Investigating the Role of Drosophila Tomosyn in Synaptic Strength and Plasticity

by

Chad W. Sauvola

B.S. Biology
B.A. Art History
Wofford College, 2015

Submitted to the Department of Brain and Cognitive Sciences
in partial fulfillment of the requirements for the degree of

Doctor of Philosophy in Neuroscience

at the

MASSACHUSETTS INSTITUTE OF TECHNOLOGY

September 2021

Author .....
Department of Brain and Cognitive Sciences
August 12, 2021

Certified by.....
J. Troy Littleton
Menicon Professor of Neuroscience
Thesis Supervisor

Accepted by .....
Rebecca Saxe
John W. Jarve (1978) Professor in Brain and Cognitive Sciences
Associate Head, Department of Brain and Cognitive Sciences

Investigating the Role of Drosophila Tomosyn in Synaptic Strength and Plasticity

by

Chad W. Sauvola

Submitted to the Department of Brain and Cognitive Sciences
on August 12, 2021, in partial fulfillment of the
requirements for the degree of
Doctor of Philosophy in Neuroscience

Abstract

Neurotransmission is an adaptation of cellular secretion characterized by precise spatial and temporal regulation of SNARE assembly that occurs at specialized presynaptic subdomains in response to transient calcium influx following an action potential. SV fusion from the presynaptic terminal results in a postsynaptic response that varies in size depending on synaptic strength. Both the postsynaptic and presynaptic terminals contribute to synaptic strength with the postsynaptic terminal regulating its own sensitivity for neurotransmitters by governing receptor field composition, and the presynaptic compartment controlling the probability of SV fusion (P_r) following an action potential. While many postsynaptic mechanisms controlling strength have been described, the presynaptic contribution remains incompletely understood. Chapter 1 describes current models of SNARE assembly and disassembly during cycles of synaptic vesicle release. Each protein described in this chapter provides a potential point of regulation for setting presynaptic strength and modulating presynaptic release during plasticity.

Chapter 2 focuses on the decoy SNARE protein Tomosyn and its role at the Drosophila larval neuromuscular junction (NMJ). Larval muscles are typically co-innervated by two glutamatergic motoneurons (Ib and Is) that show highly stereotyped differences in P_r at rest as well as differential expression of presynaptic homeostatic plasticity (PHP) when glutamate receptor function is impaired. Tonic Ib terminals display moderate initial P_r, robust potentiation, and sustained release during train stimulation whereas phasic Is terminals show high intrinsic P_r, rapid depression, and variable PHP expression. Tomosyn contributes to these differences by suppressing P_r and evoked release from tonic Ib motoneurons without affecting phasic Is release. *tomosyn* null mutants show phasic-like properties including high intrinsic P_r, enhanced depression, and impaired presynaptic homeostatic potentiation (PHP) suggesting Tomosyn regulates the tonic/phasic character and PHP expression of Drosophila synapses. The results in this chapter argue Tomosyn suppresses P_r at Ib synapses to enable tonic release and robust potentiation. Phasic release dominates when Tomosyn expression is low, contributing to the high intrinsic P_r in MNIs terminals at the expense of sustained release and robust PHP. Chapter 3 outlines future directions that might lend further insight into how Tomosyn regulates presynaptic release.

Thesis Supervisor: J. Troy Littleton
Title: Menicon Professor of Neuroscience

Acknowledgments

This thesis would not have been written without the many friends and colleagues I've made in the Littleton lab. I've been lucky. Thank you to Yulia Akbergenova for understanding my garbled thoughts and pretending I speak plain English. Thank you to Kiel Ormerod for encouraging me to go outside and for providing useful advice on our daily coffee runs. Thank you to Karen Cunningham for never making me complete a sentence. Thank you to Mónica Quiñones-Frías for encouraging me to do the experiment before talking about it. Thank you to Elizabeth Brija for diving into the nitty gritty details. Thank you to Ellen Guss for always matching my excitement level. Thank you to Dina Volfson for keeping the lab running. Thank you to everyone else in the Littleton lab for creating a fun and rigorous place to work. Finally, thank you to Troy for encouraging me to freely explore while providing the perfect amount of guidance to keep things from coming off the rails. Your good taste in research topics and your constant nudging (often pushing) in the right direction has kept me and the rest of us on track.

I'm also grateful to countless friends and family back home. Thank you to Stacey Hettes for teaching me the word "neuroscientist" and convincing me that was a cool kind of person to be. Thank you to Karen Goodchild for teaching me how to dive deep into a research topic and encouraging me to pursue the topics that interest me most. Thank you to Kaylee Boalt for constantly believing in me. I've been blessed with more family than the average person, so I'll only thank a few. Mom, thank you for teaching me to settle for nothing less than beautiful. Dad, thank you for teaching me to work hard and stop when it's good enough. Triston, InaMae, Laryn, Kyle and baby Torni thanks for teaching me that science is not the most important thing in life.

Contents

Chapter 3: Conclusions and future directions

Chapter 1

SNARE Regulatory Proteins in Synaptic Vesicle Fusion and Recycling

1.1 Introduction

Eukaryotes rely on membrane-bound organelles to organize and transport material between cellular compartments (Wickner and Schekman, 2008). Transport between membrane-bound compartments and secretion of cellular cargo requires fusion of opposing lipid bilayers (Jahn and Südhof, 1999; Rothman, 1994). A large family of membrane associated SNARE proteins constitute the minimal molecular machinery required for membrane fusion by assembling into energetically favorable coiled-coil bundles that pull opposing lipid bilayers together to induce fusion (Jahn and Scheller, 2006; Söllner et al., 1993; Südhof and Rothman, 2009). Most cargo do not require a trigger for release and are trafficked into secretory vesicles destined for immediate fusion with the plasma membrane via the constitutive secretory pathway (Burgess and Kelly, 1987). Many cells including neurons also display a regulated secretion pathway for fast stimulus-dependent cargo release, typically in response to transient rises in intracellular Ca^{2+}. Regulated secretion is mediated by a large cohort of SNARE regulatory proteins (SRPs) that control the timing and localization of SNARE assembly (Südhof and Rothman, 2009). Although some SRPs like *N*-ethylmaleimide sensitive factor (NSF), the soluble NSF attachment proteins (SNAPs) and Unc18 function in both constitutive and regulated secretion, others like Unc13, Complexin (Cpx), Synaptotagmin 1 (Syt1), Rab3-interacting molecule (RIM) and Tomosyn (Tom) provide unique temporal and spatial control of regulated secretion.

Many SRPs are present in all eukaryotes, suggesting they existed in the last common ancestor (Bennett and Scheller, 1993; Göhde et al., 2021; Littleton, 2000; Lloyd et al., 2000;

Varoqueaux and Fasshauer, 2017). Others appeared later in multi-cellular eukaryotes that required more extensive cell-cell communication (Barber et al., 2009; Ryan and Grant, 2009). Gene duplication events occurring in vertebrate lineages generated orthologs of most SRPs in chordates. This redundancy is often absent in non-vertebrate lineages, facilitating genetic analysis of conserved membrane trafficking mechanisms in simpler model eukaryotes like the budding yeast *Saccharomyces cerevisiae*, the nematode *Caenorhabditis elegans* and the fruit fly *Drosophila melanogaster* (Bargmann, 1993; DiAntonio et al., 1993; Littleton and Bellen, 1995; Novick et al., 1980; Sato et al., 2014). Behavioral screens for temperature-sensitive (TS) paralytic mutants in Drosophila identified several conserved SRPs that contribute to SV release (Babcock et al., 2004; van der Bliek and Meyerowitz, 1991; Chen et al., 1991; Guan et al., 2005; Iyer et al., 2013; Kawasaki and Ordway, 1999; Kawasaki et al., 1998; Littleton et al., 1998, 2001a; Rao et al., 2001; Siddiqi and Benzer, 1976; Tolar and Pallanck, 1998). Similarly, screens for *C. elegans* mutants displaying motor paralysis, uncoordinated locomotion or altered sensitivity to the acetylcholinesterase inhibitor aldicarb have revealed key functions for multiple SRPs (Bargmann, 1993; Brenner, 1973; Hosono et al., 1992; Miller et al., 1996; Nguyen et al., 1995; Richmond et al., 1999; Sieburth et al., 2005). Given the conservation of SRPs across evolution, reverse genetic approaches have also been used to define functions for these proteins in Drosophila and nematodes (Harris and Littleton, 2015; Richmond and Broadie, 2002; Schwarz, 1994). The accessibility of peripheral neuromuscular junctions (NMJs) for electrophysiology and imaging has also facilitated characterization of SNARE and SRP function in SV cycling in Drosophila and *C. elegans* (Jan and Jan, 1976; Melom et al., 2013; Peled and Isacoff, 2011; Richmond and Jorgensen, 1999).

The SV cycle is initiated following action potential firing and depolarization of presynaptic terminals that cause transient voltage-gated Ca^{2+} channel opening (Katz, 1969; Sudhof, 2004). Subsequent spikes in local [Ca^{2+}] trigger fusion of SVs that are docked and primed at specialized release sites known as active zones (AZs) (Ackermann et al., 2015; Ghelani and Sigrist, 2018; Zhai and Bellen, 2004). Following Ca^{2+} influx, SVs fuse at individual AZs in a probabilistic manner that is governed by a range of factors including local Ca^{2+} channel density and SV distance from the source of Ca^{2+} influx (Akbergenova et al., 2018; Böhme et al., 2016; Bucurenciu et al., 2008; Meinrenken et al., 2002; Neher and Brose, 2018). Release probability (P_r) for SV fusion can be approximated by measuring AZ P_r,

which varies across neuronal subclasses and within the AZ population of a single neuron (Akbergenova et al., 2018; Atwood and Karunanithi, 2002; Holderith et al., 2012; Karlocai et al., 2021; Koester and Johnston, 2005; Melom et al., 2013; Neher and Brose, 2018; Peled and Isacoff, 2011). Most SVs are released via Ca^{2+}-dependent evoked release, although some fuse in a stimulus-independent mode called spontaneous release. After fusion with the presynaptic plasma membrane, several endocytic routes for membrane and protein retrieval recover individual SVs, or larger membrane patches that traffic through endosomal compartments for further sorting (Chanaday et al., 2019; Gan and Watanabe, 2018; Soykan et al., 2016). Reformed SVs acidify through the action of the vesicular H^+ pump, load neurotransmitters by vesicular H^+ antiporters, and subsequently re-enter the SV pool for additional rounds of release (Sudhof, 2004).

This chapter explores current models for how SRPs guide SNAREs through their assembly/disassembly cycle, focusing on insights from invertebrate genetic studies of SV fusion. Biochemical approaches that guided reverse genetic experiments and provided context for interpreting genetic studies are also highlighted. The biochemistry and genetics of mammalian SV fusion have been described in prior reviews (Brunger et al., 2019; Neher and Brose, 2018; Rizo, 2018; Südhof, 2013). Key invertebrate and mammalian SRP phenotypes and their predicted molecular function are described in **Table 1**. This review begins with a description of the mechanism enabling SNAREs to overcome innate repulsion between opposing membranes, and the role of Unc13 and Unc18 in regulating SNARE availability for partial assembly. The SRPs Syt1 and Cpx then arrest SNARE assembly in a partially zippered state and subsequently promote Ca^{2+}-dependent fusion. After fusion, NSF and SNAPs disassemble the SNARE complex to recharge individual SNARE proteins for further cycles of release. Intrinsic SNARE properties protect SNAREs from spontaneous reassembly post-fusion with help from the SRPs Unc18 and Tomosyn. Finally, RIM and Rab3 cooperate with Unc13 to re-position endocytosed SVs for subsequent docking and priming. Each of these steps provide avenues for modulation of SV release that can impact synaptic strength and plasticity.

1.2 SV fusion is mediated by SNARE complex assembly

Lipids form stable bilayer membranes that innately repel each other through electrostatic forces and hydration repulsion (Milovanovic and Jahn, 2015; Robertson, 2018). Binding and

assembly of SNARE proteins embedded in distinct bilayers is an energetically favored event that provides sufficient input to disrupt and fuse opposing membranes (McNew et al., 2000a; Tucker et al., 2004; Weber et al., 1998). SNAREs are a large protein family characterized by a ~70 amino acid -helical heptad repeat known as the SNARE motif. Based on their primary subcellular location, SNAREs are classified as vesicular (v-) or target (t-) membrane SNAREs. A secondary classification scheme defines the proteins as Q- or R-SNAREs depending on whether a glutamine (Q) or arginine (R) is encoded at a highly conserved central hydrophilic layer within the 16-layer SNARE coil. A fusion-competent SNARE complex is formed when three Q-SNARE helices combine with one R-SNARE helix of an opposing membrane (Fasshauer et al., 1998; Weimbs et al., 1997). Across species, the SNARE complex mediating SV fusion is composed of the v-SNARE Synaptobrevin 2 (Syb2, also known as vesicular associated membrane protein (VAMP)) and the t-SNAREs Syntaxin 1 (Syx1) and Synaptosomal associated protein of 25 kilodaltons (SNAP-25) (Söllner et al., 1993). Like all known SNARE complexes, the SV SNARE complex is composed of four α-helices, a Q-helix from Syx1, two Q-helices from SNAP-25 and one R-helix from Syb2. Syb2 and Syx1 are C-terminal anchored transmembrane proteins translated on cytosolic ribosomes and post-translationally inserted into membranes by the transmembrane recognition complex (TRC) (Bennett et al., 1992a; Borgese et al., 2003; Kutay et al., 1993; Trimble et al., 1988). SNAP-25 lacks a transmembrane domain and is post-translationally embedded in membranes via palmitoylation of a cysteine-rich central region (Gonzalo and Linder, 1998; Oyler et al., 1989).

In their native state, SNAREs are disordered filaments that project from their carrier membranes into the cytosol (Fasshauer, 2003). Each protein displays selective binding to a set of cognate SNAREs that zipper together to form a highly structured four-helical SNARE bundle (McNew et al., 2000a; Sutton et al., 1998). Incorporation of individual SNARE filaments into the structured SNARE complex releases free energy that is harnessed to overcome the innate repulsion between opposing lipid membranes. Two competing models for the order of SNARE incorporation into the SNARE complex have been described (Rizo, 2018). One model proposes t-SNARE dimers of Syx1 and SNAP-25 are formed before the v-SNARE Syb2 is engaged. A more recent model argues the SRP Unc18 chaperones assembly of Syx1 and Syb2, ensuring proper alignment prior to SNAP-25 incorporation. These two models converge once cognate SNARE recognition is established to form a

partially-zippered SNARE configuration known as the trans-SNARE complex, with transmembrane segments residing on separate compartments and full SNARE assembly being temporarily arrested (**Figure 1A**). SNARE zippering is directional, initiating at the free N-terminal end and progressing through the membrane embedded C-termini (Hernandez et al., 2012; Pobbati et al., 2006; Stein et al., 2009; Sutton et al., 1998). Full zippering through the C-terminus drives fusion by converting the trans-SNARE complex to a cis-complex where all transmembrane segments are embedded in the same bilayer (**Figure 1B**). The specific arrangement of SNARE complexes between fusing membranes and the number of complexes required for SV fusion remain unclear. However, current models suggest efficient fusion requires several SNARE complexes to be arranged like "spokes on a wheel" around the fusion pore formed between opposing membranes (Hua and Scheller, 2001; Kümmel et al., 2011; Shi et al., 2012)

Genetic analysis of SNARE mutants in Drosophila and *C. elegans* support an essential and conserved role for the SNARE complex in mediating SV fusion. In Drosophila, Syx1 is essential for fusion of both SVs and post-Golgi vesicles with the plasma membrane (Broadie et al., 1995; Burgess et al., 1997; Schulze and Bellen, 1996; Schulze et al., 1995). This dual function has made it difficult to define the precise role of Syx1 in SV release, as complete absence of the protein prevents cell viability. *Syx1* null mutants develop to the late embryonic stage due to maternal deposition of Syx1 mRNA. Development is arrested once maternal mRNAs are depleted and null embryos are paralyzed due to total absence of evoked and spontaneous SV release (Schulze et al., 1995). Structure-function studies targeting distinct regions of Syx1 and TS paralytic *syx1* mutants identified in forward genetic screens are consistent with an essential role for Syx1 in SV fusion (Fergestad et al., 2001; Lagow et al., 2007; Littleton et al., 1998; Stewart et al., 2000; Wu et al., 1999). However, *syx1* mutations in distinct regions of the protein differentially alter the amount of spontaneous versus evoked release, indicating Syx1 function can be altered to change either evoked or spontaneous SV fusion pathways. Consistent with an essential role for Syx1 in invertebrate SV fusion, null mutants in *C. elegans* Syx1 (*unc-64*) are immobile and lack detectable SV release (Ogawa et al., 1998; Saifee et al., 1998).

Genetic studies of the Drosophila Syb2 and SNAP-25 homologs have revealed phenotypes that are more challenging to interpret due to potential redundancy with other SNARE isoforms. Unlike Syx1, Syb2 function in SV and post-Golgi fusion is segregated

between two Drosophila v-SNAREs, with c-Syb mediating post-Golgi fusion and n-Syb controlling SV release (Broadie et al., 1995; Chin et al., 1993; Deitcher et al., 1998; DiAntonio et al., 1993; Yoshihara et al., 1999). Although *n-Syb* null mutants show severe impairments in evoked release, a low rate of spontaneous fusion is preserved that indicates SV fusion is not eliminated. Consistently, high frequency stimulation elicits a low level of delayed evoked release (Yoshihara et al., 1999) and cleavage of n-Syb by tetanus toxin does not eliminate spontaneous fusion (Sweeney et al., 1995). *n-Syb* phenotypes can be rescued by overexpressing c-Syb, suggesting both proteins are capable of supporting SV release (Bhattacharya et al., 2002). Given overexpressed c-Syb supports relatively normal SV fusion in the absence of n-Syb, it is unclear why *n-Syb* mutants show defects primarily in evoked release. Perhaps endogenous neuronal c-Syb expression is too low to support evoked fusion, but high enough to contribute to residual spontaneous release. Alternatively, n-Syb may be specialized for evoked SV release, with spontaneous fusion supported by c-Syb and other Drosophila v-SNAREs (Littleton, 2000). Although no other v-SNARE beyond c-Syb has been shown to function in SV fusion in Drosophila, multiple v-SNAREs support spontaneous and asynchronous SV release at mammalian synapses (Lin et al., 2020; Ramirez et al., 2012). Similar to Drosophila, *C. elegans* null mutations in the Syb2 homolog (*snb-1*) are embryonic lethal, but retain uncoordinated movements that indicate a low level of residual SV release (Nonet et al., 1998).

Mutations in Drosophila *SNAP-25* indicate redundancy may also compensate for loss of t-SNARE function. The first mutant in Drosophila SNAP-25 was isolated as a TS paralytic allele caused by an amino acid substitution at a highly conserved residue (G50E) in the second SNARE motif of the protein (Rao et al., 2001). Upon exposure to the non-permissive temperature of 37°C, adult animals rapidly paralyze. *SNAP-25*^{TS} mutant larvae show elevated evoked and spontaneous release at room temperature and impaired release at 37°C. A Syx1 TS mutant (*syx1*$^{3\text{-}69}$; caused by a T254I substitution in the SNARE helix) displays a similar phenotype, indicating multiple t-SNARE mutations can alter SNARE dynamics in a manner that enhances fusion at lower temperatures and blocks release at elevated temperature (Bykhovskaia et al., 2013; Lagow et al., 2007; Littleton et al., 1998). While the mechanism underlying *SNAP-25*^{TS} release enhancement is unknown, molecular modeling suggests the *syx1*$^{3\text{-}69}$ TS mutant enhances release by altering interactions between the fusion clamp Cpx and the SNARE complex to modify SNARE zippering dynamics (Bykhovskaia et al., 2013).

Subsequent studies on SNAP-25 revealed null mutants cause pupal lethality, but do not affect SV release in larvae due to compensation from the t-SNARE homolog SNAP-24 (Vilinsky et al., 2002). Together, these data suggest SNAP-25 normally excludes endogenous SNAP-24 from participating in the SV SNARE complex, though SNAP-24 can support normal SV release when SNAP-25 is absent. *C. elegans* SNAP-25 null mutants (*ric-4*) have not been characterized electrophysiologically though they display locomotor defects that suggest RIC-4 is essential for normal synaptic function (Miller et al., 1996). In summary, genetic approaches in Drosophila and *C. elegans* indicate an essential role for Syx1 in all forms of SV fusion, with spontaneous release persisting in the absence of Syb2 and SNAP-25 likely due to compensation from non-SV SNAREs.

1.3 Unc18 and Unc13 restrict the localization of SNARE assembly to AZs by regulating Syx1 conformational transitions

Although SNARE proteins are sufficient for membrane fusion *in vitro*, SRPs are required to regulate SNARE activity *in vivo*. Given SNARE complex formation is energetically favorable, the assembly process must be tightly controlled so it occurs at the right time and place for productive fusion (Rizo, 2018). The SM proteins (Sec1/Munc18, hereafter referred to as Unc18) and the AZ-localized Unc13 family are SRPs that control the subcellular localization of SNARE assembly. Unc18 is universally required for eukaryotic membrane fusion (Südhof and Rothman, 2009), while Unc13 functions only in regulated secretion (Aravamudan et al., 1999; Richmond et al., 1999). Both proteins act primarily by controlling Syx1 availability for SNARE complex formation. Syx1 contains four α-helical domains with only the most C-terminal helix (termed the H3 domain) participating in SNARE complex formation (Fernandez et al., 1998; Sutton et al., 1998; Wu et al., 1999). The remaining N-terminal helices form a three-helix bundle called the H_{abc} domain that folds back onto the H3 SNARE motif to generate a monomeric four stranded coiled-coil bundle. The H_{abc} domain is separated from the H3 segment by a flexible hinge, allowing Syx1 to adopt an open or closed confirmation (Dulubova et al., 1999; Fernandez et al., 1998). In the closed state, the SNARE motif is locked into a grove along the length of the H_{abc} domain and blocked from participating in SNARE complex formation. When converted to the open state, the H3 domain is relieved

of H_{abc} inhibition and SNARE complex formation can proceed. Point mutations in the hinge separating the H_{abc} and H3 domains bias Syx1 toward the open conformation (open-Syx1) and enhance SV fusion in *C. elegans* (Gerber et al., 2008a; Richmond et al., 2001). These observations indicate the Syx1 closed conformation is an autoinhibitory feature that must be overcome for SV fusion to proceed, with Unc13 and Unc18 controlling this conformational switch (**Figure 2A**).

Unc18 proteins are cytosolic and can bind to Syx1 alone, Syx1 in complex with the v-SNARE, or the fully assembled SNARE complex (Baker et al., 2015; Dulubova et al., 2007; Hata et al., 1993; Khvotchev et al., 2007; Pevsner et al., 1994; Yang et al., 2000). These distinct binding interaction modes suggest Unc18 performs multiple roles in SNARE dynamics. Indeed, *in vivo* evidence indicates Unc18 both positively and negatively regulates SV release. The Drosophila Unc18 homolog ROP (Ras opposite) is essential for SV fusion, yet strongly inhibits both evoked and spontaneous release when overexpressed (**Figure 2B**) (Harrison et al., 1994; Schulze et al., 1994; Wu et al., 1998). Like Syx1, ROP functions in all modes of cellular secretion and is required for SV and post-Golgi vesicle fusion (DeBruhl et al., 2016; Harrison et al., 1994). Unc18 proteins suppress Syx1 activity in part by holding the t-SNARE in its closed state (Pevsner et al., 1994; Yang et al., 2000). This interaction is required for transport of Syx1 through the secretory pathway, reducing its ability to form ectopic SNARE complexes at inappropriate times or subcellular locations (McEwen and Kaplan, 2008; Medine et al., 2007; Rowe et al., 1999, 2001). Overexpression of Unc18 is predicted to suppress neurotransmitter release by preventing formation of fusogenic SNARE complexes due to excessive inhibition of Syx1. Heterozygotes of *Unc18* null mutants also display reduced evoked and spontaneous fusion, indicating SV release is impaired under conditions where Unc18 levels are limiting (Wu et al., 1998). Together, these data indicate SV release is bi-directionally sensitive to Unc18 abundance, suggesting synaptic levels of the protein are finely tuned for optimal presynaptic output.

Unc18 must also play a positive role in release given *Unc18* null mutants show severe secretion defects (Harrison et al., 1994; Verhage et al., 2000; Weimer et al., 2003). Multiple positive effects of Unc18 on SV release have been described, including its ability to protect SNARE complexes from disassembly by NSF and α-SNAP. Assembly of the SNARE complex *in vitro* is blocked when NSF and α-SNAP are added, suggesting SNAREs must be protected from ongoing disassembly (Ma et al., 2013; Prinslow et al., 2019; Stepien et al.,

2019). Addition of Unc18 and Unc13 to these *in vitro* assays restores the ability of SNAREs to trigger fusion, indicating the two proteins act in concert to ensure fusogenic SNARE zippering is not disrupted by premature disassembly. Unc18 also chaperones SNARE assembly by properly aligning individual SNARE helices during zippering of the 4-stranded helical bundle (Jiao et al., 2018; Ma et al., 2013). The SNARE complex is a coiled-coil structure divided into layers of hydrophobicity defined relative to the most central zero layer (Fasshauer et al., 1998). Misalignment of zippering decreases free energy released during SNARE assembly and alters the distance between fusing membranes (Fasshauer et al., 1998; Pobbati et al., 2006). *In vitro* data suggest Unc18 binds Syx1 and Syb2 in a prefusion intermediate where the two SNAREs are arrested in a partially zippered state and held in proper alignment prior to SNAP-25 arrival (**Figure 2C**) (Jiao et al., 2018; Shu et al., 2020). This role of Unc18 in SNARE assembly is supported by crystal structures of several yeast homologs that hold individual v- and t-SNAREs in proper register (Baker et al., 2015). In summary, Unc18 likely supports SV fusion by templating SNARE complex assembly and inhibiting SNARE disassembly prior to fusion. How Unc18 transitions from inhibiting Syx1 availability by holding the protein in a closed conformation to templating Syx1 and Syb2 assembly is unclear, though Unc13 is hypothesized to regulate this transition *in vivo*.

Unc13 is one of several multidomain scaffold proteins enriched at presynaptic AZs. Unlike most AZ scaffolds, Unc13 is absolutely essential for both spontaneous and evoked release (Aravamudan et al., 1999; Augustin et al., 1999; Richmond et al., 1999). Unc13 contains C2, MUN and calmodulin binding domains that each have highly conserved binding interactions across evolution (Böhme et al., 2016; Brose et al., 2000). The lipid-binding C2 domains encoded at both termini of Unc13 enable simultaneous interaction with the SV and plasma membrane to facilitate SV capture (Liu et al., 2016). The MUN domain forms a long helical rod that extends from the AZ into the cytosol, similar to other vesicle tethering factors. The MUN domain plays a critical role in SV priming by converting Syx1 from its closed to open state, leading to subsequent v-SNARE engagement and SV docking (Betz et al., 1997; Li et al., 2011; Ma et al., 2011; Wang et al., 2011). Consistent with this model, open-Syx1 mutants rescue release defects in *C. elegans Unc13* nulls, indicating *Unc13* animals lack SV fusion due to insufficient conversion of Syx1 from its closed to open state (Richmond et al., 2001).

1.4 Syt1 and Cpx regulate SNARE assembly to control the timing of Ca^{2+}-dependent fusion

Membrane fusion during constitutive secretion occurs spontaneously, with SNARE complex zippering hypothesized to occur in a single step. In contrast, SNARE assembly during regulated secretion is predicted to arrest in a partially zippered state, allowing membrane fusion to be tightly coupled to Ca^{2+} influx. Progressive step-wise zippering of the SV SNARE complex is supported by studies of the clostridial neurotoxins tetanus and botulinum that cleave individual SNAREs (Breidenbach and Brunger, 2005). After SV docking and priming, only a subset of toxin serotypes can access SNAREs for cleavage at each conformational state generated by progressive zippering (Bajohrs et al., 2004; Hayashi et al., 1994). Intermediate energy states along the trajectory of SNARE zippering are also observed *in vitro* using optical tweezers, further suggesting SNAREs assemble and disassemble in a step-wise manner (Gao et al., 2012; Zorman et al., 2014). The synaptic SRPs Cpx and Syt1 provide a neuronal-specific mechanism to further stall SNARE zippering until elevated Ca^{2+} triggers full SNARE assembly (**Figure 3A**). Cpx acts during trans-SNARE complex formation to arrest assembly in the partially zippered state (Bykhovskaia et al., 2013; Giraudo et al., 2006; Malsam et al., 2012), with Syt1 triggering full zippering and synchronous evoked fusion in response to Ca^{2+} (Chapman, 2008; Quiñones-Frías and Littleton, 2021; Südhof, 2013). The mechanisms by which these proteins regulate SNARE assembly and fusion are still being defined, but several models link their biochemical activities with defects in release observed in mutants disrupting their function.

Cpx is small cytosolic α-helical protein identified through its binding affinity for the SNARE complex (McMahon et al., 1995). The protein is composed of an N-terminal accessory helix, a central SNARE-binding helix and an unstructured C-terminus that assembles into an amphipathic helix when bound to SV membranes (Bowen et al., 2005; Buhl et al., 2013; Cho et al., 2010; Kaeser-Woo et al., 2012; Pabst et al., 2000; Snead et al., 2014; Xue et al., 2007). Mouse *Cpx* mutants have decreased evoked release, suggesting the protein facilitates SV fusion (Reim et al., 2001). Subsequent *in vitro* assays indicated Cpx primarily functions to inhibit SNARE assembly and fusion (Giraudo et al., 2006; Malsam et al., 2020). In contrast to four *Cpx* genes in mammals, Drosophila contain a single *Cpx* that facilitates genetic analysis. Null mutants in Drosophila *Cpx* revealed both positive and negative functions in SV release, including a ~100-fold increase in spontaneous fusion (**Figure 3B**)

and a ~50% decrease in evoked release (**Figure 3C**) (Huntwork and Littleton, 2007). *C. elegans Cpx* null mutants display similar defects, indicating enhanced spontaneous fusion and decreased evoked release are conserved invertebrate phenotypes associated with loss of Cpx (Buhl et al., 2013; Cho et al., 2010; Iyer et al., 2013; Jorquera et al., 2012; Martin et al., 2011; Sabeva et al., 2017; Wragg et al., 2017; Xue et al., 2009). *Cpx* mutants also disrupt the speed of evoked release, with less synchronous fusion and increased release through the slower asynchronous pathway (Jorquera et al., 2012). In addition, Cpx participates in tethering SVs to release sites by interacting with the core AZ scaffolding protein Bruchpilot (BRP) (Scholz et al., 2019). Together, these observations indicate Cpx helps target SVs to release sites, facilitates the amount and speed of evoked release, and clamps SVs in a partially zippered state that limits spontaneous fusion.

In contrast to the dramatic increase in spontaneous fusion in invertebrate *Cpx* mutants, mouse *Cpx* knockouts do not display elevated spontaneous release (Chang et al., 2015; López-Murcia et al., 2019; Xue et al., 2007, 2008; Yang et al., 2013). However, mammalian Cpx is sufficient to clamp spontaneous release in both *C. elegans* and Drosophila *Cpx* mutants (Cho et al., 2010; Wragg et al., 2017), suggesting clamping properties are intrinsic to Cpx across phyla. Cpx3 is the most effective mammalian isoform for clamping SV fusion in Drosophila and *C. elegans Cpx* mutants. The primary difference between Cpx3 and other mammalian isoforms occurs in the C-terminus, suggesting this region harbors critical determinants for clamping fusion. Although it is unclear why mammalian synapses are more resistant to enhanced spontaneous release in *Cpx* mutants, Cpx can clamp SV fusion during the asynchronous phase of evoked release in mammals (Chang et al., 2015; Yang et al., 2010). This slower component of release occurs when Ca^{2+} levels are falling from their peak concentration that drives synchronous SV fusion. Therefore, higher baseline Ca^{2+} levels in invertebrate presynaptic terminals could account for the differences in Cpx clamping. Consistent with this hypothesis, presynaptic [Ca^{2+}] can be reduced by long-term exposure to BAPTA and causes a ~50% decrease in spontaneous release in Drosophila *Cpx* mutants (Jorquera et al., 2012). These data suggest Cpx clamping acts optimally at a slightly higher baseline [Ca^{2+}], implying it may act in part by regulating the Ca^{2+} sensitivity of SV release.

Current data indicate the activating and inhibitory functions of Cpx can be genetically separated, though both require SNARE complex binding (Cho et al., 2010, 2014; Iyer et al., 2013; Krishnakumar et al., 2011; Xue et al., 2007, 2010). Several models for the inhibitory

function of Cpx have been proposed. A "zig-zag" model based on structural evidence suggests the central helix of Cpx tucks into a partially zippered SNARE complex, while the accessory helix projects out at a 45-degree angle to bind a neighboring partial SNARE assembly (Kümmel et al., 2011). This mode would allow Cpx to bridge partial SNARE assemblies in an alternating zigzag chain sandwiched between docked SVs and the plasma membrane to clamp release before Ca^{2+} influx. Mutations predicted to abolish the zig-zag array have only mild effects on SV release in Drosophila, suggesting this binding mode is unlikely to represent the primary clamping configuration of Cpx (Cho et al., 2014). A second model from biochemical studies and molecular modeling suggests competition between Syb2 and Cpx for t-SNARE binding mediates clamping, with the Cpx N-terminal accessory helix binding partially assembled SNARE complexes in a grove between Syx1 and SNAP-25 in place of Syb2 (**Figure 3D**). This would allow Cpx to destabilize the final step of SNARE zippering by excluding Syb2 from the C-terminus of the SNARE complex (Brady et al., 2021; Bykhovskaia et al., 2013; Vasin et al., 2016). Although attractive, genetic analysis of *Cpx* and *n-Syb* mutations predicted to disrupt this mode of binding only partially disrupt clamping (Vasin et al., 2016). A modified version of the competition model has also been described where Syb2, a single helix of SNAP-25, and the Cpx accessory helix form a C-terminal helical bundle that displaces Syx1 from the SNARE complex at its C-terminus (Malsam et al., 2020). Mutations disrupting this binding mode do not affect evoked release but decrease the clamping efficiency for spontaneous fusion.

Regardless of its clamping configuration, enhanced spontaneous release in *Cpx* mutants is abolished in Drosophila *Cpx, Syt1* double mutants (**Figure 3B**) (Jorquera et al., 2012). Syt1 is a SV protein with tandem C2 domains (C2A and C2B, **Figure 4A**) that bind ~ five Ca^{2+} ions via negatively charged aspartate residues encoded within protruding C2 loops (Chapman, 2008; Ubach et al., 1998). Ca^{2+} binding neutralizes the negative charge of these loops to allow C2•Ca^{2+} to partially insert into the plasma membrane (Chapman and Davis, 1998; Davletov and Südhof, 1993; Fernandez et al., 2001; Ubach et al., 2001). Ca^{2+} binding to the C2B domain of Drosophila Syt1 is critical for promoting evoked release (**Figure 4B**), with C2A-Ca^{2+} playing a supporting role (Bowers and Reist, 2020; Lee et al., 2013; Littleton et al., 2001b; Mackler et al., 2002; Paddock et al., 2008, 2011; Striegel et al., 2012a; Yoshihara et al., 2010). The genetic interactions between *Syt1* and *Cpx* suggest loss of Cpx may disrupt Syt1's ability to link its fusion activation to Ca^{2+} binding. Following loss of Cpx,

Syt1 may constitutively activate SNARE-dependent fusion in a Ca^{2+}-independent manner, leading to elevated spontaneous fusion rates.

Regulation of Syt1 activity is also likely to contribute to Cpx's positive role in promoting fusion as mutations in either gene cause similar SV release defects, though *Cpx* phenotypes are generally milder than those found in *Syt1* (Jorquera et al., 2012). Both *Cpx* and *Syt1* mutants show impaired evoked synchronous release while enhancing the number of SVs released through the slower asynchronous pathway (Guan et al., 2020; Jorquera et al., 2012; Lee and Littleton, 2015; Mackler et al., 2002; Paddock et al., 2011; Saraswati et al., 2007; Shields et al., 2020; Striegel et al., 2012b, 2012a; Yoshihara and Littleton, 2002; Yoshihara et al., 2010). Both mutants show an increased rate of spontaneous fusion (DiAntonio and Schwarz, 1994; Huntwork and Littleton, 2007; Lee et al., 2013; Littleton et al., 1993, 1994), with Cpx playing the primary role in clamping release at invertebrate terminals and Syt1 assuming this function at mammalian synapses. The Ca^{2+} sensitivity of evoked release is also reduced in either mutant (Jorquera et al., 2012; Littleton et al., 1994), suggesting a greater number of Ca^{2+} ions are required to fuse SVs in their absence. Evoked release defects in *Cpx* mutants can be partially rescued with elevated extracellular [Ca^{2+}], arguing Ca^{2+} sensitivity is impaired but not abolished (Jorquera et al., 2012). In contrast, *Syt1* mutants display severely impaired release across the entire [Ca^{2+}] range (Littleton et al., 1994; Yoshihara and Littleton, 2002). Finally, both mutants reduce the size of the readily releasable SV pool and alter the speed of SV fusion in a Ca^{2+}-dependent manner (Jorquera et al., 2012; Lee and Littleton, 2015; Mace et al., 2009; Yoshihara and Littleton, 2002). Recent structural evidence provides a potential model explaining why these SRPs phenocopy each other. Syt1 and Cpx bind the outer surface of the SNARE complex to form a split but continuous α-helix as part of a "tripartite complex" (**Figure 3A**), suggesting Syt1 and Cpx may form a single regulatory unit that reduces the energy barrier needed for full SNARE zippering (Trimbuch and Rosenmund, 2016; Zhou et al., 2017).

Beyond the tripartite SNARE binding site with Cpx, a primary SNARE complex binding interface on a distinct surface of the Syt1 C2B domain is critical for triggering SV release (Guan et al., 2017; Zhou et al., 2015a). The five key residues that form the primary binding site based on structural data were independently identified in a genetic screen for *Syt1* mutants in Drosophila (**Figure 4C**), indicating this interface is highly conserved and essential for Syt1 function (Guan et al., 2017). Disrupting SNARE binding at this site

phenocopies *Syt1* null mutants in critical ways (**Figure 4D**), including loss of synchronous fusion and elevated rates of asynchronous and spontaneous release. Current models for Syt1's role in fusion suggest SNARE binding, together with Ca^{2+}-independent lipid interactions mediated through a polybasic stretch on a separate C2B surface, sandwich Syt1 between the plasma membrane and the partially assembled SNARE complex. This positions the Ca^{2+} binding loops of Syt1's C2 domains close to the plasma membrane, enabling rapid membrane insertion of the loops following Ca^{2+} entry to trigger a conformational rotation that pulls the two fusing membranes together and initiates full SNARE zippering (Quiñones-Frías and Littleton, 2021). Ca^{2+}-dependent conformational changes in Syt1 may also dislodge Cpx to facilitate conversion from the trans- to cis-SNARE complex to drive the final fusion reaction. Displacement of Cpx would provide binding sites for α-SNAP to initiate subsequent NSF-mediated SNARE complex disassembly. Together, these data indicate Syt1 and Cpx cooperate to prevent full SNARE zippering during SV priming and later activate full fusion following Ca^{2+} influx.

1.5 The AAA+ ATPase NSF disassembles SNARE complexes to support continual SV cycling

NSF proteins are highly conserved AAA+ ATPases that disassemble SNARE complexes for both constitutive and regulated membrane trafficking (Pallanck et al., 1995a; Wilson et al., 1989). Disassembly of the SNARE complex supplies the energy input required for membrane fusion by returning SNAREs to their disordered state for future rounds of assembly (Block et al., 1988; Littleton et al., 1998; Wilson et al., 1992). The cis-SNARE complex (also called the 7S complex based on its gradient sedimentation) is highly stable and resistant to SDS denaturation, indicating a large input of cellular energy is required to break the complex apart (Fasshauer et al., 2002). Full dissociation of the SNARE complex is estimated to consume between 12 and 50 ATP molecules, generating 65 kBT of free energy that can be used to drive membrane fusion during future cycles of SNARE assembly (Cipriano et al., 2013; Yoon and Munson, 2018). NSF proteins are composed of an N-terminal domain and two AAA+ ATPase domains termed D1 and D2 (Tagaya et al., 1993; White et al., 2018). The D2 domains promote multimerization of NSF into hexamers that assemble around a single SNARE complex via interactions between the NSF N-terminal domains and SNAP proteins that preferentially associate with assembled SNARE complexes (White et al., 2018; Zhao et al.,

2015). Once the SNAP/NSF/SNARE complex is formed (termed the 20S complex, **Figure 5A**), the D1 domains of NSF use ATP hydrolysis to twist the four-helical SNARE bundle opposite to its assembled orientation until individual SNAREs are sufficiently destabilized to disassociate (Cipriano et al., 2013; Ryu et al., 2015; Zhao et al., 2015). Whether SNARE disassembly by NSF occurs in a multi-step process or all at once remains contentious. One model based on the processive mechanism of the bacterial AAA+ ATPase ClpXP suggests NSF may drive SNARE disassembly by progressing along the assembled SNARE complex in discrete steps that each require ATP hydrolysis (Saunders et al., 2020). An alternate model supported by *in vitro* single molecule assays suggests NSF may use a spring-loaded trigger mechanism to disassemble the SNARE complex in a single round of ATP hydrolysis (Ryu et al., 2015).

The Drosophila genome encodes two NSF proteins. NSF1 (*comatose*) mediates neuronal SNARE complex disassembly (Boulianne and Trimble, 1995; Ordway et al., 1994; Pallanck et al., 1995b) and NSF2 functions more broadly, including in the postsynaptic compartment (Golby et al., 2001; Stewart et al., 2002). TS behavioral screens in Drosophila uncovered numerous mutants in NSF1 that were originally named after their strong paralytic phenotype (*comatose)* (Pallanck et al., 1995a; Siddiqi and Benzer, 1976). Many *comatose* TS alleles result from single amino acid changes within a hinge region of the D1 domain that may impair the ability of NSF to twist the SNARE complex apart (Littleton et al., 2001a). Although restrictive temperatures are predicted to immediately disrupt NSF function, adult *comatose* animals behave normally for ~ one minute before paralysis (**Figure 4B**). Accumulation of assembled 7S SNARE complexes (**Figure 5B**) and a progressive impairment of synaptic transmission within the visual system (**Figure 5C**) mirror the time course for paralysis (Littleton et al., 1998, 2001a, Sanyal et al., 1999, 2001; Tolar and Pallanck, 1998). These data suggest depletion of free SNAREs available to engage in SNARE complex assembly occurs after several rounds of SV fusion following loss of NSF1 function, leading to disrupted synaptic transmission and subsequent behavioral paralysis. The time course for recovery of *comatose* mutants correlates with the duration of the prior heat shock, likely due to the slow kinetics of NSF-mediated SNARE disassembly and the increasing depletion of free SNAREs as animals are maintained for longer periods at restrictive temperatures. The delayed onset and slow recovery from behavioral paralysis in NSF TS mutants contrasts with the rapid onset and recovery observed in Syx1 TS mutants ($Syx1^{3\text{-}69}$,

Figure 5D). These kinetic differences highlight the requirement of Syx1 for immediate SV fusion and the large pre-existing pools of free SNAREs and SVs available to support ongoing release for several minutes after NSF inactivation (Littleton et al., 1998).

Although *comatose* mutations cause adult paralysis and synaptic transmission defects, the role of NSF at larval NMJs has been difficult to ascertain. *NSF1* null mutants are lethal, but die over a developmental window that spans from late embryogenesis to the pharate adult stage (Golby et al., 2001; Littleton et al., 2001a; Sanyal and Krishnan, 2001). *NSF1* null larvae display no obvious transmission defects at the NMJ even though lethality is rescued when NSF1 is re-expressed in the nervous system. *NSF2* null mutants die during early larval development and are rescued by re-expression of NSF2 in mesodermal tissues, suggesting this isoform is predominantly active within muscles and other non-neuronal cells (Golby et al., 2001). NSF2 may also have SNARE-independent presynaptic functions given *NSF2* mutants have defects in SV mobility due to decreased presynaptic actin filament assembly (Nunes et al., 2006). Overexpression of NSF2 in the nervous system is sufficient to rescue release defects in *NSF1* mutants, suggesting differences in expression pattern and abundance are likely to account for their unique phenotypes. At the adult NMJ, *comatose* mutants display normal baseline synaptic transmission and a progressive activity-dependent reduction in evoked release during repetitive stimulation (Kawasaki and Ordway, 1999; Kawasaki et al., 1998). Together with an accumulation of docked SVs observed by EM at restrictive temperatures, these data suggest disassembly of SNARE complexes by NSF helps maintain SVs in a readily-releasable state. Excess SNARE complexes in *comatose* mutants accumulate in both the presynaptic plasma membrane and on SVs (Littleton et al., 2001a; Sanyal et al., 1999, 2001; Tolar and Pallanck, 1998). Together, these data indicate NSF can break apart SNARE complexes in the plasma membrane that accumulate following fusion, as well as those already on SVs, to maintain a pool of free Syb2 to participate in trans-SNARE complex formation.

NSF relies on SNAP proteins to bind assembled SNARE complexes (Clary et al., 1990; Vivona et al., 2013). α-, β-, and γ-SNAP were initially purified from brain extracts based on their ability to promote NSF binding to SNARE-rich membranes. α-SNAP is the most extensively characterized and mediates association of NSF with the 7S SNARE complex *in vitro* and *in vivo* (Barnard et al., 1997; Söllner et al., 1993; Vivona et al., 2013; Zhao et al., 2015). The α-SNAP/SNARE complex binding interface includes residues from

all SNAREs, suggesting it only recognizes assembled SNARE complexes (Marz et al., 2003; Whiteheart et al., 1992; Wilson et al., 1992). NSF hexamers bind SNAREs via four α-SNAP proteins that form a bridge between the SNARE complex and the NSF N-terminal domains (Huang et al., 2019; White et al., 2018; Zhao and Brunger, 2016; Zhao et al., 2015; Zhou et al., 2015b). *In vitro* evidence suggests NSF and α-SNAP indiscriminately disassemble SNARE complexes regardless of individual SNARE composition, suggesting they provide the energy for most cellular fusion reactions (Vivona et al., 2013; Zhao and Brunger, 2016; Zhao et al., 2015). Although the *in vitro* function of α-SNAP in SNARE disassembly has been well characterized, *in vivo* roles have not been extensively studied. In *C. elegans,* synaptic phenotypes resulting from NSF and α-SNAP mutations have not been reported, but Drosophila *α-SNAP* null mutants are embryonic lethal (Babcock et al., 2004; Ordway et al., 1994). Similar to Syx1 and Unc18, Drosophila *α-SNAP* mutants show defects in membrane trafficking in many cell types that indicate α-SNAP function is broadly required (Babcock et al., 2004). Like *comatose* mutants, *α-SNAP* hypomorphic alleles accumulate assembled 7S SNARE complexes but show no defects in synaptic transmission at larval NMJs (Babcock et al., 2004).

The functions of β- and γ-SNAP are less clear. α-SNAP is the only SNAP that restores *in vitro* fusion deficits in yeast *sec17* (α-SNAP) mutants, suggesting SNAPs are not fully redundant (Clary et al., 1990; Griff et al., 1992; Peter et al., 1998). β-SNAP is a vertebrate-specific paralog of α-SNAP generated by a gene duplication event occurring after divergence of vertebrates and invertebrates. γ-SNAP is dissimilar in sequence to both α- and β- SNAP and may play a supportive role in NSF/SNARE complex dynamics (Peter et al., 1998; Stenbeck, 1998; Whiteheart et al., 1992). Many invertebrates lack a γ-SNAP homolog, though Drosophila has two γ-SNAP genes that have not been characterized. Although no γ-SNAP mutant has been reported in any species, RNAi knockdown of γ-SNAP indicates the protein mediates disassembly of an endosomal SNARE complex, suggesting a canonical SNAP function (Inoue et al., 2015). Although the requirement of NSF and SNAPs for SNARE complex disassembly has been well defined, the full complement of *in vivo* functions mediated by these proteins remains poorly characterized.

1.6 Multiple modes of endocytosis mediate SV and

SNARE recycling

The SV and presynaptic plasma membranes become continuous during fusion, resulting in a temporary disruption in the spatial segregation of proteins. Many neurons can continue to release SVs for minutes to hours under high exocytotic demand, releasing far more SVs than observed in synaptic terminals by EM (Ceccarelli et al., 1973). To support further rounds of release, membrane proteins must be re-segregated and SV material selectively internalized to form new vesicles (Chanaday et al., 2019; Dittman and Ryan, 2009; Gan and Watanabe, 2018). SNARE disassembly by NSF is also required to free v-SNAREs from plasma membrane t-SNAREs after fusion. SNARE disassembly by NSF is hypothesized to occur in part at peri-active zones (PAZ), a presynaptic endocytotic domain surrounding AZs where SV material is retrieved from the plasma membrane (Estes et al., 1996; Guan et al., 2020; Harris and Littleton, 2015; Littleton et al., 2001a; Maritzen and Haucke, 2018; Rodal et al., 2008; Yu et al., 2011). Live imaging of NSF and α-SNAP show they redistribute from the cytoplasm to the peri-active zone (PAZ) to bind post-fusion SNARE complexes in Drosophila *comatose* mutants (Yu et al., 2011). Although endocytosis and SNARE disassembly can act within the same membrane compartment, how NSF activity is spatially and temporally coordinated with endocytosis is unknown. Three popular models have been proposed for SV endocytosis, including "kiss-and-run" endocytosis, ultrafast endocytosis and Clathrin-mediated endocytosis (CME) (Ceccarelli et al., 1973; Fesce et al., 1994; Heuser and Reese, 1973; Watanabe et al., 2013b, 2013a).

Kiss-and-run is conceptually the simplest way to recover SVs membrane proteins, with SNARE zippering causing brief fusion pore formation that releases neurotransmitters before the pore is quickly re-closed (Chanaday et al., 2019; Cremona and De Camilli, 1997; Rizzoli and Jahn, 2007). As such, SV material is never lost to the plasma membrane and SVs are immediately recovered without losing their identity. It is unclear how NSF-mediated disassembly works in this pathway given cis-SNARE complexes would not form in a fused membrane. Kiss-and-run has been documented for dense core vesicle (DCV) cargo release and for some SVs at a few central mammalian synapses (Aravanis et al., 2003; Artalejo et al., 1998; Wen et al., 2017; Xia et al., 2009; Zhang et al., 2009). However, experimental evidence does not support this mechanism at invertebrate synapses given kiss-and-run is a Clathrin-independent process (Artalejo et al., 1998; Henkel and Almers, 1996). Acute inactivation of Clathrin at Drosophila NMJs abolishes sustained release during repetitive

stimulation and is accompanied by complete loss of SVs (Heerssen et al., 2008; Rodal and Littleton, 2008).

In contrast to kiss-and-run, CME enables SVs to be directly recovered from the plasma membrane after full collapse through progressive membrane invagination into reformed vesicles. Clathrin is a cytosolic protein that forms trimeric Y-shaped triskelions that progressively deform the plasma membrane by assembling on endocytic membrane patches to generate coated pits (Smith et al., 1998; Ungewickell and Branton, 1981). Further assembly shapes these pits into Clathrin-caged spheres that are budded from the plasma membrane (Heuser and Reese, 1973; Takei et al., 1996). GTP hydrolysis by the endocytic protein Dynamin provides energy to release nascent SVs from the plasma membrane by oligomerizing around the invaginating membrane stalk and pinching it to induce membrane fission (Ford et al., 2011; Hinshaw and Schmid, 1995; Sweitzer and Hinshaw, 1998). Hypomorphic alleles of the Drosophila Dynamin homolog *Shibire* were isolated in TS paralytic screens (van der Bliek and Meyerowitz, 1991; Chen et al., 1991; Delgado et al., 2000; van de Goor et al., 1995; Koenig and Ikeda, 1989; Poodry et al., 1973). *Shibire* mutants show fast synaptic depression and SV depletion at elevated temperatures, suggesting Dynamin is required to recover SVs for sustained release (Delgado et al., 2000; Kawasaki et al., 2000; Koenig and Ikeda, 1989; Wu et al., 2005).

Clathrin assembly is triggered by cytosolic adaptor proteins that recognize and cluster SV material into endocytic membrane patches (Haucke et al., 2011). Each SV protein is presumed to directly or indirectly associate with the general endocytic adaptor protein complex 2 (AP2) for retrieval from the membrane, with interactions between SV proteins likely contributing to AP2 recognition (Bennett et al., 1992b; Wittig et al., 2021). Syt1 is captured by the AP2 adaptor complex and Stonin2, while Syb2 is internalized by indirect AP2 association through the Clathrin adaptor AP180 (Bao et al., 2005; Chapman et al., 1998; Diril et al., 2006; Haucke et al., 2000; Kaempf et al., 2015; Littleton et al., 2001b; Martina et al., 2001; Nonet et al., 1999; Walther et al., 2004; Zhang et al., 1998, 1994). Mutations in the core α-adaptin subunit of the Drosophila AP2 complex cause embryonic lethality, with disrupted endocytosis and loss of SVs (González-Gaitán and Jäckle, 1997). Mutations in AP2 proteins in *C. elegans* also disrupt synaptic transmission and reduce SV numbers by up to 70%, with accumulation of large membrane vacuoles within synaptic terminals (Gu et al., 2008, 2013; Mullen et al., 2012). Loss of the Drosophila AP180 protein LAP causes a

reduction in SV number, accumulation of cytosolic cisternae and increased SV size (Zhang et al., 1998), similar to mutants of the *C. elegans* AP180 homolog Unc11 that display an accumulation of Snb-1 (Syb2 homolog) on the plasma membrane, impaired neurotransmitter release and enlarged SVs (Nonet et al., 1999). NSF-mediated disassembly of the SNARE complex would expose Syb2 to AP180, providing one potential switch coupling SNARE disassembly to SV endocytosis. Neurotransmission is not fully eliminated in *AP180* mutants, suggesting Syb2 can be retrieved from the plasma membrane via another mechanism. The abundant SV protein Synaptophysin simultaneously binds Syb2 and AP2 to provide a secondary pathway for SV internalization (Bonanomi et al., 2007; Gordon and Cousin, 2014, 2016, Gordon et al., 2011, 2016; Pennuto et al., 2003; Yelamanchili et al., 2005). Syx1 cannot bind Syb2 while associated with Synaptophysin, suggesting Syb2 would only be available for endocytosis recruitment after SNARE complex disassembly (Edelmann et al., 1995; Siddiqui et al., 2007). In addition, Synaptophysin may act to chaperone Syb2 and prevent premature SNARE complex re-assembly. Given the lack of a Synaptophysin homolog in Drosophila (Stevens et al., 2012), additional mechanisms to support v-SNARE endocytosis and chaperoning likely exist.

Ultrafast endocytosis is a newly proposed mechanism for Dynamin-dependent SV formation where the plasma membrane immediately buckles into the cytoplasm when SVs fuse (Gan and Watanabe, 2018; Watanabe et al., 2013b, 2013a). Optically stimulated *C. elegans* motoneurons fixed within 25 milliseconds of SV release show large membrane invaginations at the periphery of the AZ that quickly resolve into cytosolic endosomes (Watanabe et al., 2013b). Following Dynamin activity, Clathrin-mediated fission of these endosomes generates new SVs. However, it is currently unclear whether the rapidly invaginated membrane compartments observed by EM contain SV proteins that were just exocytosed. This form of endocytosis may primarily act to relieve plasma membrane tension by internalizing lipids rather than fused SV proteins. Given the slow kinetics of NSF-mediated SNARE disassembly and the rapid time-course of ultrafast endocytosis, it is unlikely NSF could disassemble cis-SNARE complexes prior to plasma membrane internalization via this mechanism. As such, ultrafast endocytosis may internalize SV material lost during prior rounds of fusion. Indeed, some SV cargo like Syt1 and Syb2 are localized to the plasma membrane in resting mammalian neurons (Fernández-Alfonso et al., 2006), potentially allowing ultrafast endocytosis to draw from a pool of SV material normally

found on the plasma membrane.

1.7 SNAREs, Rabs and Rab effectors contribute to target specificity for membrane fusion

Following endocytosis, SVs navigate a host of non-target presynaptic membrane compartments as they traffic back to AZs. Dozens of t- and v-SNAREs are encoded in eukaryotic genomes, implying a large combinatorial assortment of possible SNARE complexes across different subcellular compartments. Only a subset of these theoretical complexes associate *in vitro* and *in vivo* to promote membrane fusion (McNew et al., 2000b; Söllner et al., 1993), suggesting cognate SNARE binding contributes to fusion specificity. SRPs also facilitate specificity in membrane trafficking, with Rab proteins and their effectors acting in vesicle-target recognition upstream of SNARE interactions. Rab proteins are monomeric GTPases that specify membrane identity by associating with one or a small subset of intracellular compartments via two cysteine-linked prenyl groups (Stenmark, 2009). These lipid anchors are exposed in the Rab GTP-bound active state and occluded following GTP hydrolysis (inactive GDP-bound state), allowing Rabs to cycle on and off membranes in a GTP-dependent manner (Pereira-Leal et al., 2001; Stenmark and Olkkonen, 2001). Rabs sculpt intracellular membrane composition by recruiting and activating effector proteins that include tethering factors, SNAREs, cytoskeleton modifiers, lipid kinases/phosphatases, endocytic proteins and protein scaffolds (Grosshans et al., 2006; Stenmark, 2009). Among this group, tethering factors form critical Rab effectors for mediating membrane fusion specificity. These multimeric protein complexes project farther into the cytosol than SNARE proteins, identifying and luring vesicles via specific affinity for vesicular Rabs or SNAREs (Spang, 2016; Whyte and Munro, 2002; Witkos and Lowe, 2015; Yu and Hughson, 2010). Tethering complexes are phylogenetically diverse and include the Exocyst, Golgin, CORVET, and HOPS complexes, each tethering a distinct vesicle type to their cognate target membrane. After tethering factors bring vesicles to the appropriate target compartment, trans-SNARE assembly docks and primes them for fusion.

At the synapse, AZ components project into the cytoplasm to engage and recruit SVs to release sites via several large scaffolding proteins (Ghelani and Sigrist, 2018; Südhof, 2012; Zhai and Bellen, 2004). One of the most prominent AZ scaffold proteins in Drosophila is the ELKS/CAST-like protein BRP (Wagh et al., 2006). *Brp* null mutants lack the electron-

dense T-bar structure at Drosophila AZs and have reduced evoked release secondary to decreased AZ Ca^{2+} channel density (Kittel et al., 2006; Wagh et al., 2006). *Brp* mutants lacking only the cytosolic C-terminus of the protein (*Brp*^{nude}) have normal AZ dense body projections and Ca^{2+} channel clustering, but fail to accumulate SVs that normally surround the AZ due to defective Cpx binding (Hallermann et al., 2010; Scholz et al., 2019). *Brp*^{nude} mutants display normal evoked release at low frequency, but severely reduced release following repetitive stimulation. These data indicate BRP is not an essential tethering factor for SV docking and priming, but clusters SVs for fast refilling of release sites to support sustained activity.

Among the AZ proteins that mediate SV targeting, RIM tethers vesicles to release sites via its interaction with Rab3 (Betz et al., 2001; Han et al., 2011; Koushika et al., 2001; Schoch et al., 2002; Wang et al., 1997). *RIM* mutants have severely impaired evoked release accompanied by a dramatic reduction in SV docking (Gracheva et al., 2008; Graf et al., 2012; Han et al., 2011; Kushibiki et al., 2019; Oh et al., 2021). Together with the AZ protein SYD-2/Liprin, the *C. elegans* RIM homolog Unc10 forms filamentous projections that extend from the AZ to capture and tether Rab3 bound SVs at release sites (Gracheva et al., 2008; Stigloher et al., 2011). *Rab3* mutants also show defects in SV recruitment, but have more modest impairments in evoked release (Geppert et al., 1997; Gracheva et al., 2008; Graf et al., 2009; Nonet et al., 1997; Schlüter et al., 2006). Drosophila and *C. elegans RIM/Rab3* double mutants do not have enhanced release defects, suggesting they operate in a similar pathway. Beyond SV tethering, Drosophila *Rab3* mutants have defects in AZ maturation, with a subset of release sites lacking late AZ scaffold proteins required for efficient evoked release (Graf et al., 2009). This AZ maturation phenotype is not observed in *RIM* mutants, suggesting Rab3 interfaces with other Rab effector proteins to deliver AZ components during synaptic development.

RIM is hypothesized to partner with Unc13 to transition SVs from a tethered state to the downstream Unc18/Unc13-dependent priming mechanism (Liu et al., 2019). RIM and Unc13 display highly conserved interactions mediated by a C2 domain in Unc13 and a zinc finger domain of RIM. Disruption of the RIM/Unc13 interaction reduces the number of fusion competent SVs, suggesting efficient SV recruitment requires engagement with Unc13 (Betz et al., 2001). Homodimerization of Unc13 in *C. elegans* generates an autoinhibitory state that is relieved by RIM binding prior to SV priming (Liu et al., 2019). These biochemical

interactions suggest a model where Unc13 autoinhibition is relieved by RIM before it primes Syx1 for SNARE complex assembly. Given the RIM zinc finger domain also interacts with Rab3 (Betz et al., 2001; Liu et al., 2019; Weimer et al., 2006), priming may be coupled to SV arrival through competition for RIM binding between Unc13 and SV-bound Rab3. Release of RIM from Rab3 would allow it to activate Unc13 for Syx1 priming, with open Syx1 engaging Unc18 on a distinct interaction surface that templates the onset of SNARE complex assembly between Syx1 and SV-localized Syb2. Release defects in both *Unc10/RIM* and *Unc13* can be rescued by the open-Syx1 mutation (Tien et al., 2020), consistent with RIM-mediated SV tethering facilitating downstream SNARE-dependent SV priming.

1.8 Tomosyn acts as a decoy SNARE to negatively regulate SNARE complex assembly

SNARE proteins incompatible with membrane fusion, known as decoy SNAREs, provide an additional mechanism to ensure regulated SNARE assembly. Several decoy SNAREs have been described in mammals, but Tomosyn is the only known invertebrate decoy SNARE (Ashery et al., 2009; Gerst, 2003; Lao et al., 2000; Masuda et al., 1998; Scales et al., 2002). Tomosyn was originally identified for its ability to displace Syx1 from Unc18, and suggested to engage Syx1 and SNAP-25 in an intermediate stage of SNARE assembly preceding trans-SNARE complex formation (Fujita et al., 1998; Masuda et al., 1998; Pobbati et al., 2004). Subsequent experiments revealed Tomosyn prevents Syb2 binding to t-SNAREs, suggesting this complex is not a prefusion intermediate but may rather inhibit productive SNARE complex assembly (Yokoyama et al., 1999). Tomosyn is a large cytoplasmic protein with a Syb2-like R-SNARE motif at its C-terminus that forms a four-helical SNARE complex with synaptic t-SNAREs (**Figure 6**). However, the absence of a membrane anchor in Tomosyn prevents formation of fusogenic SNARE complexes. At the N-terminus, Tomosyn contains WD40 repeats organized into a propeller-like scaffold with homology to L(2)GL proteins (Lehman et al., 1999; Williams et al., 2011). *In vivo* studies suggest Tomosyn can also interact with SNAREs beyond its R-SNARE motif, as the yeast Tomosyn-like protein Sro7 lacks a SNARE motif and uses its scaffold domain to coordinate vesicle docking with SNARE assembly by binding the Sec9 t-SNARE (Lehman et al., 1999; McEwen et al., 2006; Yamamoto et al., 2010a; Yizhar et al., 2007).

Tomosyn overexpression reduces both constitutive and regulated secretion in a

diverse set of eukaryotes, suggesting a highly conserved inhibitory role (Chen et al., 2011; Gracheva et al., 2006; Hatsuzawa et al., 2003; Li et al., 2019; Williams et al., 2011; Yizhar et al., 2004; Zhang et al., 2006). Null mutations in *C. elegans Tomosyn* (*tom-1)* show a dramatic increase in evoked neurotransmitter release (Burdina et al., 2011; Gracheva et al., 2006; McEwen et al., 2006). Whether this phenotype is caused by reduced decoy SNARE activity remains unclear given the scaffold and SNARE domains are both required in tandem to suppress release (Burdina et al., 2011). Indeed, work in mammalian cultured cells suggests the SNARE domain may be dispensable for Tomosyn's inhibitory role given overexpression of the scaffold alone is sufficient to suppress evoked release (Yamamoto et al., 2010b). This phenotype can be reversed by elevating the extracellular [Ca^{2+}] (Yizhar et al., 2004, 2007) or by co-overexpressing a cytosolic fragment of Syt1 arguing the Tomosyn scaffold domain inhibits release by limiting Syt1's ability to trigger Ca^{2+}-dependent SNARE assembly in some mammalian cells (Yamamoto et al., 2010b). The scaffold coding section of the *tomosyn* gene contains a highly conserved region of alternative splicing that generates multiple splice variants across species (Groffen et al., 2005). The functional differences between these splice isoforms, including whether all splice variants can inhibit Syt1 function, remains unknown.

Beyond Tomosyn's coregulation of SNARE assembly with Syt1, genetic interactions in *C. elegans* suggest release suppression by Tomosyn may prevent Unc13/Unc-18-independent SNARE assembly. The total elimination of release in *unc-13* and *unc-18* single mutants indicate SV priming normally occurs exclusively via an Unc13/Unc18-dependent mechanism. Remarkably, double mutants of *tom-1*/*unc-13* and *tom-1*/*unc-18* partially restore the loss of evoked and spontaneous release in *unc-13* and *unc-18* single mutants, indicating Tomosyn suppresses a pathway that would otherwise bypass Unc13 and Unc18 to generate dysregulated priming (Gracheva et al., 2010; Hu et al., 2013; McEwen et al., 2006). *In vitro* reconstitution experiments indicate Tomosyn does not interfere with Unc13/Unc18-chaperoned SNARE assembly, suggesting Tomosyn can only engage Syx1 in an Unc13/Unc18-independent manner. NSF disassembly of the Tomosyn/t-SNARE complex leads to Unc18 capture of Syx1 for incorporation into productive SNARE complexes (Hatsuzawa et al., 2003; Li et al., 2018). *In vivo*, *tom-1* enhanced release is exaggerated by the open-Syx1 mutation, causing a further increase in *tom-1* sensitivity to the acetylcholinesterase inhibitor aldicarb (Tien et al., 2020). Enhanced SV fusion in *tom-1* exceeds the residual release in *tom-1*/*unc-13* and *tom-1*/*unc-18* double mutants, indicating

Tomosyn also suppresses SNARE assembly within the traditional Unc13/Unc18 priming pathway. Together, these data indicate Tomosyn ensures tight regulation of SNARE complex assembly by acting as a failsafe to prevent dysregulated Unc13/Unc18-independent priming of Syx1.

1.9 SRPs regulate intrinsic synaptic properties

SRPs guide SNARE interactions during multiple steps of the SV fusion cycle by localizing SNARE assembly, regulating Ca^{2+}-dependent SNARE zippering, recycling SNAREs post-fusion and inhibiting dysregulated SV priming (**Figure 7**). Given their critical roles in synaptic communication, it is not surprising that mutations in these genes cause a host of severe human neurological disorders (Abramov et al., 2021; Engel et al., 2016; Lipstein et al., 2017; Melland et al., 2021; Melom and Littleton, 2011; Redler et al., 2017; Salpietro et al., 2019). SRPs and SNAREs are broadly expressed in all neurons and are ideally positioned to regulate intrinsic synaptic release strength and presynaptic plasticity. Given presynaptic output and plasticity mechanisms display wide heterogeneity across neuronal subtypes and at individual release sites, SRPs are likely subject to transcriptional and post-translational control that alters their function. Indeed, SRPs can regulate release differences by controlling SV availability, spontaneous release rate, and SV priming location (Aponte-Santiago and Littleton, 2020; Böhme et al., 2016; Cho et al., 2015; Fulterer et al., 2018; Hu et al., 2013; Melom et al., 2013; Pooryasin et al., 2021).

Several examples of SRP regulation that alter synaptic function or plasticity have been characterized. Phosphorylation of a Drosophila Cpx isoform by protein kinase A (PKA) occurs during activity-dependent retrograde signaling that reduces its clamping function, allowing activity-dependent increases in spontaneous SV release to promote synaptic growth and development (Andreae and Burrone, 2018; Barber et al., 2009; Cho et al., 2015; Choi et al., 2014; Huntwork and Littleton, 2007; Yoshihara et al., 2005). The synaptic signaling molecule nitric oxide (NO) enhances synaptic transmission by modifying Cpx function in Drosophila, with NO-regulated S-nitrosylation of the Cpx C-terminus altering SNARE-binding and enhancing evoked release (Robinson et al., 2018). Transcriptional regulation of Cpx can also modulate synaptic strength in Drosophila, with caloric intake and insulin signaling decreasing synaptic transmission by increasing Cpx levels downstream of the translational inhibitor FOXO (Mahoney et al., 2016). Similarly, the synaptic levels of Unc18

and Syx1 are finely tuned to regulate SV priming dynamics that are required to support presynaptic homeostatic plasticity at Drosophila NMJs (Ortega et al., 2018). Alternative splicing of Unc13 in Drosophila and *C. elegans* results in unique isoforms that alter the protein's length, allowing the MUN domain to position and control SV priming at varying distances from AZ Ca^{2+} channel clusters (Böhme et al., 2016; Fulterer et al., 2018; Hu et al., 2013; Pooryasin et al., 2021; Reddy-Alla et al., 2017). In Drosophila, newly formed AZs first accumulate the long Unc13B splice variant before the shorter Unc13A variant arrives as AZs mature. Unc13B does not support efficient evoked release but is sufficient for spontaneous fusion, while Unc13A is required for SV priming for evoked but not spontaneous release (Böhme et al., 2016). Short isoforms of Unc13 in *C. elegans* also promote greater evoked release than longer isoforms (Hu et al., 2013), suggesting alternative Unc13 splicing represents a general mechanism for altering the efficiency of SV release by controlling where SV priming occurs along the AZ.

The role of Tomosyn in controlling intrinsic synaptic strength and plasticity may be unique among the SRPs given Tomosyn mutants appear healthy across species despite strong effects on evoked neurotransmitter release (Gracheva et al., 2006; McEwen et al., 2006; Sakisaka et al., 2008). This argues Tomosyn is not essential for neuronal function but may instead primarily function to finetune SV release strength in a synapse-specific manner with some synapses showing strong Tomosyn expression and others displaying little to no expression. Indeed, Tomosyn expression level is highly variable between distinct neuronal subgroups across the hippocampus, suggesting discrete synaptic populations are subject to varying levels of Tomosyn release suppression (Barak et al., 2010, 2013; Groffen et al., 2005). Hippocampal mossy fiber to CA3 (MF-CA3) synapses are characterized by high Tomosyn expression, low intrinsic release probability, and robust short-term facilitation. RNAi knockdown of Tomosyn in these terminals followed by optogenetic stimulation reveals Tomosyn expression in MF-CA3 synapses is required for this synapse's intrinsically low release probability and capacity to robustly facilitate during repetitive stimulation (Ben-Simon et al., 2015). Further, PKA phosphorylation of Tomosyn enhances SV release by inactivating Tomosyn's inhibitory function across species (Baba et al., 2005; Chen et al., 2011) and Tomosyn knockdown at MF-CA3 synapses prevents the expression of PKA-dependent presynaptic long-term potentiation suggesting Tomosyn regulates the expression of short- and long-term plasticity in this synapse (Ben-Simon et al., 2015). These data suggest

Tomosyn expression is required at some synapses to regulate intrinsic release strength and plasticity. It remains unknown whether synapses with endogenously low Tomosyn expression show differences in baseline release strength and capacity to facilitate/potentiate relative to synapses with high Tomosyn expression such as the MF-CA3 synapse.

These examples highlight only a subset of the mechanisms by which SNARE function might be dynamically controlled by SRPs. Future studies will certainly provide additional insights into how regulation of these essential presynaptic gatekeepers of brain communication contribute to the diversity of synaptic function and plasticity observed across distinct neuronal populations.

Tables and Figures

Table 1: Summary of SNARE/SRP mutant phenotypes in mice, Drosophila, and *C. elegans*

Function	Protein	Species	Gene name	Mutant	Phenotype	References
Membrane fusion	Syntaxin 1	*M. mus*	*Stx1A*	*Stx1A*^{XRA}	No abnormal phenotypes detected	
			Stx1B	*Stx1B*$^{tm1.1Rmnd}$	Premature death; minimal synaptic release defects	Wu *et al,* 2015; Gerber *et al,* 2008
				Stx1B^{Open}	Decreased RRP size, increased evoked release	
		C. ele	*unc-64*	*unc-64(js115)*	Lethal	Saifee *et al* , 1998; Liu *et al* , 2018
				unc-64(e246)	Reduced spontaneous cholinergic release, normal GABAergic release	
		D. mel	*Syx1A*	*Syx1A*$^{\Delta 229}$	Embryonic lethal; no syanptic release	Schulze *et al,* 1995; Littleton *et al* , 1998
				Syx1A$^{3-69}$	Temperature sensitive paralysis	
	Syb2	*M. mus*	*Syb2*	*Syb2*^{tm1Sud}	Embryonic lethal; 100-fold reduction in evoked release	Schoch *et al* , 2001
		C. ele	*snb-1*	*snb-1(tm6668)*	Lethal	The C. elegans Deletion Mutant Consortium, 2012; Liu et al, 2018
				snb-1(md247)	Reduced spontaneous cholinergic release, normal GABAergic release	
		D. mel	*n-Syb*	*n-syb*$^{\Delta F33B}$	Embryonic lethal; no evoked release, some spontaneous release	Deitcher *et al* , 1998
				nSyb^{l4}	Very little movement	
			Syb (c-Syb)	*syb*^{144}	Lethal	Bhattacharya *et al* , 2002
	SNAP-25	*M. mus*	*Snap25*	*Snap25*^{tm1Mcw}	Embyonic lethal; no evoked release, elevated spontaneous release	Washbourne *et al,* 2002
		C. ele	*ric-4*	*ric-4(md1088)*	Viable; aldicarb resistance, sluggish movement	Miller *et al* , 1996
		D. mel	*SNAP-25*	*snap-25*^{124}	Reduced evoked release, enhanced spontaneous release	Rao *et al* , 2001; Vilinsky *et al, 2002*
				snap-25^{TS}	Temperature sensitive paralysis	
Synaptic vesicle docking and priming	Sec1/ Munc18	*M. mus*	*Munc18-1*	*Stxbp1*^{tm1Sud}	Embryonic lethal; total absence of evoked and spontaneous release	Verhage *et al, 2000;* Miyamoto *et al* , 2017
			Munc18-2	*Stxbp2*^{tm1Bdic}	Postnatal lethality	Kim *et al* , 2012
			Munc18-3	*Stxbp3*^{tm1Yt}	Postnatal lethality; altered insulin secretion	Kanda *et al* , 2005
		C. ele	*unc-18*	*unc-18(e174)*	Unccordinated movement	Brenner, 1974
		D. mel	*rop*	*rop*^{G27}	Embryonic lethality	Harrison *et al* , 1994
	Unc13	*M. mus*	*Munc13-1*	*Munc13- 1/2*^{DKO}	Embyonic or postnatal lethality; absence of evoked and spontaneous release	Augustin *et al* , 1999; Varoqueaux et al, 2002
			Munc13-2			
			Munc13-3	*Unc13c*^{tm1Bros}	Viable; mild cerebellar synaptic phenotypes	Augustin *et al* , 2001
			Munc13-4			
		C. ele	*unc-13*	*unc-13(s69)*	Minimally viable; total absence of evoked and spontaneous release	Richmond *et el,* 1999; Richmond et al, 2001
		D. mel	*Unc13*	*unc13*^{PB400}	Embryonic lethal; near absence of evoked release and spontaneous release	Aravamudan *et al* , 1999
Synaptic vesicle targetting	Rab3	*M. mus*	*Rab3a*	*Rab3*^{ABCD}	Premature death; moderately reduced evoked responses	Schlüter *et al* , 2004
			Rab3b			
			Rab3c			
			Rab3d			
		C. ele	*rab-3*	*rab-3(js49)*	Viable; weaker pharyngeal pumping, aldicarb resistance	Nonet *et al* , 1997
		D. mel	*rab3*	*rab3*^{rup}	Viable; mild SV release phenotypes, abnormal active zone morphology	Graf *et al,* 2009
	RIM	*M. mus*	*Rim1*	*Rim1*^{alphabeta} ; *Rim2*^{alphabetagamma}	Conditional knockouts; severely impaired evoked and spontaneous release, reduced Ca^{2+} channel accumulation	Schoch *et al* , 2002; Kaeser *et al* , 2008; Kaiser *et al* , 2011
			Rim2			
			Rim3	*Rim3*^{gamma}	No abnormal phenotypes detected	
			Rim4	*Rim4*^{tm1Bllr}	Low body weight, small size	
		C. ele	*unc-10*	*unc-10(md1117)*	Viable; severely reduced evoked and spontaneous fusion	Koushika *et al* , 2001
		D. mel	*Rim*	*Rim*^{Ex73}	Viable; severely impaired release, reduced Ca^{2+} channel accumulation	Graf *et al,* 2012
Fusion clamp/ calcium sensor	Complexin	*M. mus*	*Cpx1*	*Cpxl/II*^{DKO}	Postnatal lethality; severely reduced evoked release	Reim *et al,* 2001
			Cpx2			
			Cpx3	*Cpx3/4*^{DKO}	Viable; impaired retinal neuroransmission	Xue *et al* , 2008; Reim *et al, 2009*
			Cpx4			
		C. ele	*cpx-1*	*cpx-1(ok1552)*	Viable; reduced evoked release, and enhanced spontaneous release	Martin *et al* , 2011
		D. mel	*cpx*	*cpx*^{SH1}	Viable; reduced evoked release, 100-fold enhanced spontaneous release	Huntwork and Littleton, 2007
	Syt1	*M. mus*	*Syt1*	*Syt1*^{tm1Sud}	Postnatal lethality; Severely reduced synchronous release	Geppert *et al* , 1994
		C. ele	*snt-1*	*snt-1(md290)*	Viable; reduced evoked and spontaneous release	Li *et al* , 2018
		D. mel	*syt1*	*syt1*$^{N13/AD4}$	Viable; severely reduced synchronous release	Littleton *et al* , 1994; Yoshihara and Littleton, 2002
SNARE recylcing	NSF	*M. mus*	*Nsf*	*Nsf*$^{tm1b(KOMP)Mbp}$	Embryonic lethal	Dickinson *et al* , 2016
		C. ele	*nsf-1*	*nsf-1(tm2194)*	Lethal	The *C. elegans* Deletion Mutant Consortium, 2012
		D. mel	*comt*	*comt*^{clp}	Embyonic lethal	Sidiqqi and Benzer, 1976; Sanyal and Krishnan, 2001
				comt^{ST17}	TS paralysis	
			Nsf2	*Nsf2*^{55}	Larval lethal	Golby *et al* , 2001
NSF attachment	α- / β- SNAP	*M. mus*	*Napa*	*Napa*^{tm1Caw}	Embryonic lethal	Bronson and Lane, 1990; Chae *et al* , 2004
				Napa^{hyh}	Hydrocephaly, abnormal gait	
			Napb	*Napb*^{tm1Rhee}	Viable; seizures	Burgalossi *et al,* 2010
		C. ele	*snap-1*	*snap-1(tm2068)*	Lethal	The *C. elegans* Deletion Mutant Consortium, 2012
		D. mel	*αSNAP*	*αSNAP*^{M3}	Embyonic lethal	Lukinova *et al,* 1999; Babcock *et al* , 2004
Decoy SNARE	Tomosyn	*M. mus*	*Stxbp5*	*Tomosyn*^{KO}	Viable; enhanced evoked release	Sakisaka *et al* , 2008
			Stxbp5l	*Tom2*^{KO}	Viable; enhanced SV rundown at the diaphragm neuromuscular juntion	Geerts *et al* , 2015
		C. ele	*tom-1*	*tom-1(ok285)*	Viable; enhanced evoked release, hypersensitive to aldicarb	Gracheva *et al* , 2006; Vashlishan *et al* , 2008
		D. mel	*tomosyn*			
Syb2 recylcing	AP180	*M. mus*	*AP180*	*Snap91*$^{tm1.1Tmar}$	Premature death; mishapen SVs, reduced release, mislocalized Syb2	Joo Koo *et al* , 2015
		C. ele	*unc-11*	*unc-11(e47)*	Viable; mislocalized SNB-1, mishapen SVs, decreased release	Brenner, 1974; Nonet *et al* , 1999
		D. mel	*lap*	*lap*^{1}	Minimally viable; enlarged SVs, impaired SV recycling	Zhang *et al* , 1998

Table 1. Summary of synaptic and behavioral phenotypes in *Mus musculus* (*M. mus*), *Caenorhabditis elegans* (*C. ele*) and *Drosophila melanogaster* (*D. mel*) SNARE and SRP mutants.

Figure 1

A

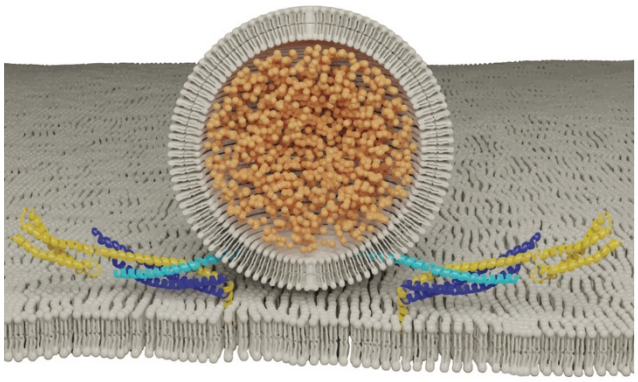

Syb2 Syx1 SNAP-25

B

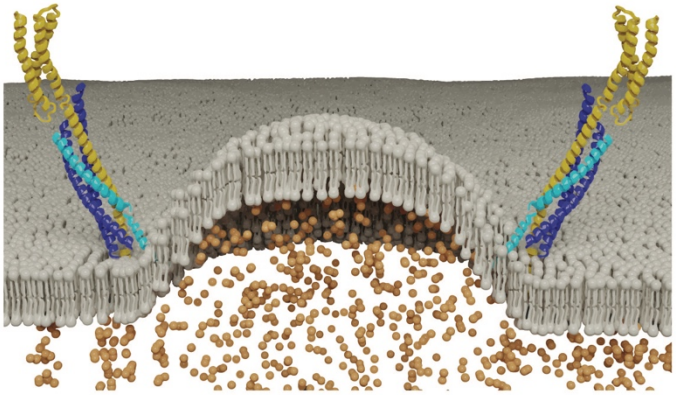

Syb2 Syx1 SNAP-25

Figure 1. SNAREs assemble between opposing membranes to drive membrane fusion and neurotransmitter release.

(A) One helix of the v-SNARE Syb2 assembles with three t-SNARE helices (one from Syx1 and two from SNAP-25) to form a four-helical trans-SNARE complex between opposing membranes. (B) Full SNARE zippering converts the trans-SNARE complex to a cis-SNARE complex to drive membrane fusion and neurotransmitter release. PDB structures in this and subsequent figures were obtained from the cited sources and rendered on membranes to highlight their role in SV fusion. Adapted from (Fernandez et al., 1998; Sutton et al., 1998).

Figure 2

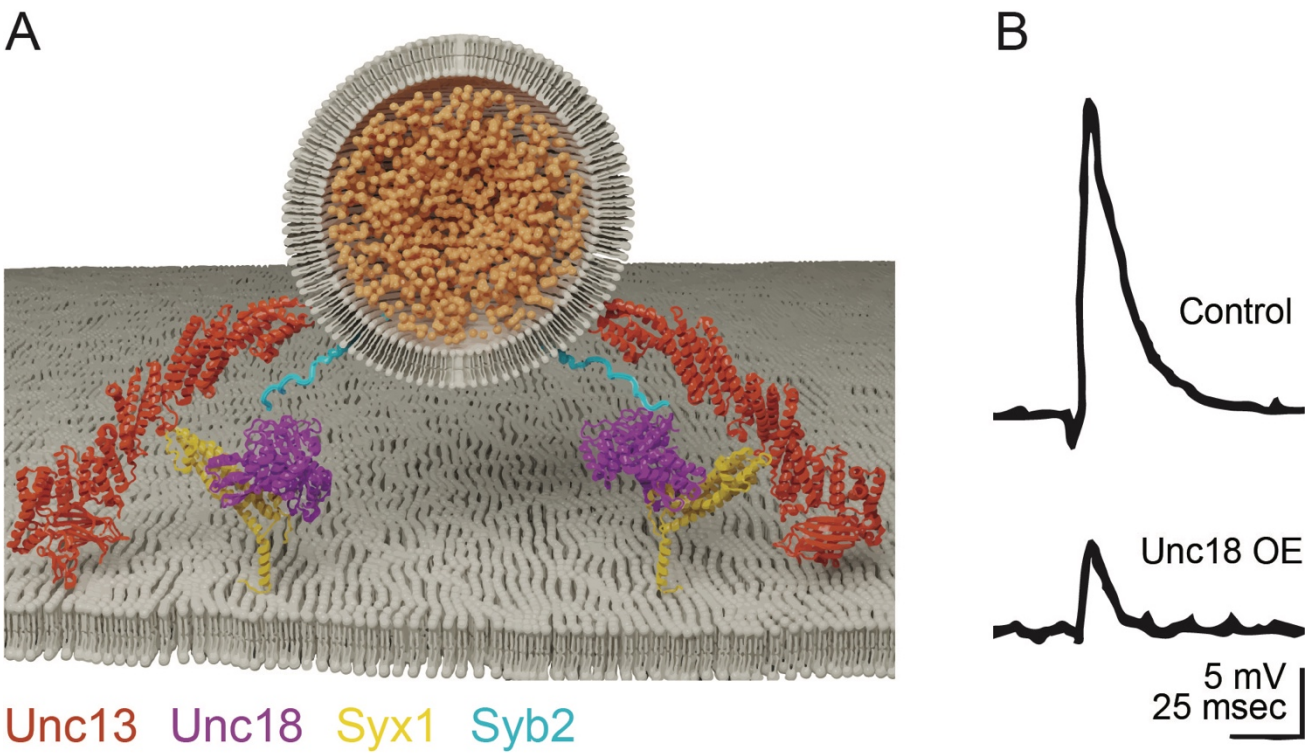
A
B
Control
Unc18 OE
5 mV
25 msec
Unc13 Unc18 Syx1 Syb2
C
Unc18 Syx1 Syb2 SNAP-25

Figure 2. Unc13 and Unc18 chaperone SNARE complex assembly by regulating Syx1. (A) Unc18 holds Syx1 in a closed conformation prior to SNARE complex assembly. Unc13 bridges the SV and plasma membranes and interacts with Syx1 to drive transition to the open-Syx1 state. Adapted from (Burkhardt et al., 2008; Liu et al., 2016; Xu et al., 2018). (B) Electrophysiological recordings of evoked responses at the Drosophila larval neuromuscular junction reveal overexpression of Unc18 impairs SV fusion. Adapted from (Schulze et al., 1994). (C) Unc18 chaperones the assembly of Syb2 and Syx1 prior to SNAP-25 inclusion into the SNARE complex. Adapted from (Burkhardt et al., 2008).

Figure 3

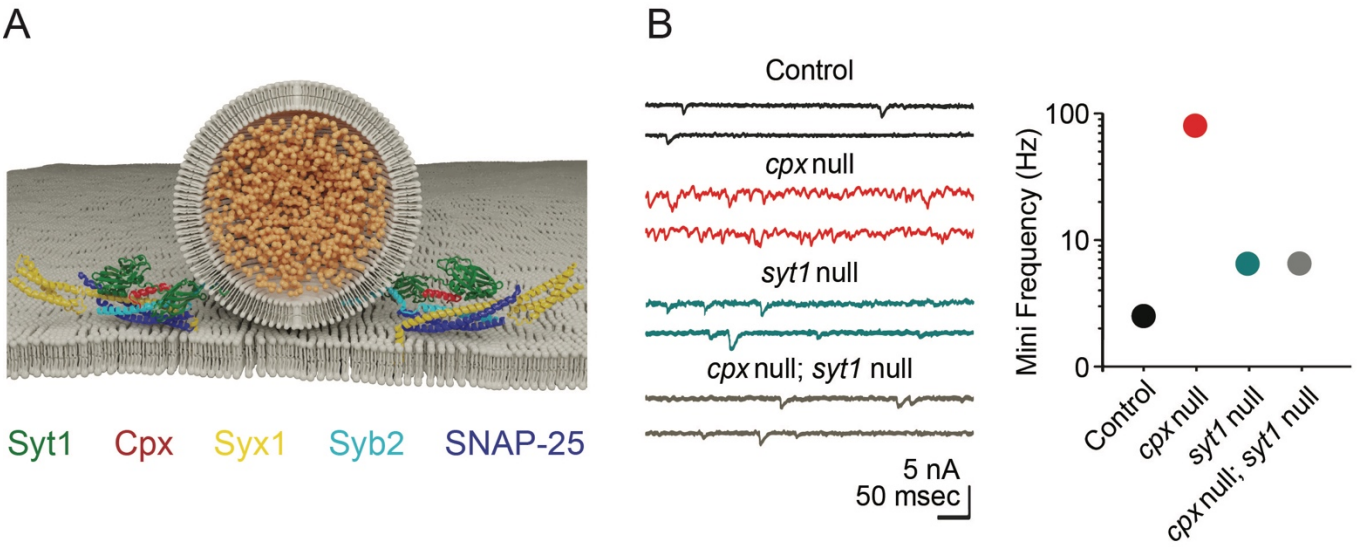
A
Syt1
Cpx
Syx1
Syb2
SNAP-25
B
Control
cpx null
syt1 null
cpx null; syt1 null
5 nA
50 msec
Mini Frequency (Hz)
100
10
0
Control
cpx null
syt1 null
cpx null; syt1 null
C
Control
cpx null
50 nA
50 msec
D
Pre-fusion
Clamped

Figure 3. Cpx clamps the SNARE complex in a partially assembled state.

(A) Cpx and Syt1 engage the SNARE complex on a shared binding interface to form a tripartite complex. Adapted from (Zhou et al., 2017). (B) Electrophysiological recordings at Drosophila larval NMJs reveal *cpx* null mutants have a dramatically increased rate of spontaneous release. Spontaneous release is restored to near normal levels in *syt1; cpx* double mutants, indicating Syt1 is required for the elevated mini rate in *cpx* single mutants. Quantification of spontaneous release rate (mini frequency) is shown on the right for the indicated genotypes. (C) Evoked response amplitude is reduced in *cpx* null mutants, indicating Cpx is also required for efficient Ca^{2+}-activated release. Panels B and C adapted from (Jorquera et al., 2012). (D) Molecular-dynamics modeling suggests Cpx may clamp SNAREs in a partially assembled state by altering the confirmation of the C-terminus of Syb2 to prevent full SNARE zippering. Adapted from (Bykhovskaia et al., 2013).

Figure 4

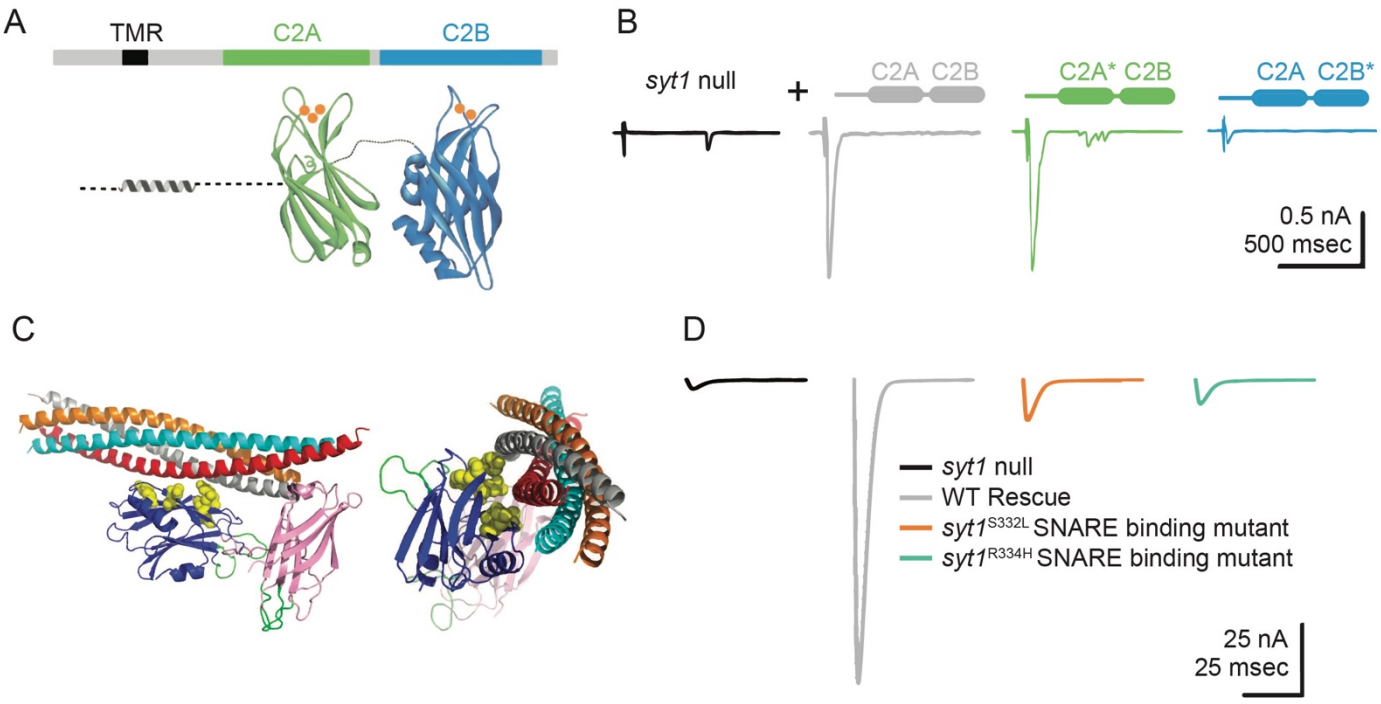
A
TMR
C2A
C2B
B
syt1 null
+
C2A C2B
C2A* C2B
C2A C2B*
0.5 nA
500 msec
C
D
syt1 null
WT Rescue
syt1S332L SNARE binding mutant
syt1R334H SNARE binding mutant
25 nA
25 msec

Figure 4. Syt1 binds Ca^{2+} and SNARE complexes to trigger synchronous SV fusion.
(A) Syt1 is tethered to SV membranes via a transmembrane region (TMR) and has two Ca^{2+}-binding C2 domains projecting into the cytosol. Ca^{2+} (orange) binds to polybasic loops projecting from each C2 domain, with C2A accommodating 3 Ca^{2+} ions and C2B binding 2 Ca^{2+} ions. (B) Two-electrode voltage clamp recordings demonstrate *syt1* nulls have dramatically impaired evoked synchronous release at Drosophila larval NMJs. Unlike rescue with wildtype (WT) *Syt1* (grey trace), transgenes with impaired C2B Ca^{2+} binding (C2B*, blue) severely impair evoked release while C2A Ca^{2+} binding mutants (C2A*, green) fail to prevent the enhanced asynchronous release observed in nulls (black). Adapted from (Yoshihara et al., 2010). (C) The Syt1 C2B domain (blue) also interacts with the SNARE complex at a primary interface independent of the Cpx-associated tripartite binding site. Critical residues coordinating binding of the Syt1 C2B domain to the SNARE complex are highlighted in yellow and were identified from crystal structures of the complex and genetic screens in Drosophila. (D) Disrupting Syt1-SNARE binding at the primary interface with two independent alleles mimics the *syt1* null phenotype. Panels C and D adapted from (Guan et al., 2017).

Figure 5

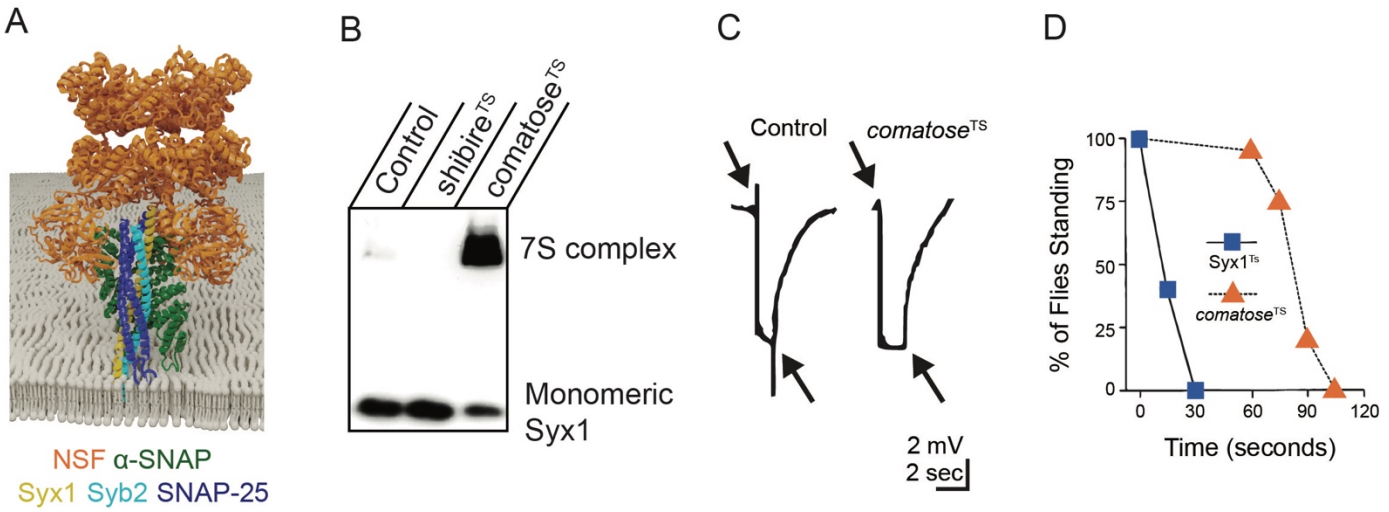
A
NSF α-SNAP
Syx1 Syb2 SNAP-25
B
Control
shibire TS
comatose TS
7S complex
Monomeric
Syx1
C
Control
comatose TS
2 mV
2 sec
D
% of Flies Standing
100
75
50
25
0
0
30
60
90
120
Time (seconds)
Syx1 Ts
comatose TS

Figure 5. NSF and α-SNAP disassemble the cis-SNARE complex to maintain a pool of available free SNAREs for sustained release.

(A) α-SNAP binds assembled SNARE complexes, enabling NSF to form a hexamer around the SNARE complex to initiate disassembly. Adapted from (Zhao et al., 2015). (B) Western blot of Drosophila brain extracts with anti-Syx1 antisera demonstrates 7S complexes accumulate at the restrictive temperature in *comatose*^{TS} mutants at the expense of monomeric Syx1. Heat-shocked *shibire*^{TS} mutants have reduced 7S complex compared to controls, indicating NSF continues to disassemble SNARE complexes within the plasma membrane when SVs are depleted. (C) Electroretinograms recorded from Drosophila TS *comatose* mutants reveal a loss of on and off transients (arrows) at elevated temperatures that occurs secondary to disrupted synaptic transmission from photoreceptors. Panels B and C adapted from (Littleton et al., 2001a). (D) Drosophila TS mutants in *Syx1* show rapid behavioral paralysis compared to the slower time-course for *comatose* TS mutations in NSF. Adapted from (Littleton et al., 1998).

Figure 6

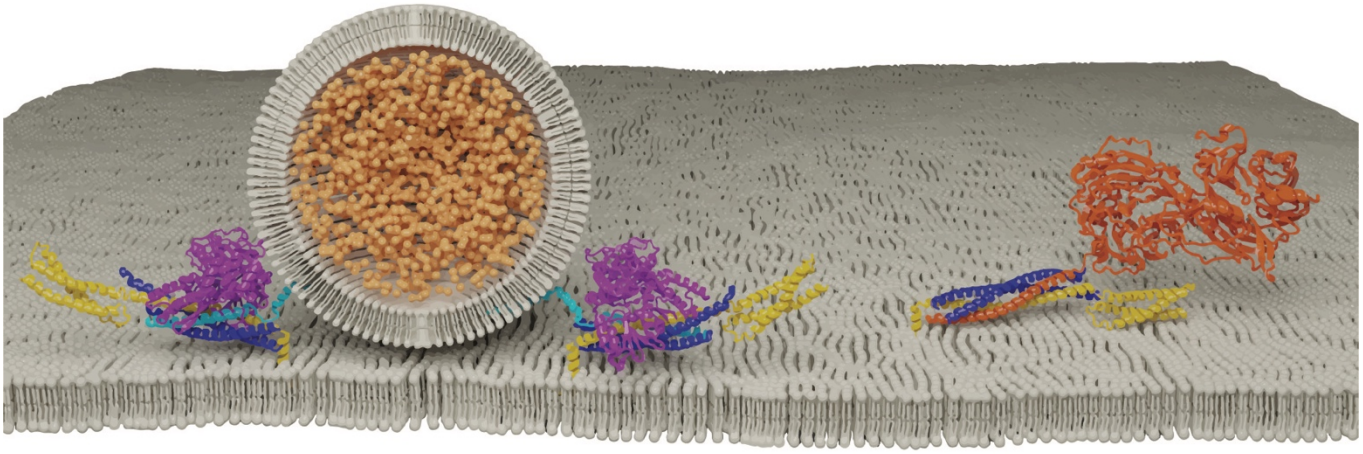

Syx1 Syb2 SNAP-25 Unc18 Tomosyn

Figure 6. **Tomosyn forms a decoy SNARE complex with Syx1 and SNAP-25 in an Unc18 and Syb2 independent manner.**

Adapted from (Hattendorf et al., 2007; Pobbati et al., 2004).

Figure 7

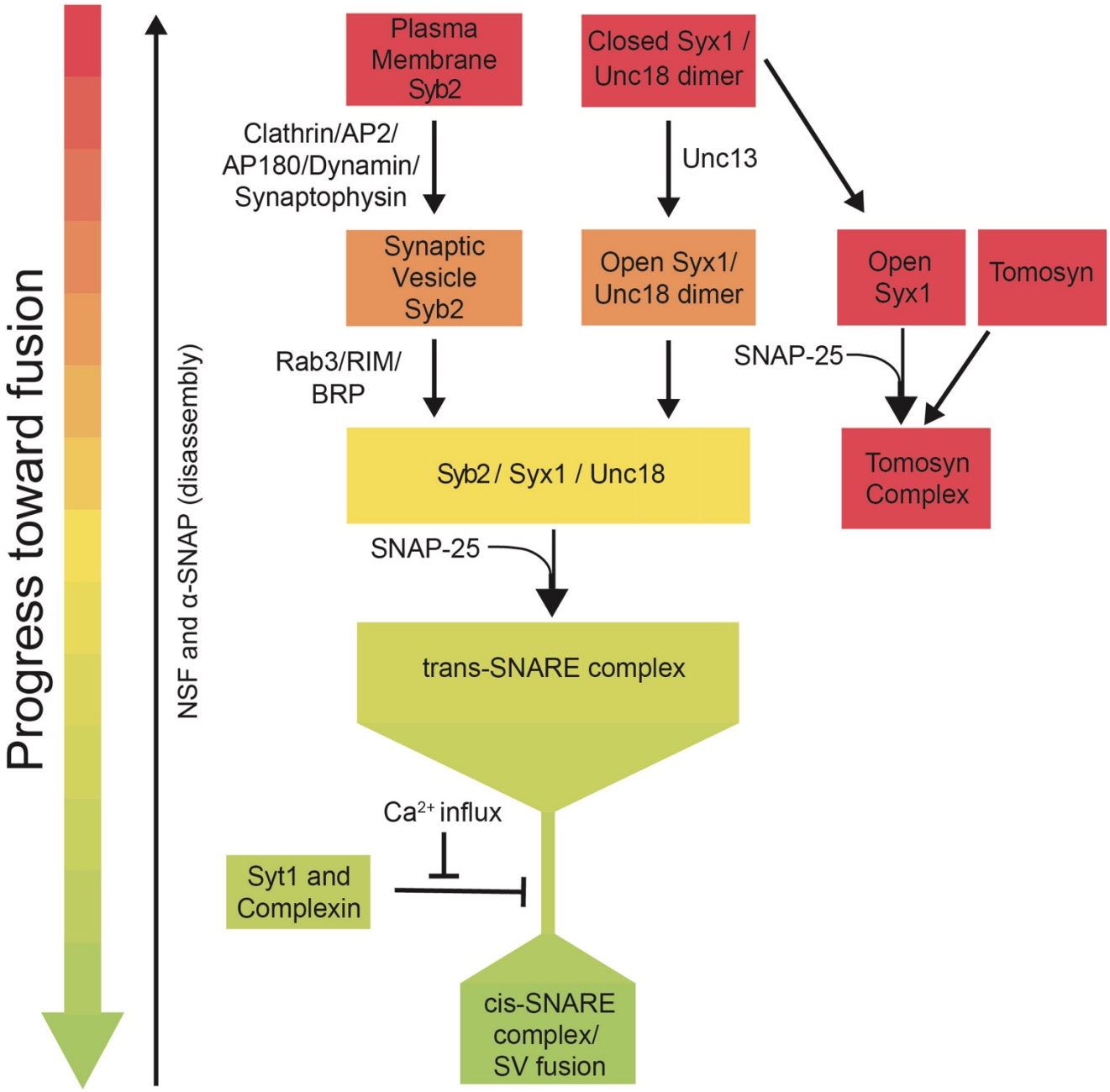
Progress toward fusion
NSF and α-SNAP (disassembly)
Plasma Membrane Syb2
Closed Syx1 / Unc18 dimer
Clathrin/AP2/ AP180/Dynamin/ Synaptophysin
Unc13
Synaptic Vesicle Syb2
Open Syx1/ Unc18 dimer
Open Syx1
Tomosyn
Rab3/RIM/ BRP
SNAP-25
Syb2 / Syx1 / Unc18
Tomosyn Complex
SNAP-25
trans-SNARE complex
Ca2+ influx
Syt1 and Complexin
cis-SNARE complex/ SV fusion

Figure 7. Summary flowchart showing current models for SRP regulation of SNARE complex assembly and SV fusion.

References

Abramov, D., Guiberson, N.G.L., and Burré, J. (2021). STXBP1 encephalopathies: Clinical spectrum, disease mechanisms, and therapeutic strategies. J. Neurochem. *157*, 165–178.

Ackermann, F., Waites, C.L., and Garner, C.C. (2015). Presynaptic active zones in invertebrates and vertebrates. EMBO Rep. *16*, 923–938.

Akbergenova, Y., and Bykhovskaia, M. (2007). Synapsin maintains the reserve vesicle pool and spatial segregation of the recycling pool in Drosophila presynaptic boutons. Brain Res. *1178*, 52–64.

Akbergenova, Y., and Bykhovskaia, M. (2010). Synapsin regulates vesicle organization and activity-dependent recycling at Drosophila motor boutons. Neuroscience *170*, 441–452.

Akbergenova, Y., Cunningham, K.L., Zhang, Y.V., Weiss, S., and Littleton, J.T. (2018). Characterization of developmental and molecular factors underlying release heterogeneity at Drosophila synapses. Elife *7*.

Andreae, L.C., and Burrone, J. (2018). The role of spontaneous neurotransmission in synapse and circuit development. J. Neurosci. Res. *96*, 354–359.

Aponte-Santiago, N.A., and Littleton, J.T. (2020). Synaptic properties and plasticity mechanisms of invertebrate tonic and phasic neurons. Front. Physiol. *11*, 611982.

Aponte-Santiago, N.A., Ormerod, K.G., Akbergenova, Y., and Littleton, J.T. (2020). Synaptic plasticity induced by differential manipulation of tonic and phasic motoneurons in drosophila. J. Neurosci. *40*, 6270–6288.

Aravamudan, B., Fergestad, T., Davis, W.S., Rodesch, C.K., and Broadie, K. (1999). Drosophila UNC-13 is essential for synaptic transmission. Nat. Neurosci. *2*, 965–971.

Aravanis, A.M., Pyle, J.L., and Tsien, R.W. (2003). Single synaptic vesicles fusing transiently and successively without loss of identity. Nature *423*, 643–647.

Artalejo, C.R., Elhamdani, A., and Palfrey, H.C. (1998). Secretion: dense-core vesicles can kiss-and-run too. Curr. Biol. *8*, R62-5.

Ashery, U., Bielopolski, N., Barak, B., and Yizhar, O. (2009). Friends and foes in synaptic transmission: the role of tomosyn in vesicle priming. Trends Neurosci. *32*, 275–282.

Atwood, H. (2008). Parallel "phasic" and "tonic" motor systems of the crayfish abdomen. J. Exp. Biol. *211*, 2193–2195.

Atwood, H.L., and Karunanithi, S. (2002). Diversification of synaptic strength: presynaptic elements. Nat. Rev. Neurosci. *3*, 497–516.

Atwood, H.L., Govind, C.K., and Wu, C.F. (1993). Differential ultrastructure of synaptic terminals on ventral longitudinal abdominal muscles in Drosophila larvae. J. Neurobiol. *24*, 1008–1024.

Augustin, I., Rosenmund, C., Südhof, T.C., and Brose, N. (1999). Munc13-1 is essential for fusion competence of glutamatergic synaptic vesicles. Nature *400*, 457–461.

Baba, T., Sakisaka, T., Mochida, S., and Takai, Y. (2005). PKA-catalyzed phosphorylation of tomosyn and its implication in Ca2+-dependent exocytosis of neurotransmitter. J. Cell Biol. *170*, 1113–1125.

Babcock, M., Macleod, G.T., Leither, J., and Pallanck, L. (2004). Genetic analysis of soluble N-ethylmaleimide-sensitive factor attachment protein function in Drosophila reveals positive and negative secretory roles. J. Neurosci. *24*, 3964--3973.

Bajohrs, M., Rickman, C., Binz, T., and Davletov, B. (2004). A molecular basis underlying differences in the toxicity of botulinum serotypes A and E. EMBO Rep. *5*, 1090–1095.

Baker, R.W., Jeffrey, P.D., Zick, M., Phillips, B.P., Wickner, W.T., and Hughson, F.M. (2015). A direct role for the Sec1/Munc18-family protein Vps33 as a template for SNARE assembly. Science *349*, 1111–1114.

Bao, H., Daniels, R.W., MacLeod, G.T., Charlton, M.P., Atwood, H.L., and Zhang, B. (2005). AP180 maintains the distribution of synaptic and vesicle proteins in the nerve terminal and indirectly regulates the efficacy of Ca2+-triggered exocytosis. J. Neurophysiol. *94*, 1888–

1903.
Barak, B., Williams, A., Bielopolski, N., Gottfried, I., Okun, E., Brown, M.A., Matti, U., Rettig, J., Stuenkel, E.L., and Ashery, U. (2010). Tomosyn expression pattern in the mouse hippocampus suggests both presynaptic and postsynaptic functions. Front. Neuroanat. *4*, 149.
Barak, B., Okun, E., Ben-Simon, Y., Lavi, A., Shapira, R., Madar, R., Wang, Y., Norman, E., Sheinin, A., Pita, M.A., et al. (2013). Neuron-specific expression of tomosyn1 in the mouse hippocampal dentate gyrus impairs spatial learning and memory. Neuromolecul. Med. *15*, 351–363.
Barber, C.F., Jorquera, R.A., Melom, J.E., and Littleton, J.T. (2009). Postsynaptic regulation of synaptic plasticity by synaptotagmin 4 requires both C2 domains. J. Cell Biol. *187*, 295–310.
Bargmann, C.I. (1993). Genetic and cellular analysis of behavior in C. elegans. Annu. Rev. Neurosci. *16*, 47–71.
Barnard, R.J., Morgan, A., and Burgoyne, R.D. (1997). Stimulation of NSF ATPase activity by alpha-SNAP is required for SNARE complex disassembly and exocytosis. J. Cell Biol. *139*, 875–883.
Bennett, M.K., and Scheller, R.H. (1993). The molecular machinery for secretion is conserved from yeast to neurons. Proc. Natl. Acad. Sci. USA *90*, 2559–2563.
Bennett, M.K., Calakos, N., and Scheller, R.H. (1992a). Syntaxin: a synaptic protein implicated in docking of synaptic vesicles at presynaptic active zones. Science *257*, 255–259.
Bennett, M.K., Calakos, N., Kreiner, T., and Scheller, R.H. (1992b). Synaptic vesicle membrane proteins interact to form a multimeric complex. J. Cell Biol. *116*, 761–775.
Ben-Simon, Y., Rodenas-Ruano, A., Alviña, K., Lam, A.D., Stuenkel, E.L., Castillo, P.E., and Ashery, U. (2015). A Combined Optogenetic-Knockdown Strategy Reveals a Major Role of Tomosyn in Mossy Fiber Synaptic Plasticity. Cell Rep. *12*, 396–404.
Betz, A., Okamoto, M., Benseler, F., and Brose, N. (1997). Direct interaction of the rat unc-13 homologue Munc13-1 with the N terminus of syntaxin. J. Biol. Chem. *272*, 2520–2526.
Betz, A., Thakur, P., Junge, H.J., Ashery, U., Rhee, J.S., Scheuss, V., Rosenmund, C., Rettig, J., and Brose, N. (2001). Functional interaction of the active zone proteins Munc13-1 and RIM1 in synaptic vesicle priming. Neuron *30*, 183–196.
Bhatnagar, S., Soni, M.S., Wrighton, L.S., Hebert, A.S., Zhou, A.S., Paul, P.K., Gregg, T., Rabaglia, M.E., Keller, M.P., Coon, J.J., et al. (2014). Phosphorylation and degradation of tomosyn-2 de-represses insulin secretion. J. Biol. Chem. *289*, 25276–25286.
Bhattacharya, S., Stewart, B.A., Niemeyer, B.A., Burgess, R.W., McCabe, B.D., Lin, P., Boulianne, G., O'Kane, C.J., and Schwarz, T.L. (2002). Members of the synaptobrevin/vesicle-associated membrane protein (VAMP) family in Drosophila are functionally interchangeable in vivo for neurotransmitter release and cell viability. Proc. Natl. Acad. Sci. USA *99*, 13867–13872.
van der Bliek, A.M., and Meyerowitz, E.M. (1991). Dynamin-like protein encoded by the Drosophila shibire gene associated with vesicular traffic. Nature *351*, 411–414.
Block, M.R., Glick, B.S., Wilcox, C.A., Wieland, F.T., and Rothman, J.E. (1988). Purification of an N-ethylmaleimide-sensitive protein catalyzing vesicular transport. Proc. Natl. Acad. Sci. USA *85*, 7852–7856.
Böhme, M.A., Beis, C., Reddy-Alla, S., Reynolds, E., Mampell, M.M., Grasskamp, A.T., Lützkendorf, J., Bergeron, D.D., Driller, J.H., Babikir, H., et al. (2016). Active zone scaffolds differentially accumulate Unc13 isoforms to tune Ca(2+) channel-vesicle coupling. Nat. Neurosci. *19*, 1311–1320.
Bonanomi, D., Rusconi, L., Colombo, C.A., Benfenati, F., and Valtorta, F. (2007). Synaptophysin I selectively specifies the exocytic pathway of synaptobrevin 2/VAMP2. Biochem. J. *404*, 525–534.
Borgese, N., Colombo, S., and Pedrazzini, E. (2003). The tale of tail-anchored proteins: coming

from the cytosol and looking for a membrane. J. Cell Biol. *161*, 1013–1019.
Boulianne, G.L., and Trimble, W.S. (1995). Identification of a second homolog of N-ethylmaleimide-sensitive fusion protein that is expressed in the nervous system and secretory tissues of Drosophila. Proc. Natl. Acad. Sci. USA *92*, 7095–7099.
Bowen, M.E., Weninger, K., Ernst, J., Chu, S., and Brunger, A.T. (2005). Single-molecule studies of synaptotagmin and complexin binding to the SNARE complex. Biophys. J. *89*, 690–702.
Bowers, M.R., and Reist, N.E. (2020). The C2A domain of synaptotagmin is an essential component of the calcium sensor for synaptic transmission. PLoS One *15*, e0228348.
Brady, J., Vasin, A., and Bykhovskaia, M. (2021). The accessory helix of complexin stabilizes a partially unzippered state of the SNARE complex and mediates the complexin clamping function in vivo. Eneuro *8*.
Breidenbach, M.A., and Brunger, A.T. (2005). New insights into clostridial neurotoxin-SNARE interactions. Trends Mol. Med. *11*, 377–381.
Brenner, S. (1973). The genetics of behaviour. Br Med Bull *29*, 269–271.
Broadie, K., Prokop, A., Bellen, H.J., O'Kane, C.J., Schulze, K.L., and Sweeney, S.T. (1995). Syntaxin and synaptobrevin function downstream of vesicle docking in Drosophila. Neuron *15*, 663–673.
Brose, N., Rosenmund, C., and Rettig, J. (2000). Regulation of transmitter release by Unc-13 and its homologues. Curr. Opin. Neurobiol. *10*, 303–311.
Brunger, A.T., Choi, U.B., Lai, Y., Leitz, J., White, K.I., and Zhou, Q. (2019). The pre-synaptic fusion machinery. Curr. Opin. Struct. Biol. *54*, 179–188.
Bucurenciu, I., Kulik, A., Schwaller, B., Frotscher, M., and Jonas, P. (2008). Nanodomain coupling between Ca2+ channels and Ca2+ sensors promotes fast and efficient transmitter release at a cortical GABAergic synapse. Neuron *57*, 536–545.
Buhl, L.K., Jorquera, R.A., Akbergenova, Y., Huntwork-Rodriguez, S., Volfson, D., and Littleton, J.T. (2013). Differential regulation of evoked and spontaneous neurotransmitter release by C-terminal modifications of complexin. Mol. Cell. Neurosci. *52*, 161–172.
Burdina, A.O., Klosterman, S.M., Shtessel, L., Ahmed, S., and Richmond, J.E. (2011). In vivo analysis of conserved C. elegans tomosyn domains. PLoS One *6*, e26185.
Burgess, T.L., and Kelly, R.B. (1987). Constitutive and regulated secretion of proteins. Annu. Rev. Cell Biol. *3*, 243–293.
Burgess, R.W., Deitcher, D.L., and Schwarz, T.L. (1997). The synaptic protein syntaxin1 is required for cellularization of Drosophila embryos. J. Cell Biol. *138*, 861–875.
Burkhardt, P., Hattendorf, D.A., Weis, W.I., and Fasshauer, D. (2008). Munc18a controls SNARE assembly through its interaction with the syntaxin N-peptide. EMBO J. *27*, 923–933.
Bykhovskaia, M., Jagota, A., Gonzalez, A., Vasin, A., and Littleton, J.T. (2013). Interaction of the complexin accessory helix with the C-terminus of the SNARE complex: molecular-dynamics model of the fusion clamp. Biophys. J. *105*, 679–690.
Ceccarelli, B., Hurlbut, W.P., and Mauro, A. (1973). Turnover of transmitter and synaptic vesicles at the frog neuromuscular junction. J. Cell Biol. *57*, 499–524.
Chanaday, N.L., Cousin, M.A., Milosevic, I., Watanabe, S., and Morgan, J.R. (2019). The Synaptic Vesicle Cycle Revisited: New Insights into the Modes and Mechanisms. J. Neurosci. *39*, 8209–8216.
Chang, S., Reim, K., Pedersen, M., Neher, E., Brose, N., and Taschenberger, H. (2015). Complexin stabilizes newly primed synaptic vesicles and prevents their premature fusion at the mouse calyx of held synapse. J. Neurosci. *35*, 8272–8290.
Chapman, E.R. (2008). How does synaptotagmin trigger neurotransmitter release? Annu. Rev. Biochem. *77*, 615–641.
Chapman, E.R., and Davis, A.F. (1998). Direct interaction of a Ca2+-binding loop of synaptotagmin with lipid bilayers. J. Biol. Chem. *273*, 13995–14001.
Chapman, E.R., Desai, R.C., Davis, A.F., and Tornehl, C.K. (1998). Delineation of the oligomerization, AP-2 binding, and synprint binding region of the C2B domain of

synaptotagmin. J. Biol. Chem. *273*, 32966–32972.
Chen, K., Richlitzki, A., Featherstone, D.E., Schwärzel, M., and Richmond, J.E. (2011). Tomosyn-dependent regulation of synaptic transmission is required for a late phase of associative odor memory. Proc. Natl. Acad. Sci. USA *108*, 18482–18487.
Chen, M.S., Obar, R.A., Schroeder, C.C., Austin, T.W., Poodry, C.A., Wadsworth, S.C., and Vallee, R.B. (1991). Multiple forms of dynamin are encoded by shibire, a Drosophila gene involved in endocytosis. Nature *351*, 583–586.
Chin, A.C., Burgess, R.W., Wong, B.R., Schwarz, T.L., and Scheller, R.H. (1993). Differential expression of transcripts from syb, a Drosophila melanogaster gene encoding VAMP (synaptobrevin) that is abundant in non-neuronal cells. Gene *131*, 175–181.
Cho, R.W., Song, Y., and Littleton, J.T. (2010). Comparative analysis of Drosophila and mammalian complexins as fusion clamps and facilitators of neurotransmitter release. Mol. Cell. Neurosci. *45*, 389–397.
Cho, R.W., Kümmel, D., Li, F., Baguley, S.W., Coleman, J., Rothman, J.E., and Littleton, J.T. (2014). Genetic analysis of the Complexin trans-clamping model for cross-linking SNARE complexes in vivo. Proc. Natl. Acad. Sci. USA *111*, 10317–10322.
Cho, R.W., Buhl, L.K., Volfson, D., Tran, A., Li, F., Akbergenova, Y., and Littleton, J.T. (2015). Phosphorylation of Complexin by PKA Regulates Activity-Dependent Spontaneous Neurotransmitter Release and Structural Synaptic Plasticity. Neuron *88*, 749–761.
Choi, B.J., Imlach, W.L., Jiao, W., Wolfram, V., Wu, Y., Grbic, M., Cela, C., Baines, R.A., Nitabach, M.N., and McCabe, B.D. (2014). Miniature neurotransmission regulates Drosophila synaptic structural maturation. Neuron *82*, 618–634.
Cipriano, D.J., Jung, J., Vivona, S., Fenn, T.D., Brunger, A.T., and Bryant, Z. (2013). Processive ATP-driven substrate disassembly by the N-ethylmaleimide-sensitive factor (NSF) molecular machine. J. Biol. Chem. *288*, 23436–23445.
Clary, D.O., Griff, I.C., and Rothman, J.E. (1990). SNAPs, a family of NSF attachment proteins involved in intracellular membrane fusion in animals and yeast. Cell *61*, 709–721.
Cremona, O., and De Camilli, P. (1997). Synaptic vesicle endocytosis. Curr. Opin. Neurobiol. *7*, 323–330.
Davletov, B.A., and Südhof, T.C. (1993). A single C2 domain from synaptotagmin I is sufficient for high affinity Ca2+/phospholipid binding. J. Biol. Chem. *268*, 26386–26390.
DeBruhl, H., Albertson, R., Swider, Z., and Sullivan, W. (2016). Rop, the Sec1/Munc18 homolog in Drosophila, is required for furrow ingression and stable cell shape during cytokinesis. J. Cell Sci. *129*, 430–443.
Deitcher, D.L., Ueda, A., Stewart, B.A., Burgess, R.W., Kidokoro, Y., and Schwarz, T.L. (1998). Distinct requirements for evoked and spontaneous release of neurotransmitter are revealed by mutations in the Drosophila gene neuronal-synaptobrevin. J. Neurosci. *18*, 2028–2039.
Delgado, R., Maureira, C., Oliva, C., Kidokoro, Y., and Labarca, P. (2000). Size of vesicle pools, rates of mobilization, and recycling at neuromuscular synapses of a Drosophila mutant, shibire. Neuron *28*, 941–953.
Deng, P., Khan, A., Jacobson, D., Sambrani, N., McGurk, L., Li, X., Jayasree, A., Hejatko, J., Shohat-Ophir, G., O'Connell, M.A., et al. (2020). Adar RNA editing-dependent and -independent effects are required for brain and innate immune functions in Drosophila. Nat. Commun. *11*, 1580.
DiAntonio, A., and Schwarz, T.L. (1994). The effect on synaptic physiology of synaptotagmin mutations in Drosophila. Neuron *12*, 909–920.
DiAntonio, A., Burgess, R.W., Chin, A.C., Deitcher, D.L., Scheller, R.H., and Schwarz, T.L. (1993). Identification and characterization of Drosophila genes for synaptic vesicle proteins. J. Neurosci. *13*, 4924–4935.
Diril, M.K., Wienisch, M., Jung, N., Klingauf, J., and Haucke, V. (2006). Stonin 2 is an AP-2-dependent endocytic sorting adaptor for synaptotagmin internalization and recycling. Dev. Cell *10*, 233–244.

Dittman, J., and Ryan, T.A. (2009). Molecular circuitry of endocytosis at nerve terminals. Annu. Rev. Cell Dev. Biol. *25*, 133–160.

Dittman, J.S., Kreitzer, A.C., and Regehr, W.G. (2000). Interplay between facilitation, depression, and residual calcium at three presynaptic terminals. J. Neurosci. *20*, 1374–1385.

Dulubova, I., Sugita, S., Hill, S., Hosaka, M., Fernandez, I., Südhof, T.C., and Rizo, J. (1999). A conformational switch in syntaxin during exocytosis: role of munc18. EMBO J. *18*, 4372–4382.

Dulubova, I., Khvotchev, M., Liu, S., Huryeva, I., Südhof, T.C., and Rizo, J. (2007). Munc18-1 binds directly to the neuronal SNARE complex. Proc. Natl. Acad. Sci. USA *104*, 2697–2702.

Edelmann, L., Hanson, P.I., Chapman, E.R., and Jahn, R. (1995). Synaptobrevin binding to synaptophysin: a potential mechanism for controlling the exocytotic fusion machine. EMBO J. *14*, 224–231.

Engel, A.G., Selcen, D., Shen, X.-M., Milone, M., and Harper, C.M. (2016). Loss of MUNC13-1 function causes microcephaly, cortical hyperexcitability, and fatal myasthenia. Neurol. Genet. *2*, e105.

Estes, P.S., Roos, J., van der Bliek, A., Kelly, R.B., Krishnan, K.S., and Ramaswami, M. (1996). Traffic of dynamin within individual Drosophila synaptic boutons relative to compartment-specific markers. J. Neurosci. *16*, 5443–5456.

Evergren, E., Benfenati, F., and Shupliakov, O. (2007). The synapsin cycle: a view from the synaptic endocytic zone. J. Neurosci. Res. *85*, 2648–2656.

Fasshauer, D. (2003). Structural insights into the SNARE mechanism. Biochim. Biophys. Acta *1641*, 87–97.

Fasshauer, D., Sutton, R.B., Brunger, A.T., and Jahn, R. (1998). Conserved structural features of the synaptic fusion complex: SNARE proteins reclassified as Q- and R-SNAREs. Proc. Natl. Acad. Sci. USA *95*, 15781–15786.

Fasshauer, D., Antonin, W., Subramaniam, V., and Jahn, R. (2002). SNARE assembly and disassembly exhibit a pronounced hysteresis. Nat. Struct. Biol. *9*, 144–151.

Fergestad, T., Wu, M.N., Schulze, K.L., Lloyd, T.E., Bellen, H.J., and Broadie, K. (2001). Targeted mutations in the syntaxin H3 domain specifically disrupt SNARE complex function in synaptic transmission. J. Neurosci. *21*, 9142–9150.

Fernandez, I., Ubach, J., Dulubova, I., Zhang, X., Südhof, T.C., and Rizo, J. (1998). Three-dimensional structure of an evolutionarily conserved N-terminal domain of syntaxin 1A. Cell *94*, 841–849.

Fernandez, I., Araç, D., Ubach, J., Gerber, S.H., Shin, O., Gao, Y., Anderson, R.G., Südhof, T.C., and Rizo, J. (2001). Three-dimensional structure of the synaptotagmin 1 C2B-domain: synaptotagmin 1 as a phospholipid binding machine. Neuron *32*, 1057–1069.

Fernández-Alfonso, T., Kwan, R., and Ryan, T.A. (2006). Synaptic vesicles interchange their membrane proteins with a large surface reservoir during recycling. Neuron *51*, 179–186.

Fesce, R., Grohovaz, F., Valtorta, F., and Meldolesi, J. (1994). Neurotransmitter release: fusion or "kiss-and-run"? Trends Cell Biol. *4*, 1–4.

Ford, M.G.J., Jenni, S., and Nunnari, J. (2011). The crystal structure of dynamin. Nature *477*, 561–566.

Fujita, Y., Shirataki, H., Sakisaka, T., Asakura, T., Ohya, T., Kotani, H., Yokoyama, S., Nishioka, H., Matsuura, Y., Mizoguchi, A., et al. (1998). Tomosyn: a syntaxin-1-binding protein that forms a novel complex in the neurotransmitter release process. Neuron *20*, 905–915.

Fulterer, A., Andlauer, T.F.M., Ender, A., Maglione, M., Eyring, K., Woitkuhn, J., Lehmann, M., Matkovic-Rachid, T., Geiger, J.R.P., Walter, A.M., et al. (2018). Active Zone Scaffold Protein Ratios Tune Functional Diversity across Brain Synapses. Cell Rep. *23*, 1259–1274.

Gan, Q., and Watanabe, S. (2018). Synaptic vesicle endocytosis in different model systems. Front. Cell Neurosci. *12*, 171.

Gao, Y., Zorman, S., Gundersen, G., Xi, Z., Ma, L., Sirinakis, G., Rothman, J.E., and Zhang, Y.

(2012). Single reconstituted neuronal SNARE complexes zipper in three distinct stages. Science *337*, 1340–1343.
Geerts, C.J., Plomp, J.J., Koopmans, B., Loos, M., van der Pijl, E.M., van der Valk, M.A., Verhage, M., and Groffen, A.J.A. (2015). Tomosyn-2 is required for normal motor performance in mice and sustains neurotransmission at motor endplates. Brain Struct. Funct. *220*, 1971–1982.
Geerts, C.J., Mancini, R., Chen, N., Koopmans, F.T.W., Li, K.W., Smit, A.B., van Weering, J.R.T., Verhage, M., and Groffen, A.J.A. (2017). Tomosyn associates with secretory vesicles in neurons through its N- and C-terminal domains. PLoS One *12*, e0180912.
Geppert, M., Goda, Y., Stevens, C.F., and Südhof, T.C. (1997). The small GTP-binding protein Rab3A regulates a late step in synaptic vesicle fusion. Nature *387*, 810–814.
Gerber, S.H., Rah, J.-C., Min, S.-W., Liu, X., de Wit, H., Dulubova, I., Meyer, A.C., Rizo, J., Arancillo, M., Hammer, R.E., et al. (2008a). Conformational switch of syntaxin-1 controls synaptic vesicle fusion. Science (New York, NY) *321*, 1507--1510.
Gerber, S.H., Rah, J.-C., Min, S.-W., Liu, X., de Wit, H., Dulubova, I., Meyer, A.C., Rizo, J., Arancillo, M., Hammer, R.E., et al. (2008b). Conformational switch of syntaxin-1 controls synaptic vesicle fusion. Science *321*, 1507–1510.
Gerst, J.E. (2003). SNARE regulators: matchmakers and matchbreakers. Biochim. Biophys. Acta *1641*, 99–110.
Ghelani, T., and Sigrist, S.J. (2018). Coupling the structural and functional assembly of synaptic release sites. Front. Neuroanat. *12*, 81.
Giraudo, C.G., Eng, W.S., Melia, T.J., and Rothman, J.E. (2006). A clamping mechanism involved in SNARE-dependent exocytosis. Science *313*, 676–680.
Gogolla, N., Leblanc, J.J., Quast, K.B., Südhof, T.C., Fagiolini, M., and Hensch, T.K. (2009). Common circuit defect of excitatory-inhibitory balance in mouse models of autism. J. Neurodev. Disord. *1*, 172–181.
Göhde, R., Naumann, B., Laundon, D., Imig, C., McDonald, K., Cooper, B.H., Varoqueaux, F., Fasshauer, D., and Burkhardt, P. (2021). Choanoflagellates and the ancestry of neurosecretory vesicles. Philos. Trans. R. Soc. Lond. B, Biol. Sci. *376*, 20190759.
Golby, J.A., Tolar, L.A., and Pallanck, L. (2001). Partitioning of N-ethylmaleimide-sensitive fusion (NSF) protein function in Drosophila melanogaster: dNSF1 is required in the nervous system, and dNSF2 is required in mesoderm. Genetics *158*, 265--278.
González-Gaitán, M., and Jäckle, H. (1997). Role of Drosophila alpha-adaptin in presynaptic vesicle recycling. Cell *88*, 767–776.
Gonzalo, S., and Linder, M.E. (1998). SNAP-25 palmitoylation and plasma membrane targeting require a functional secretory pathway. Mol. Biol. Cell *9*, 585–597.
van de Goor, J., Ramaswami, M., and Kelly, R. (1995). Redistribution of synaptic vesicles and their proteins in temperature-sensitive shibire(ts1) mutant Drosophila. Proc. Natl. Acad. Sci. USA *92*, 5739–5743.
Gordon, S.L., and Cousin, M.A. (2014). The Sybtraps: control of synaptobrevin traffic by synaptophysin, α-synuclein and AP-180. Traffic *15*, 245–254.
Gordon, S.L., and Cousin, M.A. (2016). The iTRAPs: Guardians of Synaptic Vesicle Cargo Retrieval During Endocytosis. Front. Synaptic Neurosci. *8*, 1.
Gordon, S.L., Leube, R.E., and Cousin, M.A. (2011). Synaptophysin is required for synaptobrevin retrieval during synaptic vesicle endocytosis. J. Neurosci. *31*, 14032–14036.
Gordon, S.L., Harper, C.B., Smillie, K.J., and Cousin, M.A. (2016). A fine balance of synaptophysin levels underlies efficient retrieval of synaptobrevin II to synaptic vesicles. PLoS One *11*, e0149457.
Gracheva, E.O., Burdina, A.O., Holgado, A.M., Berthelot-Grosjean, M., Ackley, B.D., Hadwiger, G., Nonet, M.L., Weimer, R.M., and Richmond, J.E. (2006). Tomosyn inhibits synaptic vesicle priming in Caenorhabditis elegans. PLoS Biol. *4*, e261.
Gracheva, E.O., Hadwiger, G., Nonet, M.L., and Richmond, J.E. (2008). Direct interactions

between C. elegans RAB-3 and Rim provide a mechanism to target vesicles to the presynaptic density. Neurosci. Lett. *444*, 137–142.
Gracheva, E.O., Maryon, E.B., Berthelot-Grosjean, M., and Richmond, J.E. (2010). Differential Regulation of Synaptic Vesicle Tethering and Docking by UNC-18 and TOM-1. Front. Synaptic Neurosci. *2*, 141.
Graf, E.R., Daniels, R.W., Burgess, R.W., Schwarz, T.L., and DiAntonio, A. (2009). Rab3 dynamically controls protein composition at active zones. Neuron *64*, 663–677.
Graf, E.R., Valakh, V., Wright, C.M., Wu, C., Liu, Z., Zhang, Y.Q., and DiAntonio, A. (2012). RIM promotes calcium channel accumulation at active zones of the Drosophila neuromuscular junction. J. Neurosci. *32*, 16586–16596.
Gratz, S.J., Ukken, F.P., Rubinstein, C.D., Thiede, G., Donohue, L.K., Cummings, A.M., and O'Connor-Giles, K.M. (2014). Highly specific and efficient CRISPR/Cas9-catalyzed homology-directed repair in Drosophila. Genetics *196*, 961–971.
Griff, I.C., Schekman, R., Rothman, J.E., and Kaiser, C.A. (1992). The yeast SEC17 gene product is functionally equivalent to mammalian alpha-SNAP protein. J. Biol. Chem. *267*, 12106–12115.
Groffen, A.J.A., Jacobsen, L., Schut, D., and Verhage, M. (2005). Two distinct genes drive expression of seven tomosyn isoforms in the mammalian brain, sharing a conserved structure with a unique variable domain. J. Neurochem. *92*, 554–568.
Grosshans, B.L., Ortiz, D., and Novick, P. (2006). Rabs and their effectors: achieving specificity in membrane traffic. Proc. Natl. Acad. Sci. USA *103*, 11821–11827.
Gu, M., Schuske, K., Watanabe, S., Liu, Q., Baum, P., Garriga, G., and Jorgensen, E.M. (2008). Mu2 adaptin facilitates but is not essential for synaptic vesicle recycling in Caenorhabditis elegans. J. Cell Biol. *183*, 881–892.
Gu, M., Liu, Q., Watanabe, S., Sun, L., Hollopeter, G., Grant, B.D., and Jorgensen, E.M. (2013). AP2 hemicomplexes contribute independently to synaptic vesicle endocytosis. Elife *2*, e00190.
Guan, Z., Saraswati, S., Adolfsen, B., and Littleton, J.T. (2005). Genome-wide transcriptional changes associated with enhanced activity in the Drosophila nervous system. Neuron *48*, 91–107.
Guan, Z., Bykhovskaia, M., Jorquera, R.A., Sutton, R.B., Akbergenova, Y., and Littleton, J.T. (2017). A synaptotagmin suppressor screen indicates SNARE binding controls the timing and Ca2+ cooperativity of vesicle fusion. Elife *6*.
Guan, Z., Quiñones-Frías, M.C., Akbergenova, Y., and Littleton, J.T. (2020). Drosophila Synaptotagmin 7 negatively regulates synaptic vesicle release and replenishment in a dosage-dependent manner. Elife *9*.
Hallermann, S., Kittel, R.J., Wichmann, C., Weyhersmüller, A., Fouquet, W., Mertel, S., Owald, D., Eimer, S., Depner, H., Schwärzel, M., et al. (2010). Naked dense bodies provoke depression. J. Neurosci. *30*, 14340–14345.
Han, Y., Kaeser, P.S., Südhof, T.C., and Schneggenburger, R. (2011). RIM determines Ca^2+ channel density and vesicle docking at the presynaptic active zone. Neuron *69*, 304–316.
Harris, K.P., and Littleton, J.T. (2015). Transmission, development, and plasticity of synapses. Genetics *201*, 345–375.
Harris, K.P., Zhang, Y.V., Piccioli, Z.D., Perrimon, N., and Littleton, J.T. (2016). The postsynaptic t-SNARE Syntaxin 4 controls traffic of Neuroligin 1 and Synaptotagmin 4 to regulate retrograde signaling. Elife *5*.
Harris, K.P., Littleton, J.T., and Stewart, B.A. (2018). Postsynaptic Syntaxin 4 negatively regulates the efficiency of neurotransmitter release. J Neurogenet *32*, 221–229.
Harrison, S.D., Broadie, K., van de Goor, J., and Rubin, G.M. (1994). Mutations in the Drosophila Rop gene suggest a function in general secretion and synaptic transmission. Neuron *13*, 555–566.
Hata, Y., Slaughter, C.A., and Südhof, T.C. (1993). Synaptic vesicle fusion complex contains unc-

18 homologue bound to syntaxin. Nature *366*, 347–351.
Hatsuzawa, K., Lang, T., Fasshauer, D., Bruns, D., and Jahn, R. (2003). The R-SNARE motif of tomosyn forms SNARE core complexes with syntaxin 1 and SNAP-25 and down-regulates exocytosis. J. Biol. Chem. *278*, 31159–31166.
Hattendorf, D.A., Andreeva, A., Gangar, A., Brennwald, P.J., and Weis, W.I. (2007). Structure of the yeast polarity protein Sro7 reveals a SNARE regulatory mechanism. Nature *446*, 567–571.
Haucke, V., Wenk, M.R., Chapman, E.R., Farsad, K., and De Camilli, P. (2000). Dual interaction of synaptotagmin with mu2- and alpha-adaptin facilitates clathrin-coated pit nucleation. EMBO J. *19*, 6011–6019.
Haucke, V., Neher, E., and Sigrist, S.J. (2011). Protein scaffolds in the coupling of synaptic exocytosis and endocytosis. Nat. Rev. Neurosci. *12*, 127–138.
Hayashi, T., McMahon, H., Yamasaki, S., Binz, T., Hata, Y., Südhof, T.C., and Niemann, H. (1994). Synaptic vesicle membrane fusion complex: action of clostridial neurotoxins on assembly. EMBO J. *13*, 5051–5061.
Heerssen, H., Fetter, R.D., and Davis, G.W. (2008). Clathrin dependence of synaptic-vesicle formation at the Drosophila neuromuscular junction. Curr. Biol. *18*, 401--409.
Henkel, A.W., and Almers, W. (1996). Fast steps in exocytosis and endocytosis studied by capacitance measurements in endocrine cells. Curr. Opin. Neurobiol. *6*, 350–357.
Hernandez, J.M., Stein, A., Behrmann, E., Riedel, D., Cypionka, A., Farsi, Z., Walla, P.J., Raunser, S., and Jahn, R. (2012). Membrane fusion intermediates via directional and full assembly of the SNARE complex. Science *336*, 1581–1584.
Heuser, J.E., and Reese, T.S. (1973). Evidence for recycling of synaptic vesicle membrane during transmitter release at the frog neuromuscular junction. J. Cell Biol. *57*, 315–344.
Hinshaw, J.E., and Schmid, S.L. (1995). Dynamin self-assembles into rings suggesting a mechanism for coated vesicle budding. Nature *374*, 190–192.
Holderith, N., Lorincz, A., Katona, G., Rózsa, B., Kulik, A., Watanabe, M., and Nusser, Z. (2012). Release probability of hippocampal glutamatergic terminals scales with the size of the active zone. Nat. Neurosci. *15*, 988–997.
Hoopengardner, B., Bhalla, T., Staber, C., and Reenan, R. (2003). Nervous system targets of RNA editing identified by comparative genomics. Science *301*, 832–836.
Hosono, R., Hekimi, S., Kamiya, Y., Sassa, T., Murakami, S., Nishiwaki, K., Miwa, J., Taketo, A., and Kodaira, K.I. (1992). The unc-18 gene encodes a novel protein affecting the kinetics of acetylcholine metabolism in the nematode Caenorhabditis elegans. J. Neurochem. *58*, 1517–1525.
Hu, Z., Tong, X.-J., and Kaplan, J.M. (2013). UNC-13L, UNC-13S, and Tomosyn form a protein code for fast and slow neurotransmitter release in Caenorhabditis elegans. Elife *2*, e00967.
Hua, Y., and Scheller, R.H. (2001). Three SNARE complexes cooperate to mediate membrane fusion. Proc. Natl. Acad. Sci. USA *98*, 8065–8070.
Huang, X., Sun, S., Wang, X., Fan, F., Zhou, Q., Lu, S., Cao, Y., Wang, Q.-W., Dong, M.-Q., Yao, J., et al. (2019). Mechanistic insights into the SNARE complex disassembly. Sci. Adv. *5*, eaau8164.
Huntwork, S., and Littleton, J.T. (2007). A complexin fusion clamp regulates spontaneous neurotransmitter release and synaptic growth. Nat. Neurosci. *10*, 1235–1237.
Inoue, H., Matsuzaki, Y., Tanaka, A., Hosoi, K., Ichimura, K., Arasaki, K., Wakana, Y., Asano, K., Tanaka, M., Okuzaki, D., et al. (2015). γ-SNAP stimulates disassembly of endosomal SNARE complexes and regulates endocytic trafficking pathways. J. Cell Sci. *128*, 2781–2794.
Iyer, J., Wahlmark, C.J., Kuser-Ahnert, G.A., and Kawasaki, F. (2013). Molecular mechanisms of COMPLEXIN fusion clamp function in synaptic exocytosis revealed in a new Drosophila mutant. Mol. Cell. Neurosci. *56*, 244–254.
Jahn, R., and Scheller, R.H. (2006). SNAREs–engines for membrane fusion. Nature Reviews

Molecular Cell Biology *7*, 631--643.
Jahn, R., and Südhof, T.C. (1999). Membrane fusion and exocytosis. Annu. Rev. Biochem. *68*, 863–911.
Jan, L.Y., and Jan, Y.N. (1976). Properties of the larval neuromuscular junction in Drosophila melanogaster. J. Physiol. (Lond.) *262*, 189–214.
Jiao, J., He, M., Port, S.A., Baker, R.W., Xu, Y., Qu, H., Xiong, Y., Wang, Y., Jin, H., Eisemann, T.J., et al. (2018). Munc18-1 catalyzes neuronal SNARE assembly by templating SNARE association. Elife *7*.
Jorquera, R.A., Huntwork-Rodriguez, S., Akbergenova, Y., Cho, R.W., and Littleton, J.T. (2012). Complexin controls spontaneous and evoked neurotransmitter release by regulating the timing and properties of synaptotagmin activity. J. Neurosci. *32*, 18234–18245.
Kaempf, N., Kochlamazashvili, G., Puchkov, D., Maritzen, T., Bajjalieh, S.M., Kononenko, N.L., and Haucke, V. (2015). Overlapping functions of stonin 2 and SV2 in sorting of the calcium sensor synaptotagmin 1 to synaptic vesicles. Proc. Natl. Acad. Sci. USA *112*, 7297–7302.
Kaeser-Woo, Y.J., Yang, X., and Südhof, T.C. (2012). C-terminal complexin sequence is selectively required for clamping and priming but not for Ca2+ triggering of synaptic exocytosis. J. Neurosci. *32*, 2877–2885.
Karlocai, M.R., Heredi, J., Benedek, T., Holderith, N., Lorincz, A., and Nusser, Z. (2021). Variability in the Munc13-1 content of excitatory release site. Elife *10*.
Katz, B.S. (1969). The Release of Neural Transmitter Substances (Sherrington Lecture): Bernard S. Katz: 9780853230601: Amazon.com: Books (Liverpool University Press).
Kawasaki, F., and Ordway, R.W. (1999). The Drosophila NSF protein, dNSF1, plays a similar role at neuromuscular and some central synapses. J. Neurophysiol. *82*, 123–130.
Kawasaki, F., Mattiuz, A.M., and Ordway, R.W. (1998). Synaptic physiology and ultrastructure in comatose mutants define an in vivo role for NSF in neurotransmitter release. J. Neurosci. *18*, 10241–10249.
Kawasaki, F., Hazen, M., and Ordway, R.W. (2000). Fast synaptic fatigue in shibire mutants reveals a rapid requirement for dynamin in synaptic vesicle membrane trafficking. Nat. Neurosci. *3*, 859–860.
Kennedy, D., and Takeda, K. (1965). Reflex control of abdominal flexor muscles in the crayfish. J. Exp. Biol. *43*, 229–246.
Kennedy, M.J., Davison, I.G., Robinson, C.G., and Ehlers, M.D. (2010). Syntaxin-4 defines a domain for activity-dependent exocytosis in dendritic spines. Cell *141*, 524–535.
Khvotchev, M., Dulubova, I., Sun, J., Dai, H., Rizo, J., and Südhof, T.C. (2007). Dual modes of Munc18-1/SNARE interactions are coupled by functionally critical binding to syntaxin-1 N terminus. J. Neurosci. *27*, 12147–12155.
Kittel, R.J., Wichmann, C., Rasse, T.M., Fouquet, W., Schmidt, M., Schmid, A., Wagh, D.A., Pawlu, C., Kellner, R.R., Willig, K.I., et al. (2006). Bruchpilot promotes active zone assembly, Ca2+ channel clustering, and vesicle release. Science *312*, 1051–1054.
Koenig, J.H., and Ikeda, K. (1989). Disappearance and reformation of synaptic vesicle membrane upon transmitter release observed under reversible blockage of membrane retrieval. J. Neurosci. *9*, 3844--3860.
Koester, H.J., and Johnston, D. (2005). Target cell-dependent normalization of transmitter release at neocortical synapses. Science *308*, 863–866.
Korkut, C., Li, Y., Koles, K., Brewer, C., Ashley, J., Yoshihara, M., and Budnik, V. (2013). Regulation of postsynaptic retrograde signaling by presynaptic exosome release. Neuron *77*, 1039–1046.
Koushika, S.P., Richmond, J.E., Hadwiger, G., Weimer, R.M., Jorgensen, E.M., and Nonet, M.L. (2001). A post-docking role for active zone protein Rim. Nat. Neurosci. *4*, 997–1005.
Krishnakumar, S.S., Radoff, D.T., Kümmel, D., Giraudo, C.G., Li, F., Khandan, L., Baguley, S.W., Coleman, J., Reinisch, K.M., Pincet, F., et al. (2011). A conformational switch in complexin is required for synaptotagmin to trigger synaptic fusion. Nat. Struc. Mol. Biol. *18*, 934–940.

Kümmel, D., Krishnakumar, S.S., Radoff, D.T., Li, F., Giraudo, C.G., Pincet, F., Rothman, J.E., and Reinisch, K.M. (2011). Complexin cross-links prefusion SNAREs into a zigzag array. Nat. Struct. Mol. Biol. *18*, 927–933.

Kurdyak, P., Atwood, H.L., Stewart, B.A., and Wu, C.F. (1994). Differential physiology and morphology of motor axons to ventral longitudinal muscles in larval Drosophila. J. Comp. Neurol. *350*, 463–472.

Kushibiki, Y., Suzuki, T., Jin, Y., and Taru, H. (2019). RIMB-1/RIM-Binding Protein and UNC-10/RIM Redundantly Regulate Presynaptic Localization of the Voltage-Gated Calcium Channel in Caenorhabditis elegans. J. Neurosci. *39*, 8617–8631.

Kutay, U., Hartmann, E., and Rapoport, T.A. (1993). A class of membrane proteins with a C-terminal anchor. Trends Cell Biol. *3*, 72–75.

Kwon, H.-B., and Castillo, P.E. (2008). Long-term potentiation selectively expressed by NMDA receptors at hippocampal mossy fiber synapses. Neuron *57*, 108–120.

Lagow, R.D., Bao, H., Cohen, E.N., Daniels, R.W., Zuzek, A., Williams, W.H., Macleod, G.T., Sutton, R.B., and Zhang, B. (2007). Modification of a hydrophobic layer by a point mutation in syntaxin 1A regulates the rate of synaptic vesicle fusion. PLoS Biol. *5*, e72.

Lao, G., Scheuss, V., Gerwin, C.M., Su, Q., Mochida, S., Rettig, J., and Sheng, Z.H. (2000). Syntaphilin: a syntaxin-1 clamp that controls SNARE assembly. Neuron *25*, 191–201.

Lee, J., and Littleton, J.T. (2015). Transmembrane tethering of synaptotagmin to synaptic vesicles controls multiple modes of neurotransmitter release. Proc. Natl. Acad. Sci. USA *112*, 3793–3798.

Lee, J., Guan, Z., Akbergenova, Y., and Littleton, J.T. (2013). Genetic analysis of synaptotagmin C2 domain specificity in regulating spontaneous and evoked neurotransmitter release. J. Neurosci. *33*, 187–200.

Lehman, K., Rossi, G., Adamo, J.E., and Brennwald, P. (1999). Yeast homologues of tomosyn and lethal giant larvae function in exocytosis and are associated with the plasma membrane SNARE, Sec9. J. Cell Biol. *146*, 125–140.

Li, B., Li, Y., Liu, F., Tan, X., Rui, Q., Tong, Y., Qiao, L., Gao, R., Li, G., Shi, R., et al. (2019). Overexpressed Tomosyn Binds Syntaxins and Blocks Secretion during Pollen Development. Plant Physiol. *181*, 1114–1126.

Li, W., Ma, C., Guan, R., Xu, Y., Tomchick, D.R., and Rizo, J. (2011). The crystal structure of a Munc13 C-terminal module exhibits a remarkable similarity to vesicle tethering factors. Structure *19*, 1443–1455.

Li, Y., Wang, S., Li, T., Zhu, L., and Ma, C. (2018). Tomosyn guides SNARE complex formation in coordination with Munc18 and Munc13. FEBS Lett. *592*, 1161–1172.

Lin, P.-Y., Chanaday, N.L., Horvath, P.M., Ramirez, D.M.O., Monteggia, L.M., and Kavalali, E.T. (2020). VAMP4 Maintains a Ca2+-Sensitive Pool of Spontaneously Recycling Synaptic Vesicles. J. Neurosci. *40*, 5389–5401.

Lipstein, N., Verhoeven-Duif, N.M., Michelassi, F.E., Calloway, N., van Hasselt, P.M., Pienkowska, K., van Haaften, G., van Haelst, M.M., van Empelen, R., Cuppen, I., et al. (2017). Synaptic UNC13A protein variant causes increased neurotransmission and dyskinetic movement disorder. J. Clin. Invest. *127*, 1005–1018.

Littleton, J.T. (2000). A genomic analysis of membrane trafficking and neurotransmitter release in Drosophila. J. Cell Biol. *150*, F77-82.

Littleton, J.T., and Bellen, H.J. (1995). Presynaptic proteins involved in exocytosis in Drosophila melanogaster: a genetic analysis. Invert Neurosci *1*, 3–13.

Littleton, J.T., Stern, M., Schulze, K., Perin, M., and Bellen, H.J. (1993). Mutational analysis of Drosophila synaptotagmin demonstrates its essential role in Ca(2+)-activated neurotransmitter release. Cell *74*, 1125–1134.

Littleton, J.T., Stern, M., Perin, M., and Bellen, H.J. (1994). Calcium dependence of neurotransmitter release and rate of spontaneous vesicle fusions are altered in Drosophila synaptotagmin mutants. Proc. Natl. Acad. Sci. USA *91*, 10888–10892.

Littleton, J.T., Chapman, E.R., Kreber, R., Garment, M.B., Carlson, S.D., and Ganetzky, B. (1998). Temperature-sensitive paralytic mutations demonstrate that synaptic exocytosis requires SNARE complex assembly and disassembly. Neuron *21*, 401–413.

Littleton, J.T., Barnard, R.J., Titus, S.A., Slind, J., Chapman, E.R., and Ganetzky, B. (2001a). SNARE-complex disassembly by NSF follows synaptic-vesicle fusion. Proc. Natl. Acad. Sci. USA *98*, 12233–12238.

Littleton, J.T., Bai, J., Vyas, B., Desai, R., Baltus, A.E., Garment, M.B., Carlson, S.D., Ganetzky, B., and Chapman, E.R. (2001b). synaptotagmin mutants reveal essential functions for the C2B domain in Ca2+-triggered fusion and recycling of synaptic vesicles in vivo. J. Neurosci. *21*, 1421–1433.

Liu, H., Li, L., Nedelcu, D., Hall, Q., Zhou, L., Wang, W., Yu, Y., Kaplan, J.M., and Hu, Z. (2019). Heterodimerization of UNC-13/RIM regulates synaptic vesicle release probability but not priming in C. elegans. Elife *8*.

Liu, X., Seven, A.B., Camacho, M., Esser, V., Xu, J., Trimbuch, T., Quade, B., Su, L., Ma, C., Rosenmund, C., et al. (2016). Functional synergy between the Munc13 C-terminal C1 and C2 domains. Elife *5*.

Liu, Z., Chen, O., Wall, J.B.J., Zheng, M., Zhou, Y., Wang, L., Vaseghi, H.R., Qian, L., and Liu, J. (2017). Systematic comparison of 2A peptides for cloning multi-genes in a polycistronic vector. Sci. Rep. *7*, 2193.

Lloyd, T.E., Verstreken, P., Ostrin, E.J., Phillippi, A., Lichtarge, O., and Bellen, H.J. (2000). A genome-wide search for synaptic vesicle cycle proteins in Drosophila. Neuron *26*, 45–50.

Lnenicka, G.A., Atwood, H.L., and Marin, L. (1986). Morphological transformation of synaptic terminals of a phasic motoneuron by long-term tonic stimulation. J. Neurosci. *6*, 2252–2258.

López-Murcia, F.J., Reim, K., Jahn, O., Taschenberger, H., and Brose, N. (2019). Acute complexin knockout abates spontaneous and evoked transmitter release. Cell Rep. *26*, 2521–2530.e5.

Lu, W., Man, H., Ju, W., Trimble, W.S., MacDonald, J.F., and Wang, Y.T. (2001). Activation of synaptic NMDA receptors induces membrane insertion of new AMPA receptors and LTP in cultured hippocampal neurons. Neuron *29*, 243–254.

Lu, Z., Chouhan, A.K., Borycz, J.A., Lu, Z., Rossano, A.J., Brain, K.L., Zhou, Y., Meinertzhagen, I.A., and Macleod, G.T. (2016). High-Probability Neurotransmitter Release Sites Represent an Energy-Efficient Design. Curr. Biol. *26*, 2562–2571.

Ma, C., Li, W., Xu, Y., and Rizo, J. (2011). Munc13 mediates the transition from the closed syntaxin-Munc18 complex to the SNARE complex. Nat. Struct. Mol. Biol. *18*, 542–549.

Ma, C., Su, L., Seven, A.B., Xu, Y., and Rizo, J. (2013). Reconstitution of the vital functions of Munc18 and Munc13 in neurotransmitter release. Science *339*, 421–425.

Mace, K.E., Biela, L.M., Sares, A.G., and Reist, N.E. (2009). Synaptotagmin I stabilizes synaptic vesicles via its C2A polylysine motif. Genesis *47*, 337--345.

Mackler, J.M., Drummond, J.A., Loewen, C.A., Robinson, I.M., and Reist, N.E. (2002). The C(2)B Ca(2+)-binding motif of synaptotagmin is required for synaptic transmission in vivo. Nature *418*, 340–344.

Madera-Salcedo, I.K., Danelli, L., Tiwari, N., Dema, B., Pacreau, E., Vibhushan, S., Birnbaum, J., Agabriel, C., Liabeuf, V., Klingebiel, C., et al. (2018). Tomosyn functions as a PKCδ-regulated fusion clamp in mast cell degranulation. Sci. Signal. *11*.

Mahoney, R.E., Azpurua, J., and Eaton, B.A. (2016). Insulin signaling controls neurotransmission via the 4eBP-dependent modification of the exocytotic machinery. Elife *5*.

Malsam, J., Parisotto, D., Bharat, T.A.M., Scheutzow, A., Krause, J.M., Briggs, J.A.G., and Söllner, T.H. (2012). Complexin arrests a pool of docked vesicles for fast Ca2+-dependent release. EMBO J. *31*, 3270–3281.

Malsam, J., Bärfuss, S., Trimbuch, T., Zarebidaki, F., Sonnen, A.F.-P., Wild, K., Scheutzow, A., Rohland, L., Mayer, M.P., Sinning, I., et al. (2020). Complexin Suppresses Spontaneous Exocytosis by Capturing the Membrane-Proximal Regions of VAMP2 and SNAP25. Cell

Rep. *32*, 107926.
Maritzen, T., and Haucke, V. (2018). Coupling of exocytosis and endocytosis at the presynaptic active zone. Neurosci. Res. *127*, 45–52.
Martin, J.A., Hu, Z., Fenz, K.M., Fernandez, J., and Dittman, J.S. (2011). Complexin has opposite effects on two modes of synaptic vesicle fusion. Curr. Biol. *21*, 97–105.
Martina, J.A., Bonangelino, C.J., Aguilar, R.C., and Bonifacino, J.S. (2001). Stonin 2: an adaptor-like protein that interacts with components of the endocytic machinery. J. Cell Biol. *153*, 1111–1120.
Marz, K.E., Lauer, J.M., and Hanson, P.I. (2003). Defining the SNARE complex binding surface of alpha-SNAP: implications for SNARE complex disassembly. J. Biol. Chem. *278*, 27000–27008.
Masuda, E.S., Huang, B.C., Fisher, J.M., Luo, Y., and Scheller, R.H. (1998). Tomosyn binds t-SNARE proteins via a VAMP-like coiled coil. Neuron *21*, 479–480.
McEwen, J.M., and Kaplan, J.M. (2008). UNC-18 promotes both the anterograde trafficking and synaptic function of syntaxin. Mol. Biol. Cell *19*, 3836–3846.
McEwen, J.M., Madison, J.M., Dybbs, M., and Kaplan, J.M. (2006). Antagonistic regulation of synaptic vesicle priming by Tomosyn and UNC-13. Neuron *51*, 303–315.
McMahon, H.T., Missler, M., Li, C., and Südhof, T.C. (1995). Complexins: cytosolic proteins that regulate SNAP receptor function. Cell *83*, 111–119.
McNew, J.A., Weber, T., Parlati, F., Johnston, R.J., Melia, T.J., Söllner, T.H., and Rothman, J.E. (2000a). Close is not enough: SNARE-dependent membrane fusion requires an active mechanism that transduces force to membrane anchors. J. Cell Biol. *150*, 105–117.
McNew, J.A., Parlati, F., Fukuda, R., Johnston, R.J., Paz, K., Paumet, F., Söllner, T.H., and Rothman, J.E. (2000b). Compartmental specificity of cellular membrane fusion encoded in SNARE proteins. Nature *407*, 153–159.
Medine, C.N., Rickman, C., Chamberlain, L.H., and Duncan, R.R. (2007). Munc18-1 prevents the formation of ectopic SNARE complexes in living cells. J. Cell Sci. *120*, 4407–4415.
Meinrenken, C.J., Borst, J.G.G., and Sakmann, B. (2002). Calcium secretion coupling at calyx of Held governed by nonuniform channel-vesicle topography. J. Neurosci. *22*, 1648–1667.
Melland, H., Carr, E.M., and Gordon, S.L. (2021). Disorders of synaptic vesicle fusion machinery. J. Neurochem. *157*, 130–164.
Melom, J.E., and Littleton, J.T. (2011). Synapse development in health and disease. Curr. Opin. Genet. Dev. *21*, 256–261.
Melom, J.E., Akbergenova, Y., Gavornik, J.P., and Littleton, J.T. (2013). Spontaneous and evoked release are independently regulated at individual active zones. J. Neurosci. *33*, 17253–17263.
Miller, K.G., Alfonso, A., Nguyen, M., Crowell, J.A., Johnson, C.D., and Rand, J.B. (1996). A genetic selection for Caenorhabditis elegans synaptic transmission mutants. Proc. Natl. Acad. Sci. USA *93*, 12593–12598.
Milovanovic, D., and Jahn, R. (2015). Organization and dynamics of SNARE proteins in the presynaptic membrane. Front. Physiol. *6*, 89.
Mullen, G.P., Grundahl, K.M., Gu, M., Watanabe, S., Hobson, R.J., Crowell, J.A., McManus, J.R., Mathews, E.A., Jorgensen, E.M., and Rand, J.B. (2012). UNC-41/stonin functions with AP2 to recycle synaptic vesicles in Caenorhabditis elegans. PLoS One *7*, e40095.
Nair, A.G., Muttathukunnel, P., and Müller, M. (2020). Distinct molecular pathways govern presynaptic homeostatic plasticity. BioRxiv.
Neher, E., and Brose, N. (2018). Dynamically Primed Synaptic Vesicle States: Key to Understand Synaptic Short-Term Plasticity. Neuron *100*, 1283–1291.
Nguyen, M., Alfonso, A., Johnson, C.D., and Rand, J.B. (1995). Caenorhabditis elegans mutants resistant to inhibitors of acetylcholinesterase. Genetics *140*, 527–535.
Nonet, M.L., Staunton, J.E., Kilgard, M.P., Fergestad, T., Hartwieg, E., Horvitz, H.R., Jorgensen, E.M., and Meyer, B.J. (1997). Caenorhabditis elegans rab-3 mutant synapses exhibit

impaired function and are partially depleted of vesicles. J. Neurosci. *17*, 8061–8073.
Nonet, M.L., Saifee, O., Zhao, H., Rand, J.B., and Wei, L. (1998). Synaptic transmission deficits in Caenorhabditis elegans synaptobrevin mutants. J. Neurosci. *18*, 70–80.
Nonet, M.L., Holgado, A.M., Brewer, F., Serpe, C.J., Norbeck, B.A., Holleran, J., Wei, L., Hartwieg, E., Jorgensen, E.M., and Alfonso, A. (1999). UNC-11, a Caenorhabditis elegans AP180 homologue, regulates the size and protein composition of synaptic vesicles. Mol. Biol. Cell *10*, 2343–2360.
Novick, P., Field, C., and Schekman, R. (1980). Identification of 23 complementation groups required for post-translational events in the yeast secretory pathway. Cell *21*, 205–215.
Nunes, P., Haines, N., Kuppuswamy, V., Fleet, D.J., and Stewart, B.A. (2006). Synaptic vesicle mobility and presynaptic F-actin are disrupted in a N-ethylmaleimide-sensitive factor allele of Drosophila. Mol. Biol. Cell *17*, 4709–4719.
Ogawa, H., Harada, S., Sassa, T., Yamamoto, H., and Hosono, R. (1998). Functional properties of the unc-64 gene encoding a Caenorhabditis elegans syntaxin. J. Biol. Chem. *273*, 2192–2198.
Oh, K.H., Krout, M.D., Richmond, J.E., and Kim, H. (2021). UNC-2 CaV2 Channel Localization at Presynaptic Active Zones Depends on UNC-10/RIM and SYD-2/Liprin-α in Caenorhabditis elegans. J. Neurosci. *41*, 4782–4794.
Ordway, R.W., Pallanck, L., and Ganetzky, B. (1994). Neurally expressed Drosophila genes encoding homologs of the NSF and SNAP secretory proteins. Proc. Natl. Acad. Sci. USA *91*, 5715–5719.
Ortega, J.M., Genç, Ö., and Davis, G.W. (2018). Molecular mechanisms that stabilize short term synaptic plasticity during presynaptic homeostatic plasticity. Elife *7*.
Oyler, G.A., Higgins, G.A., Hart, R.A., Battenberg, E., Billingsley, M., Bloom, F.E., and Wilson, M.C. (1989). The identification of a novel synaptosomal-associated protein, SNAP-25, differentially expressed by neuronal subpopulations. J. Cell Biol. *109*, 3039–3052.
Pabst, S., Hazzard, J.W., Antonin, W., Südhof, T.C., Jahn, R., Rizo, J., and Fasshauer, D. (2000). Selective interaction of complexin with the neuronal SNARE complex. Determination of the binding regions. J. Biol. Chem. *275*, 19808–19818.
Paddock, B.E., Striegel, A.R., Hui, E., Chapman, E.R., and Reist, N.E. (2008). Ca2+-dependent, phospholipid-binding residues of synaptotagmin are critical for excitation-secretion coupling in vivo. J. Neurosci. *28*, 7458–7466.
Paddock, B.E., Wang, Z., Biela, L.M., Chen, K., Getzy, M.D., Striegel, A., Richmond, J.E., Chapman, E.R., Featherstone, D.E., and Reist, N.E. (2011). Membrane penetration by synaptotagmin is required for coupling calcium binding to vesicle fusion in vivo. J. Neurosci. *31*, 2248–2257.
Palladino, M.J., Keegan, L.P., O'Connell, M.A., and Reenan, R.A. (2000). A-to-I pre-mRNA editing in Drosophila is primarily involved in adult nervous system function and integrity. Cell *102*, 437–449.
Pallanck, L., Ordway, R.W., and Ganetzky, B. (1995a). A Drosophila NSF mutant. Nature *376*, 25.
Pallanck, L., Ordway, R.W., Ramaswami, M., Chi, W.Y., Krishnan, K.S., and Ganetzky, B. (1995b). Distinct roles for N-ethylmaleimide-sensitive fusion protein (NSF) suggested by the identification of a second Drosophila NSF homolog. J. Biol. Chem. *270*, 18742–18744.
Paro, S., Li, X., O'Connell, M.A., and Keegan, L.P. (2012). Regulation and functions of ADAR in drosophila. Curr. Top. Microbiol. Immunol. *353*, 221–236.
Peled, E.S., and Isacoff, E.Y. (2011). Optical quantal analysis of synaptic transmission in wild-type and rab3-mutant Drosophila motor axons. Nat. Neurosci. *14*, 519–526.
Pennuto, M., Bonanomi, D., Benfenati, F., and Valtorta, F. (2003). Synaptophysin I controls the targeting of VAMP2/synaptobrevin II to synaptic vesicles. Mol. Biol. Cell *14*, 4909–4919.
Pereira-Leal, J.B., Hume, A.N., and Seabra, M.C. (2001). Prenylation of Rab GTPases: molecular mechanisms and involvement in genetic disease. FEBS Lett. *498*, 197–200.
Peter, F., Wong, S.H., Subramaniam, V.N., Tang, B.L., and Hong, W. (1998). Alpha-SNAP but not

gamma-SNAP is required for ER-Golgi transport after vesicle budding and the Rab1-requiring step but before the EGTA-sensitive step. J. Cell Sci. *111 (Pt 17)*, 2625–2633.
Pevsner, J., Hsu, S.C., Braun, J.E., Calakos, N., Ting, A.E., Bennett, M.K., and Scheller, R.H. (1994). Specificity and regulation of a synaptic vesicle docking complex. Neuron *13*, 353–361.
Pobbati, A.V., Razeto, A., Böddener, M., Becker, S., and Fasshauer, D. (2004). Structural basis for the inhibitory role of tomosyn in exocytosis. J. Biol. Chem. *279*, 47192–47200.
Pobbati, A.V., Stein, A., and Fasshauer, D. (2006). N- to C-terminal SNARE complex assembly promotes rapid membrane fusion. Science *313*, 673–676.
Poodry, C.A., Hall, L., and Suzuki, D.T. (1973). Developmental properties of Shibire: a pleiotropic mutation affecting larval and adult locomotion and development. Dev. Biol. *32*, 373–386.
Pooryasin, A., Maglione, M., Schubert, M., Matkovic-Rachid, T., Hasheminasab, S.-M., Pech, U., Fiala, A., Mielke, T., and Sigrist, S.J. (2021). Unc13A and Unc13B contribute to the decoding of distinct sensory information in Drosophila. Nat. Commun. *12*, 1932.
Port, F., and Bullock, S.L. (2016). Augmenting CRISPR applications in Drosophila with tRNA-flanked sgRNAs. Nat. Methods *13*, 852–854.
Prinslow, E.A., Stepien, K.P., Pan, Y.-Z., Xu, J., and Rizo, J. (2019). Multiple factors maintain assembled trans-SNARE complexes in the presence of NSF and αSNAP. Elife *8*.
Pulver, S.R., Bayley, T.G., Taylor, A.L., Berni, J., Bate, M., and Hedwig, B. (2015). IMAGING FICTIVE LOCOMOTOR PATTERNS IN LARVAL DROSOPHILA. J. Neurophysiol. *114*, jn.00731.2015.
Quiñones-Frías, M.C., and Littleton, J.T. (2021). Function of Drosophila Synaptotagmins in membrane trafficking at synapses. Cell Mol. Life Sci.
Ramirez, D.M.O., Khvotchev, M., Trauterman, B., and Kavalali, E.T. (2012). Vti1a identifies a vesicle pool that preferentially recycles at rest and maintains spontaneous neurotransmission. Neuron *73*, 121–134.
Rao, S.S., Stewart, B.A., Rivlin, P.K., Vilinsky, I., Watson, B.O., Lang, C., Boulianne, G., Salpeter, M.M., and Deitcher, D.L. (2001). Two distinct effects on neurotransmission in a temperature-sensitive SNAP-25 mutant. EMBO J. *20*, 6761–6771.
Reddy-Alla, S., Böhme, M.A., Reynolds, E., Beis, C., Grasskamp, A.T., Mampell, M.M., Maglione, M., Jusyte, M., Rey, U., Babikir, H., et al. (2017). Stable positioning of unc13 restricts synaptic vesicle fusion to defined release sites to promote synchronous neurotransmission. Neuron *95*, 1350–1364.e12.
Redler, S., Strom, T.M., Wieland, T., Cremer, K., Engels, H., Distelmaier, F., Schaper, J., Küchler, A., Lemke, J.R., Jeschke, S., et al. (2017). Variants in CPLX1 in two families with autosomal-recessive severe infantile myoclonic epilepsy and ID. Eur. J. Hum. Genet. *25*, 889–893.
Reim, K., Mansour, M., Varoqueaux, F., McMahon, H.T., Südhof, T.C., Brose, N., and Rosenmund, C. (2001). Complexins regulate a late step in Ca2+-dependent neurotransmitter release. Cell *104*, 71–81.
Richmond, J.E., and Broadie, K.S. (2002). The synaptic vesicle cycle: exocytosis and endocytosis in Drosophila and C. elegans. Curr. Opin. Neurobiol. *12*, 499–507.
Richmond, J.E., and Jorgensen, E.M. (1999). One GABA and two acetylcholine receptors function at the C. elegans neuromuscular junction. Nat. Neurosci. *2*, 791–797.
Richmond, J.E., Davis, W.S., and Jorgensen, E.M. (1999). UNC-13 is required for synaptic vesicle fusion in C. elegans. Nat. Neurosci. *2*, 959–964.
Richmond, J.E., Weimer, R.M., and Jorgensen, E.M. (2001). An open form of syntaxin bypasses the requirement for UNC-13 in vesicle priming. Nature *412*, 338–341.
Rizo, J. (2018). Mechanism of neurotransmitter release coming into focus. Protein Sci. *27*, 1364–1391.
Rizzoli, S.O., and Jahn, R. (2007). Kiss-and-run, collapse and “readily retrievable” vesicles. Traffic *8*, 1137–1144.

Robertson, J.L. (2018). The lipid bilayer membrane and its protein constituents. J. Gen. Physiol. *150*, 1472–1483.

Robinson, S.W., Bourgognon, J.-M., Spiers, J.G., Breda, C., Campesan, S., Butcher, A., Mallucci, G.R., Dinsdale, D., Morone, N., Mistry, R., et al. (2018). Nitric oxide-mediated posttranslational modifications control neurotransmitter release by modulating complexin farnesylation and enhancing its clamping ability. PLoS Biol. *16*, e2003611.

Rodal, A.A., and Littleton, J.T. (2008). Synaptic endocytosis: illuminating the role of clathrin assembly. Curr. Biol. *18*, R259-61.

Rodal, A.A., Motola-Barnes, R.N., and Littleton, J.T. (2008). Nervous wreck and Cdc42 cooperate to regulate endocytic actin assembly during synaptic growth. J. Neurosci. *28*, 8316–8325.

Rosahl, T.W., Geppert, M., Spillane, D., Herz, J., Hammer, R.E., Malenka, R.C., and Südhof, T.C. (1993). Short-term synaptic plasticity is altered in mice lacking synapsin I. Cell *75*, 661–670.

Rothman, J.E. (1994). Mechanisms of intracellular protein transport. Nature *372*, 55–63.

Rowe, J., Corradi, N., Malosio, M.L., Taverna, E., Halban, P., Meldolesi, J., and Rosa, P. (1999). Blockade of membrane transport and disassembly of the Golgi complex by expression of syntaxin 1A in neurosecretion-incompetent cells: prevention by rbSEC1. J. Cell Sci. *112 (Pt 12)*, 1865–1877.

Rowe, J., Calegari, F., Taverna, E., Longhi, R., and Rosa, P. (2001). Syntaxin 1A is delivered to the apical and basolateral domains of epithelial cells: the role of munc-18 proteins. J. Cell Sci. *114*, 3323–3332.

Rubin, R., Abbott, L.F., and Sompolinsky, H. (2017). Balanced excitation and inhibition are required for high-capacity, noise-robust neuronal selectivity. Proc. Natl. Acad. Sci. USA *114*, E9366–E9375.

Ryan, T.J., and Grant, S.G.N. (2009). The origin and evolution of synapses. Nat. Rev. Neurosci. *10*, 701–712.

Ryu, J.-K., Min, D., Rah, S.-H., Kim, S.J., Park, Y., Kim, H., Hyeon, C., Kim, H.M., Jahn, R., and Yoon, T.-Y. (2015). Spring-loaded unraveling of a single SNARE complex by NSF in one round of ATP turnover. Science *347*, 1485–1489.

Sabeva, N., Cho, R.W., Vasin, A., Gonzalez, A., Littleton, J.T., and Bykhovskaia, M. (2017). Complexin Mutants Reveal Partial Segregation between Recycling Pathways That Drive Evoked and Spontaneous Neurotransmission. J. Neurosci. *37*, 383–396.

Saifee, O., Wei, L., and Nonet, M.L. (1998). The Caenorhabditis elegans unc-64 locus encodes a syntaxin that interacts genetically with synaptobrevin. Mol. Biol. Cell *9*, 1235–1252.

Sakisaka, T., Yamamoto, Y., Mochida, S., Nakamura, M., Nishikawa, K., Ishizaki, H., Okamoto-Tanaka, M., Miyoshi, J., Fujiyoshi, Y., Manabe, T., et al. (2008). Dual inhibition of SNARE complex formation by tomosyn ensures controlled neurotransmitter release. J. Cell Biol. *183*, 323–337.

Salpietro, V., Malintan, N.T., Llano-Rivas, I., Spaeth, C.G., Efthymiou, S., Striano, P., Vandrovcova, J., Cutrupi, M.C., Chimenz, R., David, E., et al. (2019). Mutations in the neuronal vesicular SNARE VAMP2 affect synaptic membrane fusion and impair human neurodevelopment. Am. J. Hum. Genet. *104*, 721–730.

Sanyal, S., and Krishnan, K.S. (2001). Lethal comatose mutation in Drosophila reveals possible role for NSF in neurogenesis. Neuroreport *12*, 1363–1366.

Sanyal, S., Basole, A., and Krishnan, K.S. (1999). Phenotypic interaction between temperature-sensitive paralytic mutants comatose and paralytic suggests a role for N-ethylmaleimide-sensitive fusion factor in synaptic vesicle cycling in Drosophila. J. Neurosci. *19*, RC47.

Sanyal, S., Tolar, L.A., Pallanck, L., and Krishnan, K.S. (2001). Genetic interaction between shibire and comatose mutations in Drosophila suggest a role for snap-receptor complex assembly and disassembly for maintenance of synaptic vesicle cycling. Neurosci. Lett. *311*, 21–24.

Sapiro, A.L., Shmueli, A., Henry, G.L., Li, Q., Shalit, T., Yaron, O., Paas, Y., Billy Li, J., and Shohat-Ophir, G. (2019). Illuminating spatial A-to-I RNA editing signatures within the

Drosophila brain. Proc. Natl. Acad. Sci. USA *116*, 2318–2327.
Saraswati, S., Adolfsen, B., and Littleton, J.T. (2007). Characterization of the role of the Synaptotagmin family as calcium sensors in facilitation and asynchronous neurotransmitter release. Proc. Natl. Acad. Sci. USA *104*, 14122–14127.
Sato, K., Norris, A., Sato, M., and Grant, B.D. (2014). C. elegans as a model for membrane traffic. WormBook 1–47.
Saunders, R.A., Stinson, B.M., Baker, T.A., and Sauer, R.T. (2020). Multistep substrate binding and engagement by the AAA+ ClpXP protease. Proc. Natl. Acad. Sci. USA *117*, 28005–28013.
Scales, S.J., Hesser, B.A., Masuda, E.S., and Scheller, R.H. (2002). Amisyn, a novel syntaxin-binding protein that may regulate SNARE complex assembly. J. Biol. Chem. *277*, 28271–28279.
Schlüter, O.M., Basu, J., Südhof, T.C., and Rosenmund, C. (2006). Rab3 superprimes synaptic vesicles for release: implications for short-term synaptic plasticity. J. Neurosci. *26*, 1239–1246.
Schoch, S., Castillo, P.E., Jo, T., Mukherjee, K., Geppert, M., Wang, Y., Schmitz, F., Malenka, R.C., and Südhof, T.C. (2002). RIM1alpha forms a protein scaffold for regulating neurotransmitter release at the active zone. Nature *415*, 321–326.
Scholz, N., Ehmann, N., Sachidanandan, D., Imig, C., Cooper, B.H., Jahn, O., Reim, K., Brose, N., Meyer, J., Lamberty, M., et al. (2019). Complexin cooperates with Bruchpilot to tether synaptic vesicles to the active zone cytomatrix. J. Cell Biol. *218*, 1011–1026.
Schulze, K.L., and Bellen, H.J. (1996). Drosophila syntaxin is required for cell viability and may function in membrane formation and stabilization. Genetics *144*, 1713–1724.
Schulze, K.L., Littleton, J.T., Salzberg, A., Halachmi, N., Stern, M., Lev, Z., and Bellen, H.J. (1994). rop, a Drosophila homolog of yeast Sec1 and vertebrate n-Sec1/Munc-18 proteins, is a negative regulator of neurotransmitter release in vivo. Neuron *13*, 1099–1108.
Schulze, K.L., Broadie, K., Perin, M.S., and Bellen, H.J. (1995). Genetic and electrophysiological studies of Drosophila syntaxin-1A demonstrate its role in nonneuronal secretion and neurotransmission. Cell *80*, 311–320.
Schwarz, T.L. (1994). Genetic analysis of neurotransmitter release at the synapse. Curr. Opin. Neurobiol. *4*, 633–639.
Shen, W., Kilander, M.B.C., Bridi, M.S., Frei, J.A., Niescier, R.F., Huang, S., and Lin, Y.-C. (2020). Tomosyn regulates the small RhoA GTPase to control the dendritic stability of neurons and the surface expression of AMPA receptors. J. Neurosci. Res. *98*, 1213–1231.
Shi, L., Shen, Q.-T., Kiel, A., Wang, J., Wang, H.-W., Melia, T.J., Rothman, J.E., and Pincet, F. (2012). SNARE proteins: one to fuse and three to keep the nascent fusion pore open. Science *335*, 1355–1359.
Shields, M.C., Bowers, M.R., Kramer, H.L., Fulcer, M.M., Perinet, L.C., Metz, M.J., and Reist, N.E. (2020). The role of the C2A domain of synaptotagmin 1 in asynchronous neurotransmitter release. PLoS One *15*, e0232991.
Shu, T., Jin, H., Rothman, J.E., and Zhang, Y. (2020). Munc13-1 MUN domain and Munc18-1 cooperatively chaperone SNARE assembly through a tetrameric complex. Proc. Natl. Acad. Sci. USA *117*, 1036–1041.
Siddiqi, O., and Benzer, S. (1976). Neurophysiological defects in temperature-sensitive paralytic mutants of Drosophila melanogaster. Proc. Natl. Acad. Sci. USA *73*, 3253–3257.
Siddiqui, T.J., Vites, O., Stein, A., Heintzmann, R., Jahn, R., and Fasshauer, D. (2007). Determinants of synaptobrevin regulation in membranes. Mol. Biol. Cell *18*, 2037–2046.
Sieburth, D., Ch'ng, Q., Dybbs, M., Tavazoie, M., Kennedy, S., Wang, D., Dupuy, D., Rual, J.-F., Hill, D.E., Vidal, M., et al. (2005). Systematic analysis of genes required for synapse structure and function. Nature *436*, 510–517.
Smith, C.J., Grigorieff, N., and Pearse, B.M. (1998). Clathrin coats at 21 A resolution: a cellular assembly designed to recycle multiple membrane receptors. EMBO J. *17*, 4943–4953.
Snead, D., Wragg, R.T., Dittman, J.S., and Eliezer, D. (2014). Membrane curvature sensing by the

C-terminal domain of complexin. Nat. Commun. *5*, 4955.
Söllner, T., Whiteheart, S.W., Brunner, M., Erdjument-Bromage, H., Geromanos, S., Tempst, P., and Rothman, J.E. (1993). SNAP receptors implicated in vesicle targeting and fusion. Nature *362*, 318–324.
Soykan, T., Maritzen, T., and Haucke, V. (2016). Modes and mechanisms of synaptic vesicle recycling. Curr. Opin. Neurobiol. *39*, 17–23.
Spang, A. (2016). Membrane tethering complexes in the endosomal system. Front. Cell Dev. Biol. *4*, 35.
Stein, A., Weber, G., Wahl, M.C., and Jahn, R. (2009). Helical extension of the neuronal SNARE complex into the membrane. Nature *460*, 525–528.
Stenbeck, G. (1998). Soluble NSF-attachment proteins. Int. J. Biochem. Cell Biol. *30*, 573–577.
Stenmark, H. (2009). Rab GTPases as coordinators of vesicle traffic. Nat. Rev. Mol. Cell Biol. *10*, 513–525.
Stenmark, H., and Olkkonen, V.M. (2001). The Rab GTPase family. Genome Biol. *2*, REVIEWS3007.
Stepien, K.P., Prinslow, E.A., and Rizo, J. (2019). Munc18-1 is crucial to overcome the inhibition of synaptic vesicle fusion by αSNAP. Nat. Commun. *10*, 4326.
Stevens, R.J., Akbergenova, Y., Jorquera, R.A., and Littleton, J.T. (2012). Abnormal synaptic vesicle biogenesis in Drosophila synaptogyrin mutants. J. Neurosci. *32*, 18054–67, 18067a.
Stewart, B.A., Mohtashami, M., Trimble, W.S., and Boulianne, G.L. (2000). SNARE proteins contribute to calcium cooperativity of synaptic transmission. Proc. Natl. Acad. Sci. USA *97*, 13955–13960.
Stewart, B.A., Mohtashami, M., Rivlin, P., Deitcher, D.L., Trimble, W.S., and Boulianne, G.L. (2002). Dominant-negative NSF2 disrupts the structure and function of Drosophila neuromuscular synapses. J. Neurobiol. *51*, 261–271.
Stigloher, C., Zhan, H., Zhen, M., Richmond, J., and Bessereau, J.-L. (2011). The presynaptic dense projection of the Caenorhabditis elegans cholinergic neuromuscular junction localizes synaptic vesicles at the active zone through SYD-2/liprin and UNC-10/RIM-dependent interactions. J. Neurosci. *31*, 4388–4396.
Striegel, A.R., Biela, L.M., Evans, C.S., Wang, Z., Delehoy, J.B., Sutton, R.B., Chapman, E.R., and Reist, N.E. (2012a). Calcium binding by synaptotagmin's C2A domain is an essential element of the electrostatic switch that triggers synchronous synaptic transmission. J. Neurosci. *32*, 1253–1260.
Striegel, A.R., Biela, L.M., Evans, C.S., Wang, Z., Delehoy, J.B., Sutton, R.B., Chapman, E.R., and Reist, N.E. (2012b). Calcium Binding by Synaptotagmin's C2A Domain is an Essential Element of the Electrostatic Switch That Triggers Synchronous Synaptic Transmission. J. Neurosci. *32*, 1253--1260.
Sudhof, T.C. (2004). The synaptic vesicle cycle. Annu. Rev. Neurosci. *27*, 509–547.
Südhof, T.C. (2012). The presynaptic active zone. Neuron *75*, 11–25.
Südhof, T.C. (2013). Neurotransmitter release: the last millisecond in the life of a synaptic vesicle. Neuron *80*, 675–690.
Südhof, T.C., and Rothman, J.E. (2009). Membrane fusion: grappling with SNARE and SM proteins. Science *323*, 474–477.
Sun, J., Bronk, P., Liu, X., Han, W., and Südhof, T.C. (2006). Synapsins regulate use-dependent synaptic plasticity in the calyx of Held by a Ca2+/calmodulin-dependent pathway. Proc. Natl. Acad. Sci. USA *103*, 2880–2885.
Sutton, R.B., Fasshauer, D., Jahn, R., and Brunger, A.T. (1998). Crystal structure of a SNARE complex involved in synaptic exocytosis at 2.4 A resolution. Nature *395*, 347–353.
Sweeney, S.T., Broadie, K., Keane, J., Niemann, H., and O'Kane, C.J. (1995). Targeted expression of tetanus toxin light chain in Drosophila specifically eliminates synaptic transmission and causes behavioral defects. Neuron *14*, 341–351.
Sweitzer, S.M., and Hinshaw, J.E. (1998). Dynamin undergoes a GTP-dependent conformational

change causing vesiculation. Cell *93*, 1021–1029.
Tagaya, M., Wilson, D.W., Brunner, M., Arango, N., and Rothman, J.E. (1993). Domain structure of an N-ethylmaleimide-sensitive fusion protein involved in vesicular transport. J. Biol. Chem. *268*, 2662–2666.
Takei, K., Mundigl, O., Daniell, L., and De Camilli, P. (1996). The synaptic vesicle cycle: a single vesicle budding step involving clathrin and dynamin. J. Cell Biol. *133*, 1237–1250.
Tebo, A.G., and Gautier, A. (2019). A split fluorescent reporter with rapid and reversible complementation. Nat. Commun. *10*, 2822.
Tien, C.-W., Yu, B., Huang, M., Stepien, K.P., Sugita, K., Xie, X., Han, L., Monnier, P.P., Zhen, M., Rizo, J., et al. (2020). Open syntaxin overcomes exocytosis defects of diverse mutants in C. elegans. Nat. Commun. *11*, 5516.
Tolar, L.A., and Pallanck, L. (1998). NSF function in neurotransmitter release involves rearrangement of the SNARE complex downstream of synaptic vesicle docking. J. Neurosci. *18*, 10250–10256.
Trimble, W.S., Cowan, D.M., and Scheller, R.H. (1988). VAMP-1: a synaptic vesicle-associated integral membrane protein. Proc. Natl. Acad. Sci. USA *85*, 4538–4542.
Trimbuch, T., and Rosenmund, C. (2016). Should I stop or should I go? The role of complexin in neurotransmitter release. Nat. Rev. Neurosci. *17*, 118–125.
Tucker, W.C., Weber, T., and Chapman, E.R. (2004). Reconstitution of Ca2+-regulated membrane fusion by synaptotagmin and SNAREs. Science *304*, 435–438.
Ubach, J., Zhang, X., Shao, X., Südhof, T.C., and Rizo, J. (1998). Ca2+ binding to synaptotagmin: how many Ca2+ ions bind to the tip of a C2-domain? EMBO J. *17*, 3921–3930.
Ubach, J., Lao, Y., Fernandez, I., Arac, D., Südhof, T.C., and Rizo, J. (2001). The C2B domain of synaptotagmin I is a Ca2+-binding module. Biochemistry *40*, 5854–5860.
Ungewickell, E., and Branton, D. (1981). Assembly units of clathrin coats. Nature *289*, 420–422.
Varoqueaux, F., and Fasshauer, D. (2017). Getting nervous: an evolutionary overhaul for communication. Annu. Rev. Genet. *51*, 455–476.
Varoqueaux, F., Sigler, A., Rhee, J.-S., Brose, N., Enk, C., Reim, K., and Rosenmund, C. (2002). Total arrest of spontaneous and evoked synaptic transmission but normal synaptogenesis in the absence of Munc13-mediated vesicle priming. Proc. Natl. Acad. Sci. USA *99*, 9037–9042.
Vasin, A., Volfson, D., Littleton, J.T., and Bykhovskaia, M. (2016). Interaction of the Complexin Accessory Helix with Synaptobrevin Regulates Spontaneous Fusion. Biophys. J. *111*, 1954–1964.
Verhage, M., Maia, A.S., Plomp, J.J., Brussaard, A.B., Heeroma, J.H., Vermeer, H., Toonen, R.F., Hammer, R.E., van den Berg, T.K., Missler, M., et al. (2000). Synaptic assembly of the brain in the absence of neurotransmitter secretion. Science *287*, 864–869.
Vilinsky, I., Stewart, B.A., Drummond, J., Robinson, I., and Deitcher, D.L. (2002). A Drosophila SNAP-25 null mutant reveals context-dependent redundancy with SNAP-24 in neurotransmission. Genetics *162*, 259--271.
Vivona, S., Cipriano, D.J., O'Leary, S., Li, Y.H., Fenn, T.D., and Brunger, A.T. (2013). Disassembly of all SNARE complexes by N-ethylmaleimide-sensitive factor (NSF) is initiated by a conserved 1:1 interaction between α-soluble NSF attachment protein (SNAP) and SNARE complex. J. Biol. Chem. *288*, 24984–24991.
Wagh, D.A., Rasse, T.M., Asan, E., Hofbauer, A., Schwenkert, I., Dürrbeck, H., Buchner, S., Dabauvalle, M.-C., Schmidt, M., Qin, G., et al. (2006). Bruchpilot, a protein with homology to ELKS/CAST, is required for structural integrity and function of synaptic active zones in Drosophila. Neuron *49*, 833–844.
Walther, K., Diril, M.K., Jung, N., and Haucke, V. (2004). Functional dissection of the interactions of stonin 2 with the adaptor complex AP-2 and synaptotagmin. Proc. Natl. Acad. Sci. USA *101*, 964–969.
Wang, S., Yang, J., Tsai, A., Kuca, T., Sanny, J., Lee, J., Dong, K., Harden, N., and Krieger, C.

(2011). Drosophila adducin regulates Dlg phosphorylation and targeting of Dlg to the synapse and epithelial membrane. Dev. Biol. *357*, 392–403.
Wang, Y., Okamoto, M., Schmitz, F., Hofmann, K., and Südhof, T.C. (1997). Rim is a putative Rab3 effector in regulating synaptic-vesicle fusion. Nature *388*, 593–598.
Watanabe, S., Liu, Q., Davis, M.W., Hollopeter, G., Thomas, N., Jorgensen, N.B., and Jorgensen, E.M. (2013b). Ultrafast endocytosis at Caenorhabditis elegans neuromuscular junctions. Elife *2*, e00723.
Watanabe, S., Rost, B.R., Camacho-Pérez, M., Davis, M.W., Söhl-Kielczynski, B., Rosenmund, C., and Jorgensen, E.M. (2013a). Ultrafast endocytosis at mouse hippocampal synapses. Nature *504*, 242–247.
Weber, T., Zemelman, B.V., McNew, J.A., Westermann, B., Gmachl, M., Parlati, F., Söllner, T.H., and Rothman, J.E. (1998). SNAREpins: minimal machinery for membrane fusion. Cell *92*, 759–772.
Weimbs, T., Low, S.H., Chapin, S.J., Mostov, K.E., Bucher, P., and Hofmann, K. (1997). A conserved domain is present in different families of vesicular fusion proteins: a new superfamily. Proc. Natl. Acad. Sci. USA *94*, 3046–3051.
Weimer, R.M., Richmond, J.E., Davis, W.S., Hadwiger, G., Nonet, M.L., and Jorgensen, E.M. (2003). Defects in synaptic vesicle docking in unc-18 mutants. Nat. Neurosci. *6*, 1023–1030.
Weimer, R.M., Gracheva, E.O., Meyrignac, O., Miller, K.G., Richmond, J.E., and Bessereau, J.-L. (2006). UNC-13 and UNC-10/rim localize synaptic vesicles to specific membrane domains. J. Neurosci. *26*, 8040–8047.
Wen, X., Saltzgaber, G.W., and Thoreson, W.B. (2017). Kiss-and-Run Is a Significant Contributor to Synaptic Exocytosis and Endocytosis in Photoreceptors. Front. Cell Neurosci. *11*, 286.
White, K.I., Zhao, M., Choi, U.B., Pfuetzner, R.A., and Brunger, A.T. (2018). Structural principles of SNARE complex recognition by the AAA+ protein NSF. Elife *7*.
Whiteheart, S.W., Brunner, M., Wilson, D.W., Wiedmann, M., and Rothman, J.E. (1992). Soluble N-ethylmaleimide-sensitive fusion attachment proteins (SNAPs) bind to a multi-SNAP receptor complex in Golgi membranes. J. Biol. Chem. *267*, 12239–12243.
Whyte, J.R.C., and Munro, S. (2002). Vesicle tethering complexes in membrane traffic. J. Cell Sci. *115*, 2627–2637.
Wickner, W., and Schekman, R. (2008). Membrane fusion. Nat. Struct. Mol. Biol. *15*, 658–664.
Widberg, C.H., Bryant, N.J., Girotti, M., Rea, S., and James, D.E. (2003). Tomosyn interacts with the t-SNAREs syntaxin4 and SNAP23 and plays a role in insulin-stimulated GLUT4 translocation. J. Biol. Chem. *278*, 35093–35101.
Williams, A.L., Bielopolski, N., Meroz, D., Lam, A.D., Passmore, D.R., Ben-Tal, N., Ernst, S.A., Ashery, U., and Stuenkel, E.L. (2011). Structural and functional analysis of tomosyn identifies domains important in exocytotic regulation. J. Biol. Chem. *286*, 14542–14553.
Wilson, D.W., Wilcox, C.A., Flynn, G.C., Chen, E., Kuang, W.J., Henzel, W.J., Block, M.R., Ullrich, A., and Rothman, J.E. (1989). A fusion protein required for vesicle-mediated transport in both mammalian cells and yeast. Nature *339*, 355–359.
Wilson, D.W., Whiteheart, S.W., Wiedmann, M., Brunner, M., and Rothman, J.E. (1992). A multisubunit particle implicated in membrane fusion. J. Cell Biol. *117*, 531–538.
Witkos, T.M., and Lowe, M. (2015). The Golgin Family of Coiled-Coil Tethering Proteins. Front. Cell Dev. Biol. *3*, 86.
Wittig, S., Ganzella, M., Barth, M., Kostmann, S., Riedel, D., Pérez-Lara, Á., Jahn, R., and Schmidt, C. (2021). Cross-linking mass spectrometry uncovers protein interactions and functional assemblies in synaptic vesicle membranes. Nat. Commun. *12*, 858.
Wragg, R.T., Parisotto, D.A., Li, Z., Terakawa, M.S., Snead, D., Basu, I., Weinstein, H., Eliezer, D., and Dittman, J.S. (2017). Evolutionary Divergence of the C-terminal Domain of Complexin Accounts for Functional Disparities between Vertebrate and Invertebrate Complexins. Front. Mol. Neurosci. *10*, 146.

Wu, M.N., Littleton, J.T., Bhat, M.A., Prokop, A., and Bellen, H.J. (1998). ROP, the Drosophila Sec1 homolog, interacts with syntaxin and regulates neurotransmitter release in a dosage-dependent manner. EMBO J. *17*, 127–139.

Wu, M.N., Fergestad, T., Lloyd, T.E., He, Y., Broadie, K., and Bellen, H.J. (1999). Syntaxin 1A interacts with multiple exocytic proteins to regulate neurotransmitter release in vivo. Neuron *23*, 593–605.

Wu, Y., Kawasaki, F., and Ordway, R.W. (2005). Properties of short-term synaptic depression at larval neuromuscular synapses in wild-type and temperature-sensitive paralytic mutants of Drosophila. J. Neurophysiol. *93*, 2396--2405.

Xia, X., Lessmann, V., and Martin, T.F.J. (2009). Imaging of evoked dense-core-vesicle exocytosis in hippocampal neurons reveals long latencies and kiss-and-run fusion events. J. Cell Sci. *122*, 75–82.

Xu, Y., Kuhlmann, J., Brennich, M., Komorowski, K., Jahn, R., Steinem, C., and Salditt, T. (2018). Reconstitution of SNARE proteins into solid-supported lipid bilayer stacks and X-ray structure analysis. Biochim. Biophys. Acta Biomembr. *1860*, 566–578.

Xue, M., Reim, K., Chen, X., Chao, H.-T., Deng, H., Rizo, J., Brose, N., and Rosenmund, C. (2007). Distinct domains of complexin I differentially regulate neurotransmitter release. Nat. Struct. Mol. Biol. *14*, 949–958.

Xue, M., Stradomska, A., Chen, H., Brose, N., Zhang, W., Rosenmund, C., and Reim, K. (2008). Complexins facilitate neurotransmitter release at excitatory and inhibitory synapses in mammalian central nervous system. Proc. Natl. Acad. Sci. USA *105*, 7875–7880.

Xue, M., Lin, Y.Q., Pan, H., Reim, K., Deng, H., Bellen, H.J., and Rosenmund, C. (2009). Tilting the balance between facilitatory and inhibitory functions of mammalian and Drosophila Complexins orchestrates synaptic vesicle exocytosis. Neuron *64*, 367–380.

Xue, M., Craig, T.K., Xu, J., Chao, H.-T., Rizo, J., and Rosenmund, C. (2010). Binding of the complexin N terminus to the SNARE complex potentiates synaptic-vesicle fusogenicity. Nat. Struct. Mol. Biol. *17*, 568–575.

Yamamoto, Y., Fujikura, K., Sakaue, M., Okimura, K., Kobayashi, Y., Nakamura, T., and Sakisaka, T. (2010a). The tail domain of tomosyn controls membrane fusion through tomosyn displacement by VAMP2. Biochem. Biophys. Res. Commun. *399*, 24–30.

Yamamoto, Y., Mochida, S., Miyazaki, N., Kawai, K., Fujikura, K., Kurooka, T., Iwasaki, K., and Sakisaka, T. (2010b). Tomosyn inhibits synaptotagmin-1-mediated step of Ca2+-dependent neurotransmitter release through its N-terminal WD40 repeats. J. Biol. Chem. *285*, 40943–40955.

Yang, B., Steegmaier, M., Gonzalez, L.C., and Scheller, R.H. (2000). nSec1 binds a closed conformation of syntaxin1A. J. Cell Biol. *148*, 247–252.

Yang, X., Kaeser-Woo, Y.J., Pang, Z.P., Xu, W., and Südhof, T.C. (2010). Complexin clamps asynchronous release by blocking a secondary Ca(2+) sensor via its accessory α helix. Neuron *68*, 907–920.

Yang, X., Cao, P., and Südhof, T.C. (2013). Deconstructing complexin function in activating and clamping Ca2+-triggered exocytosis by comparing knockout and knockdown phenotypes. Proc. Natl. Acad. Sci. USA *110*, 20777–20782.

Yelamanchili, S.V., Reisinger, C., Becher, A., Sikorra, S., Bigalke, H., Binz, T., and Ahnert-Hilger, G. (2005). The C-terminal transmembrane region of synaptobrevin binds synaptophysin from adult synaptic vesicles. Eur. J. Cell Biol. *84*, 467–475.

Yizhar, O., Matti, U., Melamed, R., Hagalili, Y., Bruns, D., Rettig, J., and Ashery, U. (2004). Tomosyn inhibits priming of large dense-core vesicles in a calcium-dependent manner. Proc. Natl. Acad. Sci. USA *101*, 2578–2583.

Yizhar, O., Lipstein, N., Gladycheva, S.E., Matti, U., Ernst, S.A., Rettig, J., Stuenkel, E.L., and Ashery, U. (2007). Multiple functional domains are involved in tomosyn regulation of exocytosis. J. Neurochem. *103*, 604–616.

Yokoyama, S., Shirataki, H., Sakisaka, T., and Takai, Y. (1999). Three splicing variants of tomosyn

and identification of their syntaxin-binding region. Biochem. Biophys. Res. Commun. *256*, 218–222.
Yoon, T.-Y., and Munson, M. (2018). SNARE complex assembly and disassembly. Curr. Biol. *28*, R397–R401.
Yoshihara, M., and Littleton, J.T. (2002). Synaptotagmin I functions as a calcium sensor to synchronize neurotransmitter release. Neuron *36*, 897–908.
Yoshihara, M., Ueda, A., Zhang, D., Deitcher, D.L., Schwarz, T.L., and Kidokoro, Y. (1999). Selective effects of neuronal-synaptobrevin mutations on transmitter release evoked by sustained versus transient Ca2+ increases and by cAMP. J. Neurosci. *19*, 2432–2441.
Yoshihara, M., Adolfsen, B., Galle, K.T., and Littleton, J.T. (2005). Retrograde signaling by Syt 4 induces presynaptic release and synapse-specific growth. Science *310*, 858–863.
Yoshihara, M., Guan, Z., and Littleton, J.T. (2010). Differential regulation of synchronous versus asynchronous neurotransmitter release by the C2 domains of synaptotagmin 1. Proc. Natl. Acad. Sci. USA *107*, 14869–14874.
Yu, I.-M., and Hughson, F.M. (2010). Tethering factors as organizers of intracellular vesicular traffic. Annu. Rev. Cell Dev. Biol. *26*, 137–156.
Yu, H., Rathore, S.S., Gulbranson, D.R., and Shen, J. (2014). The N- and C-terminal domains of tomosyn play distinct roles in soluble N-ethylmaleimide-sensitive factor attachment protein receptor binding and fusion regulation. J. Biol. Chem. *289*, 25571–25580.
Yu, W., Kawasaki, F., and Ordway, R.W. (2011). Activity-dependent interactions of NSF and SNAP at living synapses. Mol. Cell. Neurosci. *47*, 19–27.
Zhai, R.G., and Bellen, H.J. (2004). The architecture of the active zone in the presynaptic nerve terminal. Physiology (Bethesda) *19*, 262–270.
Zhang, B., Koh, Y.H., Beckstead, R.B., Budnik, V., Ganetzky, B., and Bellen, H.J. (1998). Synaptic vesicle size and number are regulated by a clathrin adaptor protein required for endocytosis. Neuron *21*, 1465–1475.
Zhang, J.Z., Davletov, B.A., Südhof, T.C., and Anderson, R.G. (1994). Synaptotagmin I is a high affinity receptor for clathrin AP-2: implications for membrane recycling. Cell *78*, 751–760.
Zhang, Q., Li, Y., and Tsien, R.W. (2009). The dynamic control of kiss-and-run and vesicular reuse probed with single nanoparticles. Science *323*, 1448–1453.
Zhang, W., Lilja, L., Mandic, S.A., Gromada, J., Smidt, K., Janson, J., Takai, Y., Bark, C., Berggren, P.-O., and Meister, B. (2006). Tomosyn is expressed in beta-cells and negatively regulates insulin exocytosis. Diabetes *55*, 574–581.
Zhao, M., and Brunger, A.T. (2016). Recent Advances in Deciphering the Structure and Molecular Mechanism of the AAA+ ATPase N-Ethylmaleimide-Sensitive Factor (NSF). J. Mol. Biol. *428*, 1912–1926.
Zhao, M., Wu, S., Zhou, Q., Vivona, S., Cipriano, D.J., Cheng, Y., and Brunger, A.T. (2015). Mechanistic insights into the recycling machine of the SNARE complex. Nature *518*, 61–67.
Zhou, S., and Yu, Y. (2018). Synaptic E-I Balance Underlies Efficient Neural Coding. Front. Neurosci. *12*, 46.
Zhou, Q., Lai, Y., Bacaj, T., Zhao, M., Lyubimov, A.Y., Uervirojnangkoorn, M., Zeldin, O.B., Brewster, A.S., Sauter, N.K., Cohen, A.E., et al. (2015a). Architecture of the synaptotagmin-SNARE machinery for neuronal exocytosis. Nature *525*, 62–67.
Zhou, Q., Huang, X., Sun, S., Li, X., Wang, H.-W., and Sui, S.-F. (2015b). Cryo-EM structure of SNAP-SNARE assembly in 20S particle. Cell Res. *25*, 551–560.
Zhou, Q., Zhou, P., Wang, A.L., Wu, D., Zhao, M., Südhof, T.C., and Brunger, A.T. (2017). The primed SNARE-complexin-synaptotagmin complex for neuronal exocytosis. Nature *548*, 420–425.
Zorman, S., Rebane, A.A., Ma, L., Yang, G., Molski, M.A., Coleman, J., Pincet, F., Rothman, J.E., and Zhang, Y. (2014). Common intermediates and kinetics, but different energetics, in the assembly of SNARE proteins. Elife *3*, e03348.

Chad W. Sauvola performed most of the work described in this chapter. Yulia Akbergenova imaged the electron microscopy samples and performed all live imaging experiments. Karen L. Cunningham performed nearly all immunohistochemistry experiments. Nicole Aponte-Santiago generated the *tomosyn* null alleles.

Chapter 2

The decoy SNARE Tomosyn sets tonic versus phasic release properties and is required for homeostatic synaptic plasticity

2.1 Introduction

Ca^{2+}-dependent fusion of synaptic vesicles (SVs) is the primary mechanism for neurotransmission and is mediated by the soluble N-ethylmaleimide sensitive factor attachment protein receptor (SNARE) family (Jahn and Scheller, 2006; Söllner et al., 1993; Sudhof, 2004; Weber et al., 1998). Following an action potential, SNARE proteins located on the SV and plasma membrane zipper into an energetically favorable coiled-coil bundle to induce SV fusion (Jahn and Scheller, 2006; Söllner et al., 1993; Südhof and Rothman, 2009). Neurotransmitter release results in a postsynaptic response that varies in size depending on the strength of the synapse, which can be regulated from both pre-and post-synaptic compartments. The postsynaptic cell controls sensitivity to neurotransmitters by governing receptor field composition, while the presynaptic neuron establishes the probability of SV fusion (P_r) (Citri and Malenka, 2008; Körber and Kuner, 2016; Nicoll, 2003; Yang and Calakos, 2013). Highly stereotyped differences in P_r exist across neurons, with many neuronal populations broadly classified as tonic or phasic depending on their spiking patterns, P_r and short-term plasticity characteristics (Atwood and Karunanithi, 2002; Dittman et al., 2000; Lnenicka and Keshishian, 2000). How cell-intrinsic properties establish differences in presynaptic P_r between neuronal classes, and how release strength is further refined via plasticity, remain incompletely understood.

The *Drosophila melanogaster* larval neuromuscular junction (NMJ) has emerged as an important model for characterizing mechanisms mediating synaptic communication and

tonic versus phasic release properties (Aponte-Santiago and Littleton, 2020; Aponte-Santiago et al., 2020; Genç and Davis, 2019; Lu et al., 2016; Newman et al., 2017; Wang et al., 2021). Larval body wall muscles are co-innervated by two glutamatergic motoneuron populations that drive locomotion, including the tonic-like Ib and phasic-like Is subtypes (Aponte-Santiago et al., 2020; Harris and Littleton, 2015; Jan and Jan, 1976; Lnenicka and Keshishian, 2000). Tonic Ib terminals display lower initial P_r and sustained release during stimulation, whereas phasic Is terminals show high intrinsic P_r and rapid depression (Lu et al., 2016; Newman et al., 2017). The Drosophila NMJ also undergoes robust presynaptic homeostatic potentiation (PHP) that rapidly increases P_r to compensate for disruptions to postsynaptic glutamate receptor (GluR) function (Böhme et al., 2019; Gratz et al., 2019; Li et al., 2018; Müller et al., 2012; Ortega et al., 2018; Weyhersmüller et al., 2011). In addition to intrinsic release differences between Ib and Is neurons, they also display distinct PHP properties depending on mechanisms of GluR impairment and extracellular Ca^{2+} concentration (Newman *et al*., 2017, Genç *et al*., 2019). How tonic and phasic neurons differentially regulate P_r at rest and during plasticity is largely unknown.

The highly conserved SNARE regulatory protein Tomosyn negatively controls SV release and has been proposed to participate in synaptic plasticity (Ben-Simon et al., 2015; Chen et al., 2011; Gracheva et al., 2006; McEwen et al., 2006). Tomosyn has an N-terminal WD40 repeat domain and a C-terminal SNARE motif with homology to the SV v-SNARE Synaptobrevin 2 (Syb2) (Fasshauer et al., 1998; Hatsuzawa et al., 2003; Hattendorf et al., 2007; Pobbati et al., 2004; Williams et al., 2011). Tomosyn inhibits presynaptic release by binding the t-SNAREs Syntaxin1 (Syx1) and SNAP-25 to prevent Syb2 incorporation into the SNARE complex fusion machinery (Hatsuzawa et al., 2003; Lehman et al., 1999; Sakisaka et al., 2008; Williams et al., 2011).

To further examine the role of Tomosyn in synaptic transmission and plasticity, we used CRISPR to generate mutations in the sole Drosophila *tomosyn* gene. Structure-function analysis revealed the SNARE domain is critical for release inhibition, while the scaffold region promotes enrichment of Tomosyn to SV rich sites. Despite enhanced evoked release, *tomosyn* mutants fail to maintain high levels of SV output during sustained stimulation due to rapid depletion of the immediately releasable SV pool. Tomosyn is highly enriched at Ib synapses and generates tonic neurotransmission properties characterized by low P_r and sustained release in this population of motoneurons. Indeed, optogenetic stimulation and

optical quantal analysis demonstrate an exclusive role for Tomosyn in regulating intrinsic release strength in tonic motoneurons. PHP expression primarily occurs at tonic synapses and is abolished in *tomosyn* mutants, suggesting Tomosyn is also essential for acute PHP expression. Together, these data support a model where Tomosyn mediates the tonic properties of Ib motoneurons by suppressing P_r to slow the rate of SV usage, while removing Tomosyn suppression enables P_r enhancement during PHP. Conversely, the absence of Tomosyn in Is motoneurons facilitates phasic release properties by enabling an intrinsically high P_r that quickly depletes the releasable SV pool, resulting in rapid synaptic depression and reduced capacity for PHP.

2.2 Results

Drosophila contains a single conserved Tomosyn gene encoding two splice variants

The Drosophila Tomosyn homolog is highly conserved with other Tomosyn proteins across the animal kingdom, displaying high sequence conservation in critical domains including the C-terminal SNARE motif. This region enables formation of a SNARE complex composed of the Tomosyn C-terminus and the t-SNAREs Syx1A and SNAP-25 (Fasshauer et al., 1998; Hatsuzawa et al., 2003; Pobbati et al., 2004; Williams et al., 2011). BLOSUM62 alignment using the C-terminal tail of the yeast homolog Sro7 as an outgroup indicates the Tomosyn SNARE motif forms a phylogenetically distinct group from other v-SNAREs despite their shared affinity for t-SNAREs (**Figure 1A**). Homology modeling suggests the C-terminus of Drosophila Tomosyn forms a SNARE complex with synaptic t-SNAREs similar in structure to that of mammalian Tomosyn (**Figure 1B**). A conserved ERG sequence within the C-terminal SNARE motif enables zippering of Tomosyn with t-SNAREs in a complex that prevents association with the SV fusion clamp Complexin (Cpx), in contrast to SNARE complexes containing Syb2 (**Figure 1C and 1D**).

Similar to other species, Drosophila *tomosyn* is alternatively spliced at exon 13 to generate two splice variants, Tomosyn13A and Tomosyn13B, that encode distinct parts of the WD40 repeat scaffold. The sequence of exon 13A is highly conserved across insect genomes, while the 13B exon sequence is poorly conserved (**Figure 1E**). As such, Tomosyn13A is likely to be the more functionally conserved isoform. Iterative homology modeling of Tomosyn13A suggests it forms a double barrel structure with three disordered loops projecting from the core WD40 scaffold domain (**Figure 1F**), as predicted for

mammalian Tomosyn-1 and Tomosyn-2 proteins (Williams et al., 2011). Exon 13 encodes one of the loops protruding from the WD40 core, suggesting alternative splicing regulates secondary features of Tomosyn beyond its SNARE-binding properties. Together, these data suggest Drosophila Tomosyn has conserved features with its mammalian counterparts.

Tomosyn mutants display increased evoked and spontaneous neurotransmitter release

To assay the function of Tomosyn at Drosophila synapses, CRISPR/Cas9 was used to generate two mutant alleles of the *tomosyn* gene on the X-chromosome (**Figure 1E**). A deletion mutant of *tomosyn* was generated using homology-directed repair to replace the entire coding sequence with a DsRed cassette ($tomosyn^{NA1}$). A frame shift mutant with an early stop codon ($tomosyn^{FS1}$) was also isolated using a gRNA that targets the 5' end of the *tomosyn* coding region. $Tomosyn^{NA1}$ mutants were used for most of this study, though both alleles displayed similar phenotypes (**Figures 2 and Figure 3**). $Tomosyn^{NA1}$ males are homozygous viable and eclose as adults at similar rates with a genomic background control ($n \geq 95$ eclosed flies; Chi-square test, $p = 0.9163$). Homozygous adult females were observed less frequently, suggesting the existence of sex divergent roles. Tomosyn has been suggested to inhibit SV SNARE complex formation by competing for t-SNARE binding with the v-SNARE Syb2. To determine if Drosophila Tomosyn plays a similar role in negatively regulating SNARE complex formation, SDS-resistant SNARE complex (7S complex) abundance was assayed. Western blots of control and $tomosyn^{NA1}$ brain lysates with Syntaxin1A antisera demonstrated a 2.7-fold increase in SNARE complex levels in the absence of Tomosyn (**Figure 1G**), consistent with Tomosyn inhibition of SNARE assembly.

To characterize synaptic transmission at Tomosyn-deficient synapses, two-electrode voltage clamp (TEVC) recordings were performed at 3rd instar muscle 6 NMJs in larval segment A4. $Tomosyn^{NA1}$ null hemizygous males displayed a 62% increase in the amplitude of evoked excitatory junctional currents (eEJCs) in 0.3 mM extracellular Ca^{2+}, indicating Tomosyn normally suppresses neurotransmitter release (**Figure 2A-2C**). A similar 51% increase in evoked release was found in the $tomosyn^{FS1}$ frameshift null mutant (**Figure 3A-3C**). Enhanced release in *tomosyn* mutants could result from a larger postsynaptic response to single SVs (quantal size) or fusion of a greater number of SVs per stimulus (quantal content). Quantal size as measured by miniature excitatory junctional current (mEJC) amplitude was unchanged in $tomosyn^{NA1}$ (**Figure 2D-2F**). Instead, *tomosyn* mutant terminals

released 70% more SVs across the active zone (AZ) population in response to a single stimulus (**Figure 2G and 2H**), with an average increase in quantal content from 84 SVs released in controls to 143 in *tomosyn*^{NA1}. In higher extracellular Ca^{2+} (2.0 mM) saline, evoked responses in *tomosyn*^{NA1} mutants remained larger and displayed a slower evoked charge transfer that resulted in a 43% increase in EJC area (Figure 2I-2M). The enhancement in delayed SV release is consistent with Drosophila RNAi knockdowns and *tomosyn* mutants in other species (Chen et al., 2011; Gracheva et al., 2006; McEwen et al., 2006; Sakisaka et al., 2008). *Tomosyn*^{NA1} mutants also showed a 3.5-fold increase in the rate of stimulation-independent spontaneous miniature release events (**Figure 2N and 2O**), a phenotype not previously reported. To confirm the elevated mini frequency is not due to a second-site mutation, *tomosyn*^{NA1} mutants were crossed with animals containing a deficiency (*Df(1)ED7161*) spanning the *tomosyn* locus. This allelic combination showed similar increases in spontaneous release (**Figure 2N and 2O**), as did the *tomosyn*^{FS1} allele (Figure S2D and S2E). *Tomosyn*^{NA1}*/Df(1)7161* trans-heterozygous null females showed even larger evoked responses compared to *tomosyn*^{NA1} hemizygous males or controls (**Figure 2A-2C**). Together with the reduction in homozygous female viability, sex-specific differences in Tomosyn function are likely to account for these enhanced phenotypes. *Tomosyn* null males were used for the remainder of the study to avoid phenotypic gender differences.

To test conservation of Tomosyn function, Drosophila Tomosyn or human Tomosyn-1 transgenes were pan-neuronally expressed in the *tomosyn*^{NA1} null background using the Gal4/UAS expression system. Both homologs rescued the increased evoked and spontaneous release phenotypes in *tomosyn*^{NA1} mutants (**Figure 4A and 4B**). Unexpectedly, human Tomosyn-1 decreased SV release to a greater extent than larvae rescued with Drosophila Tomosyn or controls. Immunohistochemistry to a Myc epitope attached to the transgenic Tomosyn proteins revealed human Tomosyn-1 was more abundant in presynaptic terminals than Drosophila Tomosyn (**Figure 4C and 4D**), suggesting dosage-sensitive inhibition of SV fusion is likely to account for enhanced suppression by the human homolog. Together, these data indicate Tomosyn decreases both evoked and spontaneous SV release at Drosophila NMJs, with these properties retained in human Tomosyn.

The C-terminal SNARE domain of Tomosyn is essential for release suppression while the N-terminal scaffold promotes SV enrichment

To determine critical domains within Tomosyn that mediate suppression of SV release, full-length or truncation mutants were expressed in the *tomosyn*^{NA1} background using the Gal4/UAS system (**Figure 5 and Figure 6**). Both Tomosyn13A and 13B splice variants restored neurotransmitter release in *tomosyn*^{NA1} (**Figure 5A and 5B**). Eliminating the SNARE motif from either splice isoform abolished rescue, while expressing the Tomosyn SNARE domain alone partially rescued enhanced release in *tomosyn*^{NA1} (**Figure 5A**). Although the SNARE motif is necessary for Tomosyn function, the failure to fully rescue release defects suggests the scaffold domain is required for complete Tomosyn-induced release suppression. The scaffold could be independently required to suppress release or act together with the SNARE domain to inhibit fusion. Co-expression of the scaffold and SNARE domains as independent transgenes failed to reconstitute full-length Tomosyn function, indicating these domains must be linked and act cooperatively to fully downregulate presynaptic release (**Figure 5A**).

To examine the role of the N-terminal scaffolding region, immunocytochemistry was performed to assay subsynaptic localization of Tomosyn and the individual domains by staining for an attached Myc epitope. Full-length Tomosyn was present throughout the periphery of presynaptic boutons as observed for other SV proteins (**Figure 6A and 6B**), consistent with the presence of Tomosyn on SVs in *C. elegans* and mammals (Geerts et al., 2017; McEwen et al., 2006). Both Tomosyn13A and 13B show stronger co-localization with the SV protein Synapsin than with the neuronal plasma membrane marker anti-HRP (**Figure 6A and 6B**). Tomosyn13A and the 13A scaffold domain alone showed similar SV enrichment, suggesting the SNARE motif is dispensable for SV localization. The Tomosyn13B scaffold domain was slightly less efficient at localizing this isoform to SV rich sites. In contrast to the scaffold domain, the SNARE motif alone had reduced SV co-localization compared to full-length Tomosyn. Together, these data indicate the scaffold domain functions to enhance Tomosyn localization to SVs.

To determine whether Tomosyn bidirectionally modulates SV release, Tomosyn was overexpressed in a wildtype background. Full-length Tomosyn13A suppressed evoked and spontaneous release by 33% and 40%, respectively (**Figure 7A and 7B**). Tomosyn13B overexpression was less effective at reducing release, although the 13B scaffold alone modestly decreased mini frequency (**Figure 7B**). Overexpression of the mammalian Tomosyn scaffold alone has been previously shown to reduce SV fusion (Yamamoto et al.,

2010; Yizhar et al., 2004, 2007), suggesting the Tomosyn 13B scaffold may have similar properties. Overexpression of the remaining Tomosyn truncation mutants, including the SNARE motif alone, failed to inhibit evoked or spontaneous release. These data indicate Tomosyn13A acts as a bidirectional modulator of presynaptic output and requires both the scaffold and SNARE domains to control SV release.

Tomosyn restricts SV release in a Ca^{2+}- and Synaptotagmin-independent manner

Beyond its role as a decoy SNARE, Tomosyn has been suggested to decrease release by binding to the Ca^{2+} sensor Synaptotagmin 1 (Syt1) and reduce its ability to activate fusion (Yamamoto et al., 2010). If a Syt1-Tomosyn interaction mediates SV release inhibition in Drosophila, loss of Syt1 should eliminate Tomosyn's ability to decrease SV fusion. To test this model, neurotransmitter release in *tomosyn, syt1* double null mutants (*tomosyn^{NA1}*; *syt1$^{AD4/N13}$*) was characterized. Most of the evoked response in *tomosyn^{NA1}* is Syt1-dependent, as double mutants had a large reduction in evoked release compared to controls (**Figure 8A**). However, *tomosyn;syt1* evoked responses were 86% larger than those of *syt1* null mutants alone (**Figure 8A and 8B**), indicating Tomosyn inhibits release independent of Syt1. *Syt1* mutants also show increases in the slower asynchronous phase of evoked fusion (Jorquera et al., 2012; Yoshihara and Littleton, 2002). Asynchronous release was increased 1.7-fold in *tomosyn;syt1* double mutants compared to *syt1* null mutants alone (**Figure 8C-8F**), indicating Tomosyn normally reduces both synchronous and asynchronous SV fusion. Similar to the ability of Tomosyn to suppress spontaneous release at wildtype synapses, the elevated mini frequency normally observed in *syt1* mutants is also enhanced 2.8-fold in *tomosyn;syt1* double mutants (**Figure 8G and 8H**). Together, these data indicate Syt1 and Tomosyn regulate evoked and spontaneous SV fusion through independent mechanisms.

Another member of the Synaptotagmin family, Syt7, regulates evoked release by controlling the size and usage of the fusogenic SV pool in Drosophila (Guan et al., 2020). Like *tomosyn^{NA1}*, *Syt7* null mutants (*syt7^{M1}*) display increased quantal content and no change in Ca^{2+} cooperativity, suggesting Syt7 and Tomosyn may restrict SV availability and fusion via a similar mechanism. To test this hypothesis, we generated and characterized *tomosyn^{NA1};;;syt7^{M1}* double mutants. Both evoked release and mini frequency at *syt7^{M1}* mutant NMJs was enhanced by loss of Tomosyn (**Figure 8I-8L**), indicating the two proteins act through independent mechanisms to negatively regulate SV fusion. In addition, increased

evoked release in *tomosyn, syt7* double mutants indicate presynaptic output can still be enhanced beyond that observed in the absence of Tomosyn alone.

We next assayed if Tomosyn inhibition of SV release is Ca^{2+}-sensitive by recording evoked responses across a range of extracellular [Ca^{2+}]. Loss of Tomosyn enhanced release across the entire Ca^{2+} range but did not alter the Ca^{2+} cooperativity of release (**Figure 9A and 9B**). Paired-pulse stimulation in Ca^{2+} conditions that matched first pulse EJC amplitudes between *tomosyn*^{NA1} and controls revealed facilitation was also preserved in the absence of Tomosyn (**Figure 9C and 9D**). At interstimulus intervals (ISI) of 25 and 50 msec, *tomosyn* mutants displayed enhanced paired-pulse facilitation (PPF). At 75 msec ISI, PPF is preserved but not significantly enhanced (**Figure 9E and 9F**). The lack of defective PPF suggests Tomosyn is unlikely to reduce fusogenicity of individual SVs. Given *tomosyn* mutants do not decrease the Ca^{2+} dependence of fusion or PPF, Tomosyn must inhibit SV release through an independent mechanism. Loss of Tomosyn also leads to enhanced synchronous and asynchronous release, together with elevated rates of spontaneous SV fusion. These data indicate Tomosyn controls SV supply in a fusion-mode-independent manner, likely by regulating release site number or SV availability through sequestration of available t-SNAREs.

Tomosyn mutants have more docked SVs at individual release sites

The increased evoked response in *tomosyn* mutants could reflect an increased number of AZs per NMJ, a higher number of docked SVs per AZ, or an increase in individual SV fusogenicity. Given *tomosyn*^{NA1} mutants display enhanced PPF, increased SV fusogenicity is unlikely. To determine if AZ number or SV docking is increased, immunocytochemistry and transmission electron microscopy (TEM) were used to characterize the morphology and ultrastructure of *tomosyn*^{NA1} NMJs. Staining for the AZ scaffold protein Bruchpilot (BRP) revealed AZ number was unchanged at *tomosyn*^{NA1} synapses (**Figure 10A and 10B**). Additionally, BRP abundance at individual AZs was not altered (**Figure 10C**), indicating release site number and AZ scaffold accumulation are not affected. To further probe NMJ morphology, bouton size and number were analyzed in *tomosyn* mutants. Despite a slightly smaller bouton area at Ib NMJs in *tomosyn*^{NA1}, total NMJ area was unchanged due to a mild increase in the number of boutons per NMJ (**Figure 10D-10F**). Is terminals showed no morphological differences from controls (**Figure 10D and 10E**). Immunostaining for Syt1

indicated total SV abundance is not altered in *tomosyn* mutants (**Figure 10G-10H**). Together, these data indicate morphological defects or AZ number does not account for enhanced release in *tomosyn* mutants.

TEM was used to determine whether enhanced SV docking contributes to increased SV release in *tomosyn* mutants. Despite no gross changes to bouton ultrastructure (**Figure 11A**), Ib terminals had a 52% increase in the number of docked SVs per AZ in $tomosyn^{NA1}$ (**Figure 11B and 11C**). Increased docking was observed over the entire length of the AZ, with no change in the absolute fraction of docked SVs at any point along the 400 nm trajectory from the electron dense T-bar center compared to controls (**Figure 11D and 11E**). The average distance between neighboring SVs was also unchanged (**Figure 11F**), suggesting SV clustering is not altered. *Tomosyn* mutants also showed a larger number of SVs within 100 and 150 nm concentric circles positioned over the AZ center (**Figure 11G and 11H**). Average SV diameter (**Figure 11I**) and SV density within the bouton were unchanged (**Figure 11J**), indicating Tomosyn does not affect SV formation or total SV number. Together, these data suggest Tomosyn suppresses release by decreasing SV availability at AZs, with enhanced SV docking occurring in the absence of the protein downstream of increased t-SNARE availability and enhanced SNARE complex formation.

Tomosyn decreases the rate of SV usage during high frequency stimulation

Endogenous activity at larval NMJs is controlled by central pattern generators (CPGs) that trigger intermittent high frequency motoneuron bursting (5-40 Hz) to drive locomotion (Jan and Jan, 1976; Lu et al., 2016; Pulver et al., 2015). To examine how elevated release in *tomosyn* mutants change across different rates of neuronal firing, synaptic output was compared between low (0.33 Hz) and high (10 Hz) frequency stimulation in 2 mM extracellular Ca^{2+}. Consistent with the enhanced single eEJC phenotype, low frequency stimulation (0.33 Hz) resulted in a 4.3-fold increase in the EJC area of the first evoked response, followed by subsequent depression that stabilized at a 1.4-fold increased quantal content per action potential in $tomosyn^{NA1}$ (**Figure 12A and 12B**). At 10 Hz stimulation, *tomosyn* mutant terminals displayed more robust synaptic depression, with quantal content quickly dropping below control levels early in the stimulation train (**Figure 12A and 12B**). Controls NMJs had lower initial quantal content at 10 Hz, and showed a gradual depression in release that was eventually equivalent to synaptic output of $tomosyn^{NA1}$ terminals by the

30th stimulus (**Figure 12C**). The size of the immediately releasable SV pool (IRP), approximated by the cumulative number of quanta released within 30 stimuli, showed no difference between *tomosyn*^{NA1} and controls (**Figure 12D**). However, the depression rate was dramatically enhanced in *tomosyn* mutants (**Figure 12E**), indicating Tomosyn normally restricts release from the IRP. To approximate the size of the larger readily releasable SV pool (RRP) and the SV recycling rate, 10 Hz stimulation was continued for 1500 stimuli to reach steady state where the number of SVs released equals the number of recycled SVs (Thanawala and Regehr, 2016). The recycling rate in *tomosyn*^{NA1} mutants was not significantly different from controls, though the RRP size was increased by 42% (**Figure 12F-12I**). Together these data indicate Tomosyn is required to support sustained release by normally preventing a population of SVs from participating in the fusion cycle during stimulation.

Tomosyn differentially regulates SV release from tonic Ib and phasic Is motoneurons

Tonic Ib and phasic Is motoneurons differ in their ability to sustain release during stimulus trains, with Ib synapses showing continued release and Is terminals displaying high initial P_r and rapid depression (Aponte-Santiago and Littleton, 2020; Lu et al., 2016). Given the phasic release character of *tomosyn* mutant synapses (**Figure 12A-12E**), we examined if Tomosyn normally functions to differentially regulate release from Ib and Is motoneuron populations. To probe endogenous expression of Tomosyn, the GFP variant mClover3 was inserted into the *tomosyn* 13A genomic locus (*tomosyn*$^{13A\text{-}Clover}$) using CRISPR (**Figure 1E**). Immunostaining for Tomosyn$^{13A\text{-}Clover}$ revealed a 2.1-fold enrichment of endogenous Tomosyn in Ib terminals relative to Is (**Figure 13A and 13B**). To determine whether this difference in expression resulted in a functional change in neurotransmitter release between the two classes of motoneurons, optogenetics was used to isolate Ib and Is evoked responses using motoneuron-specific Gal4 drivers to express UAS-Channelrhodopsin2 (Aponte-Santiago et al., 2020; Dawydow et al., 2014; Pérez-Moreno and O'Kane, 2019). Optogenetic stimulation of Ib synapses in *tomosyn*^{NA1} mutants showed a 3.8-fold increase in evoked EJC area (**Figure 13C and 13D**). In contrast, optogenetic stimulation of *tomosyn*^{NA1} Is terminals revealed no differences in evoked output, indicating the enhanced evoked release in *tomosyn* mutants is solely contributed from increased release from Ib terminals. These data indicate higher expression of Tomosyn in Ib motoneurons results in greater intrinsic release suppression.

These motoneuron populations also show stereotyped difference in single AZ P_r, with Is having intrinsically higher P_r than Ib. To determine whether Tomosyn differentially regulates P_r, optical quantal analysis was performed in the *tomosyn*^{FS1} null mutant. This mutant lacks the DsRed reporter cassette found in *tomosyn*^{NA1} and has less background fluorescence during live imaging. To detect single SV release events at individual AZs, a membrane-targeted GCaMP7s was expressed in postsynaptic muscles along with a tagged GluR subunit (GluRIIA-RFP) to identify individual PSDs as previously described (Akbergenova et al., 2018). Nerve stimulation in control animals demonstrated Is motoneurons have a 2.4-fold higher average AZ P_r (0.17±0.007) compared to Ib motoneurons (0.07±0.004). In contrast, *tomosyn*^{FS1} mutants displayed higher P_r at Ib AZs than Is due to increased Ib P_r and no effect on Is P_r (**Figure 13E-13G**). Together, these data indicate Tomosyn suppresses release from tonic synapses and contributes to the intrinsic release differences between these motoneuron subclasses. Loss of Tomosyn in Ib terminals changes both the initial P_r and short-term depression properties so that they now display phasic release similar to their Is counterparts.

Tomosyn is required for presynaptic homeostatic potentiation

Reductions in postsynaptic GluR function at Drosophila NMJs trigger a rapid and robust increase in presynaptic quantal content that homeostatically compensates for decreased quantal size (Davis et al., 1998; Frank et al., 2006; Li et al., 2018; Petersen et al., 1997). Given Tomosyn is a key regulator of quantal content, and prior data suggest PHP is more robust at tonic Ib synapses (Newman et al., 2017), we assayed if Tomosyn is required for PHP in tonic motoneurons. An allosteric inhibitor of Drosophila GluRs (Gyki) was used to acutely reduce quantal size and induce PHP as previously described (Nair et al., 2020). Following addition of Gyki into the extracellular saline, quantal size as measured by mini amplitude was reduced in both control and *tomosyn*^{NA1} mutants (**Figure 14A-14C**). Mini frequency was not significantly changed following Gyki application, indicating spontaneous fusion events remained detectable (**Figure 15A and 15B**). Control animals compensated for the reduction in quantal size with a 62% increase in quantal content that preserved the original evoked response amplitude (**Figure 14D-14F**). In contrast, *tomosyn*^{NA1} NMJs showed no significant enhancement in quantal content after Gyki application, indicating PHP expression is impaired. Loss of PHP in *tomosyn* could result from a general occlusion secondary to

elevated baseline release, or Tomosyn could be a key effector for PHP with post-translational modification decreasing its inhibitory function. To test if impaired PHP in *tomosyn* mutants is due to occlusion, the quantal content of potentiated NMJs in 0.35 mM extracellular [Ca^{2+}] was compared to non-potentiated NMJs at 1.5 mM [Ca^{2+}]. In elevated Ca^{2+}, quantal content was greater than after Gyki-induced potentiation in low Ca^{2+} for controls (46% increase) and *tomosyn*^{NA1} (61% increase), indicating lack of potentiation in *tomosyn* mutants is not due to release saturation (**Figure 15C**). Together with the observation that *tomosyn, syt7* double mutants display even higher levels of evoked release than *tomosyn* mutants alone in low Ca^{2+} (**Figure 8J**), these data suggest Tomosyn is required for normal expression of Gyki-induced PHP and represents a key effector for enhancing presynaptic output during this form of plasticity.

The two motoneuron subclasses also differ in their ability to express PHP, with tonic Ib neurons showing more robust PHP in *GluRIIA* mutants (Newman et al., 2017). To determine whether differential Tomosyn expression in Ib and Is motoneurons affects expression of Gyki-induced PHP, optical quantal mapping was used to monitor AZ P_r at individual release sites in Ib and Is terminals before and after drug application. Because Gyki reduces the fluorescent change (ΔF) from quantal release by decreasing postsynaptic Ca^{2+} influx from GluRs (**Figure 15D**), transgenic animals expressing the more sensitive GCaMP variant GCaMP8s (Zhang et al., 2020) fused to a myristoylation domain were generated to ensure SV release events could still be detected after Gyki application. Control Ib terminals showed a rapid and robust 1.8-fold increase in average AZ P_r 15 minutes after Gyki incubation (**Figure 16A-16D**). Enhanced SV release occurred across the AZ population and was independent of initial AZ P_r. In addition, a population of previously silent AZs were recruited during evoked stimulation following Gyki application (**Figure 16A**). These data indicate PHP following acute GluR impairment is mediated by a compensatory increase in single AZ P_r across the majority of the AZ population, as well by recruitment of previously silent AZs. In contrast to the robust effect at Ib synapses, Is terminals showed no significant change in AZ P_r or any recruitment of silent AZs following Gyki application (**Figure 16A, 16E-16G**), indicating this form of PHP is predominantly expressed from Ib motoneurons. *Tomosyn* mutants showed no significant increase in AZ P_r at either Ib or Is terminals following Gyki application (**Figure 16A-16G**). Together, these data indicate Gyki-induced PHP is Tomosyn-dependent and occurs exclusively at tonic Ib terminals. Loss of tomosyn

generates synaptic responses and a lack of PHP similar to that observed in phasic Is neurons, indicating Tomosyn levels represent a key presynaptic mechanism for generating tonic versus phasic presynaptic output.

2.3 Discussion

The findings reported here indicate the conserved presynaptic release suppressor Tomosyn has a key function in setting presynaptic output and plasticity properties for a tonic/phasic pair of motoneurons that co-innervate Drosophila larval muscles. CRISPR-generated mutations in the sole Drosophila *tomosyn* locus revealed synchronous, asynchronous and spontaneous SV release are all elevated in the absence of the protein. While single evoked responses were enhanced in the absence of Tomosyn, rapid depression of release was observed during train stimulation, suggesting loss of Tomosyn biases synapses toward a more phasic SV release pattern. To directly test whether Tomosyn plays a unique role in tonic synapses, tonic Ib and phasic Is motoneurons were separately stimulated using optogenetics to measure their isolated contributions. These experiments revealed a dramatic 4-fold increase in evoked output in Ib neurons with no change to Is release. Optical quantal analysis confirmed the Ib specific effect of Tomosyn and demonstrated enhanced evoked response in *tomosyn* null mutants is due to higher intrinsic P_r across the entire AZ population of this tonic population. Quantitative confocal imaging of endogenously-tagged Tomosyn indicated a near absence the protein at Is terminals, consistent with Tomosyn's exclusive role in regulating Ib release. These data argue the intrinsically high P_r and rapid depression normally found in Is motoneurons is due in part to a lack of Tomosyn inhibition of SV usage at phasic synapses. High frequency stimulation experiments demonstrate Tomosyn does not regulate the size of the immediately releasable SV pool (IRP) but rather regulates IRP usage to ensure sustained availability of SVs during prolonged stimulation, as the IRP is strongly biased towards early release in *tomosyn* nulls. We propose a model where Drosophila synapses are phasic by default, with tonic sustained release requiring higher expression of Tomosyn to create a fusion bottleneck that enables extended periods of stable release by slowing the rate of SV usage.

How Tomosyn normally suppresses release has been a point of contention in the field (Sakisaka et al., 2008; Yamamoto et al., 2010; Yizhar et al., 2004, 2007). The most widely hypothesized mechanism is that Tomosyn competes with the SV v-SNARE Syb2 for binding

to t-SNAREs. By forming fusion-incompetent SNARE complexes containing Tomosyn/Syx1/SNAP-25 that must be disassembled by NSF, a pool of t-SNAREs is kept in reserve that can be mobilized by inactivating or degrading Tomosyn. Western blot measurements demonstrate enhanced SNARE complex formation in Drosophila *tomosyn* null mutants, supporting the model that Tomosyn's SNARE domain acts as a canonical decoy SNARE in Drosophila to inhibit productive SNARE complex assembly. Expression of the Tomosyn scaffold alone also failed to rescue the null phenotype, while overexpression of the scaffold had no effect on evoked release. As such, these data indicate that while the scaffold is required for full Tomosyn function, it does not directly inhibit fusion. Our observations are consistent with the mechanism proposed in *C. elegans,* but differ from that suggested in mammalian cultured cells (Burdina et al., 2011; Yamamoto et al., 2010; Yizhar et al., 2007). We also observed that expression of the Tomosyn SNARE domain alone partially rescues the *tomosyn* null phenotype, demonstrating Tomosyn's inhibitory function maps to the SNARE motif. Work in mammalian cultured neurons indicated the Tomosyn scaffold binds Syt1 to inhibit Ca^{2+}-dependent fusion. However, *tomosyn/syt1* double mutants reveal Tomosyn suppresses release independent of Syt1 in Drosophila, arguing the scaffold must serve a function that enhances the inhibitory activity of the SNARE domain independent of Syt1. To test whether the scaffold regulates SNARE localization to support efficient inhibition of release, immunohistochemistry was used to determine the localization of full-length and truncated Tomosyn rescue constructs. Drosophila Tomosyn co-localizes with SVs, as has been reported in *C. elegans* and mammals (Geerts et al., 2017; McEwen et al., 2006). The Tomosyn SNARE motif mislocalized without the WD40 scaffold, arguing this region indirectly supports Tomosyn's inhibitory activity by ensuring proper localization of the SNARE domain so it can compete with SV Syb2 v-SNARE binding. Consistent with functional conservation, human Tomosyn rescued the elevated evoked and spontaneous release at *tomosyn* null mutant NMJs. In addition, overexpression of either Drosophila or human Tomosyn in a wildtype background decreased release, indicating presynaptic output is bi-directionally controlled by Tomosyn levels.

In addition to regulation of intrinsic release differences between tonic and phasic motoneurons, we also found that Tomosyn regulates presynaptic homeostatic potentiation (PHP), a form of synaptic plasticity well described at Drosophila NMJs (Böhme et al., 2019; Frank, 2014; Genç and Davis, 2019; Goel et al., 2019; Gratz et al., 2019). When GluR

function is impaired, the presynaptic terminal upregulates P_r to compensate for reduced evoked response amplitude. Inducing PHP with the allosteric GluR inhibitor Gyki (Nair et al., 2020) revealed Tomosyn is required for expression of this form of acute PHP. Unlike the GluR pore blocker PhTx, expression of Gyki-induced PHP results in enhanced short-term facilitation at the NMJ, which may reflect a shift in the relative contribution of Ib/Is plasticity to the evoked response during PHP expression (Nair et al., 2020). Consistently, defective PHP expression in *tomosyn* nulls is explained by impaired Ib potentiation. Given the strength of Tomosyn inhibition in Ib, relieving this neuron of Tomosyn inhibition would generate up to a 4-fold enhancement in evoked release, more than sufficient to compensate for a 2-fold reduction in evoked response size from two equally contributing motoneurons. Indeed, AZ P_r mapping revealed Ib synapses potentiated 1.8-fold in the presence of Gyki, whereas Is showed no AZ P_r enhancement. Although future studies will be required to determine the molecular pathway by which Tomosyn mediates PHP expression, prior studies have linked Tomosyn function to several PKA-dependent plasticity pathways (Baba et al., 2005; Ben-Simon et al., 2015; Chen et al., 2011). Phosphorylation of Tomosyn by PKA reduces it SNARE binding properties and partially inactivates the protein. Given Gyki-induced PHP expression requires presynaptic protein kinase D (PKD) (Nair et al., 2020), an attractive hypothesis is that PKD directly phosphorylates Tomosyn to reduce its ability to inhibit SNARE complex formation. This would mimic a *tomosyn* null phenotype, promoting SV docking and enhanced SV availability by increasing the number of free t-SNAREs. The overall effect would be to increase the apparent P_r at individual AZs as we observed with quantal imaging by generating more SVs that are available to respond to presynaptic Ca^{2+} influx.

Despite Tomosyn's importance in regulating release character between tonic and phasic terminals of the larval NMJ, *tomosyn* null mutants are viable into the adult stage. Given Tomosyn is dispensable for viability, the entire range of Tomosyn expression can be used by distinct populations of neurons *in vivo*. Consistently, Tomosyn protein expression is nearly absent from phasic Is terminals, with expression only observed in tonic Ib synapses. Ib terminals display a shift toward phasic release in *tomosyn* null mutants, with no apparent effect on Is, representing a collapse of synaptic diversity in the absence of the protein. Similar to Tomosyn, null mutants of Syt7 are viable with only mild behavioral abnormalities, yet show dramatically enlarged evoked responses at the larval NMJ (Guan et al., 2020).

Tomosyn/*syt7* double mutants show even greater enhanced release, arguing multiple non-essential release components may independently fine tune release between neuronal subtypes. Together, these experiments demonstrate Tomosyn is a highly conserved release inhibitor that varies in expression between distinct neuronal subtypes to regulate intrinsic P_r and plasticity, providing a potent mechanism to control presynaptic diversity across the nervous system.

2.4 Materials and Methods

Fly stocks

Drosophila melanogaster were cultured on standard medium between 22 and 25°C. 3rd instar larvae were used for all *in vivo* and immunostaining experiments. Adult brain extracts were used for western blot analysis. Males were preferentially used in this study to facilitate genetic crossing schemes and avoid sex-specific phenotypic differences. *Tomosyn* null mutants used in the study include *tomosyn*^{NA1} (this study)**,** *tomosyn*^{FS1} (this study), and Df(1)ED7161 (Bloomington Drosophila Stock Center (BDSC) #9217). Strains used for rescue experiments include *elav*^{C155}-GAL4 (BDSC#8765), UAS-Tom13A-6xMyc (this study), UAS-Tom13A-ΔSNARE-6xMyc (this study), UAS-Tom13B-6xMyc (this study), UAS-Tom13B-ΔSNARE-6xMyc (this study), UAS-4xMyc-TomSNARE (this study), and UAS-HumanTom1-6xMyc (this study). Double mutant experiments were performed with *syt1*^{AD4} (DiAntonio and Schwarz, 1994), *syt1*^{N13} (Littleton et al., 1993), *syt7* control (Guan et al., 2020), and *syt7*^{M1} (Guan et al., 2020). For single neuron optical stimulation experiments, the Ib-specific Gal4 driver GMR94G06 (BDSC #40701) and the Is-specific Gal4 driver GMR27F01 (BDSC #49227) was used to drive expression of UAS-ChR2-T159C (Dawydow et al., 2014) in Ib or Is motoneurons innervating larval muscle 1. For AZ P_r mapping experiments, Mef2-Gal4 (BDSC #27390), 44H10-LexA (provided by Gerry Rubin), LexAOp-myr-jGCaMP7S (this study), UAS-myr-jGCaMP8s (this study), GluRIIA-RFP (provided by Stephan Sigrist), and GluRIIB-GFP (provided by Stephan Sigrist) transgenic lines were used.

Genome engineering and UAS/LexA constructs

To generate *tomosyn*^{NA1}, two guide RNAs (gRNAs) flanking the *tomosyn* locus were selected using the CRISPR Optimal Target Finder (Gratz et al., 2014). These gRNAs were

fused with the pCFD4 expression vector (Addgene #49411) (Port et al., 2014) according to the Gibson assembly protocol using NEBuilder HighFidelity DNA Assembly Cloning Kit (E5520). Gibson assembly was used to generate a donor construct encoding a floxed P3>DsRed reporter cassette (Addgene #51434) flanked with homology arms directly outside of the *tomosyn* gene isolated using PCR. These constructs were co-injected into vasa-Cas9 embryos (BDSC #56552) and DsRed positive transformants were selected by BestGene Inc (Chino Hills, CA, USA). To generate $tomosyn^{FS1}$, the pCFD4 gRNA construct was injected without a donor, and frame shift mutants were identified by PCR and sequencing. The Cas9 chromosome was removed from both lines by backcrossing to $w^{-/-}$ (BDSC #3605). For both $tomosyn^{NA1}$ and $tomosyn^{FS1}$, unmodified progeny of the CRISPR-injected embryos were used as genetic background controls. To generate $tomosyn^{13A\text{-}Clover}$, gRNAs targeting exon13A of *tomosyn* were cloned into pCFD5 (Addgene #73914) (Port and Bullock, 2016) and co-injected with a donor plasmid by BestGene Inc. The donor was made by amplifying homology arms from the genome by PCR and fusing them by Gibson assembly with a cDNA coding for 6xHis-mClover3 (Addgene #74252) (Bajar et al., 2016) in frame with exon 13A. To generate rescue constructs, the relevant cDNAs were synthesized by GENEWIZ, Inc (South Plainfield, NJ, USA) and cloned into pBid-UASc (Addgene #35200) (Wang et al., 2012) using EcoRI and XbaI. These constructs were injected into embryos containing the VK27 attP acceptor site by BestGene, Inc (BDSC #9744). Positive transformants were selected and balanced. The fluorescent Ca^{2+} sensor GCaMP7s was tethered to the plasma membrane with an N-terminal myristoylation (myr) sequence. A cDNA encoding the first 90 amino acids of Src64b, containing a myristoylation target sequence, was PCR amplified from the pBid-UAS-myr plasmid (Akbergenova et al., 2018) and fused with the GCaMP7s cDNA (Addgene # 104463) (Dana et al., 2019) and EcoRI/XbaI digested pBid-LexA (a gift from Brian McCabe) using Gibson assembly. pBid-UAS-myr-jGCaMP8s was made by fusing a GCaMP8s cDNA (Addgene # 162374) (Zhang et al., 2020) with BglII/XbaI digested pBid-UAS-myr using Gibson assembly. These constructs were injected by BestGene, Inc into embryos containing the attP2 acceptor site and positive transformants were isolated (BDSC #8622).

Bioinformatics

NCBI BLAST was used to identify homologs of Drosophila nSyb and Tomosyn in *C.*

elegans, *N. vectensis*, *M. lignano, O. sinensis, C. teleta, A. planci, D. rerio*, *M. musculus*, and *H. sapiens*. The C-terminal tail of *S. cerevisiase* Sro7 was used as the outgroup. UCSC Genome Browser's Cons 124 feature was used to assess sequence conservation with Drosophila *tomosyn* as the reference sequence (htpp://genome.ucsc.edu). The Póle Rhône-Alpes de Bioinformatique (PRABI; https://npsa-prabi.ibcp.fr) coiled-coil prediction tool was used to identify the C-terminal SNARE domain of each protein and the BLOSUM62 algorithm of the Matlab 2020a seqpdist function was used to create sequence alignment. Phylogenetic trees were generated with the seqlinkage Matlab function.

Protein sequences used for alignment and phylogenetic tree construction:

Protein	Species	NCBI accession number
Tomosyn	*N. vectensis*	EDO30312.1
	M. lignano	PAA82513.1
	O. sinensis	XP_036368981.1
	C. teleta	ELU03639.1
	A. planci	XP_022100438.1
	D. rerio	XP_021334414.1
	M. musculus	XP_006512991.1
	H. sapiens	NP_001121187.1
	D. melanogaster	NP_001162735.1
	C. elegans	AAX89146.1
Synaptobrevin/VAMP2	*N. vectensis*	XP_001634446.2
	M. lignano	PAA92592.1
	O. sinensis	XP_029648798.1
	C. teleta	ELU12629.1
	A. planci	XP_022085538.1
	D. rerio	NP_956299.1
	M. musculus	NP_033523.1
	H. sapiens	NP_001317054.1
	D. melanogaster	NP_477058.1
	C. elegans	NP_001379956.1

	S. cerevisiae	NP_594120.1
Sro7	*S. cerevisiae*	NP_015357.1

Western blot analysis and Immunocytochemistry

Western blotting of adult head lysates (ten heads per/lane) was performed using standard laboratory procedures with mouse anti-Syx1a (8C3, 1:1000; Developmental Studies Hybridoma Bank (DSHB, Iowa City, IA)) anti-Myc (GeneTex: GTX29106, 1:1000) and mouse anti-Tub (Sigma: T5168, 1:1,000,000). The boiling step was omitted to preserve the 7S complex. IR Dye 680LT-conjugated goat anti-mouse (1:10,000, LICOR; 926-68020) was used as the secondary antibody. Visualization was performed with a LI-COR Odyssey Imaging System (LI-COR Biosciences, Lincoln, MA, USA) and analysis was performed using the Plot Lanes and Measure Areas function of FIJI image analysis software (Schindelin et al., 2012).

Immunostaining for AZ and bouton counting was performed on wandering 3rd instar larvae dissected in Ca^{2+}-free HL3.1 and fixed for 7 min in Ca^{2+}-free HL3.1 containing 4% PFA. Larvae were blocked and permeabilized for 1 hr in PBS containing 0.1% Triton X-100, 2.5% NGS, 2.5% BSA and 0.1% sodium azide. Larvae were incubated overnight with primary antibody at 4°C and 2 hr in secondary antibody at room temperature. Samples were mounted on slides with Vectashield (Vector Laboratories, Burlingame, CA). Antibodies used for immunolabeling were: rabbit anti-GFP at 1:1000 (ab6556; Abcam, Cambridge, UK), mouse anti-BRP at 1:500 (Nc82; DSHB), mouse anti-Synapsin at 1:500 (3C11; DSHB), rabbit anti-Myc at 1:500 (GTX29106; GeneTex, Irvine, CA, USA), rabbit anti-Syt1 (gift of Noreen Reist) at 1:500, and DyLight 649 conjugated anti-HRP at 1:1000 (#123-605-021; Jackson Immuno Research, West Grove, PA, USA). Secondary antibodies for morphology and co-localization experiments were used at 1:500: goat anti-rabbit Alexa Fluor 488-conjugated antibody (A-11008; Thermofisher) and goat anti-mouse Alexa Fluor 546-conjugated antibody (A-11030; ThermoFisher). The secondary antibody used for anti-GFP staining was goat anti-rabbit Alexa Flour 488-conjugated antibody (A-11008; Thermofisher) used at 1:500. Immunoreactive proteins were imaged at segments A3 and A4 of muscle fiber 4 for all experiments, except for anti-GFP staining, which was imaged at muscles 6/7. Images were acquired on a PerkinElmer Ultraview Vox spinning disk confocal microscope system using a 63x oil immersion objective. Ib and Is terminals were identified based on bouton and

NMJ size, with Is having characteristically smaller boutons and total NMJ size. NMJ morphology, staining intensity, and co-localization between channels were analyzed using Volocity 6.3.1 software.

Electrophysiology

Postsynaptic currents from the indicated genotypes were recorded from 3rd instar larvae at muscle fiber 6 (unless otherwise noted) of segment A4 using two-electrode voltage clamp with a −80 mV holding potential in HL3.1 saline solution (in mM, 70 NaCl, 5 KCl, 10 NaHCO3, 4 MgCl2, 5 trehalose, 115 sucrose, 5 HEPES, pH 7.18) as previously described (Jorquera et al., 2012). Final [Ca^{2+}] was adjusted to the level indicated. All electrophysiology experiments were performed at room temperature. Inward currents recorded during TEVC are labeled on a reverse axis in the figures for simplicity. Asynchronous release contribution was approximated by fitting the weighted average of two logarithmic regressions with separate time constants to the normalized cumulative charge transfer of evoked responses as previously described (Jorquera et al., 2012). The Ca^{2+} cooperativity of release was determined from the Hill coefficient of a 4-parameter logistic regression of evoked responses fit to the linear range (0.1 to 0.75 mM Ca^{2+}). Data acquisition and analysis was performed using Axoscope 9.0 and Clampfit 9.0 software (Molecular Devices, Sunnyvale, CA, USA). mEJCs were analyzed with Mini Analysis software 6.0.3 (Synaptosoft, Decatur, GA, USA). Motor nerves innervating the musculature were severed and placed into a suction electrode. Action potential stimulation was applied at 0.33 Hz (unless indicated) using a programmable stimulator (Master8, AMPI; Jerusalem, Israel).

Optogenetic experiments were performed in the same way with the following modifications. Postsynaptic currents were recorded from 3rd instar larvae at segment A4 of muscle fiber 1. Evoked postsynaptic currents were generated using the Master8 stimulator and an LED driver (LED-D1B, THORLABS, Newton, NJ, USA) to generate 470 nm light pulses from an attached LED (M470F3, THORLABS, Newton, NJ, USA). Ib and Is currents were separately evoked by driving expression of channelrhodopsin (UAS-ChR2-T159C, provided by Robert Kittel) under the control of GMR94G06-Gal4 (BDSC #40701) or GMR27F01-Gal4 (BDSC# 49227), respectively.

Gyki application and PHP analysis

Gyki was diluted fresh each day in HL3.1 to a final concentration of 10 uM. The final Ca^{2+} concentration was adjusted to the level indicated. The Gyki solution was bath applied to fully dissected larvae for 15 minutes as previously described (Nair et al., 2020). Subsequent recordings were performed in the continued presence of bath applied Gyki.

Optical AZ P_r Mapping

AZ P_r mapping experiments were performed on a Zeiss Axio Imager equipped with a spinning-disk confocal head (CSU-X1; Yokagawa, Japan) and ImagEM X2 EM-CCD camera (Hamamatsu, Hamamatsu City, Japan) as previously described (Akbergenova et al., 2018). For P_r mapping of *tomosyn*^{FS1}, myristoylated-GCaMP7s was expressed in larval muscles with GMR44H10-LexA (provided by Gerald Rubin). Individual PSDs were visualized at segments A2-A4 of muscle fiber 4 by expression of GluRIIA-RFP and GluRIIB-GFP (hereafter referred to as GluR) under control of their endogenous promoters (provided by Stephan Sigrist). An Olympus LUMFL N 60X objective with a 1.10 NA was used to acquire GCaMP7s imaging data at 8 Hz. 3rd instar larvae were dissected in Ca^{2+}-free HL3 containing 20 mM $MgCl_2$. After dissection, preparations were maintained in HL3 with 20 mM $MgCl_2$ and 1.0 mM Ca^{2+} for 5 min. A dual channel multiplane stack was imaged at the beginning of each experiment to identify GluR-positive PSDs. Single focal plane videos were then recorded while motoneurons innervating the muscles were stimulated with a suction electrode at 0.3 Hz for 3 minutes. GluR PSD position was re-imaged every 25 sec during experimentation. The dual channel stack was merged with single plane images using the max intensity projection algorithm from Volocity 6.3.1 software. The position of all GluR PSDs was then added to the myr-GCaMP7s stimulation video. GluR positive PSDs were detected automatically using the spot finding function of Volocity and equal size ROIs were assigned to the PSD population. In cases where the software failed to label visible GluR PSDs, ROIs were added manually. GCaMP7s peak flashes were detected and assigned to ROIs based on centroid proximity. Evoked events were identified as frames with three or more simultaneous GCaMP events across the arbor. The time and location of Ca^{2+} events were imported into Excel or Matlab for further analysis. Evoked GCaMP events per ROI were divided by the number of stimulations to calculate AZ P_r.

AZ P_r experiments with Gyki were performed in the same way with the following modifications. Mef2-Gal4 (BDSC #27390) was used to drive expression of UAS-myr-

GCaMP8s in larval muscles. Dissected preparations were maintained in HL3 containing 10 mM $MgCl_2$ and 0.5 mM Ca^{2+} and imaged at muscle fibers 6/7. The HL3 solution was exchanged for an identical solution containing 10 uM Gyki and incubated for 15 minutes. A second imaging session was recorded at each NMJ after Gyki incubation. AZ locations were identified by labeling peaks for all events and regions of highest peak densities were assigned as ROIs. Release events were assigned to ROIs using the centroid proximity algorithm in Volocity 6.3.1.

Electron microscopy

Tomosyn^{NA1} and control 3rd instar larvae were dissected in Ca^{2+}-free HL3 saline and fixed in 1% glutaraldehyde, 4% formaldehyde and 0.1 M sodium cacodylate buffered saline (CBS) with 1 mM magnesium chloride for 10 min at room temperature as previously described (Akbergenova and Bykhovskaia, 2009). After fixative exchange, samples were microwaved in a BioWave Pro Pelco (Ted Pella, Inc, Redding, CA, USA) using the following fixation protocol: (1) 100W 1 min, (2) 1 min off, (3) 100W 1 min, (4) 300W 20 secs, (5) 20 secs off, (6) 300W 20 secs. Steps 4–6 were repeated twice more. Samples were then washed in CBS and stained *en bloc* for 30 min in 1% osmium tetroxide. Following another CBS wash, samples were stained *en bloc* for 30 mins in 2% uranyl acetate and briefly incubated in sequentially anhydrous solutions of ethanol and then pure anhydrous acetone. Epoxy resin infiltration was performed by incubating the dehydrated samples in a series of acetone/epoxy mixtures, with the acetone percentage decreasing in each successive step (Embed 812; Electron Microscopy Sciences). Thin sections (40–50 nm) were collected on Formvar/carbon-coated copper slot grids and stained on grid for ~5 min with lead citrate. Sections were imaged at 49,000 × magnification at 120 kV using a Tecnai G2 electron microscope (FEI, Hillsboro, OR, USA) equipped with a charge-coupled device camera (Gatan, Pleasanton, CA, USA). Micrographs of type Ib boutons from segment 4 of muscle fibers 6/7 were analyzed using Volocity 6.3.1. SV centers were annotated as points, T-bar bases as single pixel ROIs, and electron densities as contoured lines. Distances between these features were calculated using the Measure Distance function to determine SV spacing, SV number, and docked SV number (SVs with centers <50 nm to the electron dense AZ).

Quantification and Statistics

Statistical analysis and graphing were performed with GraphPad Prism (San Diego, CA, USA). In two cases, outliers were identified and removed using the default settings of the Identify Outlier function in Prism9 (mini frequency of elav-Gal4,*tomosyn*^{NA1} in Fig. 2Q, excluded mini frequency was 23.3 Hz; mini frequency of *syt7*^{M1} in Fig. 4M, excluded mini frequency was 6.20 Hz). Electrophysiological traces were generated using the plot function in Matlab R2020A (MathWorks, Natick, MA, USA). Statistical significance was determined using Student's *t* test for comparisons between two groups, or a One-way ANOVA followed by Tukey's multiple comparisons test for comparisons between three or more groups unless noted. In the figures, the center of each distribution is plotted as the median value and reported in the figure legends as the median, mean ± SEM, *n*. In the main text, the centers and *n* are reported as mean ± SEM, *n*. In all cases *n* represents the number of individual NMJs analyzed unless otherwise noted. The number of larvae used per group in each experiment is indicated in the figure legends. Asterisks in the figures denote p-values of: *, $p \leq 0.05$; **, $p \leq 0.01$; ***, $p \leq 0.001$; and ****, $p \leq 0.0001$.

Figures

Figure 1

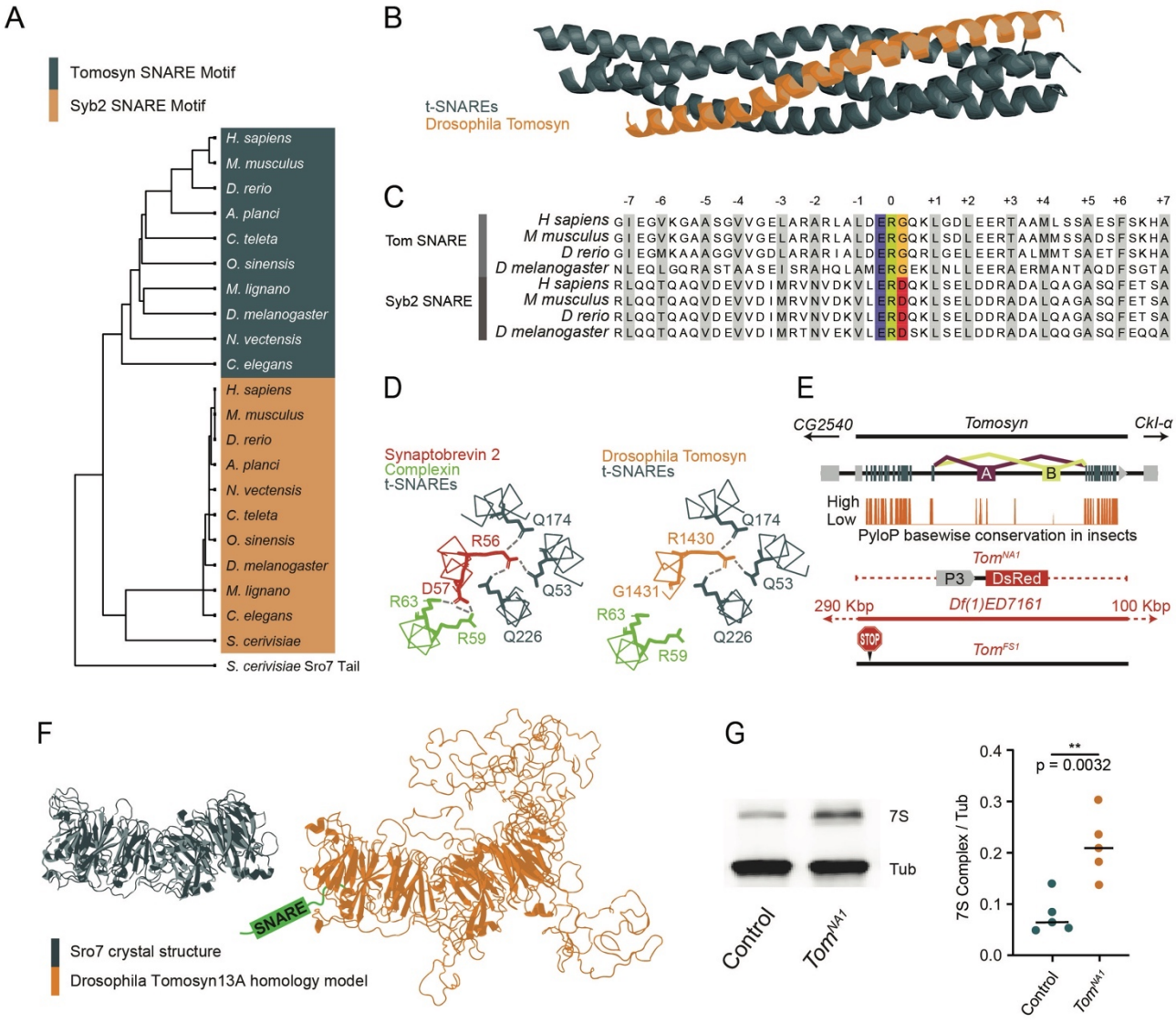
A
Tomosyn SNARE Motif
Syb2 SNARE Motif
H. sapiens
M. musculus
D. rerio
A. planci
C. teleta
O. sinensis
M. lignano
D. melanogaster
N. vectensis
C. elegans
H. sapiens
M. musculus
D. rerio
A. planci
N. vectensis
C. teleta
O. sinensis
D. melanogaster
M. lignano
C. elegans
S. cerivisiae
S. cerivisiae Sro7 Tail
B
t-SNAREs
Drosophila Tomosyn
C
-7 -6 -5 -4 -3 -2 -1 0 +1 +2 +3 +4 +5 +6 +7
Tom SNARE
Syb2 SNARE
H sapiens GIEGVKGAASGVVGELARARLALDERGQKLGDLEERTAAMLSSAESFSKHA
M musculus GIEGVKGAASGVVGELARARLALDERGQKLSDLEERTAAMMSSADSFSKHA
D rerio GIEGMKAAAGGVVGDLARARIALDERGQRLGELEERTALMMTSAETFSKHA
D melanogaster NLEQLGQRASTAASEISRAHQLAMERGEKLNLLEERAERMANTAQDFSGTA
H sapiens RLQQTQAQVDEVVDIMRVNVDKVLERDQKLSELDDRADALQAGASQFETSA
M musculus RLQQTQAQVDEVVDIMRVNVDKVLERDQKLSELDDRADALQAGASQFETSA
D rerio RLQQTQAQVDEVVDIMRVNVDKVLERDQKLSELDDRADALQAGASQFETSA
D melanogaster RLQQTQAQVDEVVDIMRTNVEKVLERDSKLSELDDRADALQQGASQFEQQA
D
Synaptobrevin 2
Complexin
t-SNAREs
Q174
R56
Q53
D57
R63
R59
Q226
Drosophila Tomosyn
t-SNAREs
Q174
R1430
Q53
G1431
R63
R59
Q226
E
CG2540
Tomosyn
CkI-α
A
B
High
Low
PyloP basewise conservation in insects
Tom^NA1
P3
DsRed
290 Kbp
Df(1)ED7161
100 Kbp
STOP
Tom^FS1
F
SNARE
Sro7 crystal structure
Drosophila Tomosyn13A homology model
G
7S
Tub
Control
Tom^NA1
**
p = 0.0032
7S Complex / Tub
0.4
0.3
0.2
0.1
0.0
Control
Tom^NA1

Figure 1. Generation of mutations in the conserved Drosophila Tomosyn homolog

(A) BLOSUM62 alignment tree of Tomosyn SNARE motifs and Syb2 SNARE motifs across the indicated species. The C-terminal tail of *Saccharomyces cerevisiae* Sro7 was used as an outgroup. (B) Homology model of the Drosophila Tomosyn SNARE motif in complex with the Syx1A and SNAP-25 t-SNAREs. (C) Sequence alignment between the Syb2 SNARE sequence and the Tomosyn SNARE motif from humans (*H sapiens*), mouse (*M musculus*), zebrafish (*D rerio*), and Drosophila (*D melanogaster*). (D) Transverse section through a model of the SNARE bundle indicating the Syb2 complex binds Complexin, in contrast to the Tomosyn/t-SNARE complex (adapted from (Pobbati et al., 2004). (E) Genomic structure of Drosophila *tomosyn* shows mutually exclusive splicing at coding exon 13 (top). Basewise conservation of the *tomosyn* gene across insect genomes using PhyloP (middle). Diagram of *tomosyn* CRIPSR mutants generated in this study, including $tomosyn^{NA1}$ that replaces the locus with a DsRed cassette and $tomosyn^{FS1}$ that induces an early frameshift stop codon. A deficiency (*Df(1)ED7161*) spanning the *tomosyn* locus is also shown. (F) Structure of the *Saccharomyces cerevisiae* L(2)GL scaffold protein Sro7 (left, adapted from (Hattendorf et al., 2007) and iterative homology model of Drosophila Tomosyn13A (right, adapted from (Williams et al., 2011). (G) Representative Western blot of adult brain lysates stained with anti-Syx1A to label the 7S SNARE complex and anti-Tubulin as a loading control. The ratio of 7S complex/Tubulin intensity for control (0.06528, 0.07891 ± 0.01658, $n = 5$ samples, 10 brains per sample) and $tomosyn^{NA1}$ (0.2082, 0.2127 ± 0.06183, $n = 5$ samples, 10 brains per sample; Student's t test, $p = 0.0032$) is shown on the right. The median is plotted in this and all remaining figures. Statistical data is reported as the median, mean ± SEM for this and all other figures.

Figure 2

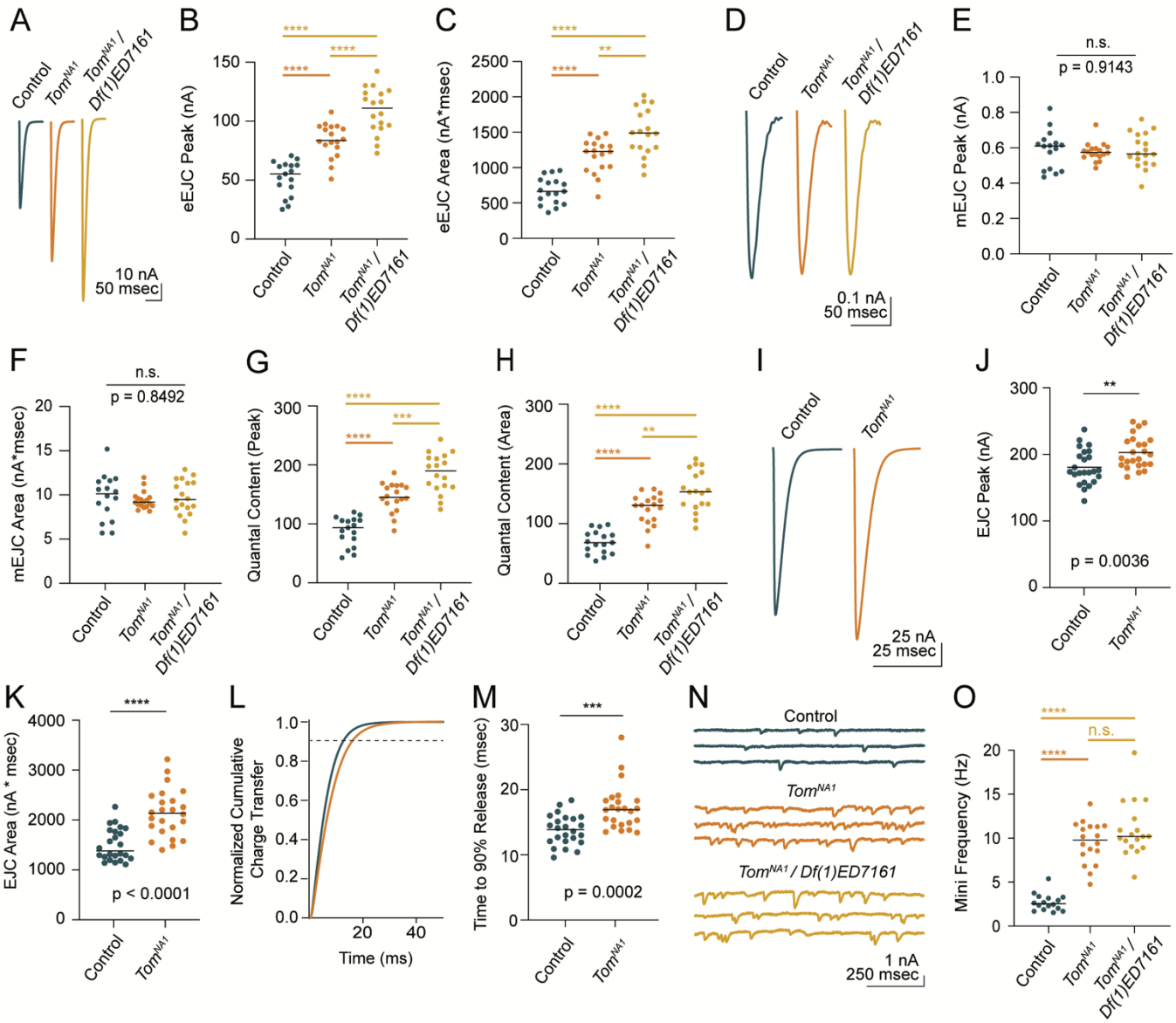
A
Control
Tom^NA1
Tom^NA1 / Df(1)ED7161
10 nA
50 msec
B
eEJC Peak (nA)
****
****
****
Control
Tom^NA1
Tom^NA1 / Df(1)ED7161
C
eEJC Area (nA*msec)
****
**
****
D
0.1 nA
50 msec
E
mEJC Peak (nA)
n.s.
p = 0.9143
F
mEJC Area (nA*msec)
n.s.
p = 0.8492
G
Quantal Content (Peak)
H
Quantal Content (Area)
I
25 nA
25 msec
J
EJC Peak (nA)
**
p = 0.0036
K
EJC Area (nA * msec)
****
p < 0.0001
L
Normalized Cumulative Charge Transfer
Time (ms)
M
Time to 90% Release (msec)
***
p = 0.0002
N
Tom^NA1 / Df(1)ED7161
1 nA
250 msec
O
Mini Frequency (Hz)
****
n.s.
****

Figure 2. *Tomosyn* mutants show elevated evoked and spontaneous release

(A) Average evoked eEJC traces in 0.3 mM Ca^{2+} from the indicated genotypes. (B) Quantification of average eEJC peak amplitude (nA) per NMJ in 0.3 mM Ca^{2+} (control: 55.3, 51.78 ± 3.522, n = 17; *tomosyn*^{NA1}: 83.74, 83.74 ± 3.378, n = 18; *tomosyn*^{NA1}*/Df(1)ED7161*: 111.0, 108.8 ± 4.578, n = 18; $p < 0.0001$; ≥ 10 larvae per group) (C) Quantification of average eEJC area (nA*msec) per NMJ in 0.3 mM Ca^{2+} (control: 663.2, 670.7 ± 45.60, n = 17; *tomosyn*^{NA1}: 1228, 1167 ± 56.66, n = 18; *tomosyn*^{NA1}*/Df(1)ED7161*: 1488, 1499 ± 78.35, n = 18; $p < 0.0001$; ≥ 10 larvae per group). (D) Average mEJC traces for the indicated genotypes. (E) Quantification of average mEJC peak amplitude (nA) per NMJ (control: 0.6104, 0.5898 ± 0.02706, n = 16; *tomosyn*^{NA1}: 0.5985, 0.5771 ± 0.01221, n = 18; *tomosyn*^{NA1}*/Df(1)ED7161*: 0.5657, 0.5846 ± 0.02287, n = 18; p = 0.9143; ≥ 10 larvae per group). (F) Quantification of average mEJC area (nA*msecs) per NMJ (control: 10.12, 9.743 ± 0.6477, n = 16; *tomosyn*^{NA1}: 9.172, 9.396 ± 0.2328, n = 18; *tomosyn*^{NA1}*/ Df(1)ED7161*: 9.476, 9.697 ± 0.4741, n = 18; p = 0.8496; ≥ 10 larvae per group). (G) Quantification of evoked quantal content in 0.3 mM Ca^{2+} per NMJ calculated using peak EJC (control: 93.75, 87.79 ± 5.971, n = 17; *tomosyn*^{NA1}: 145.1, 145.1 ± 5.854 n = 18; *tomosyn*^{NA1}*/Df(1)ED7161*: 189.9, 186.2 ± 7.831, n = 18; $p < 0.0001$; ≥ 10 larvae per group). (H) Quantification of evoked quantal content in 0.3 mM Ca^{2+} per NMJ calculated using EJC area (control: 68.07, 68.84 ± 4.680, n = 17; *tomosyn*^{NA1}: 130.7, 124.2 ± 6.030, n = 18; *tomosyn*^{NA1}*/Df(1)ED7161*: 153.5, 154.6 ± 8.080, n = 18; $p < 0.0001$; ≥ 10 larvae per group). (I) Average eEJC traces in 2.0 mM Ca^{2+} for the indicated genotypes. (J) Quantification of average eEJC peak amplitude (nA) per NMJ in 2.0 mM Ca^{2+} (control: 174.4, 181.0 ± 5.313, n = 24; *tomosyn*^{NA1}: 197.1, 203.2 ± 4.948 n = 24; p = 0.0036; ≥ 18 larvae per group). (K) Quantification of average eEJC area (nA*msec) per NMJ in 2.0 mM Ca^{2+} (control: 1372, 1496 ± 66.60, n = 24; *tomosyn*^{NA1}: 2134, 2140 ± 97.90, n = 24; $p < 0.0001$; ≥ 18 larvae). (L) Normalized cumulative charge transfer in 2.0 mM Ca^{2+}; dashed line represents 90% cumulative release. (M) Quantification of time (msec) when average eEJC reaches 90% charge transfer per NMJ in 2.0 mM Ca^{2+} (control: 13.85, 13.79 ± 0.4711, n = 24; *tomosyn*^{NA1}: 16.95, 17.19 ± 0.7025, n = 24; p = 0.0002; ≥ 18 larvae per group). (N) Representative mEJC traces for the indicated genotypes. (O) Quantification of mEJC frequency (Hz) per NMJ (control: 2.547, 2.701 ± 0.2436, n = 16; *tomosyn*^{NA1}: 9.783, 9.522 ± 0.5590, n = 18; *tomosyn*^{NA1}*/Df(1)ED7161*: 10.19, 10.97 ± 0.7395, n = 18; $p < 0.0001$; ≥ 10 larvae per group).

Figure 3

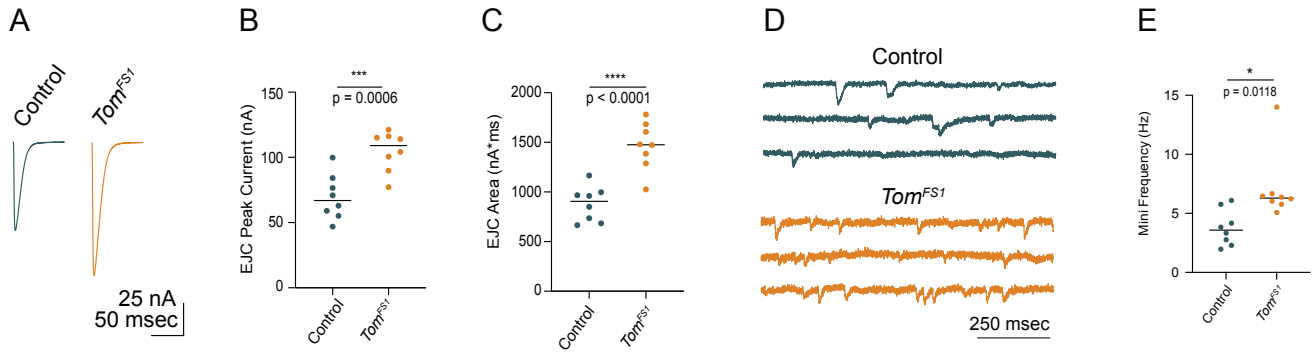
A
Control
Tom^FS1
25 nA
50 msec
B
EJC Peak Current (nA)
150
100
50
0
***
p = 0.0006
Control
Tom^FS1
C
EJC Area (nA*ms)
2000
1500
1000
500
0
****
p < 0.0001
Control
Tom^FS1
D
Control
Tom^FS1
250 msec
E
Mini Frequency (Hz)
15
10
5
0
*
p = 0.0118
Control
Tom^FS1

Figure 3. *tomosyn*^{FS1} null mutants display elevated evoked and spontaneous neurotransmitter release

(A) Average eEJC traces in 0.3 mM Ca^{2+} for the indicated genotypes. (B) Quantification of average eEJC peak amplitude (nA) per NMJ in 0.3 mM Ca^{2+} (control: 66.93, 69.45 ± 6.062,l n = 8; *tomosyn*^{FS1}: 109.1, 104.8 ± 5.333, n = 8; p = 0.0006; ≥ 4 larvae per group). (C) Quantification of average eEJC area (nA*msec) per NMJ in 0.3 mM Ca^{2+} (control: 906.1, 878.3 ± 62.09, n = 8; *tomosyn*^{FS1}: 1476, 1465 ± 84.26, n = 8; $p < 0.0001$; ≥ 4 larvae per group) (D) Representative mEJC traces for the indicated genotypes. (E) Quantification of average mEJC peak amplitude (nA) per NMJ (control: 3.583, 3.779 ± 0.5376, n = 8; *tomosyn*^{FS1}: 6.300, 7.075 ± 1.005, n = 8; p = 0.0118; ≥ 4 larvae per group).

Figure 4

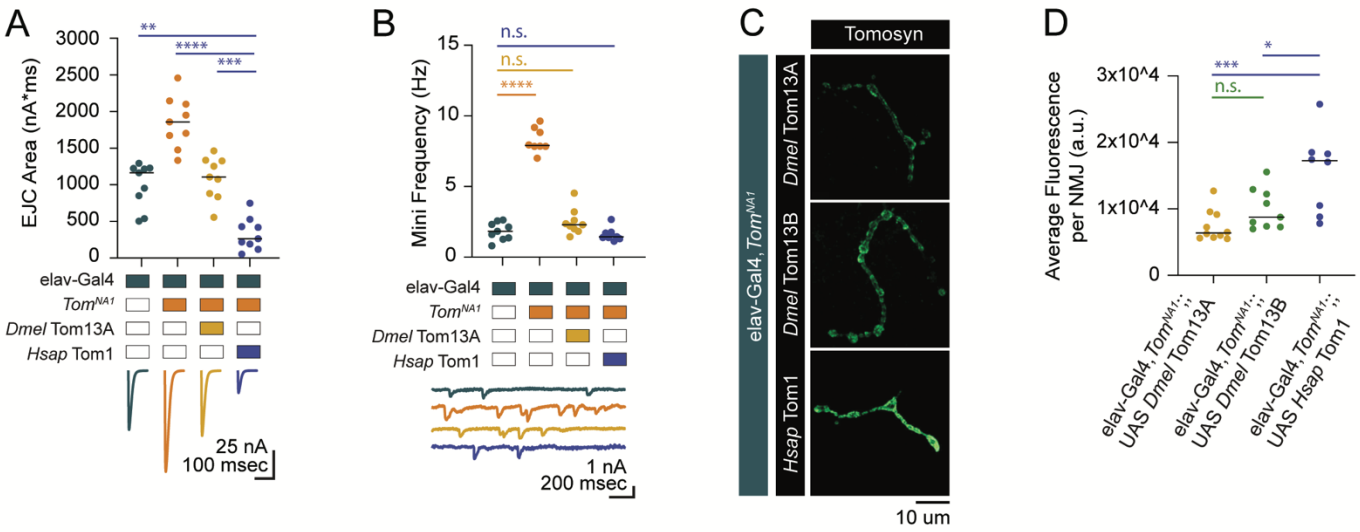
A
EJC Area (nA*ms)
3000
2500
2000
1500
1000
500
0
**
****
***
elav-Gal4
Tom^NA1
Dmel Tom13A
Hsap Tom1
25 nA
100 msec
B
Mini Frequency (Hz)
15
10
5
0
n.s.
n.s.
****
elav-Gal4
Tom^NA1
Dmel Tom13A
Hsap Tom1
1 nA
200 msec
C
Tomosyn
elav-Gal4, Tom^NA1
Dmel Tom13A
Dmel Tom13B
Hsap Tom1
10 um
D
Average Fluorescence per NMJ (a.u.)
3x10^4
2x10^4
1x10^4
0
***
n.s.
*
elav-Gal4, Tom^NA1;;; UAS Dmel Tom13A
elav-Gal4, Tom^NA1;;; UAS Dmel Tom13B
elav-Gal4, Tom^NA1;;; UAS Hsap Tom1

Figure 4. *Tomosyn* mutants are rescued by neuronal expression of Drosophila and human Tomosyn

(A) Quantification of evoked peak current amplitude (nA) in 0.3 mM Ca^{2+} in controls, *tomosyn*^{NA1} mutants and *tomosyn*^{NA1} mutants rescued with Drosophila (*Dmel* Tom13A) or human (*Hsap* Tom1) *tomosyn* (elav-Gal4: 1165, 996.6 ± 101.7, $n = 9$; elav-Gal4,*tomosyn*^{NA1}: 1860, 1856 ± 117.2, $n = 9$; elav-Gal4,*tomosyn*^{NA1}>UAS-Drosophila Tom13A: 1106, 1093 ± 96.98, $n = 9$ NMJs; elav-Gal4,*tomosyn*^{NA1}>UAS-Human Tom1: 262.7, 330 ± 73.47, $n = 9$; $p < 0.0001$; ≥ 5 larvae per group). (B) Quantification of mEJC rate (Hz) for the indicated genotypes (elav-Gal4: 1.833, 1.836 ± 0.2098, $n = 9$; elav-Gal4,*tomosyn*^{NA1}: 7.901, 8.268 ± 0.3066, $n = 9$; elav-Gal4,*tomosyn*^{NA1}>UAS-*Dmel*Tom13A: 2.300, 2.497 ± 0.3029, $n = 9$; elav-Gal4,*tomosyn*^{NA1}>UAS-*Hsap*Tom1: 1.438, 1.605 ± 0.1487, $n = 9$; $p < 0.0001$; ≥ 5 larvae per group). (C) Representative confocal images of Myc-tagged Drosophila (*Dmel* Tom13A and *Dmel* Tom13B) and human (*Hsap* Tom1) Tomosyn rescue constructs at the 3rd instar larval NMJ. (D) Quantification of fluorescence intensity (arbitrary fluorescence units) of Myc-tagged Tomosyn rescue constructs (elav-Gal4,*tomosyn*^{NA1}>UAS-*Dmel* Tom13A: 6391, 7437 ± 742.9, $n = 10$; elav-Gal4,*tomosyn*^{NA1}>UAS-*Dmel*Tom13B: 8764, 10,003 ± 1013, $n = 9$; elav-Gal4,*tomosyn*^{NA1}>UAS-*Hsap* Tom1: 17,253, 15,528 ± 2141, $n = 8$; $p = 0.001$; ≥ 6 larvae per group).

Figure 5

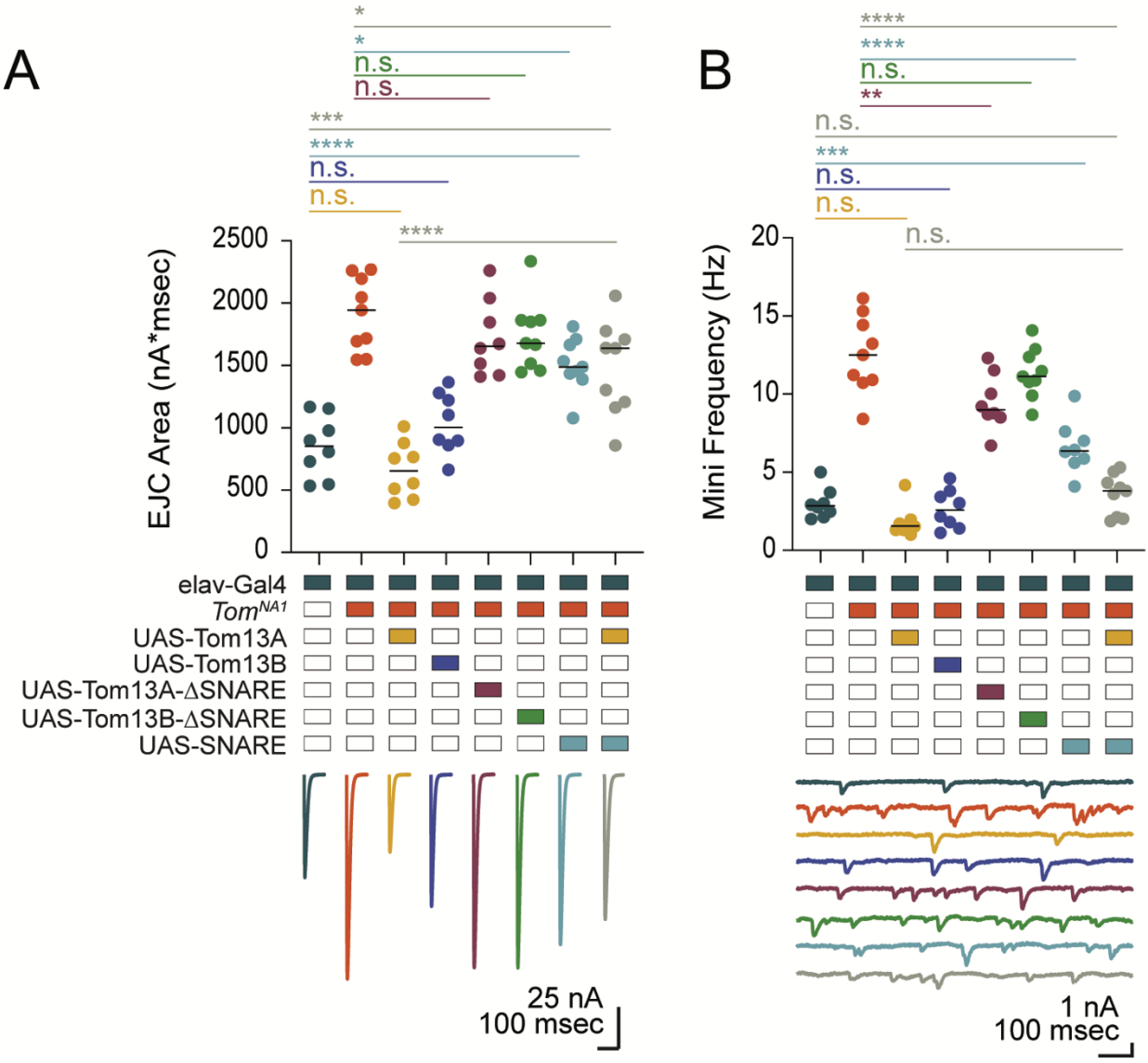
A
B
EJC Area (nA*msec)
2500
2000
1500
1000
500
0
Mini Frequency (Hz)
20
15
10
5
0
n.s.
****
***
**
*
elav-Gal4
Tom^NA1
UAS-Tom13A
UAS-Tom13B
UAS-Tom13A-ΔSNARE
UAS-Tom13B-ΔSNARE
UAS-SNARE
25 nA
100 msec
1 nA
100 msec

Figure 5. The Tomosyn SNARE domain mediates release suppression

(A) Quantification of evoked eJC area (nA*msec) with Tomosyn rescue constructs in 0.3 mM Ca^{2+} (elav-Gal4: 853.9, 852.3 ± 86.62, n = 8; elav-Gal4,*tomosyn*^{NA1}: 1942, 1915 ± 98.61, n = 9; elav-Gal4,*tomosyn*^{NA1}>UAS-Tom13A: 655.2, 662.2 ± 79.03, n = 8; elav-Gal4,*tomosyn*^{NA1}>UAS-Tom13B: 1004, 1037 ± 86.03, n = 8; elav-Gal4,*tomosyn*^{NA1}>UAS-Tom13A-ΔSNARE: 1656, 1726 ± 107.5, n = 8; elav-Gal4,*tomosyn*^{NA1}>UAS-Tom13B-ΔSNARE: 1678, 1742 ± 92.94, n = 9; elav-Gal4,*tomosyn*^{NA1}>UAS-SNARE: 1488, 1508 ± 71.46, n = 9; elav-Gal4,*tomosyn*^{NA1}>UAS-SNARE,UAS-Tom13A: 1639, 1484 ± 124.5, n = 9; $p < 0.0001$; Šidak's multiple comparisons test, p-values indicated in figure; ≥ 4 larvae per group). (B) Quantification of mEJC rate (Hz) with Tomosyn rescue constructs (elav-Gal4: 2.850, 3.000 ± 0.3429, n = 8; elav-Gal4,*tomosyn*^{NA1}: 12.50, 12.54 ± 0.8283, n = 9; elav-Gal4,*tomosyn*^{NA1}>UAS-Tom13A: 1.550, 1.817 ± 0.3511, n = 8; elav-Gal4,*tomosyn*^{NA1}>UAS-Tom13B: 2.600, 2.671 ± 0.4371, n = 8; elav-Gal4,*tomosyn*^{NA1}>UAS-Tom13A-ΔSNARE: 8.983, 9.467 ± 0.6319, n = 8; elav-Gal4,*tomosyn*^{NA1}>UAS-Tom13B-ΔSNARE: 11.13, 11.34 ± 0.5356, n = 9; elav-Gal4,*tomosyn*^{NA1}>UAS-SNARE: 6.367, 6.596 ± 0.5937, n = 8; elav-Gal4,*tomosyn*^{NA1}>UAS-SNARE,UAS-Tom13AΔSNARE: 3.815, 3.571 ± 0.4309, n = 9; $p < 0.0001$; Šidak's multiple comparisons test, p-values indicated in figure; ≥ 4 larvae per group).

Figure 6

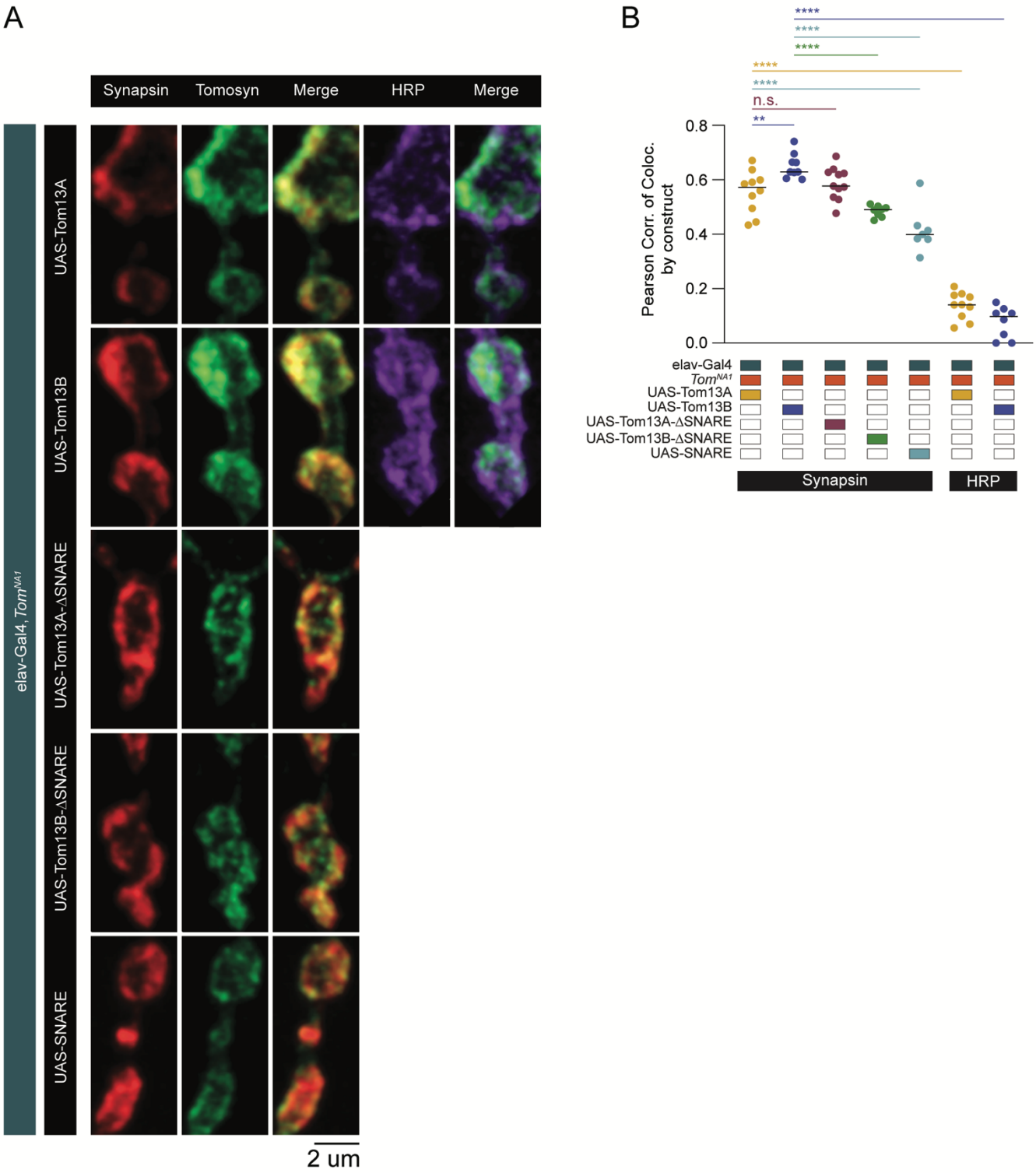
A
Synapsin
Tomosyn
Merge
HRP
Merge
elav-Gal4, Tom^NA1
UAS-Tom13A
UAS-Tom13B
UAS-Tom13A-ΔSNARE
UAS-Tom13B-ΔSNARE
UAS-SNARE
2 um
B
****
****
****
****
****
n.s.
**
Pearson Corr. of Coloc. by construct
0.8
0.6
0.4
0.2
0.0
elav-Gal4
Tom^NA1
UAS-Tom13A
UAS-Tom13B
UAS-Tom13A-ΔSNARE
UAS-Tom13B-ΔSNARE
UAS-SNARE
Synapsin
HRP

Figure 6. The Tomosyn scaffold domain promotes SV enrichment

(A) Representative confocal images of NMJs immunostained for Tomosyn (anti-Myc), Synapsin (3C11) and HRP in a panel of Tomosyn rescue constructs (full-length Tomosyn 13A and 13B: UAS-Tom13A and UAS-Tom13B; SNARE deletions of Tomosyn 13A and 13B: UAS-Tom13A-ΔSNARE and UAS-Tom13B-ΔSNARE; SNARE domain alone: UAS-SNARE). (B) Pearson correlation of co-localization between Tomosyn rescue constructs and Synapsin (elav-Gal4,*tomosyn*^{NA1}>UAS-Tom13A: 0.05725, 0.5559 ± 0.02471, n = 10; elav-Gal4,*tomosyn*^{NA1}>UAS-Tom13B: 0.6290, 0.6509 ± 0.01516, n = 9; elav-Gal4,*tomosyn*^{NA1}>UAS-Tom13A-ΔSNARE: 0.5770, 0.5869 ± 0.01794, n = 11; elav-Gal4,*tomosyn*^{NA1}>UAS-Tom13B-ΔSNARE: 0.4905, 0.4850 ± 0.007283, n = 8; elav-Gal4,*tomosyn*^{NA1}>UAS-SNARE: 0.3990, 0.4161 ± 0.03189, n = 7) and between Tomosyn rescue constructs and HRP (elav-Gal4,*tomosyn*^{NA1}>UAS-Tom13A: 0.1405, 0.1372 ± 0.01571, n = 10; elav-Gal4,*tomosyn*^{NA1}>UAS-Tom13B: 0.09780, 0.07658 ± 0.02059, n = 8; $p < 0.0001$, Šidak's multiple comparisons test, p-values indicated in figure; ≥ 6 larvae per group).

Figure 7

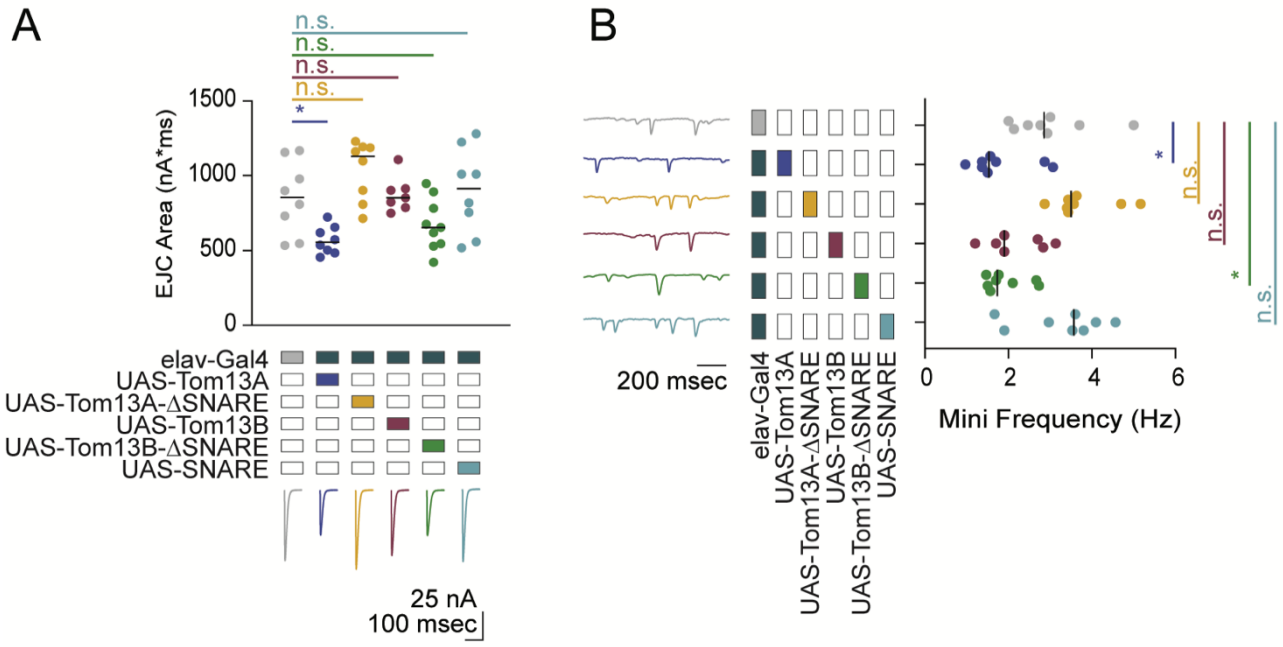
A
n.s.
n.s.
n.s.
n.s.
*
1500
1000
500
0
EJC Area (nA*ms)
elav-Gal4
UAS-Tom13A
UAS-Tom13A-ΔSNARE
UAS-Tom13B
UAS-Tom13B-ΔSNARE
UAS-SNARE
25 nA
100 msec
B
200 msec
elav-Gal4
UAS-Tom13A
UAS-Tom13A-ΔSNARE
UAS-Tom13B
UAS-Tom13B-ΔSNARE
UAS-SNARE
0
2
4
6
Mini Frequency (Hz)
*
n.s.
n.s.
*
n.s.

Figure 7. Tomosyn13A bidirectionally modulates evoked and spontaneous SV release

(A) Quantification of evoked response area (nA*msec) after Tomosyn overexpression in 0.3 mM Ca^{2+}. These experiments were performed in the same experiment as Fig. 3C. The elav-Gal4 data is reproduced here for comparison (elav-Gal4: 853.9, 852.3 ± 86.62, n = 8; elav-Gal4>UAS-Tom13A: 555.3, 569.0 ± 32.45, n = 8; elav-Gal4>UAS-Tom13A-ΔSNARE: 1130, 1037 ± 70.41, n = 8; elav-Gal4>UAS-Tom13B: 851.4, 876.1 ± 44.35, n = 7; elav-Gal4>UAS-Tom13B-ΔSNARE: 654.0, 674.1 ± 57.48, n = 9; elav-Gal4>UAS-SNARE: 913.4, 896.7 ± 100.4, n = 8; p = 0.0003; Dunnett's multiple comparisons test, p-values indicated in figure; ≥ 4 larvae per group). (B) Quantification of mEJC rate (Hz) following Tomosyn overexpression. These experiments were performed in the same experiment as Fig. 3D. The elav-Gal4 data is reproduced here for comparison (elav-Gal4: 2.850, 3.000 ± 0.3429, n = 8; elav-Gal4>UAS-Tom13A: 1.533, 1.800 ± 0.2661, n = 8; elav-Gal4>UAS-Tom13A-ΔSNARE: 3.500, 3.775 ± 0.2691, n = 8; elav-Gal4>UAS-Tom13B: 1.900, 2.195 ± 0.2651, n = 7; elav-Gal4>UAS-Tom13B-ΔSNARE: 1.733, 1.938 ± 0.1807, n = 8; elav-Gal4>UAS-SNARE: 3.567, 3.267 ± 0.3627, n = 8; $p < 0.0001$; Dunnett's multiple comparisons test, p-values indicated in figure; ≥ 4 larvae per group).

Figure 8

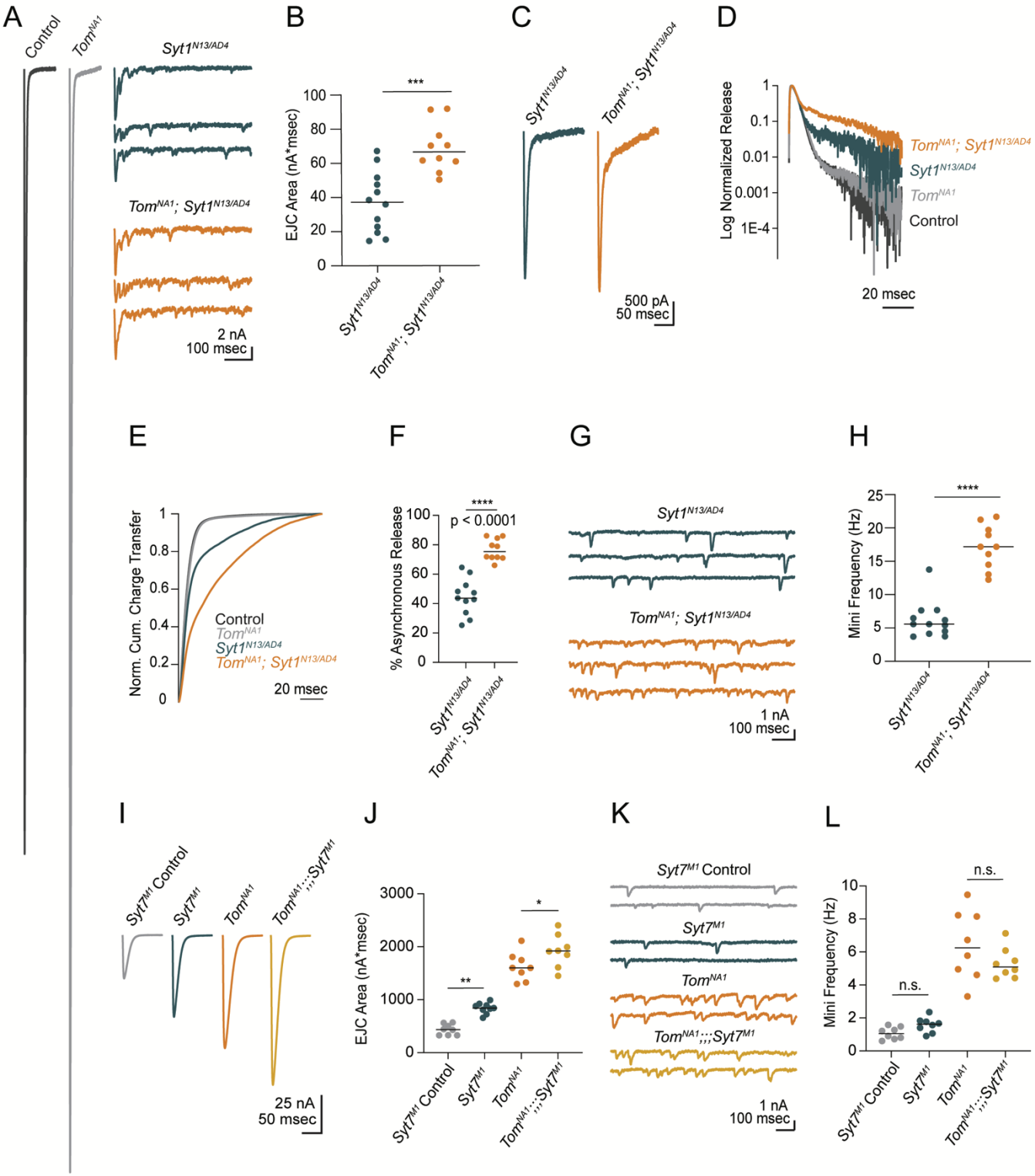
A
Control
Tom^NA1
Syt1^N13/AD4
Tom^NA1; Syt1^N13/AD4
2 nA
100 msec
B
EJC Area (nA*msec)
***
Syt1^N13/AD4
Tom^NA1; Syt1^N13/AD4
C
Syt1^N13/AD4
Tom^NA1; Syt1^N13/AD4
500 pA
50 msec
D
Log Normalized Release
Tom^NA1; Syt1^N13/AD4
Syt1^N13/AD4
Tom^NA1
Control
20 msec
E
Norm. Cum. Charge Transfer
Control
Tom^NA1
Syt1^N13/AD4
Tom^NA1; Syt1^N13/AD4
20 msec
F
% Asynchronous Release
****
p < 0.0001
Syt1^N13/AD4
Tom^NA1; Syt1^N13/AD4
G
Syt1^N13/AD4
Tom^NA1; Syt1^N13/AD4
1 nA
100 msec
H
Mini Frequency (Hz)
****
Syt1^N13/AD4
Tom^NA1; Syt1^N13/AD4
I
Syt7^M1 Control
Syt7^M1
Tom^NA1
Tom^NA1;;;Syt7^M1
25 nA
50 msec
J
EJC Area (nA*msec)
**
*
Syt7^M1 Control
Syt7^M1
Tom^NA1
Tom^NA1;;;Syt7^M1
K
Syt7^M1 Control
Syt7^M1
Tom^NA1
Tom^NA1;;;Syt7^M1
1 nA
100 msec
L
Mini Frequency (Hz)
n.s.
n.s.
Syt7^M1 Control
Syt7^M1
Tom^NA1
Tom^NA1;;;Syt7^M1

Figure 8: Tomosyn inhibits release independent of Synaptotagmin 1 and 7.

(**A**) Average evoked response in 2.0 mM Ca^{2+} for control and *tomosyn*^{NA1} (left) compared to representative traces of *syt1* null mutants (*Syt1*$^{N13/AD4}$) and *tomosyn*/*syt1* double mutants (*Tom*^{NA1}*;Syt1*$^{N13/AD4}$, right). (B) Quantification of average evoked response area (nA*msec) per NMJ in 2.0 mM Ca^{2+} (*syt1*$^{N13/AD4}$: 37.22, 37.13 ± 5.139, n = 12; *tomosyn*^{NA1}/*syt1*$^{N13/AD4}$: 66.59, 69.05 ± 4.471, n = 10; p = 0.0002; ≥ 5 larvae per group). (C) Average EJC response in 2.0 mM Ca^{2+} per genotype. (D) Log normalized average evoked response per genotype in 2.0 mM Ca^{2+}. (E) Normalized cumulative charge transfer for the average evoked response per genotype in 2.0 mM Ca^{2+}. (F) The slow component of evoked release was identified by fitting a double logarithmic function to the average normalized cumulative charge transfer per NMJ in 2.0 mM Ca^{2+} and plotted as a percent of total charge transfer (*syt1*$^{N13/AD4}$: 43.69, 44.55 ± 3.717, n = 11; *tomosyn*^{NA1}/*syt1*$^{N13/AD4}$: 75.38, 76.72 ± 2.295, n = 10; $p < 0.0001$; ≥ 5 larvae per group). (G) Representative mEJC traces per genotype. (H) Quantification of mEJC rate (Hz) per NMJ (*syt1*$^{N13/AD4}$: 5.567, 6.192 ± 0.7904, n = 12; *tomosyn*^{NA1}, *syt1*$^{N13/AD4}$: 17.17, 17.17 ± 1.034, n = 10; $p < 0.0001$; ≥ 5 larvae per group). (I) Average evoked response in 0.3 mM Ca^{2+} of control (*Syt7*^{M1} control), *syt7* null (*Syt7*^{M1}), *tomosyn* null (*tomosyn*^{NA1}), and *tomosyn*/*syt7* double null (*tomosyn*^{NA1}*;;;Syt7*^{M1}). (J) Quantification of average evoked response area (nA*msec) per NMJ in 0.3 mM Ca^{2+} (control: 437.4, 437.4 ± 36.11, n = 8; *syt7*^{M1}: 844.6, 840.4 ± 33.77, n = 9; *tomosyn*^{NA1}: 1602, 1627 ± 94.19, n = 8; *tomosyn*^{NA1}, *syt7*^{M1}: 1920, 1923 ± 108.4, n = 8; $p < 0.0001$; ≥ 5 larvae per group). (K) Representative mEJC traces per genotype. (L) Quantification of mEJC rate per NMJ (Hz) (control: 1.056, 1.070 ± 0.1290, n = 8; *syt7*^{M1}: 1.617, 1.569 ± 0.161, n = 8; *tomosyn*^{NA1}: 6.256, 6.404 ± 0.7475, n = 8; *tomosyn*^{NA1}, *syt7*^{M1}: 5.092, 5.304 ± 0.3292, n = 8; $p < 0.0001$; ≥ 5 larvae per group).

Figure 9

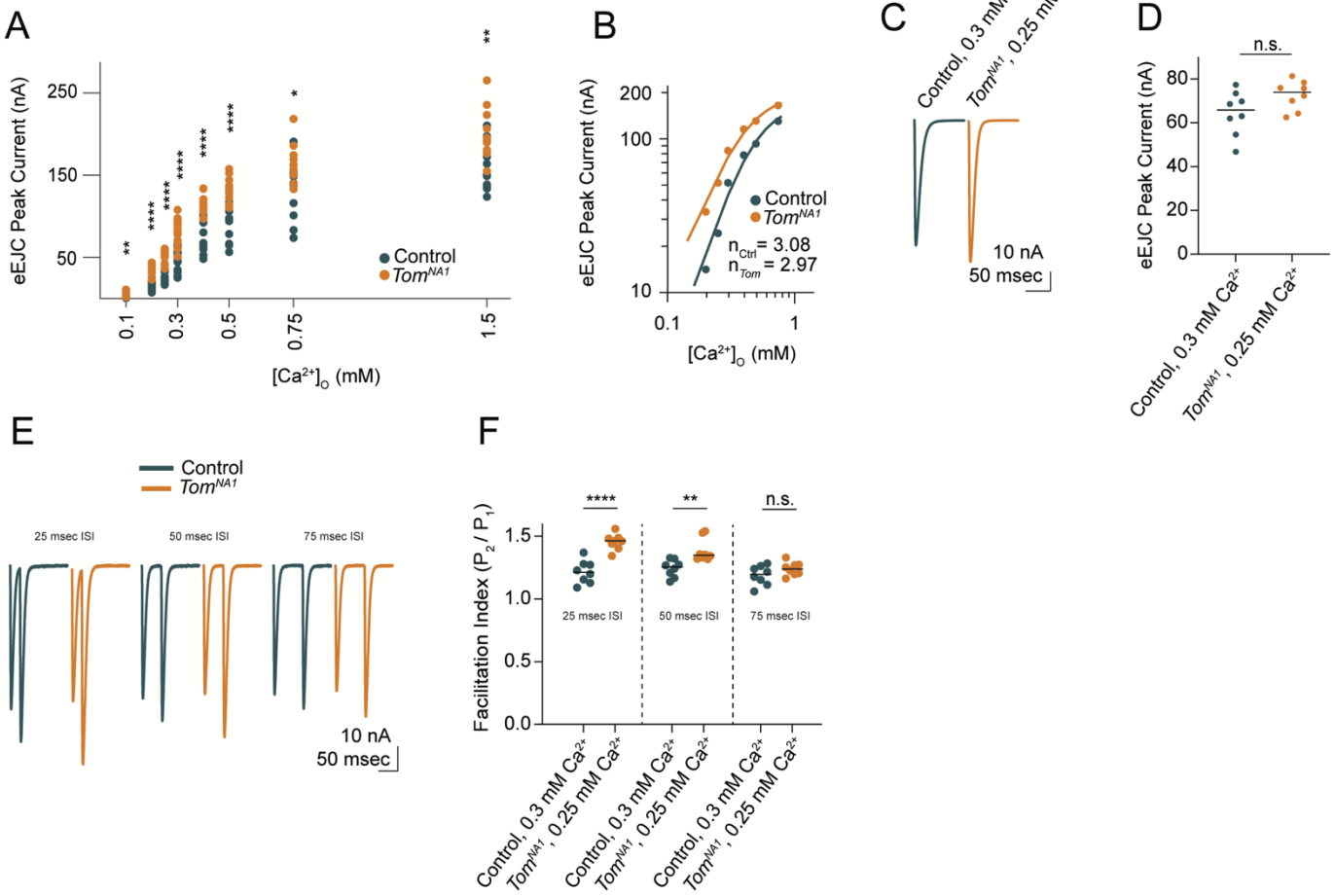
A
eEJC Peak Current (nA)
250
150
50
Control
Tom^NA1
0.1
0.3
0.5
0.75
1.5
[Ca2+]O (mM)
**
****
****
****
****
*
**
B
eEJC Peak Current (nA)
200
100
10
Control
Tom^NA1
n_Ctrl = 3.08
n_Tom = 2.97
0.1
1
[Ca2+]O (mM)
C
Control, 0.3 mM Ca2+
Tom^NA1, 0.25 mM Ca2+
10 nA
50 msec
D
n.s.
eEJC Peak Current (nA)
80
60
40
20
0
Control, 0.3 mM Ca2+
Tom^NA1, 0.25 mM Ca2+
E
Control
Tom^NA1
25 msec ISI
50 msec ISI
75 msec ISI
10 nA
50 msec
F
****
**
n.s.
Facilitation Index (P2 / P1)
1.5
1.0
0.5
0.0
25 msec ISI
50 msec ISI
75 msec ISI
Control, 0.3 mM Ca2+
Tom^NA1, 0.25 mM Ca2+

Figure 9. Tomosyn inhibits release via a Ca^{2+}-independent mechanism

(A) Quantification of average EJC peak amplitude (nA) per NMJ across a range of Ca^{2+} concentrations, including 0.1 mM (control: 0.7351, 0.8639 ± 0.1197, n = 12; *tomosyn*^{NA1}: 2.846, 3.779 ± 0.7682, n = 12; p = 0.0011; ≥ 7 larvae per group), 0.2 mM (control: 13.29, 14.14 ± 1.591, n = 12; *tomosyn*^{NA1}: 35.03, 33.49 ± 2.207, n = 13; $p < 0.0001$; ≥ 8 larvae per group), 0.25 mM (control: 22.87, 24.31 ± 1.876, n = 12; *tomosyn*^{NA1}: 54.26, 51.66 ± 2.273, n = 12; $p < 0.0001$; ≥ 7 larvae per group), 0.3 mM (control: 55.30, 51.78 ± 3.522, n = 17; *tomosyn*^{NA1}: 83.74, 83.74 ± 3.378, n = 128 $p < 0.0001$; ≥ 10 larvae per group), 0.4 mM (control: 73.90, 78.32 ± 5.599, n = 14; *tomosyn*^{NA1}: 114.7, 115.5 ± 3.090, n = 12; $p < 0.0001$; ≥ 10 larvae per group), 0.5 mM (control: 97.09, 92.87 ± 6.413, n = 12; *tomosyn*^{NA1}: 128.6, 130.7 ± 4.415, n = 12; $p < 0.0001$; ≥ 10 larvae per group), 0.75 mM (control: 139.3, 130.2 ± 11.49, n = 10; *tomosyn*^{NA1}: 159.8, 164.7 ± 7.758, n = 10; p = 0.0229; ≥ 7 larvae per group), and 1.5 mM (control: 150.5, 159.8 ± 8.010, n = 12; *tomosyn*^{NA1}: 191.2, 198.1 ± 8.781, n = 12; p = 0.0039; ≥ 7 larvae per group). (B) Log-log plot of evoked response peak amplitude across the Ca^{2+} range, fit with a 4-parameter logistic regression. The Hill slope is not significantly different between groups (control: 3.08 ± 0.48; *tomosyn*^{NA1}: 2.97 ± 0.28; extra sum-of-squares F test, p = 0.8272). (C) Average evoked response in Ca^{2+} concentrations where first evoked response amplitude is similar between control and *tomosyn*^{NA1} (0.3 mM for control, 0.25 mM for *tomosyn*^{NA1}). (D) Quantification of average EJC amplitude (nA) per NMJ (control, 0.3 mM Ca^{2+}: 65.81, 64.44 ± 3.566, n = 8; *tomosyn*^{NA1}, 0.25 mM Ca^{2+}: 74.02, 72.58 ± 2.346, n = 8; p = 0.0773; ≥ 7 larvae per group). (E) Representative paired-pulse recordings with interstimulus intervals (ISI) of 25 msec, 50 msec, and 75 msec. (F) Quantification of the average facilitation index per NMJ, calculated as the fold change in evoked peak current amplitude between pulse 1 and pulse 2. Three different ISIs were tested, including 25 msec (control, 0.3 mM Ca^{2+}: 1.214, 1.216 ± 0.03225, n = 8; *tomosyn*^{NA1}, 0.25 mM Ca^{2+}: 1.463, 1.455 ± 0.02237, n = 8; $p < 0.0001$; ≥ 7 larvae per group), 50 msec (control, 0.3 mM Ca^{2+}: 1.256, 1.244 ± 0.02428, n = 8; *tomosyn*^{NA1}, 0.25 mM Ca^{2+}: 1.349, 1.386 ± 0.03265, n = 8; p = 0.0035; ≥ 7 larvae per group) and 75 msec (control, 0.3 mM Ca^{2+}: 1.197, 1.189 ± 0.02715, n = 8; *tomosyn*^{NA1}, 0.25 mM Ca^{2+}: 1.239, 1.240 ± 0.01851, n = 8; p = 0.1396; ≥ 7 larvae per group).

Figure 10

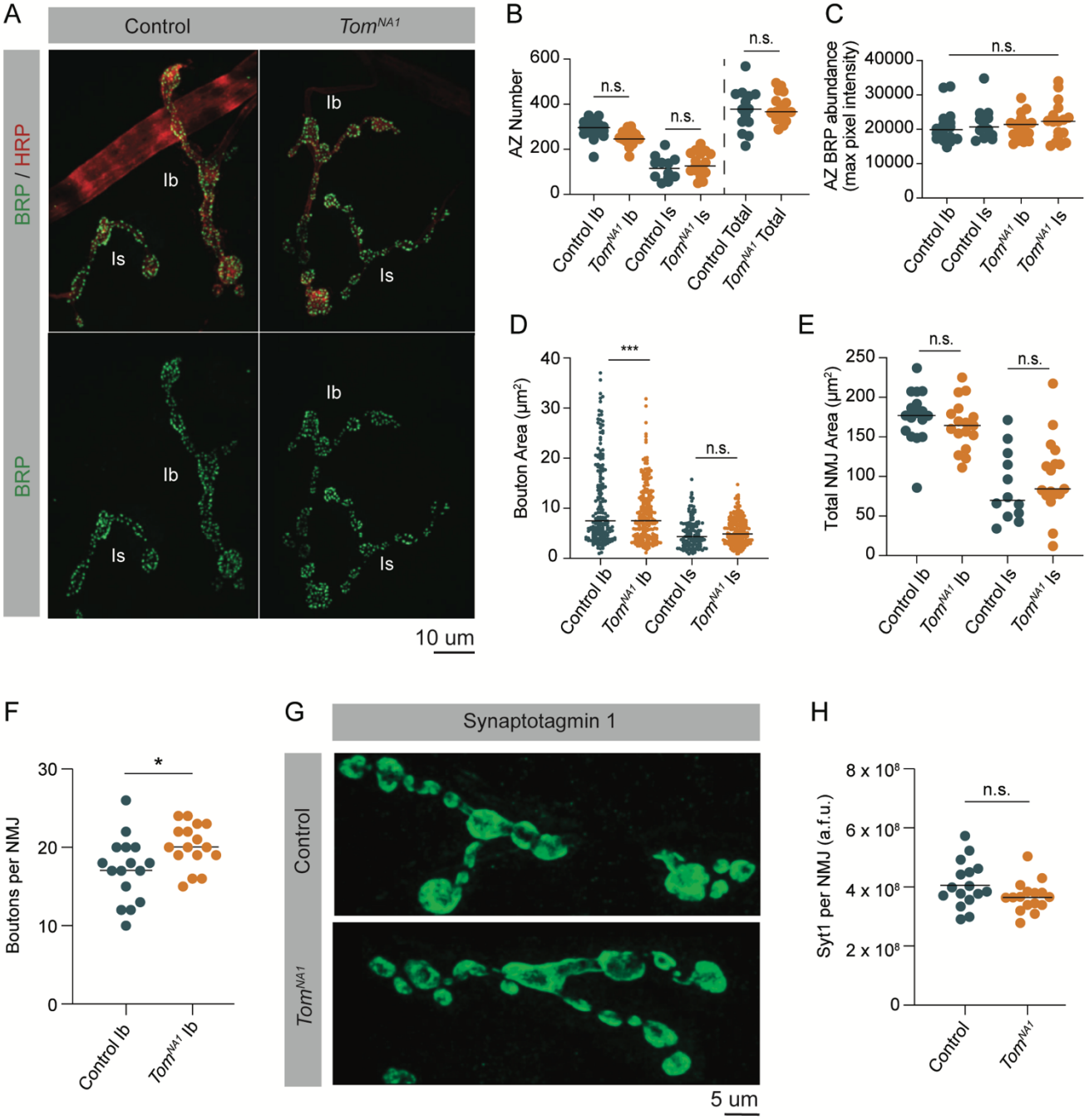
A
Control
Tom^NA1
BRP / HRP
BRP
Ib
Is
10 um
B
AZ Number
n.s.
Control Ib
Tom^NA1 Ib
Control Is
Tom^NA1 Is
Control Total
Tom^NA1 Total
C
AZ BRP abundance (max pixel intensity)
D
Bouton Area (µm²)
***
E
Total NMJ Area (µm²)
F
Boutons per NMJ
*
G
Synaptotagmin 1
Control
Tom^NA1
5 um
H
Syt1 per NMJ (a.f.u.)

Figure 10. Loss of Tomosyn does not affect AZ number, NMJ area or SV abundance

(A) Representative confocal images of immunohistochemistry against the BRP (nc82) and neuronal membranes (anti-HRP). (B) Quantification of AZ number per muscle 4 NMJ for Ib, Is and both (control, Ib: 296.0, 288.2 ± 10.71, n = 17; control, Is: 115.5, 115.8 ± 14.97, n = 12; *tomosyn*^{NA1}, Ib: 246.0, 249.7 ± 7.824, n = 17; *tomosyn*^{NA1}, Is: 126.0, 134.1 ± 12.52, n = 17; control, total: 378.0, 374.8 ± 25.07, n = 14; *tomosyn*^{NA1}, total: 366.0, 383.9 ± 14.74, n = 17; p = 0.0001; ≥ 7 larvae per group). (C) Quantification of the average BRP abundance per AZ per muscle 4 NMJ, measured as average of maximum pixel intensity of each BRP puncta in arbitrary fluorescence intensity units (control, Ib: 19911, 20722 ± 1210, n = 17; control, Is: 20682, 21733 ± 1448, n = 12; *tomosyn*^{NA1}, Ib: 21430, 20681 ± 895.7, n = 17; *tomosyn*^{NA1}, Is: 22275, 22172 ± 1372, n = 17; p = 0.7654; ≥ 7 larvae per group). (D) Quantification of average bouton size (um^2) per muscle 4 NMJ measured as the HRP positive area of each bouton swelling along the arbor (control, Ib: 7.489, 12.16 ± 1.013, n = 195; control, Is: 4.342, 4.974 ± 0.2488, n = 140; *tomosyn*^{NA1}, Ib: 7.508, 8.953 ± 0.3671, n = 241; *tomosyn*^{NA1}, Is: 4.873, 5.413 ± 0.1777, n = 229; p = 0.7654; ≥ 7 larvae per group). (E) Quantification of muscle 4 NMJ area (um^2) measured as HRP positive area (control, Ib: 176.9, 176.0 ± 8.056, n = 17; control, Is: 69.76, 88.9 ± 12.89, n = 12; *tomosyn*^{NA1}, Ib: 164.5, 164.7 ± 7.527, n = 17; *tomosyn*^{NA1}, Is: 84.32, 99.69 ± 11.80, n = 17; p < 0.0001; ≥ 7 larvae per group). (F) Quantification of muscle 4 bouton number per Ib motoneuron (control: 17.50, 17.19 ± 1.030, n = 16; *tomosyn*^{NA1}: 20, 20.19 ± 0.7025, n = 16; p = 0.0225 ≥ 7 larvae per group). (G) Representative confocal images of NMJ immunohistochemistry against the SV marker Syt1. (H) Quantification of Syt1 expression (sum of arbitrary fluorescence units) per Ib motoneuron (control: 3.913*10^8, 4.083*10^8 ± 0.949* 10^8, n = 16; *tomosyn*^{NA1}: 3.3900* 10^8, 3.6713*10^8 ± 0.1297*10^8, n = 16; p = 0.0892 ≥ 7 larvae per group).

Figure 11

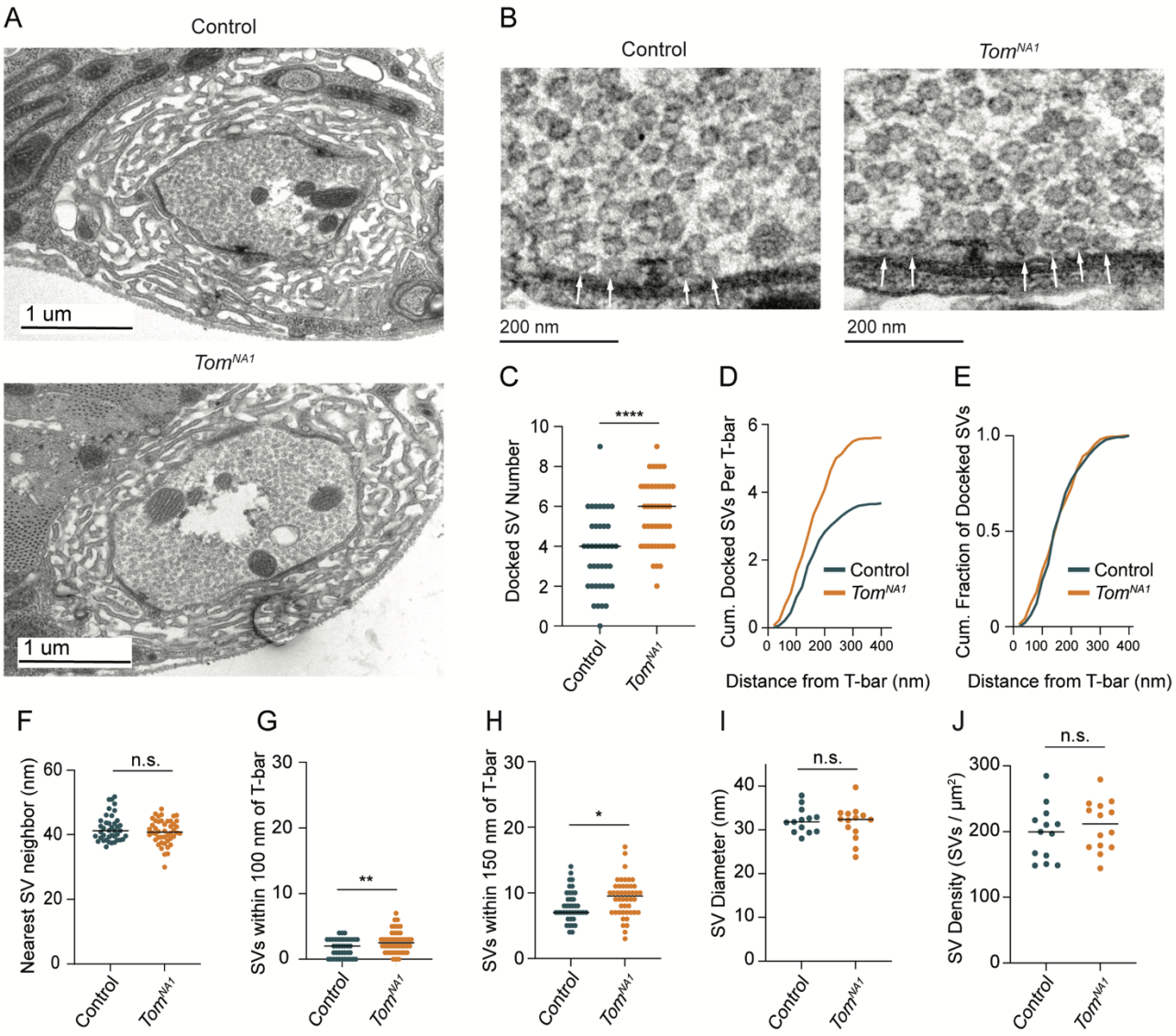
A
Control
1 um
Tom^NA1
1 um
B
Control
Tom^NA1
200 nm
200 nm
C
Docked SV Number
****
Control
Tom^NA1
D
Cum. Docked SVs Per T-bar
Control
Tom^NA1
Distance from T-bar (nm)
E
Cum. Fraction of Docked SVs
Control
Tom^NA1
Distance from T-bar (nm)
F
Nearest SV neighbor (nm)
n.s.
Control
Tom^NA1
G
SVs within 100 nm of T-bar
**
Control
Tom^NA1
H
SVs within 150 nm of T-bar
*
Control
Tom^NA1
I
SV Diameter (nm)
n.s.
Control
Tom^NA1
J
SV Density (SVs / µm²)
n.s.
Control
Tom^NA1

Figure 11. Tomosyn negatively regulates SV docking

(A) Representative TEMs of bouton cross-sections in Ib of the indicated genotypes. (B) Representative micrographs of Ib AZ of the indicated genotypes. Note the electron density along the plasma membrane and the T-bar marking the center of each AZ. Arrows indicate docked synaptic vesicles. (C) Quantification of docked SV number along each AZ electron density (control: 4, 3.7 ± 0.3, n = 40 AZs; *tomosyn*^{NA1}: 6, 5.609 ± 0.2437, n = 48 AZs; $p <$ 0.0001; 3 larvae per group). (D) Average cumulative number of docked SVs at each distance from the T-bar center. (E) Docked SV distance from the AZ center, plotted as the cumulative fraction of docked SVs at each distance from T-bar. (F) Quantification per micrograph of average distance (nm) from each SV to its nearest neighbor (control: 41.16, 42.02 ± 0.6476, n = 40 micrographs; *tomosyn*^{NA1}: 40.78 nm, 40.91 ± 0.5561, n = 46 micrographs; p = 0.1931; 3 larvae per group). (G) Quantification of SV number closer than 100 nm to the T-bar (control: 1, 1.075 ± 0.1535, n = 40 AZs; *tomosyn*^{NA1}: 2, 1.739 ± 0.1927, n = 46 AZs; p = 0.0099; 3 larvae per group). (H) Quantification of SV number closer than 150 nm to the T-bar (control: 7, 7.950 ± 0.3772, n = 40 AZs; *tomosyn*^{NA1}: 9.5, 9.261 ± 0.4164, n = 46 AZs; p = 0.0236; 3 larvae per group). (I) Quantification of average SV diameter (nm) per micrograph (control: 31.81, 32.11 ± 0.7935, n = 13 boutons; *tomosyn*^{NA1}: 32.40, 31.59 ± 1.050, n = 14 boutons; p = 0.7005; 3 larvae per group). (J) Quantification of average SV density per bouton area (SVs/um^2) per micrograph (control: 199.6, 197.9 ± 11.52, n = 13 boutons; *tomosyn*^{NA1}: 211.8, 209.2 ± 10.24, n = 14 boutons; p = 0.4690; 3 larvae per group).

Figure 12

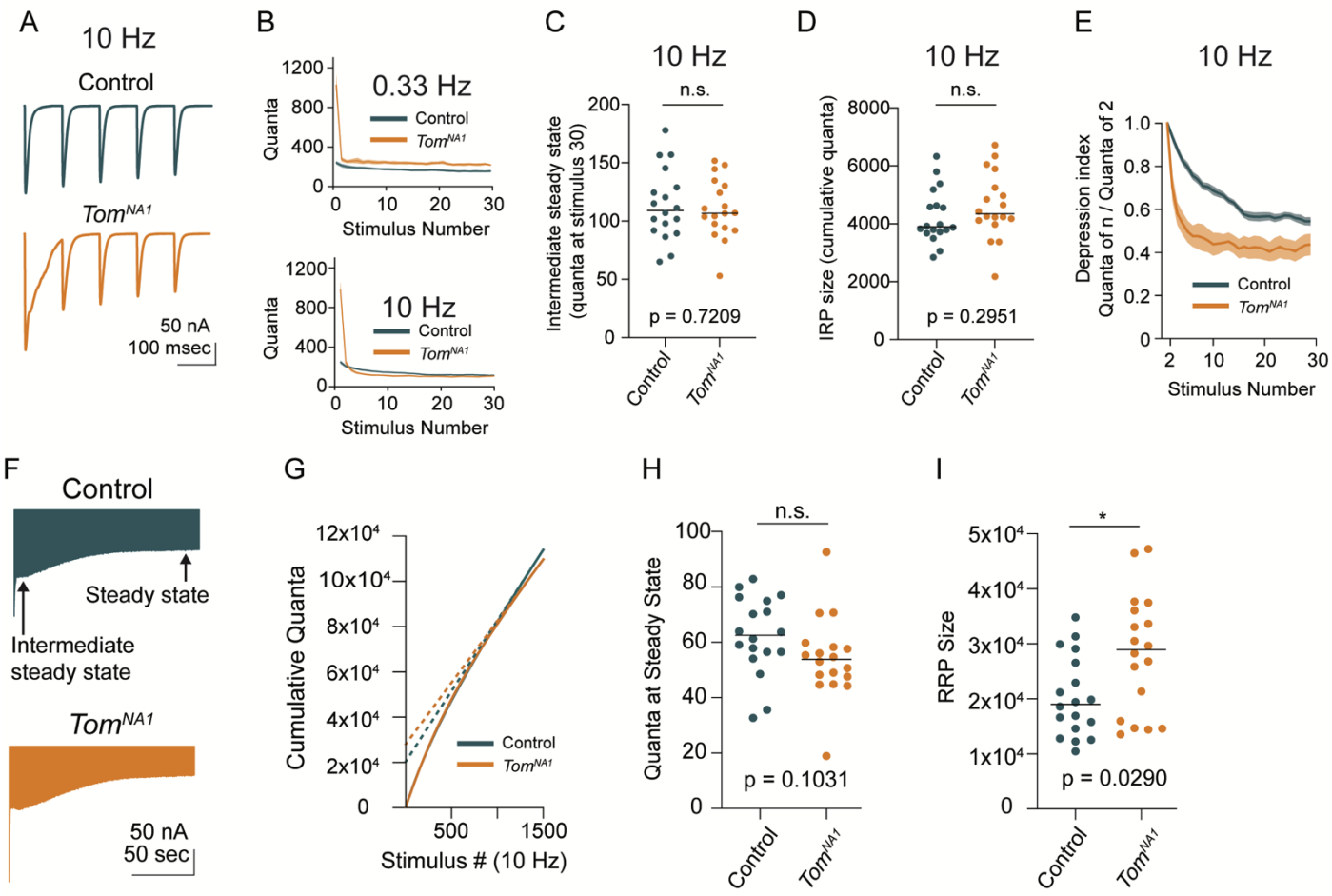
A
10 Hz
Control
Tom^NA1
50 nA
100 msec
B
0.33 Hz
Control
Tom^NA1
Quanta
Stimulus Number
10 Hz
C
10 Hz
n.s.
Intermediate steady state (quanta at stimulus 30)
p = 0.7209
D
10 Hz
n.s.
IRP size (cumulative quanta)
p = 0.2951
E
10 Hz
Depression index Quanta of n / Quanta of 2
Stimulus Number
F
Control
Steady state
Intermediate steady state
Tom^NA1
50 nA
50 sec
G
Cumulative Quanta
Control
Tom^NA1
Stimulus # (10 Hz)
H
n.s.
Quanta at Steady State
p = 0.1031
I
*
RRP Size
p = 0.0290

Figure 12. Tomosyn regulates SV usage during train stimulation

(A) Average evoked response trains during 10 Hz stimulation in 2.0 mM Ca^{2+}. Stimulus artifacts were removed for clarity. (B) Evoked quantal content in 2.0 mM Ca^{2+} (quanta) during a 0.33 Hz stimulus train (top) and during a 10 Hz stimulus train (bottom). Lines indicate mean values, with SEM noted by the shaded area (SEM is partly obscured in these plots by the line indicating the mean). (C) Quantification of the evoked response size (quanta) at the intermediate steady state, approximated as the size of stimulus 30 following 10 Hz stimulation in 2.0 mM Ca^{2+} (control: 109.0, 113.8 ± 7.217, n = 18; *tomosyn*^{NA1}: 106.8, 8.110 ± 5.964, n = 18; p = 0.7209; ≥ 12 larvae per group). (D) Quantification of the immediately releasable pool size, approximated as the cumulative quanta released within 30 stimulations at 10 Hz in 2.0 mM Ca^{2+} (control: 3899, 4247 ± 219.5, n = 18; *tomosyn*^{NA1}: 4314, 4615 ± 268.1, n = 18; p = 0.2951; ≥ 12 larvae per group). (E) The depression index was calculated as the ratio of stimulus n to stimulus 2 during a 10 Hz train in 2.0 mM Ca^{2+}. At stimulus 30, the depression index is as follows (control: 0.5565, 0.5527 ± 0.1885, n = 18; *tomosyn*^{NA1}: 0.3961, 0.4277 ± 0.03628, n = 17; p = 0.0039; ≥ 12 larvae per group). (F) Average evoked response trains during 10 Hz stimulation through 1500 stimulations in 2.0 mM Ca^{2+}. The intermediate steady state and final steady state are represented with arrows. (G) Average cumulative quanta per stimulus per genotype (solid line), with back extrapolation of the RRP size minus steady state recycling (dashed line). (H) Quantification of evoked response size at steady state (quanta) following 1500 stimulations at 10 Hz in 2.0 mM Ca^{2+} (control: 62.51, 62.36 ± 3.329, n = 18; *tomosyn*^{NA1}: 53.85, 54.29 ± 3.486, n = 18; p = 0.0315; ≥ 12 larvae per group). (I) Quantification of RRP size in quanta (control: 19041, 20333 ± 1724, n = 18; *tomosyn*^{NA1}: 28956, 28189 ± 2537, n = 18; p = 0.0290; ≥ 12 larvae per group).

Figure 13

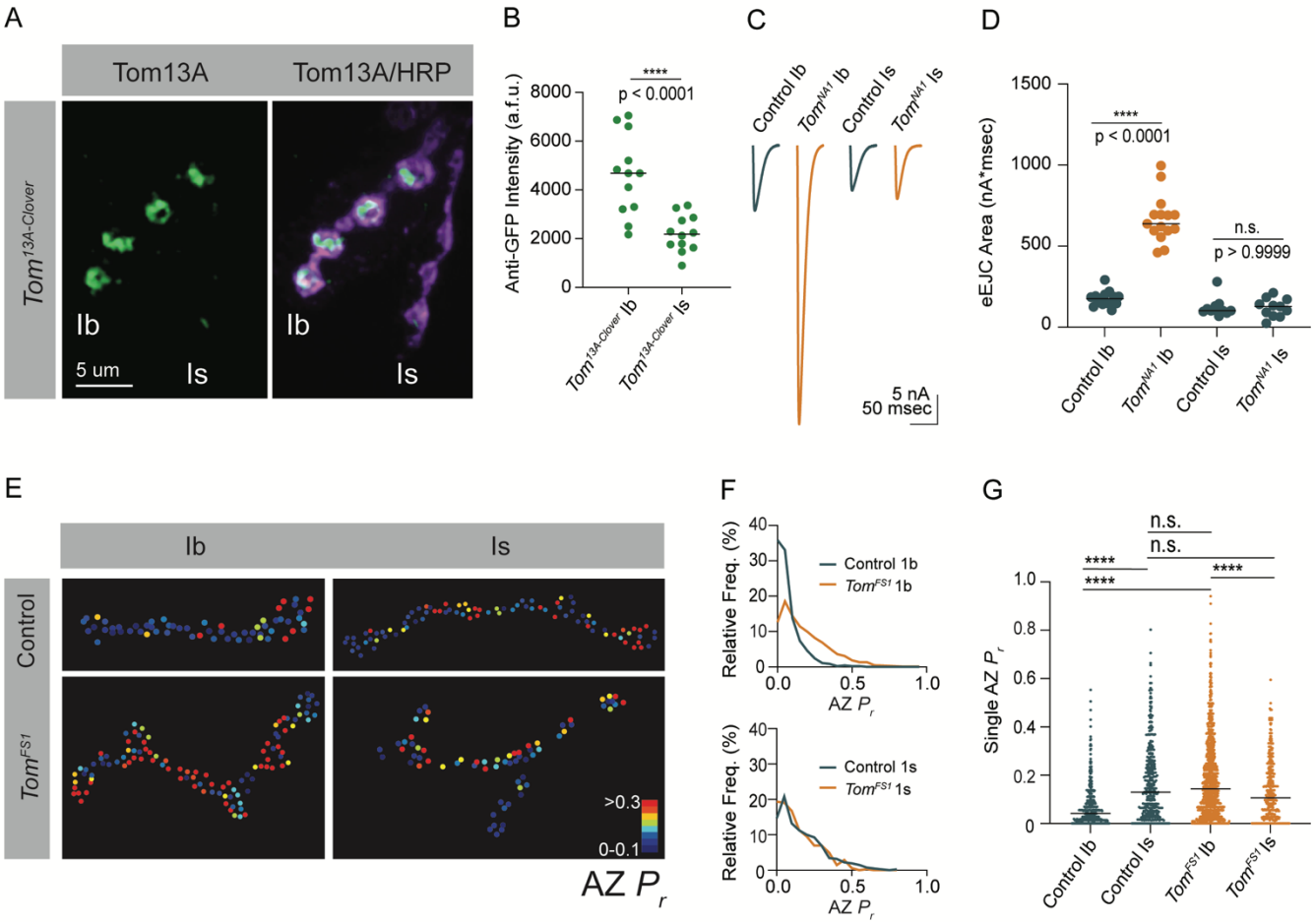
A
Tom13A
Tom13A/HRP
Tom13A-Clover
Ib
Is
5 um
B
Anti-GFP Intensity (a.f.u.)
8000
6000
4000
2000
0
****
p < 0.0001
Tom13A-Clover Ib
Tom13A-Clover Is
C
Control Ib
TomNA1 Ib
Control Is
TomNA1 Is
5 nA
50 msec
D
eEJC Area (nA*msec)
1500
1000
500
0
****
p < 0.0001
n.s.
p > 0.9999
Control Ib
TomNA1 Ib
Control Is
TomNA1 Is
E
Ib
Is
Control
TomFS1
>0.3
0-0.1
AZ Pr
F
Relative Freq. (%)
Control 1b
TomFS1 1b
AZ Pr
Control 1s
TomFS1 1s
G
Single AZ Pr
n.s.
n.s.
****
****
****
Control Ib
Control Is
TomFS1 Ib
TomFS1 Is

Figure 13. Tomosyn regulates tonic versus phasic neurotransmitter release properties

(A) Representative confocal images of NMJ immunohistochemistry against *tomosyn*$^{13A\text{-}Clover}$ (anti-GFP). (B) Quantification of Tomosyn13A-Clover expression level (arbitrary fluorescence units) in Ib and Is terminals (*tomosyn*$^{13A\text{-}Clover}$, Ib: 4680, 4601 ± 475.1, n = 12; *tomosyn*$^{13A\text{-}Clover}$, Is: 2180, 2201 ± 215.7, n = 12; $p < 0.0001$; ≥ 4 larvae per group). (C) Average optically evoked responses from motoneurons expressing channelrhodopsin 2 using drivers that specifically drive expression in Ib (GMR94G06) or Is (GMR27F01). (D) Quantification of optically evoked response area (nA*msec) in Ib and Is (GMR94G06>UAS-ChR2: 175.2, 175.7 ± 12.31, n = 14; *tomosyn*^{NA1}, GMR94G06>UAS-ChR2: 638.0, 667.1 ± 37.91, n = 15; GMR27F01>UAS-ChR2: 101.9, 121.1 ± 17.05, n = 11; *tomosyn*^{NA1}, GMR27F01>UAS-ChR2: 128.7, 120.6 ± 17.01, n = 11; $p < 0.0001$; ≥ 5 larvae per group). (E) Representative maps of quantal imaging for average P_r of individual AZs at Ib or Is terminals in control or *tomosyn*^{FS1} mutants. (F) Histogram of single AZ P_r at Ib (top) and Is (bottom) for the indicated genotypes. (G) Quantification of single AZ P_r per motoneuron per genotype (the mean is plotted, control Ib: 0.04150, 0.06938 ± 0.003829, n = 463 AZs; control Is: 0.1295, 0.1664 ± 0.007488, n = 409 AZs; *tomosyn*^{FS1} Ib: 0.1434, 0.1846 ± 0.004917, n = 1075 AZs; *tomosyn*^{FS1} Is: 0.1066, 0.1389 ± 0.006720, n = 346 AZs; $p < 0.0001$; ≥ 4 larvae per group).

Figure 14

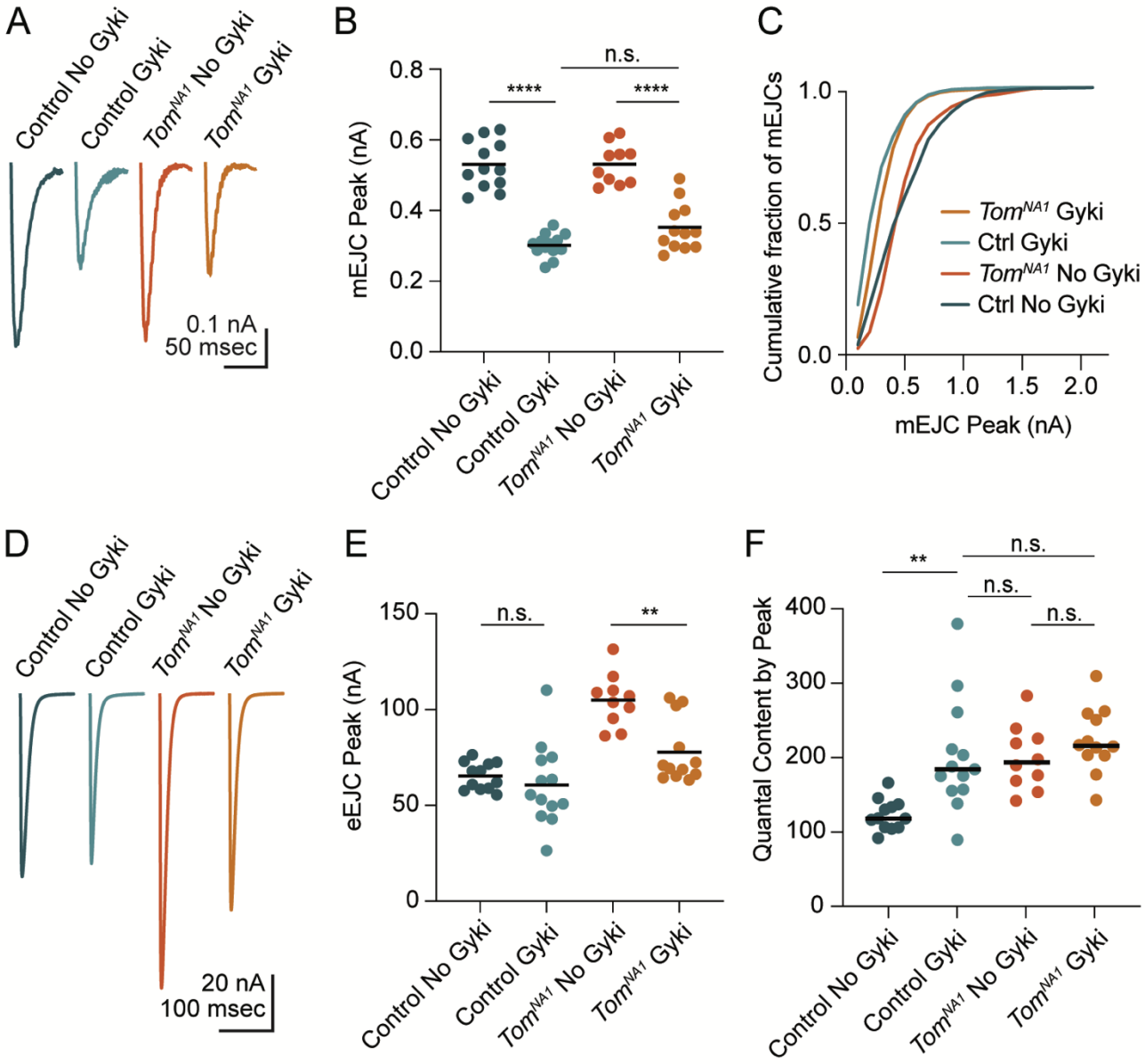
A
Control No Gyki
Control Gyki
TomNA1 No Gyki
TomNA1 Gyki
0.1 nA
50 msec
B
mEJC Peak (nA)
0.8
0.6
0.4
0.2
0.0
n.s.
****
****
Control No Gyki
Control Gyki
TomNA1 No Gyki
TomNA1 Gyki
C
Cumulative fraction of mEJCs
1.0
0.5
0.0
0.0
0.5
1.0
1.5
2.0
mEJC Peak (nA)
TomNA1 Gyki
Ctrl Gyki
TomNA1 No Gyki
Ctrl No Gyki
D
Control No Gyki
Control Gyki
TomNA1 No Gyki
TomNA1 Gyki
20 nA
100 msec
E
eEJC Peak (nA)
150
100
50
0
n.s.
**
Control No Gyki
Control Gyki
TomNA1 No Gyki
TomNA1 Gyki
F
Quantal Content by Peak
400
300
200
100
0
**
n.s.
n.s.
n.s.
Control No Gyki
Control Gyki
TomNA1 No Gyki
TomNA1 Gyki

Figure 14. Tomosyn is essential for Gyki-induced presynaptic homeostatic potentiation (PHP)

(A) Average mEJC amplitudes in the presence and absence of the allosteric GluR inhibitor Gyki (10 uM). (B) Quantification of average mEJC peak current (nA) per NMJ (control, no Gyki: 0.5161, 0.5302 ± 0.01964 n = 12; control, Gyki: 0.3062, 0.3019 ± 0.009029, n = 13; *tomosyn*^{NA1}, no Gyki: 0.5318, 0.5312 ± 0.01789, n = 10; *tomosyn*^{NA1}, Gyki: 0.3373, 0.3521 ± 0.01934, n = 12; $p < 0.0001$; ≥ 7 larvae per group). (C) Histogram showing cumulative fraction of mEJCs by peak current. (D) Average eEJC peak amplitude (nA) following 15 minute incubation in Gyki (10 uM). (E) Quantification of average eEJC peak (nA) per NMJ in 0.35 mM Ca^{2+} (control, no Gyki: 65.02, 65.28 ± 2.062 n = 12; control, Gyki: 55.52, 60.67 ± 5.819, n = 13; *tomosyn*^{NA1}, no Gyki: 105.5, 104.9 ± 4.315, n = 10; *tomosyn*^{NA1}, Gyki: 70.10, 77.82 ± 4.778, n = 12; $p < 0.0001$; ≥ 7 larvae per group). (F) Quantification of average evoked quantal content per NMJ in 0.35 mM Ca^{2+} approximated by peak current (control, no Gyki: 120.3, 124.9 ± 5.927 n = 12; control, Gyki: 185.7, 202.6 ± 20.54, n = 13; *tomosyn*^{NA1}, no Gyki: 195.2, 200.9 ± 13.47, n = 10; *tomosyn*^{NA1}, Gyki: 217.1, 224.2 ± 12.40, n = 12; $p < 0.0001$; ≥ 7 larvae per group).

Figure 15

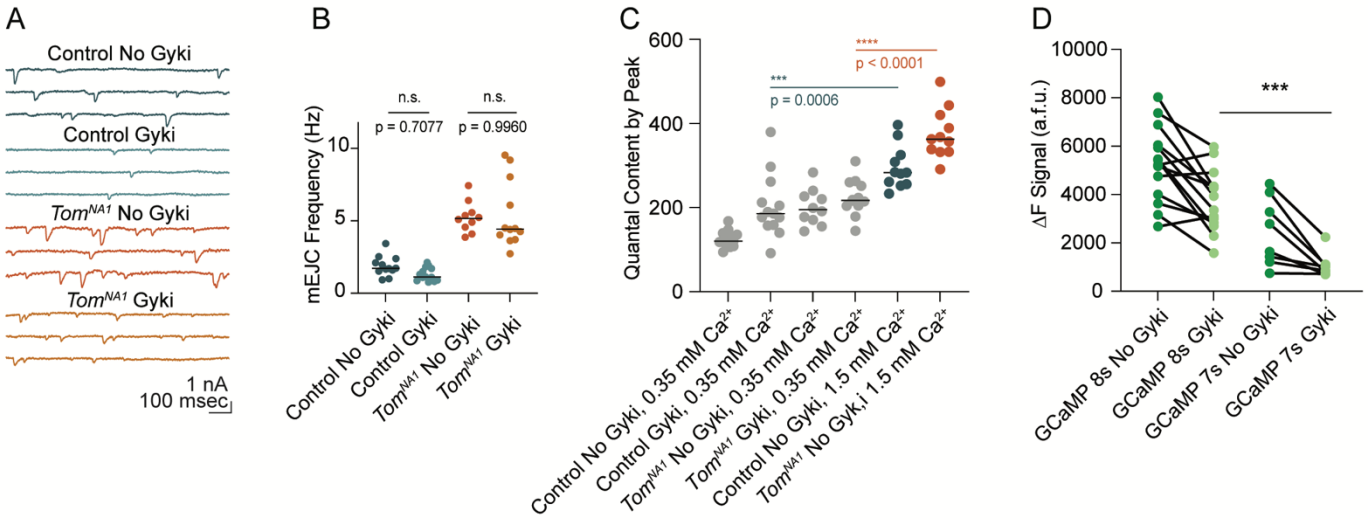
A
Control No Gyki
Control Gyki
TomNA1 No Gyki
TomNA1 Gyki
1 nA
100 msec
B
mEJC Frequency (Hz)
n.s.
p = 0.7077
n.s.
p = 0.9960
Control No Gyki
Control Gyki
TomNA1 No Gyki
TomNA1 Gyki
C
Quantal Content by Peak
***
p = 0.0006
****
p < 0.0001
Control No Gyki, 0.35 mM Ca2+
Control Gyki, 0.35 mM Ca2+
TomNA1 No Gyki, 0.35 mM Ca2+
TomNA1 Gyki, 0.35 mM Ca2+
Control No Gyki, 1.5 mM Ca2+
TomNA1 No Gyki, 1.5 mM Ca2+
D
ΔF Signal (a.f.u.)
***
GCaMP 8s No Gyki
GCaMP 8s Gyki
GCaMP 7s No Gyki
GCaMP 7s Gyki

Figure 15. mEJC detection and non-saturation of quantal content following Gyki application

(A) Representative mEJC traces per genotype. (B) Quantification of mEJC frequency per NMJ (control, no Gyki: 1.717, 1.883 ± 0.1972 $n = 12$; control, Gyki: 1.133, 1.314 ± 0.1280, $n = 13$; *tomosyn*^{NA1}, no Gyki: 5.165, 5.253 ± 0.3340, $n = 10$; *tomosyn*^{NA1}, Gyki: 4.433, 5.380 ± 0.6626, $n = 12$; $p < 0.0001$; ≥ 7 larvae per group). (C) Quantification of average evoked quantal content per NMJ in 0.35 mM Ca^{2+} (reproduced from Fig. 8 F for comparison) and 1.5 mM Ca^{2+} (control, no Gyki: 283.1, 295.8 ± 15.43, $n = 11$; *tomosyn*^{NA1}, no Gyki: 362.5, 375.9 ± 17.81, $n = 11$; $p < 0.0001$; ≥ 7 larvae per group). (D) Average ΔF signal (arbitrary fluorescence units) per NMJ before and after Gyki using the indicated GCaMP variants (GCaMP 8s, no Gyki: 5321, 5270 ± 415.6, $n = 14$; GCaMP8s, Gyki: 3647, 3733 ± 340.0, $n = 14$; GCaMP7s, no Gyki: 2216, 2455 ± 493.0, $n = 8$; GCaMP 7s, Gyki: 933.9, 1061 ± 175.9, $n = 8$; $p < 0.0001$; ≥ 4 larvae per group).

Figure 16

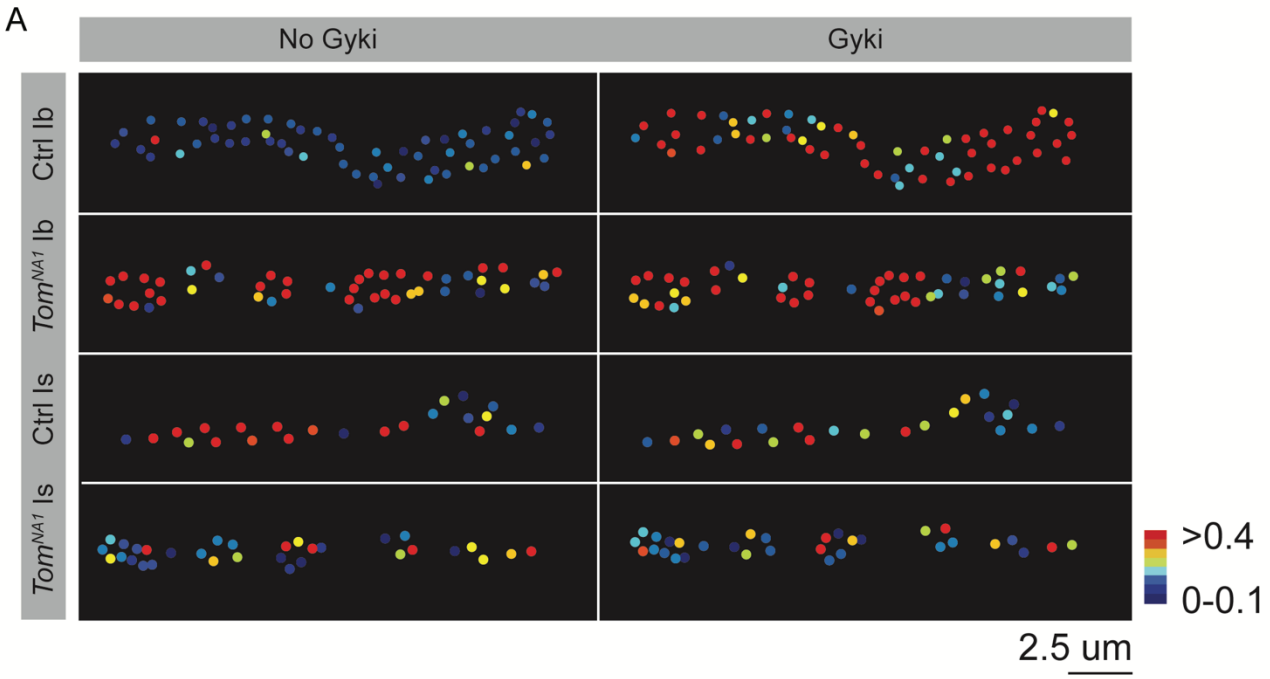
A
No Gyki
Gyki
Ctrl Ib
Tom^NA1 Ib
Ctrl Is
Tom^NA1 Is
>0.4
0-0.1
2.5 um

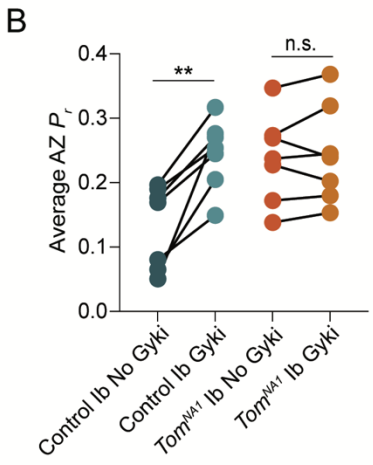
B
Average AZ Pr
**
n.s.
Control Ib No Gyki
Control Ib Gyki
Tom^NA1 Ib No Gyki
Tom^NA1 Ib Gyki

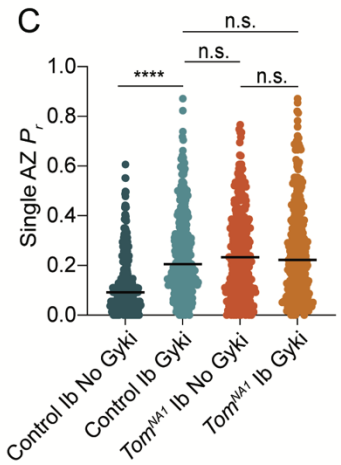
C
Single AZ Pr
n.s.
n.s.
****
n.s.
Control Ib No Gyki
Control Ib Gyki
Tom^NA1 Ib No Gyki
Tom^NA1 Ib Gyki

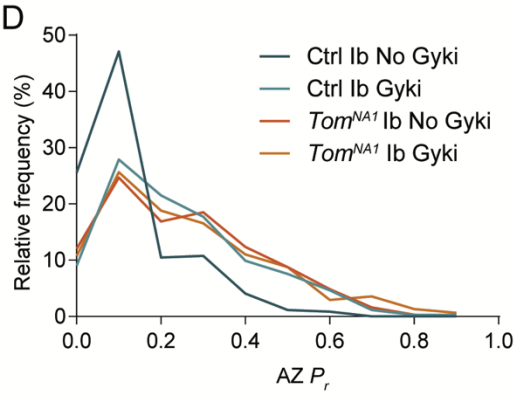
D
Relative frequency (%)
Ctrl Ib No Gyki
Ctrl Ib Gyki
Tom^NA1 Ib No Gyki
Tom^NA1 Ib Gyki
AZ Pr

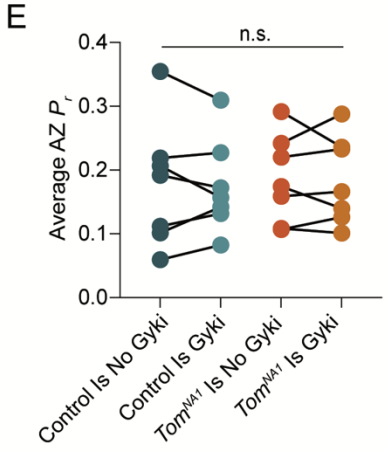
E
Average AZ Pr
n.s.
Control Is No Gyki
Control Is Gyki
Tom^NA1 Is No Gyki
Tom^NA1 Is Gyki

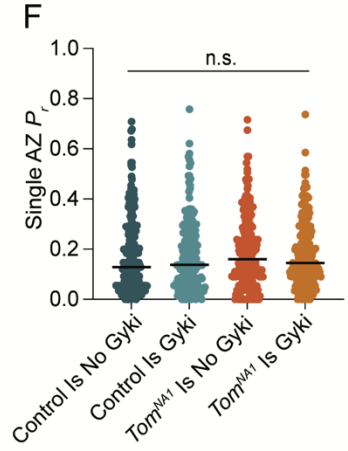
F
Single AZ Pr
n.s.
Control Is No Gyki
Control Is Gyki
Tom^NA1 Is No Gyki
Tom^NA1 Is Gyki

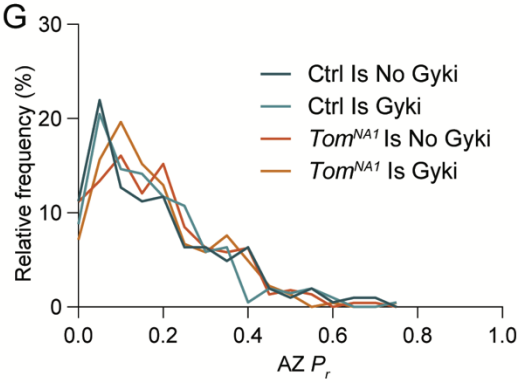
G
Relative frequency (%)
Ctrl Is No Gyki
Ctrl Is Gyki
Tom^NA1 Is No Gyki
Tom^NA1 Is Gyki
AZ Pr

Figure 16. Tomosyn is essential for Gyki-induced P_r enhancement

(G) Representative maps from quantal imaging of AZ P_r in Ib and Is before and after Gyki incubation. (H) Average AZ P_r per Ib NMJ before and after Gyki (control Ib, no Gyki: 0.1690, 0.1325 ± 0.02419, n = 7; control Ib, Gyki: 0.2538, 0.2451 ± 0.02049, n = 7; *tomosyn*^{NA1} Ib, no Gyki: 0.2373, 0.2377 ± 0.02602, n = 7; *tomosyn*^{NA1} Ib, Gyki: 0.2395, 0.2438 ± 0.02894, n = 7; p = 0.0094; ≥ 4 larvae per group). (I) Single AZ P_r at Ib NMJs before and after Gyki (control Ib, no Gyki: 0.09200, 0.1275 ± 0.006387, n = 344; control Ib, Gyki: 0.2051, 0.2412 ± 0.009160, n = 344; *tomosyn*^{NA1} Ib, no Gyki: 0.2325, 0.2515 ± 0.01016, n = 308; *tomosyn*^{NA1} Ib, Gyki: 0.2220, 0.2601 ± 0.001117, n = 308; p < 0.0001; ≥ 4 larvae per group). (J) Histogram of single AZ P_r at Ib NMJs before and after Gyki. (K) Average AZ P_r per Is NMJ before and after Gyki (control Is, no Gyki: 0.1917, 0.1777 ± 0.03719, n = 7; control Is, Gyki: 0.1568, 0.1746 ± 0.02786, n = 7; *tomosyn*^{NA1} Is, no Gyki: 0.1740, 0.1859 ± 0.02609, n = 7; *tomosyn*^{NA1} Is, Gyki: 0.1662, 0.1843 ± 0.02598, n = 7; p = 0.9918; ≥ 4 larvae per group). (L) Single AZ P_r at Is NMJs before and after Gyki (control Is, no Gyki: 0.1291, 0.1817 ± 0.01094, n = 205; control Is, Gyki: 0.1382, 0.1752 ± 0.009807, n = 205; *tomosyn*^{NA1} Is, no Gyki: 0.1605, 0.1844 ± 0.009462, n = 224; *tomosyn*^{NA1} Is, Gyki: 0.1454, 0.1813 ± 0.008662, n = 224; p = 0.9246; ≥ 4 larvae per group). (M) Histogram of single AZ P_r at Is NMJs before and after Gyki.

References

Akbergenova, Y., and Bykhovskaia, M. (2009). Enhancement of the endosomal endocytic pathway increases quantal size. Mol. Cell. Neurosci. *40*, 199–206.

Akbergenova, Y., Cunningham, K.L., Zhang, Y.V., Weiss, S., and Littleton, J.T. (2018). Characterization of developmental and molecular factors underlying release heterogeneity at Drosophila synapses. Elife *7*.

Aponte-Santiago, N.A., and Littleton, J.T. (2020). Synaptic properties and plasticity mechanisms of invertebrate tonic and phasic neurons. Front. Physiol. *11*, 611982.

Aponte-Santiago, N.A., Ormerod, K.G., Akbergenova, Y., and Littleton, J.T. (2020). Synaptic plasticity induced by differential manipulation of tonic and phasic motoneurons in drosophila. J. Neurosci. *40*, 6270–6288.

Atwood, H.L., and Karunanithi, S. (2002). Diversification of synaptic strength: presynaptic elements. Nat. Rev. Neurosci. *3*, 497–516.

Baba, T., Sakisaka, T., Mochida, S., and Takai, Y. (2005). PKA-catalyzed phosphorylation of tomosyn and its implication in Ca2+-dependent exocytosis of neurotransmitter. J. Cell Biol. *170*, 1113–1125.

Bajar, B.T., Wang, E.S., Lam, A.J., Kim, B.B., Jacobs, C.L., Howe, E.S., Davidson, M.W., Lin, M.Z., and Chu, J. (2016). Improving brightness and photostability of green and red fluorescent proteins for live cell imaging and FRET reporting. Sci. Rep. *6*, 20889.

Ben-Simon, Y., Rodenas-Ruano, A., Alviña, K., Lam, A.D., Stuenkel, E.L., Castillo, P.E., and Ashery, U. (2015). A Combined Optogenetic-Knockdown Strategy Reveals a Major Role of Tomosyn in Mossy Fiber Synaptic Plasticity. Cell Rep. *12*, 396–404.

Böhme, M.A., McCarthy, A.W., Grasskamp, A.T., Beuschel, C.B., Goel, P., Jusyte, M., Laber, D., Huang, S., Rey, U., Petzoldt, A.G., et al. (2019). Rapid active zone remodeling consolidates presynaptic potentiation. Nat. Commun. *10*, 1085.

Burdina, A.O., Klosterman, S.M., Shtessel, L., Ahmed, S., and Richmond, J.E. (2011). In vivo analysis of conserved C. elegans tomosyn domains. PLoS One *6*, e26185.

Chen, K., Richlitzki, A., Featherstone, D.E., Schwärzel, M., and Richmond, J.E. (2011). Tomosyn-dependent regulation of synaptic transmission is required for a late phase of associative odor memory. Proc. Natl. Acad. Sci. USA *108*, 18482–18487.

Cho, R.W., Song, Y., and Littleton, J.T. (2010). Comparative analysis of Drosophila and mammalian complexins as fusion clamps and facilitators of neurotransmitter release. Mol. Cell. Neurosci. *45*, 389–397.

Citri, A., and Malenka, R.C. (2008). Synaptic plasticity: multiple forms, functions, and mechanisms. Neuropsychopharmacology *33*, 18–41.

Dana, H., Sun, Y., Mohar, B., Hulse, B.K., Kerlin, A.M., Hasseman, J.P., Tsegaye, G., Tsang, A., Wong, A., Patel, R., et al. (2019). High-performance calcium sensors for imaging activity in neuronal populations and microcompartments. Nat. Methods *16*, 649–657.

Davis, G.W., DiAntonio, A., Petersen, S.A., and Goodman, C.S. (1998). Postsynaptic PKA controls quantal size and reveals a retrograde signal that regulates presynaptic transmitter release in Drosophila. Neuron *20*, 305–315.

Dawydow, A., Gueta, R., Ljaschenko, D., Ullrich, S., Hermann, M., Ehmann, N., Gao, S., Fiala, A., Langenhan, T., Nagel, G., et al. (2014). Channelrhodopsin-2-XXL, a powerful optogenetic tool for low-light applications. Proc. Natl. Acad. Sci. USA

111, 13972–13977.
DiAntonio, A., and Schwarz, T.L. (1994). The effect on synaptic physiology of synaptotagmin mutations in Drosophila. Neuron *12*, 909–920.
Dittman, J.S., Kreitzer, A.C., and Regehr, W.G. (2000). Interplay between facilitation, depression, and residual calcium at three presynaptic terminals. J. Neurosci. *20*, 1374–1385.
Fasshauer, D., Sutton, R.B., Brunger, A.T., and Jahn, R. (1998). Conserved structural features of the synaptic fusion complex: SNARE proteins reclassified as Q- and R-SNAREs. Proc. Natl. Acad. Sci. USA *95*, 15781–15786.
Frank, C.A. (2014). Homeostatic plasticity at the Drosophila neuromuscular junction. Neuropharmacology *78*, 63–74.
Frank, C.A., Kennedy, M.J., Goold, C.P., Marek, K.W., and Davis, G.W. (2006). Mechanisms underlying the rapid induction and sustained expression of synaptic homeostasis. Neuron *52*, 663–677.
Geerts, C.J., Mancini, R., Chen, N., Koopmans, F.T.W., Li, K.W., Smit, A.B., van Weering, J.R.T., Verhage, M., and Groffen, A.J.A. (2017). Tomosyn associates with secretory vesicles in neurons through its N- and C-terminal domains. PLoS One *12*, e0180912.
Genç, Ö., and Davis, G.W. (2019). Target-wide Induction and Synapse Type-Specific Robustness of Presynaptic Homeostasis. Curr. Biol. *29*, 3863–3873.e2.
Goel, P., Dufour Bergeron, D., Böhme, M.A., Nunnelly, L., Lehmann, M., Buser, C., Walter, A.M., Sigrist, S.J., and Dickman, D. (2019). Homeostatic scaling of active zone scaffolds maintains global synaptic strength. J. Cell Biol. *218*, 1706–1724.
Gracheva, E.O., Burdina, A.O., Holgado, A.M., Berthelot-Grosjean, M., Ackley, B.D., Hadwiger, G., Nonet, M.L., Weimer, R.M., and Richmond, J.E. (2006). Tomosyn inhibits synaptic vesicle priming in Caenorhabditis elegans. PLoS Biol. *4*, e261.
Gratz, S.J., Ukken, F.P., Rubinstein, C.D., Thiede, G., Donohue, L.K., Cummings, A.M., and O'Connor-Giles, K.M. (2014). Highly specific and efficient CRISPR/Cas9-catalyzed homology-directed repair in Drosophila. Genetics *196*, 961–971.
Gratz, S.J., Goel, P., Bruckner, J.J., Hernandez, R.X., Khateeb, K., Macleod, G.T., Dickman, D., and O'Connor-Giles, K.M. (2019). Endogenous Tagging Reveals Differential Regulation of Ca2+ Channels at Single Active Zones during Presynaptic Homeostatic Potentiation and Depression. J. Neurosci. *39*, 2416–2429.
Guan, Z., Quiñones-Frías, M.C., Akbergenova, Y., and Littleton, J.T. (2020). Drosophila Synaptotagmin 7 negatively regulates synaptic vesicle release and replenishment in a dosage-dependent manner. Elife *9*.
Harris, K.P., and Littleton, J.T. (2015). Transmission, development, and plasticity of synapses. Genetics *201*, 345–375.
Hatsuzawa, K., Lang, T., Fasshauer, D., Bruns, D., and Jahn, R. (2003). The R-SNARE motif of tomosyn forms SNARE core complexes with syntaxin 1 and SNAP-25 and down-regulates exocytosis. J. Biol. Chem. *278*, 31159–31166.
Hattendorf, D.A., Andreeva, A., Gangar, A., Brennwald, P.J., and Weis, W.I. (2007). Structure of the yeast polarity protein Sro7 reveals a SNARE regulatory mechanism. Nature *446*, 567–571.
Jahn, R., and Scheller, R.H. (2006). SNAREs--engines for membrane fusion. Nat. Rev. Mol. Cell Biol. *7*, 631–643.
Jan, L.Y., and Jan, Y.N. (1976). Properties of the larval neuromuscular junction in Drosophila melanogaster. J. Physiol. (Lond.) *262*, 189–214.

Jorquera, R.A., Huntwork-Rodriguez, S., Akbergenova, Y., Cho, R.W., and Littleton, J.T. (2012). Complexin controls spontaneous and evoked neurotransmitter release by regulating the timing and properties of synaptotagmin activity. J. Neurosci. *32*, 18234–18245.

Körber, C., and Kuner, T. (2016). Molecular machines regulating the release probability of synaptic vesicles at the active zone. Front. Synaptic Neurosci. *8*, 5.

Lehman, K., Rossi, G., Adamo, J.E., and Brennwald, P. (1999). Yeast homologues of tomosyn and lethal giant larvae function in exocytosis and are associated with the plasma membrane SNARE, Sec9. J. Cell Biol. *146*, 125–140.

Li, X., Goel, P., Chen, C., Angajala, V., Chen, X., and Dickman, D.K. (2018). Synapse-specific and compartmentalized expression of presynaptic homeostatic potentiation. Elife *7*.

Littleton, J.T., Stern, M., Schulze, K., Perin, M., and Bellen, H.J. (1993). Mutational analysis of Drosophila synaptotagmin demonstrates its essential role in Ca(2+)-activated neurotransmitter release. Cell *74*, 1125–1134.

Lnenicka, G.A., and Keshishian, H. (2000). Identified motor terminals in Drosophila larvae show distinct differences in morphology and physiology. J. Neurobiol. *43*, 186–197.

Lu, Z., Chouhan, A.K., Borycz, J.A., Lu, Z., Rossano, A.J., Brain, K.L., Zhou, Y., Meinertzhagen, I.A., and Macleod, G.T. (2016). High-Probability Neurotransmitter Release Sites Represent an Energy-Efficient Design. Curr. Biol. *26*, 2562–2571.

McEwen, J.M., Madison, J.M., Dybbs, M., and Kaplan, J.M. (2006). Antagonistic regulation of synaptic vesicle priming by Tomosyn and UNC-13. Neuron *51*, 303–315.

Müller, M., Liu, K.S.Y., Sigrist, S.J., and Davis, G.W. (2012). RIM controls homeostatic plasticity through modulation of the readily-releasable vesicle pool. J. Neurosci. *32*, 16574–16585.

Nair, A.G., Muttathukunnel, P., and Müller, M. (2020). Distinct molecular pathways govern presynaptic homeostatic plasticity. BioRxiv.

Newman, Z.L., Hoagland, A., Aghi, K., Worden, K., Levy, S.L., Son, J.H., Lee, L.P., and Isacoff, E.Y. (2017). Input-Specific Plasticity and Homeostasis at the Drosophila Larval Neuromuscular Junction. Neuron *93*, 1388–1404.e10.

Nicoll, R.A. (2003). Expression mechanisms underlying long-term potentiation: a postsynaptic view. Philos. Trans. R. Soc. Lond. B, Biol. Sci. *358*, 721–726.

Ortega, J.M., Genç, Ö., and Davis, G.W. (2018). Molecular mechanisms that stabilize short term synaptic plasticity during presynaptic homeostatic plasticity. Elife *7*.

Pérez-Moreno, J.J., and O'Kane, C.J. (2019). GAL4 drivers specific for type ib and type is motor neurons in drosophila. G3 (Bethesda) *9*, 453–462.

Petersen, S.A., Fetter, R.D., Noordermeer, J.N., Goodman, C.S., and DiAntonio, A. (1997). Genetic analysis of glutamate receptors in Drosophila reveals a retrograde signal regulating presynaptic transmitter release. Neuron *19*, 1237–1248.

Pobbati, A.V., Razeto, A., Böddener, M., Becker, S., and Fasshauer, D. (2004). Structural basis for the inhibitory role of tomosyn in exocytosis. J. Biol. Chem. *279*, 47192–47200.

Port, F., and Bullock, S.L. (2016). Augmenting CRISPR applications in Drosophila with tRNA-flanked sgRNAs. Nat. Methods *13*, 852–854.

Port, F., Chen, H.-M., Lee, T., and Bullock, S.L. (2014). Optimized CRISPR/Cas tools for efficient germline and somatic genome engineering in Drosophila. Proc. Natl. Acad. Sci. USA *111*, E2967-76.

Pulver, S.R., Bayley, T.G., Taylor, A.L., Berni, J., Bate, M., and Hedwig, B. (2015). IMAGING FICTIVE LOCOMOTOR PATTERNS IN LARVAL DROSOPHILA. J. Neurophysiol. *114*, jn.00731.2015.

Sakisaka, T., Yamamoto, Y., Mochida, S., Nakamura, M., Nishikawa, K., Ishizaki, H., Okamoto-Tanaka, M., Miyoshi, J., Fujiyoshi, Y., Manabe, T., et al. (2008). Dual inhibition of SNARE complex formation by tomosyn ensures controlled neurotransmitter release. J. Cell Biol. *183*, 323–337.

Schindelin, J., Arganda-Carreras, I., Frise, E., Kaynig, V., Longair, M., Pietzsch, T., Preibisch, S., Rueden, C., Saalfeld, S., Schmid, B., et al. (2012). Fiji: an open-source platform for biological-image analysis. Nat. Methods *9*, 676–682.

Söllner, T., Whiteheart, S.W., Brunner, M., Erdjument-Bromage, H., Geromanos, S., Tempst, P., and Rothman, J.E. (1993). SNAP receptors implicated in vesicle targeting and fusion. Nature *362*, 318–324.

Sudhof, T.C. (2004). The synaptic vesicle cycle. Annu. Rev. Neurosci. *27*, 509–547.

Südhof, T.C., and Rothman, J.E. (2009). Membrane fusion: grappling with SNARE and SM proteins. Science *323*, 474–477.

Thanawala, M.S., and Regehr, W.G. (2016). Determining synaptic parameters using high-frequency activation. J. Neurosci. Methods *264*, 136–152.

Wang, J.-W., Beck, E.S., and McCabe, B.D. (2012). A modular toolset for recombination transgenesis and neurogenetic analysis of Drosophila. PLoS One *7*, e42102.

Wang, Y., Lobb-Rabe, M., Ashley, J., Anand, V., and Carrillo, R.A. (2021). Structural and functional synaptic plasticity induced by convergent synapse loss in the drosophila neuromuscular circuit. J. Neurosci. *41*, 1401–1417.

Weber, T., Zemelman, B.V., McNew, J.A., Westermann, B., Gmachl, M., Parlati, F., Söllner, T.H., and Rothman, J.E. (1998). SNAREpins: minimal machinery for membrane fusion. Cell *92*, 759–772.

Weyhersmüller, A., Hallermann, S., Wagner, N., and Eilers, J. (2011). Rapid active zone remodeling during synaptic plasticity. J. Neurosci. *31*, 6041–6052.

Williams, A.L., Bielopolski, N., Meroz, D., Lam, A.D., Passmore, D.R., Ben-Tal, N., Ernst, S.A., Ashery, U., and Stuenkel, E.L. (2011). Structural and functional analysis of tomosyn identifies domains important in exocytotic regulation. J. Biol. Chem. *286*, 14542–14553.

Xue, M., Lin, Y.Q., Pan, H., Reim, K., Deng, H., Bellen, H.J., and Rosenmund, C. (2009). Tilting the balance between facilitatory and inhibitory functions of mammalian and Drosophila Complexins orchestrates synaptic vesicle exocytosis. Neuron *64*, 367–380.

Yamamoto, Y., Mochida, S., Miyazaki, N., Kawai, K., Fujikura, K., Kurooka, T., Iwasaki, K., and Sakisaka, T. (2010). Tomosyn inhibits synaptotagmin-1-mediated step of Ca2+-dependent neurotransmitter release through its N-terminal WD40 repeats. J. Biol. Chem. *285*, 40943–40955.

Yang, Y., and Calakos, N. (2013). Presynaptic long-term plasticity. Front. Synaptic Neurosci. *5*, 8.

Yizhar, O., Matti, U., Melamed, R., Hagalili, Y., Bruns, D., Rettig, J., and Ashery, U. (2004). Tomosyn inhibits priming of large dense-core vesicles in a calcium-dependent manner. Proc. Natl. Acad. Sci. USA *101*, 2578–2583.

Yizhar, O., Lipstein, N., Gladycheva, S.E., Matti, U., Ernst, S.A., Rettig, J., Stuenkel, E.L., and Ashery, U. (2007). Multiple functional domains are involved in tomosyn regulation of exocytosis. J. Neurochem. *103*, 604–616.

Yoshihara, M., and Littleton, J.T. (2002). Synaptotagmin I functions as a calcium sensor to synchronize neurotransmitter release. Neuron *36*, 897–908.

Zhang, Y., Rózsa, M., Bushey, D., Zheng, J., Reep, D., Broussard, G.J., Tsang, A., Tsegaye, G., Patel, R., Narayan, S., et al. (2020). jGCaMP8 Fast Genetically Encoded Calcium Indicators. Janelia Research Campus.

Chapter 3

Conclusions and Future Directions

3.1 Major Conclusions

My thesis work demonstrates Tomosyn functions as a negative regulator of presynaptic release in Drosophila, similar to its role in *C. elegans* and mouse models. In addition, I show that Tomosyn levels vary between tonic and phasic motoneurons and helps establish the unique release properties of these two neuronal classes. Eliminating *tomosyn* increases synaptic strength at the larval neuromuscular junction (NMJ), though it is still unclear how this alters overall nervous system function in relation to behavior. Preliminary data suggest $tomosyn^{NA1}$ adults show sluggish movement and a shortened lifespan, indicating the enhanced release may come at a cost for viability (**Figure 1A, B**). Given the central nervous system of nearly all animals is composed of a mixture of excitatory and inhibitory cells whose activities must be balanced to execute behaviors (Gogolla et al., 2009; Rubin et al., 2017; Zhou and Yu, 2018), differences in Tomosyn expression between excitatory and inhibitory neurons could contribute to the behavioral impairment in *tomosyn* mutants. However, it is unclear whether loss of Tomosyn enhances synaptic function at all neurons, as central pattern generator (CPG)-driven release patterns are more complex than the minimal stimulation paradigms used to experimentally assess synaptic strength (Lu et al., 2016; Pulver et al., 2015). Stimulation conditions better approximating the high firing rate of the CPG demonstrate *tomosyn* null synapses fail to sustain high release during stimulus trains, suggesting endogenous synaptic strength may be decreased rather than increased for neurons with high firing rates in the absence of Tomosyn. I interpret the inability to sustain release as a shift toward phasic release in synapses lacking Tomosyn.

Many additional lines of evidence suggest Tomosyn expression level regulates tonic versus phasic release properties. First, Tomosyn is differentially expressed between a tonic/phasic pair of motoneurons at the larval NMJ with higher expression in the tonic Ib than the phasic Is. Second, optogenetic isolation of evoked responses from Ib and Is in *tomosyn*

null mutants reveals a dramatic increase in Ib release whereas Is release is unaffected, suggesting Tomosyn inhibits SV fusion primarily at tonic synapses. Third, optical quantal analysis reveals the intrinsic difference in release strength between Ib and Is is eliminated in *tomosyn* nulls, demonstrating Tomosyn expression is required to establish baseline difference in tonic/phasic response between terminals. Finally, impaired postsynaptic glutamate receptor function fails to induce robust potentiation in Ib motoneurons when Tomosyn is absent, a phenotype characteristic of phasic Is synapses. Wildtype animals show a difference in average bouton size between Ib and Is, with Ib (big) having larger boutons and Is (small) displaying a smaller average bouton size. Interestingly, presynaptic morphology is changed in *tomosyn* null mutants, resulting in a decreased average bouton size in Ib with no obvious phenotype in Is. This morphological difference further argues Tomosyn primarily regulates Ib properties and has a lesser role in Is. It may also suggest Tomosyn helps establish morphological differences between these motoneurons as a consequence of the altered activity pattern. A reciprocal finding has been observed in crayfish, where artificial tonic frequency firing of phasic motoneurons converts their terminals to a more tonic appearance (Lnenicka et al., 1986). *Tomosyn* null mutant Ib terminals resemble the intrinsic properties of wildtype Is synapses, arguing in favor of a model where Drosophila neurons are slated for phasic properties and Tomosyn expression is required to confer tonic release properties. However, *tomosyn* null mutants display no change to SV size or SV density within the bouton by EM and no change to quantal size by electrophysiology. Given wildtype Is boutons are characterized by lower SV density and larger average quantal size, factors other than low Tomosyn expression must also be required to generate the intrinsic properties of Is terminals.

Using structure/function analysis we demonstrated the SNARE domain of Tomosyn is critical for release suppression and its scaffold helps localize Tomosyn to SVs. Without the SNARE domain Tomosyn fails to inhibit release, arguing the inhibitory function of Tomosyn maps to its SNARE domain. Consistently, expression of the Tomosyn SNARE alone partially restores Tomosyn function in the null mutant background. This construct is not as efficiently targeted to SVs as full-length Tomosyn, suggesting the scaffold domain is required for proper localization of the protein. In contrast to the SNARE domain, the scaffold domain alone colocalizes with SVs nearly as well as full-length Tomosyn, demonstrating this region regulates Tomosyn localization. However, the scaffold region shows almost no inhibitory activity on release, suggesting this region does not function to suppress release. This contrasts

with data from mammalian cell culture which argues the scaffold independently inhibits release by suppressing the ability of the Ca^{2+} sensor Synaptotagmin 1 (Syt1) to activate the SNARE complex (Yamamoto et al., 2010b). This mechanism does not appear to be essential for the inhibitory function of Drosophila Tomosyn as Tomosyn continues to suppress SV release in the absence of Syt1. Another unique feature of Drosophila Tomosyn is the essential role of the protein in suppressing spontaneous release. In contrast to most reports in other model organisms, *tomosyn* null Drosophila show an enhanced spontaneous release rate. This phenotype remained when the *tomosyn* null allele was crossed to an independent deficiency strain, and the phenotype was rescued by re-introducing a full-length Tomosyn transgene, indicating enhanced spontaneous release is directly caused by loss of Tomosyn. The difference in phenotype between Drosophila and other model systems may therefore reflect a difference in Tomosyn function between species. Alternatively, this may reflect a difference in Tomosyn function between distinct synaptic populations as a null mutation in the mammalian Tomosyn ortholog, Tomosyn-2 results in increased spontaneous release at mouse neuromuscular junctions (Geerts et al., 2015).

3.2 Future Directions

Our work has established the Drosophila NMJ as a model synapse to study Tomosyn's role in regulating intrinsic synaptic properties and neurotransmitter release. Many questions remain about Tomosyn function and will be discussed as possible future directions in this section.

Dosage sensitivity of Tomosyn in regulating tonic versus phasic release

Although many neurons can be broadly classified as tonic/phasic based on their initial release probability and response to train stimulation, the synaptic release character of individual synapses within these two subgroups also displays significant heterogeneity. For example, the tonic Ib motoneurons of the larval neuromuscular junction show moderate sustained release from the onset of stimulation (Aponte-Santiago et al., 2020; Atwood et al., 1993; Kurdyak et al., 1994; Lu et al., 2016). In contrast, tonic motoneurons of the Crayfish abdomen as well as mammalian parallel fiber to Purkinje cell synapses show weak initial evoked responses followed by strong short-term facilitation in response to prolonged stimulation (Atwood, 2008; Atwood and Karunanithi, 2002; Dittman et al., 2000; Kennedy

and Takeda, 1965). Our data suggest moderate expression of Tomosyn in Ib motoneurons of Drosophila larvae is required for the tonic release character of this synapse, and overexpression of both Drosophila and human Tomosyn further suppresses release probability (P_r) below wildtype levels during single stimulation. However, we did not test whether Tomosyn overexpression alters the synaptic response during train stimulation at the larval NMJ. It is possible Tomosyn overexpression makes the Ib synapse even more tonic by suppressing initial release to enable facilitation rather than sustained release during stimulus trains.

If Tomosyn were to regulate tonic release in a dosage-dependent manner the synapse would likely require a Ca^{2+}-sensitive mechanism to overcome Tomosyn inhibition. Such a mechanism is unlikely to be intrinsic to Tomosyn itself, as null mutants show enhanced release across a wide range of external Ca^{2+} concentrations with no apparent effect on the cooperativity of release, suggesting the inhibitory mechanism of Tomosyn is insensitive to Ca^{2+}. It is therefore more likely Tomosyn expression level regulates tonic/phasic release unidirectionally by creating a bottleneck in the SV fusion cycle that sets evoked response size in proportion to the level of Tomosyn expression. This hypothesis could be directly tested by subjecting NMJs overexpressing Tomosyn to a train stimulation protocol. Sustained or depressed evoked responses during repetitive stimulation would be consistent with a Ca^{2+}-insensitive role for Tomosyn in setting an upper limit on evoked response size. However, if train stimulation results in facilitation this would argue Tomosyn expression level bidirectionally regulates tonic release character likely through some Ca^{2+}-dependent mechanism of SV mobilization or docking/priming.

We were unable to demonstrate whether elevated Tomosyn expression in the Is converts this synapse from phasic to tonic release as pan-neuronal expression of UAS-Tomosyn-Myc with the elav-Gal4 driver resulted in very little to no Tomosyn expression in this terminal. Preliminary experiments using a strong Is-specific driver (Fmr1-Gal4) revealed no change in the single AZ P_r of Is synapses, revealing either Is resistance to Tomosyn inhibition or lack of UAS-Tomosyn-Myc expression in Is despite the strong driver. The latter explanation is supported by preliminary data from the lab. Single cell RNA-sequencing of Ib and Is motoneurons suggests the *tomosyn13A* splice variant is equally transcribed in Ib and Is. In contrast, results presented in chapter 2 demonstrate the mature protein is expressed ~2-fold higher in Ib than Is and optogenetic stimulation of *tomosyn* null mutants argues no

significant Tomosyn inhibition is present in the Is motoneuron. These data suggest some translational or post-translational mechanism restricts the level of Tomosyn protein expression in Is. To determine whether post-translational degradation accounts for the difference in transcript and protein abundance, a targeted screen for restored expression of endogenously tagged Tomosyn13A-GFP in Is motoneurons could be performed using RNAi constructs that target the ubiquitin ligase gene family. If a post-translational Tomosyn degradation mechanism exists in Drosophila, this screen would likely uncover the molecular pathway mediating this degradation. Is-specific knockdown of the requisite factors to restore Tomosyn expression could then be tested for their tonic/phasic release properties.

Enhancement of the tomosyn phenotype

Beyond Tomosyn, few presynaptic mutants have been described that cause enhanced release. Synaptotagmin 7 (Syt7) is a presynaptic protein that was recently shown to inhibit evoked release in Drosophila by limiting incorporation of SVs into the readily releasable pool (Guan et al., 2020). *tomosyn/syt7* double mutants show enhanced evoked release above either single mutant, suggesting at least two independent pathways negatively regulate SV fusion at the Drosophila NMJ. Whether other mutants with similar phenotypes operate within one of these pathways or regulate release via yet another mechanism is an interesting topic for future study. A point mutant in Drosophila Syx1 ($syx1^{3\text{-}69}$) causes an amino acid substitution at a residue that coordinates Syx1 binding with SNAP-25 and Syb2 near the transmembrane domain of the protein (Lagow et al., 2007; Littleton et al., 1998). These mutants paralyze at restrictive temperature (Littleton et al., 1998) and display similar synaptic defects to the *tomosyn* null at room temperature including an elevated spontaneous release rate, enhanced evoked response size, and greater 7S SNARE complex formation (Lagow et al., 2007). A recent study suggests release defects of $syx1^{3\text{-}69}$ may result from impaired binding of the fusion clamp Complexin (Cpx) to the partially assembled SNARE complex (Vasin et al., 2016), however this model does not account for the enhanced evoked release observed in $syx1^{3\text{-}69}$ mutants. It is possible this mutant alters the binding interaction between Syx1 and Tomosyn, explaining the similar phenotypes between *tomosyn* and $syx1^{3\text{-}69}$. This model could be tested by bringing the $syx1^{3\text{-}69}$ mutation into the *tomosyn* null background. If these two mutants enhance the release defects of each other, this would suggest these two mutants increase SNARE assembly and SV fusion via separate mechanisms. If instead these mutants

fail to enhance each other, this might suggest *syx1*$^{3\text{-}69}$ increases release by decreasing Tomosyn's ability to inhibit fusion providing an explanation for the similar phenotypes.

The SV-associated protein Synapsin associates with SVs to restrict their mobility using a mechanism that is reversed by elevated Ca^{2+} concentration to facilitate SV mobilization during stimulus trains (Akbergenova and Bykhovskaia, 2010; Evergren et al., 2007; Rosahl et al., 1993; Sun et al., 2006). Null mutants of Drosophila *synapsin* show greater SV mobility within the cytosol yet display no apparent release defects in response to single stimuli and only mild reductions in evoked response size following several minutes of high frequency stimulation (Akbergenova and Bykhovskaia, 2007, 2010). Increased SV mobility might be expected to increase the size of the immediately releasable SV pool to cause enhanced evoked responses. However it is possible a Tomosyn bottleneck in SV availability is sufficient to mask the phenotype of *synapsin* mutants. This hypothesis could be tested by performing electrophysiology in *tomosyn;synapsin* double mutants. Enhancement of the *tomosyn* phenotype in the double mutant background would demonstrate *tomosyn* is epistatic to *synapsin*, suggesting Tomosyn regulates quantal content regardless of the number of mobile SVs within the cytosol. Further, train stimulation experiments may lend insight into whether Tomosyn and Synapsin co-regulate tonic release. Enhanced depression during train stimulation in double mutants would suggest Synapsin restricts the rate at which *tomosyn* single mutants can exhaust the presynaptic supply of SVs.

Co-regulation of release by Tomosyn and other SNARE regulatory proteins

The SNARE regulatory proteins Unc13 and Unc18 regulate SNARE assembly by controlling the conformational state of Syx1, as described in chapter 1. Briefly, Syx1 can adopt at least two conformations including a closed conformation that prevents SNARE complex assembly and an open conformation that allows SNARE assembly to proceed. Unc18 has been shown to play a dual role, both holding Syx1 in its closed conformation to inhibit SV fusion and chaperoning the assembly of Syx1 with the v-SNARE Syb2 as a step toward activating SV release. Unc13 is thought to be involved in the transition between the inhibitory and the activating functions of Unc18 on SNARE assembly (Dulubova et al., 1999, 2007; Gerber et al., 2008b; Khvotchev et al., 2007; Richmond et al., 2001). Null mutants in Unc13 and Unc18 nearly eliminate all evoked and spontaneous release across species, demonstrating these proteins are critical for SNARE assembly and SV fusion (Aravamudan

et al., 1999; Augustin et al., 1999; Harrison et al., 1994; Varoqueaux et al., 2002; Verhage et al., 2000). Work at *C. elegans* NMJs reveals loss of Tomosyn partially restores the release defects of *unc13* and *unc18*, suggesting Tomosyn normally prevents Unc13- and Unc18-independent SNARE assembly (Gracheva et al., 2006, 2010; Hu et al., 2013; McEwen et al., 2006). Whether this mechanism is employed by other synapses is currently unknown. Given Drosophila null mutants of *unc13* and the *unc18* homolog *rop* are embryonic lethal, mutant experiments would either need to be performed at the embryonic NMJ or using a conditional knockout approach. Cell-type specific CRISPR/Cas9 using the Gal4/UAS system to drive expression of guide RNAs targeting *unc13* and *rop* in a single motoneuron may be used to generate a knockout without affecting overall viability. Using this system in the *tomosyn* null background would enable electrophysiological recordings from *tomosyn;unc13* and *tomosyn;rop* double mutant NMJs. If Tomosyn suppresses Unc13- and Rop-independent priming in Drosophila, the evoked response size and the spontaneous release rate of double mutant NMJs should be enhanced above either *unc13* or *rop* single knockouts. Although we have not yet performed double mutant experiments, preliminary overexpression experiments suggest Tomosyn and Unc13 interact to control SV priming at the Drosophila NMJ. Overexpression of an Unc13-GFP transgene did not affect evoked response size at the NMJ in a wildtype background (**Figure 2A, B**). However, overexpression of Unc13-GFP further enhanced the evoked response size in the *tomosyn* null background, suggesting Tomosyn may restrict the ability of Unc13 to prime vesicles in addition to its role in preventing Unc13-independent priming.

Presence of a negatively charged aspartate residue (D) directly downstream of the zero-layer arginine (R) in Syb2 is a highly conserved feature of fusogenic v-/R-SNAREs (Fasshauer et al., 1998). This D residue is critical for coordinating Cpx binding to the SNARE complex suggesting this residue has been conserved to enable Cpx binding (Pobbati et al., 2004). A single amino acid substitution from D to the simplest uncharged amino acid glycine (G) is a highly conserved feature of Tomosyn across species and has been shown to prevent Cpx binding to the Tomosyn SNARE complex *in vitro* (Pobbati et al., 2004), suggesting Cpx interaction with the Tomosyn SNARE complex has been strongly selected against. Why this residue change is so strongly conserved remains unknown. *cpx* mutant Drosophila show a dramatic ~100-fold increase in spontaneous SV fusion (Huntwork and Littleton, 2007; Jorquera et al., 2012) and posttranslational modification of Cpx causes an acute increase to

the spontaneous release rate (Cho et al., 2015) suggesting the rate of spontaneous release is tuned by the functional pool of Cpx at the NMJ. It is possible Cpx binding to the Tomosyn complex would limit Cpx's availability to clamp the fusogenic SNARE complex. This model could be tested by rescuing *tomosyn* mutants with constructs encoding D in the place of G directly downstream of the zero-layer R. If this mutant rescue construct disrupts Cpx clamping by competing with fusogenic complexes for Cpx binding, this would likely result in an increased spontaneous release rate. Alternatively, it is possible this G residue is important for some function unrelated to Cpx. These mutant rescue experiments would help clarify whether selection against Cpx binding explains this highly conserved Tomosyn feature.

Assessing SNARE dynamics in vivo

Whether the Tomosyn SNARE motif contains features that uniquely enable it to act as a decoy SNARE is not known. Tomosyn proteins across species share homology with the Syb2 family of v-SNAREs, however these two families show sequence differences and represent phylogenetically distinct groups. To test the model that Tomosyn inhibits release by mimicking Syb2 to lock the t-SNAREs in a non-fusogenic complex, the Tomosyn SNARE motif could be exchanged for the Syb2 SNARE motif. A chimeric protein with the Tomosyn scaffold and the Syb2 v-SNARE could be tested for its ability to suppress evoked and spontaneous release in the *tomosyn* null mutant. If this construct rescues release, it would argue the Tomosyn SNARE motif is not unique in its ability to inhibit release. Conversely, if this construct fails to rescue release this would argue the Tomosyn SNARE motif is specialized in some way to enable decoy SNARE activity. It will also be interesting to directly compare the rescue efficiencies of full-length Tomosyn and the Syb2/Tomosyn chimeric protein. *In vitro* studies have demonstrated Syb2 and the Tomosyn SNARE form similarly stable SNARE complexes and fail to displace each other (Pobbati et al., 2004). If this is true *in vivo*, one might expect to see no difference in rescue efficiency between Tomosyn and the Tomosyn/Syb2 fusion protein. However, if these two rescue constructs differ in their ability to inhibit release it is more likely one of the two SNARE motifs binds t-SNAREs more efficiently when attached to the Tomosyn scaffold.

Tomosyn inhibition of SNARE complex assembly has not directly been directly visualized *in vivo*. To test this, I generated a biosensor intended to monitor SNARE assembly

within living neurons. This sensor uses the splitFAST system which is composed of two protein components that reversibly assemble to bind a bath-applied fluorogenic compound (^{TF}Lime) that fluoresces only when bound to the assembled FAST complex (Tebo and Gautier, 2019). The large piece of splitFAST was added to the cytosolic N-terminus of nSyb and the smaller piece was attached to the N-terminus of SNAP-25 (**Figure 3A**). A fluorescent signal should only occur when SNAP-25 and nSyb are in complex. The LexA/LexAop expression system is used to drive expression of these two transgenes, which are encoded within the same polycistronic cDNA separated by a P2A "self-cleaving" peptide sequence (Liu et al., 2017). Preliminary experiments are promising, showing a strong fluorescent signal in larval motoneurons (**Figure 3B**). Further characterization is needed to determine whether this construct can be used to approximate bulk trans-SNARE complex assembly *in vivo*. First, western blot analysis must be used to stain against Syb and SNAP-25 to determine whether the P2A peptide sequence efficiently cleaves this construct. Next, fluorescent signal should be assessed in the background of temperature-sensitive paralytic mutants of NSF (*comatose^{TS}*) and Syx1 (*syx1$^{3\text{-}69}$*). At restrictive temperatures, *comatose^{TS}* prevents cis-SNARE complex disassembly post-fusion resulting in progressive buildup of cis-SNAREs whereas *syx1$^{3\text{-}69}$* shows nearly no assembled SNAREs at elevated temperature by western blot (Littleton et al., 1998). If this sensor is working as expected, *comatose^{TS}* should show increased fluorescence intensity at restrictive temperatures and *syx1$^{3\text{-}69}$* should show lower fluorescence. Assuming the sensor accurately reports SNARE assembly, I will then bring this sensor into the *tomosyn* null mutant background to determine whether bulk SNARE assembly is altered in the absence of Tomosyn.

Transcriptional and post-translational regulation of Tomosyn function

Alternative splicing of the *tomosyn* mRNA sequence may provide a mechanism to regulate the strength of Tomosyn's inhibitory activity. As discussed in chapter 2, alternative splicing of the L(2)GL scaffold coding region is a conserved feature of Tomosyn (Groffen et al., 2005), however the physiological relevance of this splicing is not clear. Our data suggest the inhibitory strength of Tomosyn may differ between splice variants as overexpression of Tomosyn13A, but not 13B, suppresses evoked and spontaneous release below wildtype levels. To test whether alternative splicing endogenously regulates Tomosyn function, CRISPR/Cas9 was used to generate isoform specific null mutants in Tomosyn13A and 13B

by separately inserting a stop codon after the splice acceptor site in each alternatively spliced exon (**Figure 4A**). Preliminary experiments revealed evoked responses of both *tomosyn13A*$^{\Delta}$ and *tomosyn13B*$^{\Delta}$ phenocopied the *tomosyn* null (**Figure 4B**) in contrast to rescue experiments described in chapter 2 which demonstrated co-expression of both isoforms is not required to suppress release. It is possible these mutants disrupt normal splicing of *tomosyn,* resulting in failure to express either full-length isoform. However, *tomosyn13A*$^{\Delta}$ and *tomosyn13B*$^{\Delta}$ showed no significant spontaneous release defects arguing some residual Tomosyn function is retained (**Figure 4C**). These results are difficult to interpret given the high variability in the isoform-specific null mutants and should therefore be repeated with larger sample sizes to better represent the biological range of phenotypes associated with *tomosyn*$^{13A\Delta}$ and *tomosyn*$^{13B\Delta}$. Western blot analysis should also be performed to ensure normal expression of the unaffected splice variant in each of these mutants. However, our attempts to generate antisera against three predicted antigenic fragments of Tomosyn were unsuccessful. We also attempted to purify full-length Tomosyn from transgenic *E. coli* but failed to solubilize the protein from bacterial pellets. Biochemistry studies of mammalian Tomosyn proteins have used cultured insect Sf9 cells to purify Tomosyn (Bhatnagar et al., 2014; Yu et al., 2014) suggesting this approach may work to isolate full-length Drosophila Tomosyn for use in antibody production and biochemistry experiments. If this fails, northern blot analysis might be used to ensure *tomosyn* pre-mRNAs are properly spliced despite the DsRed insertions in *tomosyn*$^{13A\Delta}$ and *tomosyn*$^{13B\Delta}$.

Mammalian studies have demonstrated Tomosyn function is regulated post-translationally by Protein Kinase A (PKA) phosphorylation. Tomosyn more effectively suppress SV release when it cannot be phosphorylated by PKA suggesting this kinase regulates Tomosyn's ability to inhibit release (Baba et al., 2005). Indeed, presynaptic knockdown of Tomosyn at hippocampal synapses reduces PKA-dependent long-term potentiation (LTP) arguing PKA inactivation of Tomosyn is required for some forms of presynaptic plasticity (Ben-Simon et al., 2015). Given presynaptic Protein Kinase D (PKD) activity is essential for expression of Gyki-induced presynaptic homeostatic potentiation (PHP) (Nair et al., 2020), whether PKA regulates Drosophila Tomosyn function in a similar manner is of interest. Inactivation of Tomosyn by PKD phosphorylation may underlie the acute increase in quantal content that occurs during PHP expression and would explain the inability of both *tomosyn* and *PKD* mutants to potentiate following Gyki incubation. Whether

Tomosyn is phosphorylated by PKD might be tested *in vitro* using a kinase assay on purified Tomosyn followed by mutational analysis to determine which residues are targeted for phosphorylation, if any. The *in vivo* function of these residues could then be tested using site-directed mutagenesis to generate mutant transgenes, followed by electrophysiology to determine whether these mutants can rescue PHP expression in the *tomosyn* null background.

The RNA editing enzyme ADAR (adenosine deaminase acting on RNA) modifies specific nucleotide sequences of mRNA transcripts, which can result in changes to the coding sequence (Buhl et al., 2013; Deng et al., 2020; Hoopengardner et al., 2003; Palladino et al., 2000; Paro et al., 2012). Transcriptional profiling of the Drosophila adult brain has demonstrated *tomosyn* is targeted by ADAR within the scaffold coding region, resulting in a coding change at amino acid 440 from serine to glycine (Sapiro et al., 2019). Homology modelling suggests this serine residue occurs along a face of the scaffold predicted to regulate access of the C-terminal SNARE motif (Hattendorf et al., 2007; Lehman et al., 1999). Further, phosphorylation prediction with the NetPhos3.1 algorithm strongly suggests this serine is phosphorylated raising the possibility that ADAR editing of Tomosyn may alter the way the scaffold and SNARE domains interact. To test this prediction, site-directed mutagenesis might be used to generate Tomosyn transgenes with a phospho-mimetic substitution (S440D) and the phospho-incompetent substitution generated by ADAR (S440G). These transgenes can then be compared to the wildtype unedited Tomosyn sequence for their ability to rescue the *tomosyn* null phenotype. Given the SNARE domain is the critical domain mediating Tomosyn's ability to suppress release, altered rescue efficiency in these lines might indicate the scaffold domain regulates SNARE activity via this ADAR-edited residue. This may also lend further insight into why the scaffold and SNARE must occur in tandem to fully reconstitute Tomosyn function as demonstrated in chapter 2.

Determining whether Tomosyn has a postsynaptic role in Drosophila

Localization studies in mammalian neurons demonstrate Tomosyn is also present in dendritic arbors, suggesting Tomosyn may play an additional postsynaptic role (Barak et al., 2010; Geerts et al., 2017). While the Tomosyn scaffold domain has been suggested to regulate dendritic morphology by regulating the monomeric GTPase RhoA (Shen et al., 2020), whether the Tomosyn SNARE domain plays a postsynaptic role remains unknown. SNARE function in the postsynaptic compartment mediates delivery of cargo to the membrane and

regulates release of retrograde signaling molecules onto presynaptic targets (Cho et al., 2015; Harris et al., 2016; Korkut et al., 2013; Kwon and Castillo, 2008; Lu et al., 2001; Yoshihara et al., 2005). In mammalian neurons, the t-SNARE Syntaxin 4 (Syx4) is required for membrane insertion of AMPA type glutamate receptors into dendritic spines during long-term potentiation as well as regulating the release of other cargoes (Kennedy et al., 2010). While a direct interaction between Syx4 and Tomosyn has not been demonstrated in the nervous system, work in cultured adipocytes and mast cells demonstrates Tomosyn inhibits Syx4-dependent cargo release (Madera-Salcedo et al., 2018; Widberg et al., 2003), suggesting Tomosyn may act as a decoy SNARE during formation of the Syx4 complex as well. Together, these data suggest Tomosyn may regulate Syx4-mediated retrograde signaling and receptor trafficking within the postsynaptic terminal.

The Drosophila Syx4 homolog is localized to the postsynaptic terminal and null mutants show abnormal presynaptic morphology and impaired structural plasticity (Harris et al., 2016). Assuming the model that Tomosyn regulates Syx4-dependent retrograde signaling and cargo traffic, postsynaptic overexpression of Tomosyn might suppress Syx4 activity and may cause a full or partial phenocopy of the *syx4* null mutant. To test this model, larvae overexpressing Tomosyn13A in muscles could be tested for irregular presynaptic morphology and AZ structure, as *syx4* mutants show reduced bouton number and greater voltage-gated calcium channel abundance per AZ (Harris et al., 2016, 2018). If muscle overexpression of Tomosyn affects the gross morphology of the presynaptic terminal or active zone structure, this would suggest Tomosyn acts postsynaptically to regulate presynaptic structure. Further, *syx4* mutants show increased evoked response size (Harris et al., 2018) suggesting Tomosyn overexpression in the muscle may lead to enlarged evoked responses if Tomosyn inhibits Syx4 function in the postsynaptic compartment.

3.3 Materials and Methods

Fly stocks

Drosophila melanogaster were cultured on standard medium between 22 and 25°C. Third instar larvae were used for all experiments in this chapter. Strains used include $elav^{C155}$-GAL4 (BDSC#8765), UAS-Unc13A-GFP (Böhme et al., 2016), vGluT-LexA (Choi et al., 2014), LexAop-mCherry (Choi et al., 2014), LexAop-NFAST-nSyb-P2A-CFAST10-SNAP25 (SNARE biosensor; this study), $tomosyn^{13A\Delta}$ (this study), and $tomosyn^{13B\Delta}$ (this

study).

Genome engineering and LexA line construction

To generate *tomosyn*$^{13A\Delta}$, four guide RNAs (gRNAs) flanking the splice acceptor of exon 13A were selected using the CRISPR Optimal Target Finder (Gratz et al., 2014). These gRNAs were cloned into the pCFD5 expression vector (Addgene #73914) (Port and Bullock, 2016) according to the Gibson assembly protocol using NEBuilder HighFidelity DNA Assembly Cloning Kit (E5520). Gibson assembly was also used to generate a donor construct encoding a floxed P3>DsRed reporter cassette (Addgene #51434) in the reverse orientation and flanked with homology arms unpstream and downstream of the splice acceptor site of exon13A. These constructs were co-injected into vasa-Cas9 embryos (BDSC #56552) and Ds>Red positive transformants were selected by BestGene Inc (Chino Hills, CA, USA). *tomosyn*$^{13B\Delta}$ was made in the same way as *tomosyn*$^{13A\Delta}$.

To generate the SNARE biosensor, a cDNA was synthesized *de novo* by GENEWIZ, Inc (South Plainfield, NJ, USA). splitFAST sequences were obtained from the pAG241-FKBP-NFAST and pAG241-FKBP-CFAST10 plasmid sequences (Addgene #130812 and #130814, respectively) (Tebo and Gautier, 2019). The final cDNA was subcloned into the pBID-LexA-DSCP expression vector (gift from Brian McCabe) using restriction digestion with EcoRI and XbaI and standard ligation. This construct was injected into embryos containing the VK00027 attP acceptor site and positive transformants were selected and balanced by BestGene Inc.

Lifespan and behavioral analysis

For the lifespan analysis, age matched male flies of the desired genotypes were housed in vials containing standard medium, no more than 10 flies per vial. Flies were kept at 25ºC on 12h hour light/dark cycle and transferred at least once every three days, when deaths were recorded. For the behavioral analysis, age matched male flies of the desired genotypes were placed into small glass tubes (1 fly per tube) and loaded into an MB5 Multibeam Activity Monitor (TriKinetics Inc, Waltham, MA). Flies were allowed to acclimate for ~30 minutes before behavioral analysis was initiated. Flies were allowed to freely behave for ~15 minutes while the number of interbeam movements per minute per fly were tallied by DamSystemMB1v6 software (TriKinetics Inc).

Electrophysiology

Postsynaptic currents from the indicated genotypes were recorded from 3rd instar larvae at muscle fiber 6 of segments A3 and A4 using two-electrode voltage clamp with a –80 mV holding potential in HL3.1 saline solution (in mM, 70 NaCl, 5 KCl, 10 NaHCO3, 4 MgCl2, 5 trehalose, 115 sucrose, 5 HEPES, pH 7.18) as previously described (Jorquera et al., 2012). Final [Ca^{2+}] was adjusted to the level indicated in the text. All electrophysiology experiments were performed at room temperature. Inward currents recorded during TEVC are labeled on a reverse axis in the figures for simplicity. Data acquisition and analysis was performed using Axoscope 9.0 and Clampfit 9.0 software (Molecular Devices, Sunnyvale, CA, USA). Motor nerves innervating the musculature were severed and placed into a suction electrode. Action potential stimulation was applied at 0.33 Hz using a programmable stimulator (Master8, AMPI; Jerusalem, Israel).

^{TF}Lime Application

^{TF}Lime was diluted with DMSO to a 1000x stock concentration of 5 mM. Stock solution was diluted to the working concentration in HL3.1. Dissected larvae were incubated in ^{TF}Lime for ~30 seconds before imaging.

Live imaging

Live imaging was performed on a Zeiss Axio Imager equipped with a spinning-disk confocal head (CSU-X1; Yokagawa, Japan) and ImagEM X2 EM-CCD camera (Hamamatsu, Hamamatsu City, Japan). An Olympus LUMFL N 60X objective with a 1.10 NA was used to acquire imaging data of muscle fibers 6 and 7 in third instar larvae.

Statistical analysis and graphing

Statistical analysis and graphing were performed with GraphPad Prism (San Diego, CA, USA). Electrophysiological traces were generated using the plot function in Matlab R2020A (MathWorks, Natick, MA, USA). Statistical significance was determined using Student's *t* test for comparisons between two groups, or a One-way ANOVA followed by Tukey's multiple comparisons test for comparisons between three or more groups unless otherwise noted. In the figures, the center of each distribution is plotted as the median value

and reported in the figure legends as the median, mean ± SEM, *n*. In all cases *n* represents the number of individual NMJs analyzed unless otherwise noted in the figure legends. The number of larvae used per group in each experiment is indicated in the figure legends. Asterisks in the figures denote p-values of: *, $p \leq 0.05$; **, $p \leq 0.01$; ***, $p \leq 0.001$; and ****, $p \leq 0.0001$.

Figures

Figure 1

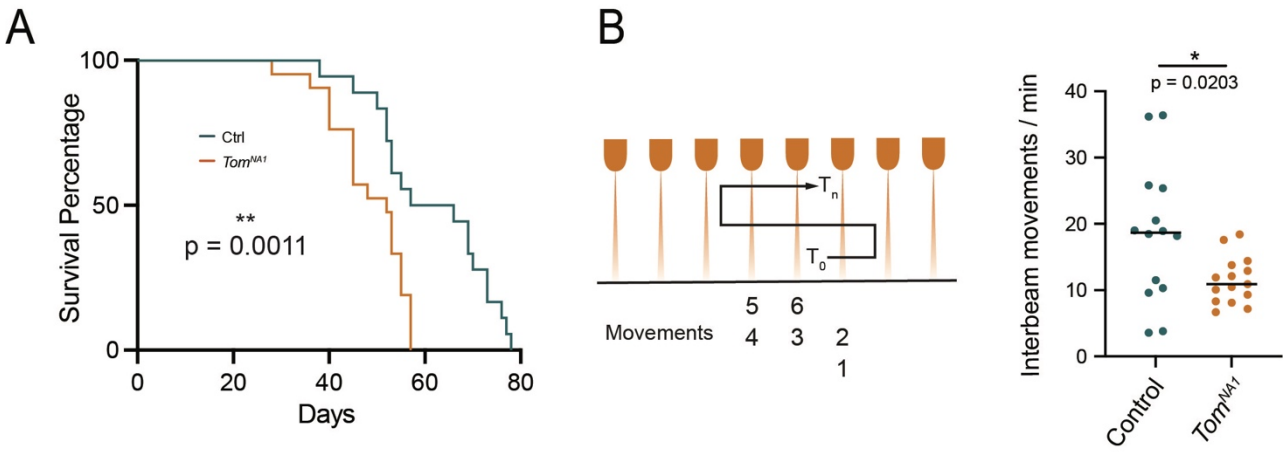
A
100
50
0
Survival Percentage
Ctrl
Tom^NA1
**
p = 0.0011
0
20
40
60
80
Days
B
T_n
T_0
Movements
5 6
4 3 2
1
*
p = 0.0203
40
30
20
10
0
Interbeam movements / min
Control
Tom^NA1

Figure 1: *Tomosyn* mutants have a shortened lifespan and show sluggish behavior.

(A) Percent of flies surviving over time (control: 61.50 days median survival, n = 18; $tomosyn^{NA1}$: 52.00 days median survival, n = 21; Mantel-Cox test, $X^2 = 10.72$, p = 0.0011). (B) Diagram illustrating how inter-beam moves are counted (left). Average inter-beam movements per fly per genotype (control: 18.68, 18.40 ± 2.743, n = 14 flies; $tomosyn^{NA1}$: 10.90, 11.48 ± 0.9066, n = 15 flies; p = 0.0203).

Figure 2

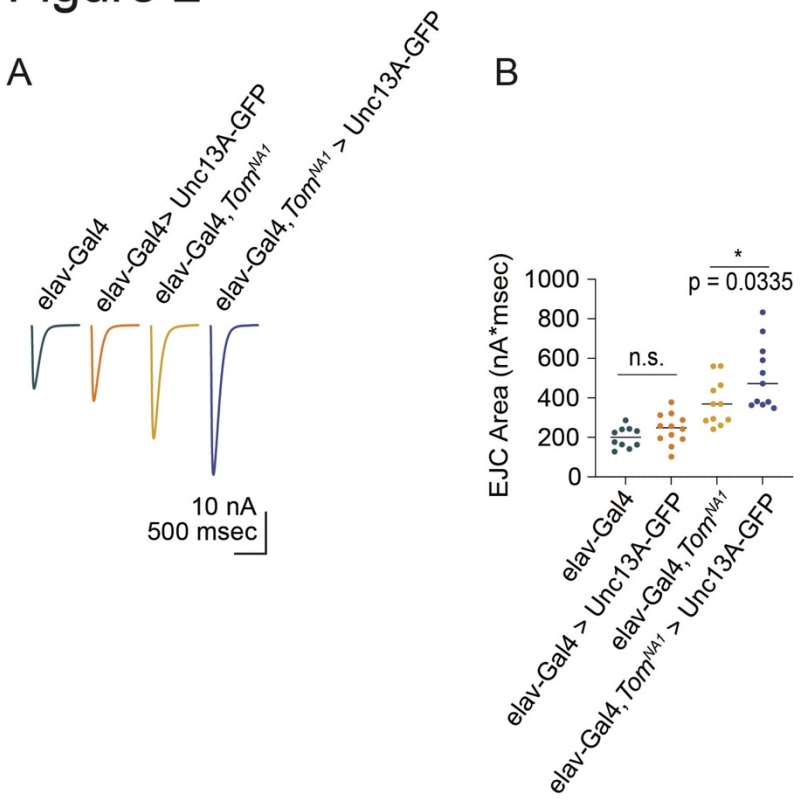
A
elav-Gal4
elav-Gal4> Unc13A-GFP
elav-Gal4, Tom^NA1
elav-Gal4, Tom^NA1 > Unc13A-GFP
10 nA
500 msec
B
EJC Area (nA*msec)
1000
800
600
400
200
0
n.s.
*
p = 0.0335
elav-Gal4
elav-Gal4 > Unc13A-GFP
elav-Gal4, Tom^NA1
elav-Gal4, Tom^NA1 > Unc13A-GFP

Figure 2: Tomosyn limits the activity of Unc13.

(A) Average evoked excitatory junctional current (eEJC) in 0.3 mM Ca^{2+}. (B) Quantification of average eEJC area (nA*msec) per NMJ in 0.3 mM Ca^{2+} (elav-Gal4: 200.3, 199.8 ± 16.49, n = 10; elav-Gal4>UAS-Unc13A-GFP: 248.9, 242.6 ± 22.26, n = 12; elav-Gal4,*tomosyn*^{NA1}: 368.7, 375.3 ± 34.86, n = 11; elav-Gal4,*tomosyn*^{NA1}>Unc13A-GFP: 472.4, 511.9 ± 50.63, n = 11; $p < 0.0001$; ≥ 3 larvae per group).

Figure 3

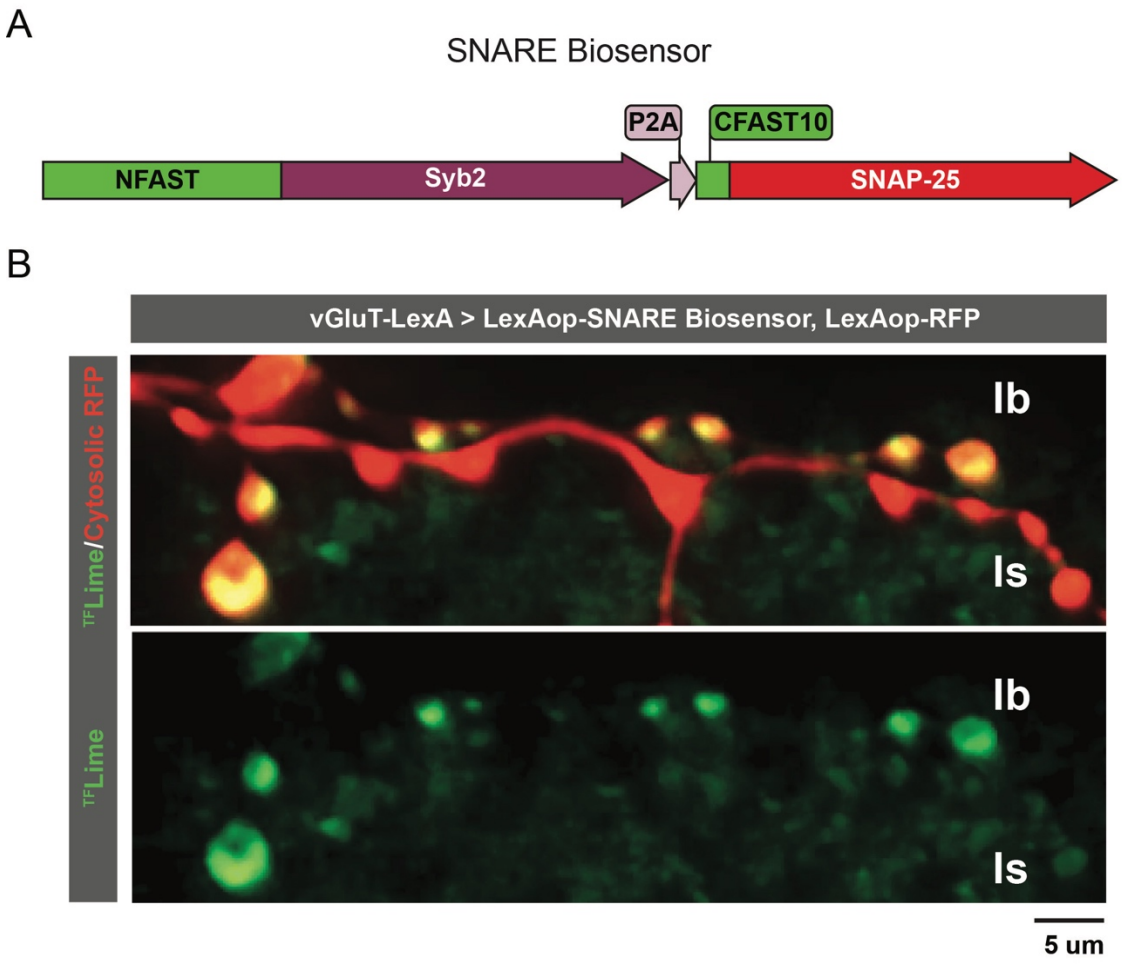
A
SNARE Biosensor
P2A
CFAST10
NFAST
Syb2
SNAP-25
B
vGluT-LexA > LexAop-SNARE Biosensor, LexAop-RFP
TFLime/Cytosolic RFP
TFLime
Ib
Is
Ib
Is
5 um

Figure 3: Testing a new biosensor to monitor SNARE assembly *in vivo.*

(A) Schematic representation of the SNARE biosensor design. (B) Live imaging of a cytosolically driven RFP (mCherry) and the SNARE biosensor. The fluorogenic ligand (^{TF}Lime) of this biosensor shows strong fluorescence signal in the presynaptic motoneuron.

Figure 4

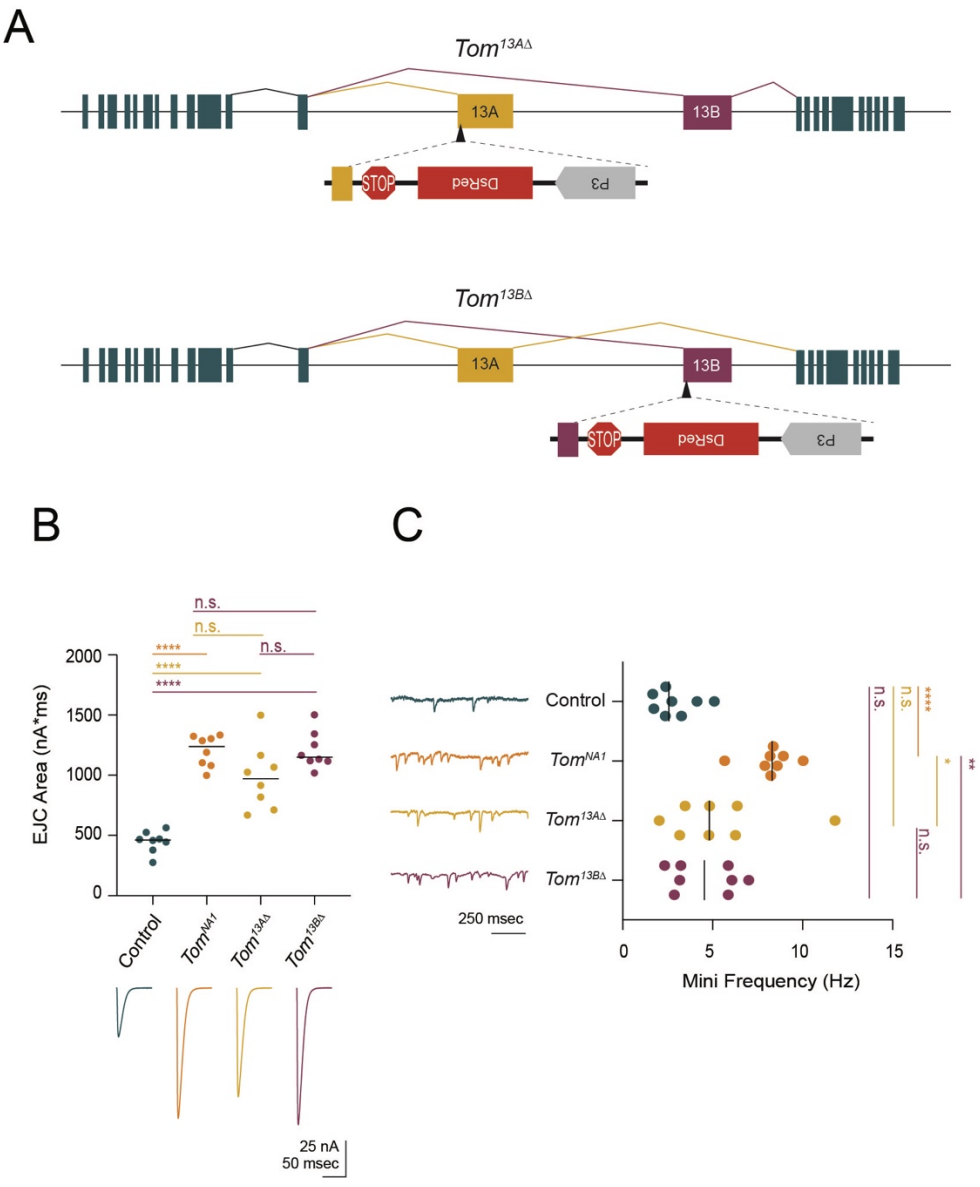
A
Tom13AΔ
13A
13B
STOP
DsRed
P3
Tom13BΔ
13A
13B
STOP
DsRed
P3
B
C
n.s.
n.s.
n.s.
****
****
****
2000
1500
1000
500
0
EJC Area (nA*ms)
Control
TomNA1
Tom13AΔ
Tom13BΔ
25 nA
50 msec
Control
TomNA1
Tom13AΔ
Tom13BΔ
250 msec
n.s.
n.s.
****
*
**
n.s.
0
5
10
15
Mini Frequency (Hz)

Figure 4: Isoform-specific *tomosyn* nulls show variable and intermediate release phenotypes.

(A) Schematic showing the genome modifications in *tomosyn*$^{13A\Delta}$ and *tomosyn*$^{13B\Delta}$. (B) Quantification of average eEJC area (nA*msec) per NMJ in 0.3 mM Ca^{2+} (control: 462.8, 448.4 ± 31.32, n = 8; *tomosyn*^{NA1}: 1239, 1203 ± 45.43, n = 8; *tomosyn*$^{13A\Delta}$: 970.7, 984.4 ± 95.59, n = 8; *tomosyn*$^{13B\Delta}$: 1150, 1207 ± 54.51, n = 8; p <0.0001; ≥ 4 larvae per group). (C) Quantification of average spontaneous release rate (Hz) per NMJ (control: 2.567, 2.925 ± 0.4212, n = 8; *tomosyn*^{NA1}: 8.300, 8.242 ± 0.4347, n = 8; *tomosyn*$^{13A\Delta}$: 4.817, 5.342 ± 1.064, n = 8; *tomosyn*$^{13B\Delta}$: 4.550, 4.550 ± 0.6432, n = 8; p <0.0001; ≥ 4 larvae per group).

References

Akbergenova, Y., and Bykhovskaia, M. (2007). Synapsin maintains the reserve vesicle pool and spatial segregation of the recycling pool in Drosophila presynaptic boutons. Brain Res. *1178*, 52–64.

Akbergenova, Y., and Bykhovskaia, M. (2010). Synapsin regulates vesicle organization and activity-dependent recycling at Drosophila motor boutons. Neuroscience *170*, 441–452.

Aponte-Santiago, N.A., Ormerod, K.G., Akbergenova, Y., and Littleton, J.T. (2020). Synaptic plasticity induced by differential manipulation of tonic and phasic motoneurons in drosophila. J. Neurosci. *40*, 6270–6288.

Aravamudan, B., Fergestad, T., Davis, W.S., Rodesch, C.K., and Broadie, K. (1999). Drosophila UNC-13 is essential for synaptic transmission. Nat. Neurosci. *2*, 965–971.

Atwood, H. (2008). Parallel "phasic" and "tonic" motor systems of the crayfish abdomen. J. Exp. Biol. *211*, 2193–2195.

Atwood, H.L., and Karunanithi, S. (2002). Diversification of synaptic strength: presynaptic elements. Nat. Rev. Neurosci. *3*, 497–516.

Atwood, H.L., Govind, C.K., and Wu, C.F. (1993). Differential ultrastructure of synaptic terminals on ventral longitudinal abdominal muscles in Drosophila larvae. J. Neurobiol. *24*, 1008–1024.

Augustin, I., Rosenmund, C., Südhof, T.C., and Brose, N. (1999). Munc13-1 is essential for fusion competence of glutamatergic synaptic vesicles. Nature *400*, 457–461.

Baba, T., Sakisaka, T., Mochida, S., and Takai, Y. (2005). PKA-catalyzed phosphorylation of tomosyn and its implication in Ca2+-dependent exocytosis of neurotransmitter. J. Cell Biol. *170*, 1113–1125.

Barak, B., Williams, A., Bielopolski, N., Gottfried, I., Okun, E., Brown, M.A., Matti, U., Rettig, J., Stuenkel, E.L., and Ashery, U. (2010). Tomosyn expression pattern in the mouse hippocampus suggests both presynaptic and postsynaptic functions. Front. Neuroanat. *4*, 149.

Ben-Simon, Y., Rodenas-Ruano, A., Alviña, K., Lam, A.D., Stuenkel, E.L., Castillo, P.E., and Ashery, U. (2015). A Combined Optogenetic-Knockdown Strategy Reveals a Major Role of Tomosyn in Mossy Fiber Synaptic Plasticity. Cell Rep. *12*, 396–404.

Bhatnagar, S., Soni, M.S., Wrighton, L.S., Hebert, A.S., Zhou, A.S., Paul, P.K., Gregg, T., Rabaglia, M.E., Keller, M.P., Coon, J.J., et al. (2014). Phosphorylation and degradation of tomosyn-2 de-represses insulin secretion. J. Biol. Chem. *289*, 25276–25286.

Böhme, M.A., Beis, C., Reddy-Alla, S., Reynolds, E., Mampell, M.M., Grasskamp, A.T., Lützkendorf, J., Bergeron, D.D., Driller, J.H., Babikir, H., et al. (2016). Active zone scaffolds differentially accumulate Unc13 isoforms to tune Ca(2+) channel-vesicle coupling. Nat. Neurosci. *19*, 1311–1320.

Buhl, L.K., Jorquera, R.A., Akbergenova, Y., Huntwork-Rodriguez, S., Volfson, D., and Littleton, J.T. (2013). Differential regulation of evoked and spontaneous neurotransmitter release by C-terminal modifications of complexin. Mol. Cell. Neurosci. *52*, 161–172.

Cho, R.W., Buhl, L.K., Volfson, D., Tran, A., Li, F., Akbergenova, Y., and Littleton, J.T. (2015). Phosphorylation of Complexin by PKA Regulates Activity-Dependent Spontaneous Neurotransmitter Release and Structural Synaptic Plasticity. Neuron *88*, 749–761.

Choi, B.J., Imlach, W.L., Jiao, W., Wolfram, V., Wu, Y., Grbic, M., Cela, C., Baines, R.A., Nitabach, M.N., and McCabe, B.D. (2014). Miniature neurotransmission regulates Drosophila synaptic structural maturation. Neuron *82*, 618–634.

Deng, P., Khan, A., Jacobson, D., Sambrani, N., McGurk, L., Li, X., Jayasree, A., Hejatko, J., Shohat-Ophir, G., O'Connell, M.A., et al. (2020). Adar RNA editing-dependent and -

independent effects are required for brain and innate immune functions in Drosophila. Nat. Commun. *11*, 1580.

Dittman, J.S., Kreitzer, A.C., and Regehr, W.G. (2000). Interplay between facilitation, depression, and residual calcium at three presynaptic terminals. J. Neurosci. *20*, 1374–1385.

Dulubova, I., Sugita, S., Hill, S., Hosaka, M., Fernandez, I., Südhof, T.C., and Rizo, J. (1999). A conformational switch in syntaxin during exocytosis: role of munc18. EMBO J. *18*, 4372–4382.

Dulubova, I., Khvotchev, M., Liu, S., Huryeva, I., Südhof, T.C., and Rizo, J. (2007). Munc18-1 binds directly to the neuronal SNARE complex. Proc. Natl. Acad. Sci. USA *104*, 2697–2702.

Evergren, E., Benfenati, F., and Shupliakov, O. (2007). The synapsin cycle: a view from the synaptic endocytic zone. J. Neurosci. Res. *85*, 2648–2656.

Fasshauer, D., Sutton, R.B., Brunger, A.T., and Jahn, R. (1998). Conserved structural features of the synaptic fusion complex: SNARE proteins reclassified as Q- and R-SNAREs. Proc. Natl. Acad. Sci. USA *95*, 15781–15786.

Geerts, C.J., Mancini, R., Chen, N., Koopmans, F.T.W., Li, K.W., Smit, A.B., van Weering, J.R.T., Verhage, M., and Groffen, A.J.A. (2017). Tomosyn associates with secretory vesicles in neurons through its N- and C-terminal domains. PLoS One *12*, e0180912.

Gerber, S.H., Rah, J.-C., Min, S.-W., Liu, X., de Wit, H., Dulubova, I., Meyer, A.C., Rizo, J., Arancillo, M., Hammer, R.E., et al. (2008). Conformational switch of syntaxin-1 controls synaptic vesicle fusion. Science *321*, 1507–1510.

Gogolla, N., Leblanc, J.J., Quast, K.B., Südhof, T.C., Fagiolini, M., and Hensch, T.K. (2009). Common circuit defect of excitatory-inhibitory balance in mouse models of autism. J. Neurodev. Disord. *1*, 172–181.

Gracheva, E.O., Burdina, A.O., Holgado, A.M., Berthelot-Grosjean, M., Ackley, B.D., Hadwiger, G., Nonet, M.L., Weimer, R.M., and Richmond, J.E. (2006). Tomosyn inhibits synaptic vesicle priming in Caenorhabditis elegans. PLoS Biol. *4*, e261.

Gracheva, E.O., Maryon, E.B., Berthelot-Grosjean, M., and Richmond, J.E. (2010). Differential Regulation of Synaptic Vesicle Tethering and Docking by UNC-18 and TOM-1. Front. Synaptic Neurosci. *2*, 141.

Gratz, S.J., Ukken, F.P., Rubinstein, C.D., Thiede, G., Donohue, L.K., Cummings, A.M., and O'Connor-Giles, K.M. (2014). Highly specific and efficient CRISPR/Cas9-catalyzed homology-directed repair in Drosophila. Genetics *196*, 961–971.

Groffen, A.J.A., Jacobsen, L., Schut, D., and Verhage, M. (2005). Two distinct genes drive expression of seven tomosyn isoforms in the mammalian brain, sharing a conserved structure with a unique variable domain. J. Neurochem. *92*, 554–568.

Guan, Z., Quiñones-Frías, M.C., Akbergenova, Y., and Littleton, J.T. (2020). Drosophila Synaptotagmin 7 negatively regulates synaptic vesicle release and replenishment in a dosage-dependent manner. Elife *9*.

Harris, K.P., Zhang, Y.V., Piccioli, Z.D., Perrimon, N., and Littleton, J.T. (2016). The postsynaptic t-SNARE Syntaxin 4 controls traffic of Neuroligin 1 and Synaptotagmin 4 to regulate retrograde signaling. Elife *5*.

Harris, K.P., Littleton, J.T., and Stewart, B.A. (2018). Postsynaptic Syntaxin 4 negatively regulates the efficiency of neurotransmitter release. J Neurogenet *32*, 221–229.

Harrison, S.D., Broadie, K., van de Goor, J., and Rubin, G.M. (1994). Mutations in the Drosophila Rop gene suggest a function in general secretion and synaptic transmission. Neuron *13*, 555–566.

Hattendorf, D.A., Andreeva, A., Gangar, A., Brennwald, P.J., and Weis, W.I. (2007). Structure of the yeast polarity protein Sro7 reveals a SNARE regulatory mechanism. Nature *446*, 567–571.

Hoopengardner, B., Bhalla, T., Staber, C., and Reenan, R. (2003). Nervous system targets of RNA editing identified by comparative genomics. Science *301*, 832–836.

Hu, Z., Tong, X.-J., and Kaplan, J.M. (2013). UNC-13L, UNC-13S, and Tomosyn form a protein code for fast and slow neurotransmitter release in Caenorhabditis elegans. Elife *2*, e00967.
Huntwork, S., and Littleton, J.T. (2007). A complexin fusion clamp regulates spontaneous neurotransmitter release and synaptic growth. Nat. Neurosci. *10*, 1235–1237.
Jorquera, R.A., Huntwork-Rodriguez, S., Akbergenova, Y., Cho, R.W., and Littleton, J.T. (2012). Complexin controls spontaneous and evoked neurotransmitter release by regulating the timing and properties of synaptotagmin activity. J. Neurosci. *32*, 18234–18245.
Kennedy, D., and Takeda, K. (1965). Reflex control of abdominal flexor muscles in the crayfish. J. Exp. Biol. *43*, 229–246.
Kennedy, M.J., Davison, I.G., Robinson, C.G., and Ehlers, M.D. (2010). Syntaxin-4 defines a domain for activity-dependent exocytosis in dendritic spines. Cell *141*, 524–535.
Khvotchev, M., Dulubova, I., Sun, J., Dai, H., Rizo, J., and Südhof, T.C. (2007). Dual modes of Munc18-1/SNARE interactions are coupled by functionally critical binding to syntaxin-1 N terminus. J. Neurosci. *27*, 12147–12155.
Korkut, C., Li, Y., Koles, K., Brewer, C., Ashley, J., Yoshihara, M., and Budnik, V. (2013). Regulation of postsynaptic retrograde signaling by presynaptic exosome release. Neuron *77*, 1039–1046.
Kurdyak, P., Atwood, H.L., Stewart, B.A., and Wu, C.F. (1994). Differential physiology and morphology of motor axons to ventral longitudinal muscles in larval Drosophila. J. Comp. Neurol. *350*, 463–472.
Kwon, H.-B., and Castillo, P.E. (2008). Long-term potentiation selectively expressed by NMDA receptors at hippocampal mossy fiber synapses. Neuron *57*, 108–120.
Lagow, R.D., Bao, H., Cohen, E.N., Daniels, R.W., Zuzek, A., Williams, W.H., Macleod, G.T., Sutton, R.B., and Zhang, B. (2007). Modification of a hydrophobic layer by a point mutation in syntaxin 1A regulates the rate of synaptic vesicle fusion. PLoS Biol. *5*, e72.
Lehman, K., Rossi, G., Adamo, J.E., and Brennwald, P. (1999). Yeast homologues of tomosyn and lethal giant larvae function in exocytosis and are associated with the plasma membrane SNARE, Sec9. J. Cell Biol. *146*, 125–140.
Littleton, J.T., Chapman, E.R., Kreber, R., Garment, M.B., Carlson, S.D., and Ganetzky, B. (1998). Temperature-sensitive paralytic mutations demonstrate that synaptic exocytosis requires SNARE complex assembly and disassembly. Neuron *21*, 401–413.
Liu, Z., Chen, O., Wall, J.B.J., Zheng, M., Zhou, Y., Wang, L., Vaseghi, H.R., Qian, L., and Liu, J. (2017). Systematic comparison of 2A peptides for cloning multi-genes in a polycistronic vector. Sci. Rep. *7*, 2193.
Lu, W., Man, H., Ju, W., Trimble, W.S., MacDonald, J.F., and Wang, Y.T. (2001). Activation of synaptic NMDA receptors induces membrane insertion of new AMPA receptors and LTP in cultured hippocampal neurons. Neuron *29*, 243–254.
Lu, Z., Chouhan, A.K., Borycz, J.A., Lu, Z., Rossano, A.J., Brain, K.L., Zhou, Y., Meinertzhagen, I.A., and Macleod, G.T. (2016). High-Probability Neurotransmitter Release Sites Represent an Energy-Efficient Design. Curr. Biol. *26*, 2562–2571.
Madera-Salcedo, I.K., Danelli, L., Tiwari, N., Dema, B., Pacreau, E., Vibhushan, S., Birnbaum, J., Agabriel, C., Liabeuf, V., Klingebiel, C., et al. (2018). Tomosyn functions as a PKCδ-regulated fusion clamp in mast cell degranulation. Sci. Signal. *11*.
McEwen, J.M., Madison, J.M., Dybbs, M., and Kaplan, J.M. (2006). Antagonistic regulation of synaptic vesicle priming by Tomosyn and UNC-13. Neuron *51*, 303–315.
Nair, A.G., Muttathukunnel, P., and Müller, M. (2020). Distinct molecular pathways govern presynaptic homeostatic plasticity. BioRxiv.
Palladino, M.J., Keegan, L.P., O'Connell, M.A., and Reenan, R.A. (2000). A-to-I pre-mRNA editing in Drosophila is primarily involved in adult nervous system function and integrity. Cell *102*, 437–449.
Paro, S., Li, X., O'Connell, M.A., and Keegan, L.P. (2012). Regulation and functions of ADAR in drosophila. Curr. Top. Microbiol. Immunol. *353*, 221–236.

Pobbati, A.V., Razeto, A., Böddener, M., Becker, S., and Fasshauer, D. (2004). Structural basis for the inhibitory role of tomosyn in exocytosis. J. Biol. Chem. *279*, 47192–47200.
Port, F., and Bullock, S.L. (2016). Augmenting CRISPR applications in Drosophila with tRNA-flanked sgRNAs. Nat. Methods *13*, 852–854.
Pulver, S.R., Bayley, T.G., Taylor, A.L., Berni, J., Bate, M., and Hedwig, B. (2015). IMAGING FICTIVE LOCOMOTOR PATTERNS IN LARVAL DROSOPHILA. J. Neurophysiol. *114*, jn.00731.2015.
Richmond, J.E., Weimer, R.M., and Jorgensen, E.M. (2001). An open form of syntaxin bypasses the requirement for UNC-13 in vesicle priming. Nature *412*, 338–341.
Rosahl, T.W., Geppert, M., Spillane, D., Herz, J., Hammer, R.E., Malenka, R.C., and Südhof, T.C. (1993). Short-term synaptic plasticity is altered in mice lacking synapsin I. Cell *75*, 661–670.
Rubin, R., Abbott, L.F., and Sompolinsky, H. (2017). Balanced excitation and inhibition are required for high-capacity, noise-robust neuronal selectivity. Proc. Natl. Acad. Sci. USA *114*, E9366–E9375.
Sapiro, A.L., Shmueli, A., Henry, G.L., Li, Q., Shalit, T., Yaron, O., Paas, Y., Billy Li, J., and Shohat-Ophir, G. (2019). Illuminating spatial A-to-I RNA editing signatures within the Drosophila brain. Proc. Natl. Acad. Sci. USA *116*, 2318–2327.
Shen, W., Kilander, M.B.C., Bridi, M.S., Frei, J.A., Niescier, R.F., Huang, S., and Lin, Y.-C. (2020). Tomosyn regulates the small RhoA GTPase to control the dendritic stability of neurons and the surface expression of AMPA receptors. J. Neurosci. Res. *98*, 1213–1231.
Sun, J., Bronk, P., Liu, X., Han, W., and Südhof, T.C. (2006). Synapsins regulate use-dependent synaptic plasticity in the calyx of Held by a Ca2+/calmodulin-dependent pathway. Proc. Natl. Acad. Sci. USA *103*, 2880–2885.
Tebo, A.G., and Gautier, A. (2019). A split fluorescent reporter with rapid and reversible complementation. Nat. Commun. *10*, 2822.
Varoqueaux, F., Sigler, A., Rhee, J.-S., Brose, N., Enk, C., Reim, K., and Rosenmund, C. (2002). Total arrest of spontaneous and evoked synaptic transmission but normal synaptogenesis in the absence of Munc13-mediated vesicle priming. Proc. Natl. Acad. Sci. USA *99*, 9037–9042.
Vasin, A., Volfson, D., Littleton, J.T., and Bykhovskaia, M. (2016). Interaction of the Complexin Accessory Helix with Synaptobrevin Regulates Spontaneous Fusion. Biophys. J. *111*, 1954–1964.
Verhage, M., Maia, A.S., Plomp, J.J., Brussaard, A.B., Heeroma, J.H., Vermeer, H., Toonen, R.F., Hammer, R.E., van den Berg, T.K., Missler, M., et al. (2000). Synaptic assembly of the brain in the absence of neurotransmitter secretion. Science *287*, 864–869.
Widberg, C.H., Bryant, N.J., Girotti, M., Rea, S., and James, D.E. (2003). Tomosyn interacts with the t-SNAREs syntaxin4 and SNAP23 and plays a role in insulin-stimulated GLUT4 translocation. J. Biol. Chem. *278*, 35093–35101.
Yamamoto, Y., Mochida, S., Miyazaki, N., Kawai, K., Fujikura, K., Kurooka, T., Iwasaki, K., and Sakisaka, T. (2010). Tomosyn inhibits synaptotagmin-1-mediated step of Ca2+-dependent neurotransmitter release through its N-terminal WD40 repeats. J. Biol. Chem. *285*, 40943–40955.
Yoshihara, M., Adolfsen, B., Galle, K.T., and Littleton, J.T. (2005). Retrograde signaling by Syt 4 induces presynaptic release and synapse-specific growth. Science *310*, 858–863.
Yu, H., Rathore, S.S., Gulbranson, D.R., and Shen, J. (2014). The N- and C-terminal domains of tomosyn play distinct roles in soluble N-ethylmaleimide-sensitive factor attachment protein receptor binding and fusion regulation. J. Biol. Chem. *289*, 25571–25580.
Zhou, S., and Yu, Y. (2018). Synaptic E-I Balance Underlies Efficient Neural Coding. Front. Neurosci. *12*, 46.